AD-A042 327 GENERAL ELECTRIC CO CINCINNATI OHIO AIRCRAFT ENGINE GROUP F/G 14/2
HIGH VELOCITY JET NOISE SOURCE LOCATION AND REDUCTION. TASK 1. --ETC(U)
FEB 77 C T SAVELL, E J STRINGAS DOT-OS-30034
UNCLASSIFIED R77AEG188 FAA-RD-76-79-1A NL

1 OF 3
ADA042327

REPORT NO. FAA-RD-76-79,Ia

(9)

HIGH VELOCITY JET NOISE SOURCE LOCATION AND REDUCTION

TASK I Supplement - CERTIFICATION OF THE GENERAL ELECTRIC JET NOISE ANECHOIC TEST FACILITY

FEBRUARY 22, 1977
FINAL REPORT

Prepared for

U.S. DEPARTMENT OF TRANSPORTATION
FEDERAL AVIATION ADMINISTRATION
Systems Research & Development Service
Washington, D.C. 20590

NOTICE

(19) 76-79-1a

1. Report No. FAA-RD-76-79, Ia	2. Government Accession No.	3. Recipient's Catalog No. 22 Feb 77
4. Title and Subtitle HIGH VELOCITY JET NOISE SOURCE LOCATION AND REDUCTION, TASK 1, SUPPLEMENT - CERTIFICATION OF THE GENERAL ELECTRIC JET NOISE ANECHOIC TEST FACILITY,		5. Report Date February 22, 1977 6. Performing Organization Code
7. Author(s) C.T. Savell (Task 1 Technical Director and Editor) et.al. E.J. Stringas (Technical Project Manager)		8. Performing Organization Report No. R77AEG188 10. Work Unit No.
9. Performing Organization Name and Address General Electric Company Group Advanced Engineering Division Aircraft Engine Group Cincinnati, Ohio 45215	(12) 236 p.	11. Contract or Grant No. DOT-OS-30034 13. Type of Report and Period Covered Task 1 Supplement October 1975-March 1976
12. Sponsoring Agency Name and Address U.S. Department of Transportation, Federal Aviation Administration Systems Research and Development Service Washington, D.C. 20590	(9) Final Rept.	14. Sponsoring Agency Code ARD-550

15. Supplementary Notes This report is in partial fulfillment of the subject program. Related documents to be issued in the course of the program include final reports of the following tasks: Task 2 - Theoretical Developments & Basic Experiments; Task 3 - Experimental Investigation of Suppression Principles; Task 4 - Development/Evaluation of Techniques for "Inflight" Investigation; Task 5 - Investigation of "Inflight" Aeroacoustic Effects; Task 6 - Noise Abatement Nozzle Design Guide.

16. Abstract

This report summarizes the certification testing of the General Electric Jet Noise Anechoic Test Facility to be used under the subject program. The precision and accuracy of acoustic measurements are evaluated in terms of:

- Anechoic and far-field environment;
- Ambient levels in the chamber;
- Contamination from piping and combustors;
- Contamination from electronic noise floor;
- Variation of the frequency response of the data acquisition and reduction systems;
- Inaccuracies in aerodynamic instrumentation or fluctuations in the jet aero conditions; and
- Precision errors in the air attenuation model due to environmental fluctuations, gradients and measurement inaccuracies

Jet noise measurements from circular conical nozzles are compared with classical referee data.

17. Key Words (Suggested by Author(s))	18. Distribution Statement
Acoustic facility certification, air attenuation, electronic noise floor, circular nozzle jet noise	Document is available to the public through the National Technical Information Service, Springfield, Virginia

19. Security Classif. (of this report)	20. Security Classif. (of this page)	21. No. of Pages	22. Price*
UNCLASSIFIED	UNCLASSIFIED	~~218~~ 237	

*For sale by the National Technical Information Service, Springfield, Virginia 22151

METRIC CONVERSION FACTORS

Approximate Conversions to Metric Measures

Symbol	When You Know	Multiply by	To Find	Symbol
		LENGTH		
in	inches	*2.5	centimeters	cm
ft	feet	30	centimeters	cm
yd	yards	0.9	meters	m
mi	miles	1.6	kilometers	km
		AREA		
in^2	square inches	6.5	square centimeters	cm^2
ft^2	square feet	0.09	square meters	m^2
yd^2	square yards	0.8	square meters	m^2
mi^2	square miles	2.6	square kilometers	km^2
	acres	0.4	hectares	ha
		MASS (weight)		
oz	ounces	28	grams	g
lb	pounds	0.45	kilograms	kg
	short tons (2000 lb)	0.9	tonnes	t
		VOLUME		
tsp	teaspoons	5	milliliters	ml
Tbsp	tablespoons	15	milliliters	ml
fl oz	fluid ounces	30	milliliters	ml
c	cups	0.24	liters	l
pt	pints	0.47	liters	l
qt	qwarts	0.95	liters	l
gal	gallons	3.8	liters	l
ft^3	cubic feet	0.03	cubic meters	m^3
yd^3	cubic yards	0.76	cubic meters	m^3
		TEMPERATURE (exact)		
°F	Fahrenheit temperature	5/9 (after subtracting 32)	Celsius temperature	°C

*1 in = 2.54 (exactly). For other exact conversions and more detailed tables, see NBS Misc. Publ. 286, Units of Weights and Measures, Price $2.25, SD Catalog No. C13.10:286.

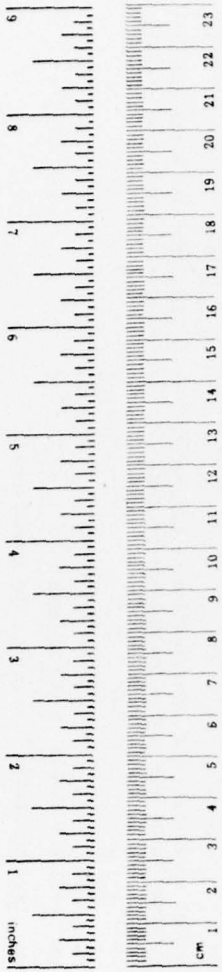

Approximate Conversions from Metric Measures

Symbol	When You Know	Multiply by	To Find	Symbol
		LENGTH		
mm	millimeters	0.04	inches	in
cm	centimeters	0.4	inches	in
m	meters	3.3	feet	ft
m	meters	1.1	yards	yd
km	kilometers	0.6	miles	mi
		AREA		
cm^2	square centimeters	0.16	square inches	in^2
m^2	square meters	1.2	square yards	yd^2
km^2	square kilometers	0.4	square miles	mi^2
ha	hectares (10,000 m^2)	2.5	acres	
		MASS (weight)		
g	grams	0.035	ounces	oz
kg	kilograms	2.2	pounds	lb
t	tonnes (1000 kg)	1.1	short tons	
		VOLUME		
ml	milliliters	0.03	fluid ounces	fl oz
l	liters	2.1	pints	pt
l	liters	1.06	quarts	qt
l	liters	0.26	gallons	gal
m^3	cubic meters	35	cubic feet	ft^3
m^3	cubic meters	1.3	cubic yards	yd^3
		TEMPERATURE (exact)		
°C	Celsius temperature	9/5 (then add 32)	Fahrenheit temperature	°F

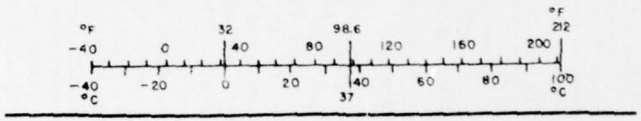

PREFACE

This report describes the work performed under Task 1 of the DOT/FAA High Velocity Jet Noise Source Location and Reduction program (Contract DOT-OS-30034). The objectives of the program were:

- Investigation of the aerodynamic and acoustic mechanisms of various jet noise suppressors, including scaling effects
- Analytical and experimental studies of the acoustic source distribution in such suppressors, including identification of source location, nature and strength and noise reduction potential
- Investigation of inflight effects on the aerodynamic and acoustic performance of these suppressors.

The results of these investigations lead to the preparation of a design guide report for predicting the overall characteristics of suppressor concepts from models to full-scale static, to inflight conditions, as well as a quantitative and qualitative prediction of the phenomena involved.

The work effect in this program was organized under the following major Tasks, each of which is reported in a separate final report:

Task 1 - Activation of Facilities and Validation of Source Location Techniques.

Task 2 - Theoretical Developments and Basic Experiments.

Task 3 - Experimental Investigation of Suppression Principles.

Task 4 - Development and Evaluation of Techniques for Inflight Investigation.

Task 5 - Investigation of Inflight Aero-Acoustic Effects on Suppressed Exhausts.

Task 6 - Preparation of Noise Abatement Nozzle Design Guide Report.

Task 1, the subject of report (FAA-RD-76-79,I) was formulated to investigate candidate test facilities and noise source location techniques (including their accuracies and limitations) in order to assure that data acquired under this and future programs would be properly validated. The present volume is a supplement to that report, **FAA-RD-76-79, Ia, covering** certification of the General Electric Jet Noise Anechoic Test Facility.

Task 2 was a theoretical effort complemented by theory verification experiments which extended across the entire contract period of performance. Task 3 represented a substantial contract effort to gather various test data on a wide range of high velocity jet nozzle suppressors. These data, intended to help identify several "optimum" nozzles for inflight testing under Task 5, provide an extensive high quality data bank useful to preparation of the Task 6 design guide as well as to future studies.

Task 4 was similar to Task 1, except that it dealt with the specific test facility requirements, measurement techniques and analytical methods necessary to evaluate the inflight noise characteristics of simple and complex suppressor nozzles. This effort provided the capability to conduct the "flight" effects test programs of Task 5.

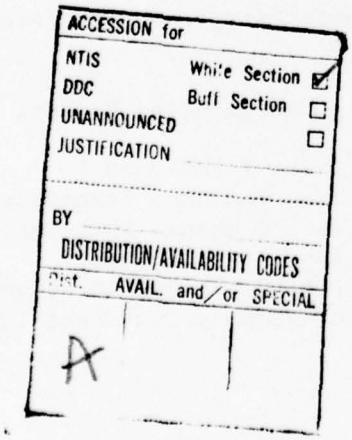

TABLE OF CONTENTS

TABLE OF CONTENTS (Concluded)

LIST OF ILLUSTRATIONS

LIST OF ILLUSTRATIONS (Continued)

LIST OF ILLUSTRATIONS (Continued)

LIST OF ILLUSTRATIONS (Continued)

LIST OF ILLUSTRATIONS (Continued)

LIST OF ILLUSTRATIONS (Continued)

LIST OF ILLUSTRATIONS (Continued)

LIST OF ILLUSTRATIONS (Continued)

LIST OF ILLUSTRATIONS (Continued)

LIST OF ILLUSTRATIONS (Continued)

LIST OF ILLUSTRATIONS (Concluded)

LIST OF TABLES

1.0 SUMMARY

This report contains the results of the supplemental Task 1 effort under contract DOT-OS-30034 involving the activation and certification of the General Electric Anechoic Jet Noise facility. The operating limits are presented on Figure 1-1.

Nozzle flow testing can be accomplished in the facility to a temperature of 1667 K (3000° R) and to a pressure ratio of 4.0.

The 1/3-octave SPL precision accuracy of the facility is within ± 2.5 dB standard deviation over the 400 Hz to 80 kHz frequency range of interest and within ± 1 dB between 630 Hz and 31.5 kHz. The chief sources of precision error are flow noise at low frequency and tape recorder floor and air attenuation measurement inaccuracies at high frequencies. The anechoic environment is excellent over the range from 200 Hz to 80 kHz. As shown on the figure, acoustic testing should not be conducted below 213 m/sec (700 ft/sec) up to 1111 K (2000° R) or below a pressure ratio of 1.1 from 1111 K (2000° R) to 1390 K (2500° R) and below a pressure ratio of 1.8 above 1390 K (2500° R).

The standard microphone stations are in the far-field for nozzles smaller than 17.3 cm (6.8 in.) effective diameter. Environmental gradients are extreme at low velocities and very high temperatures near the chamber roof and corner. Contamination from the chamber ambient noise and microphone noise floors are insignificant. Tape dynamic range becomes a problem at the angles closest to the jet axis.

The accuracy of the aerodynamic and acoustic instrumentation is excellent. The largest variability occurs when using the high temperature platinum rakes at low temperatures. Flow noise contamination within 6 dB of the jet level is possible at very low jet velocities.

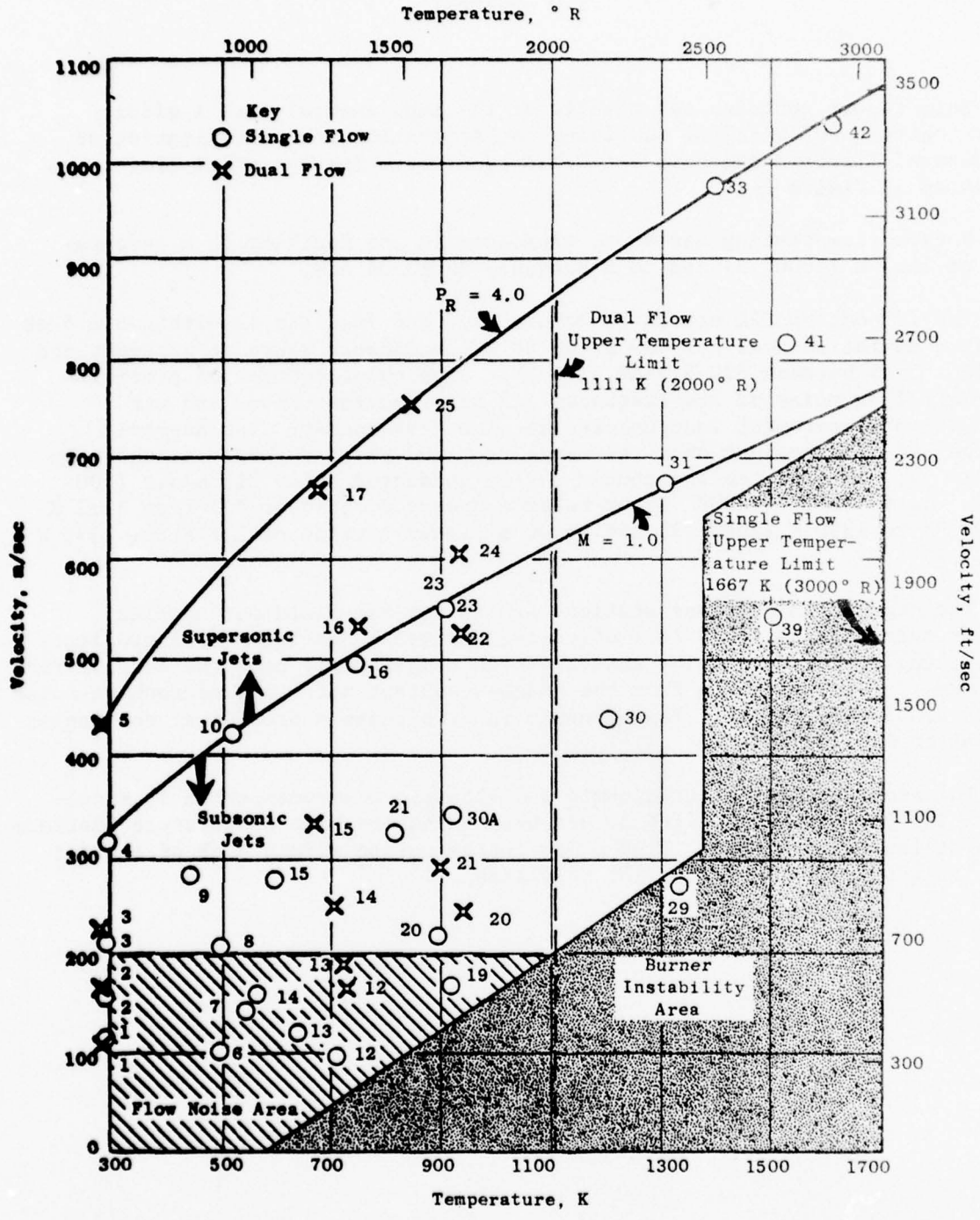

Figure 1-1. General Electric Anechoic Jet Noise Facility Operating Limits.

2.0 DESCRIPTION OF FACILITY

2.1 GENERAL

The General Electric Jet Noise Anechoic Chamber was built to support research in jet engine aircraft noise. The facility was several years in the design and construction phases, with the necessary funding provided by General Electric Corporate Funds. It will be utilized for support of internal acoustic development programs as well as acoustic programs sponsored by the various Government agencies engaged in jet noise research.

The facility can accommodate model exhaust nozzle configurations of approximately 2 mm (1/16 inch) to 17.3-cm (6.8-in.) diameter, which simulate turbojet and low bypass turbofans as well as conventional high bypass ratio turbofan applications. It is capable of exact temperature and pressure simulation as experienced on current and anticipated future, advanced, multicycle-engine systems.

The air supply system currently has secondary flow capability for simulating turbofan and duct-burning applications. Expansion to a tertiary flow system is underway, enabling open-throat anechoic free-jet testing of single- and dual-flow models. The tertiary flow system is scheduled for completion in early 1977.

The anechoic chamber is located at General Electric's Aircraft Engine Group in Evendale, Ohio. It is situated in the northeast corner of the Building 500 complex. The facility was built in an area formerly occupied by Cell 41, an engine test cell constructed for use on the X211 Atomic Engine Program. The basic shell of the anechoic test chamber, shown on Figure 2-1, was originally used as the exhaust stack. This cylindrical building is 21.95 meters (72 feet) high and 13.1 meters (43 feet) in diameter. The engine cell is now used for hardware preparation and storage and will be used for installation of the air source to be used on the tertiary flow system. The old engine test control room was divided, with part of it now used as the control room for the anechoic facility and the other part used as office area for the Acoustic Evaluation Engineering staff. This layout is depicted on Figures 2-2 and 2-3. The test chamber itself is divided into several major areas as shown on Figure 2-4.

The lower chamber is used as an air plenum, allowing for the entrained air flow (induced during operation) to pass in through the inlet silencers and up through the false floor (as shown on Figure 2-5) into the anechoic chamber. The entrained air becomes uniformly distributed within the plenum, thus eliminating any significant velocity effects throughout the chamber during operation. The design of the lower chamber was determined through scale-model testing, with a design velocity requirement of 2.13 m/sec (7 ft/sec) or less. Actual measurements of entrained-flow velocity were performed during chamber checkout as discussed in Section 3.3. Surfaces in the lower chamber are acoustically treated to prevent noises generated in the

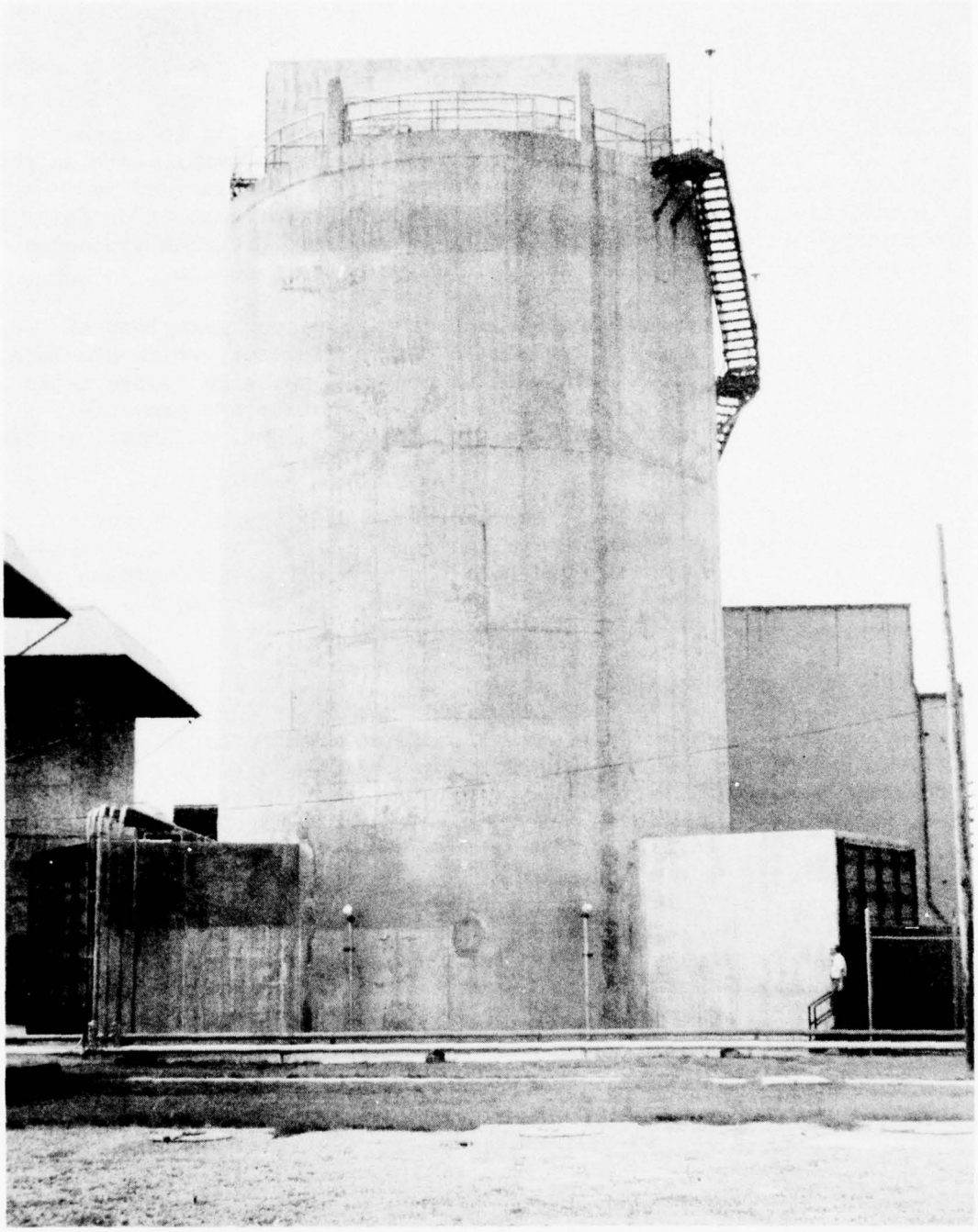

Figure 2-1. External View of the General Electric Anechoic Jet Noise Test Facility.

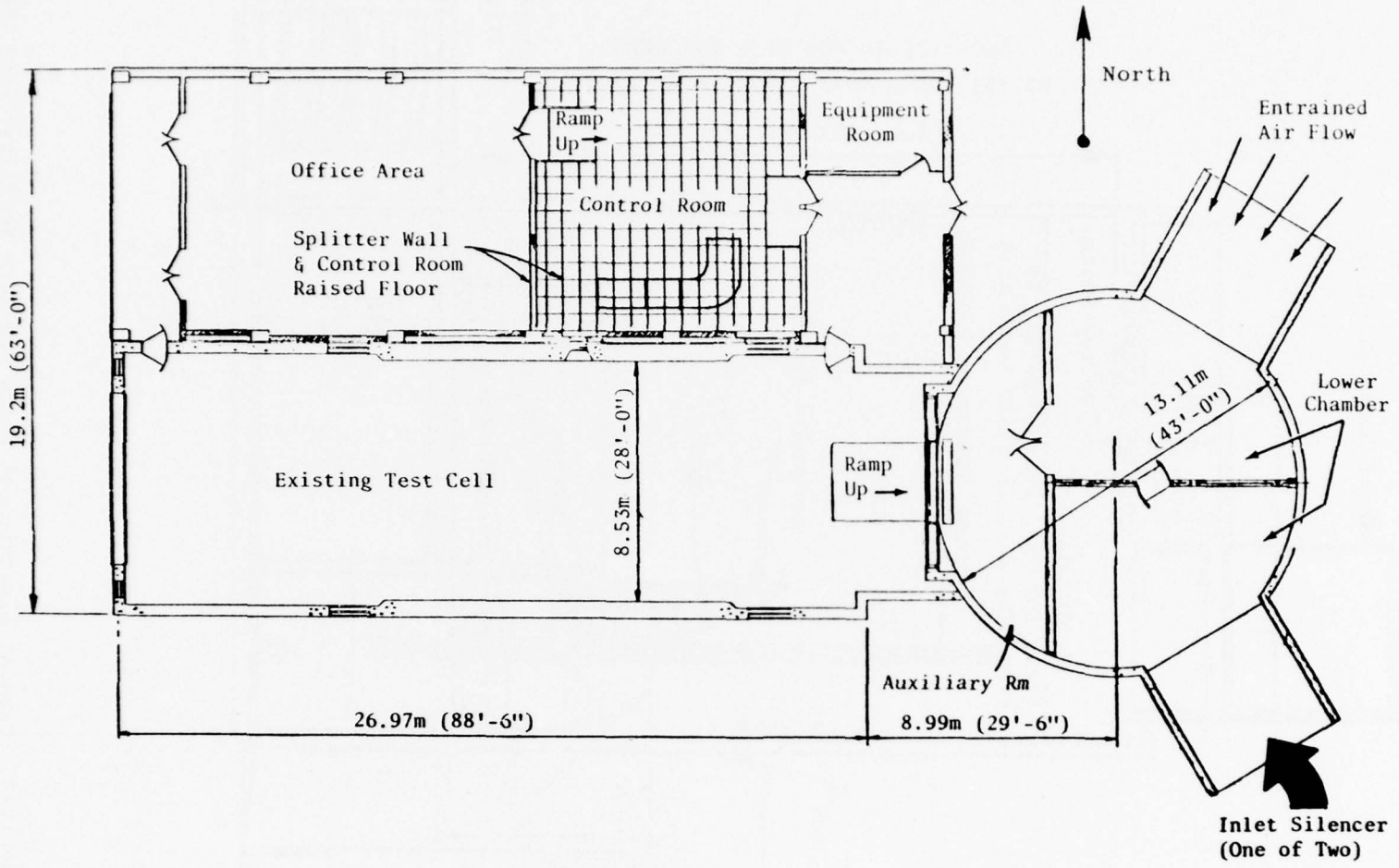

Figure 2-2. General Electric Jet Noise Anechoic Facility Floor Plan.

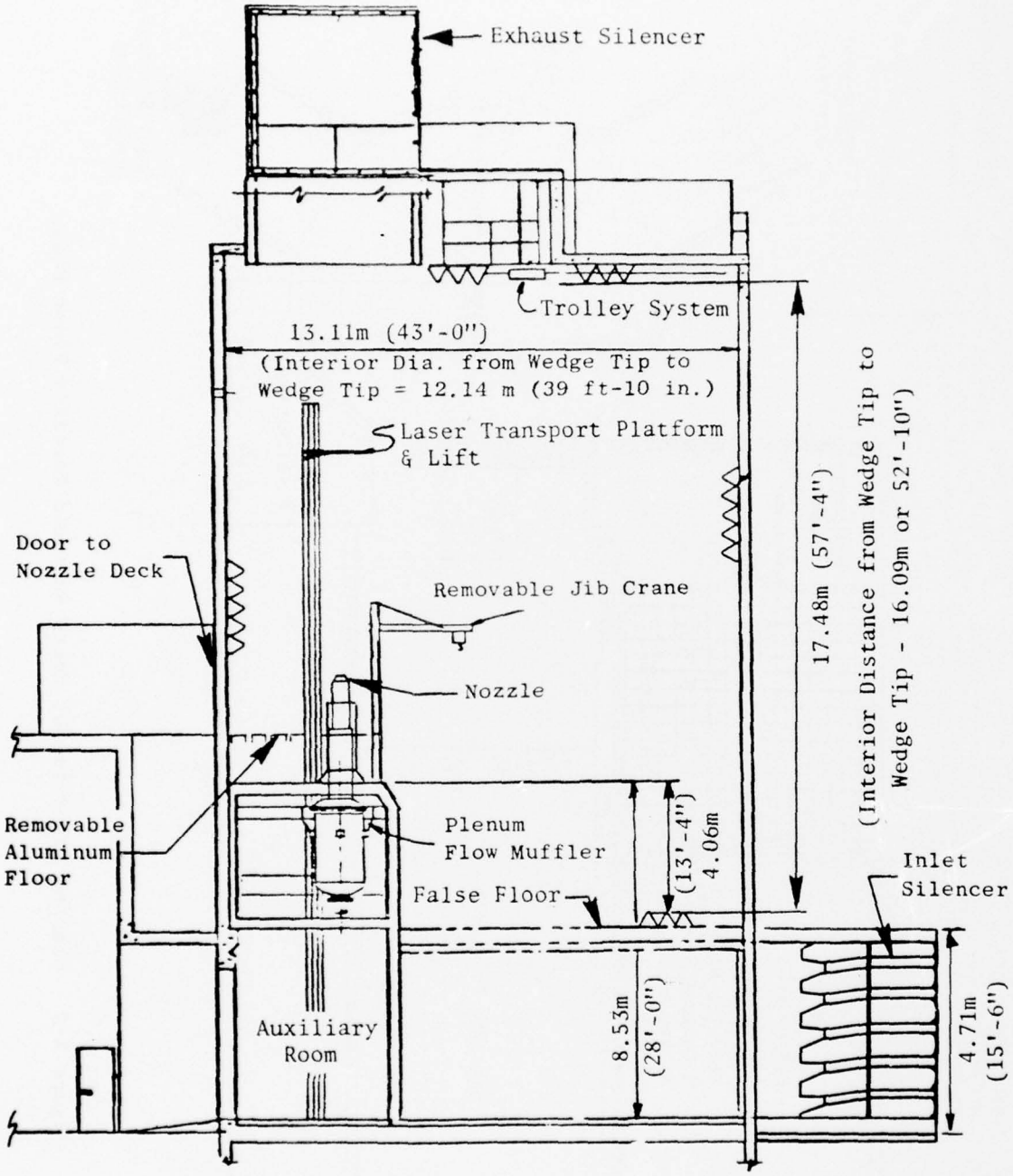

Figure 2-3. General Electric Jet Noise Anechoic Facility Cross Section.

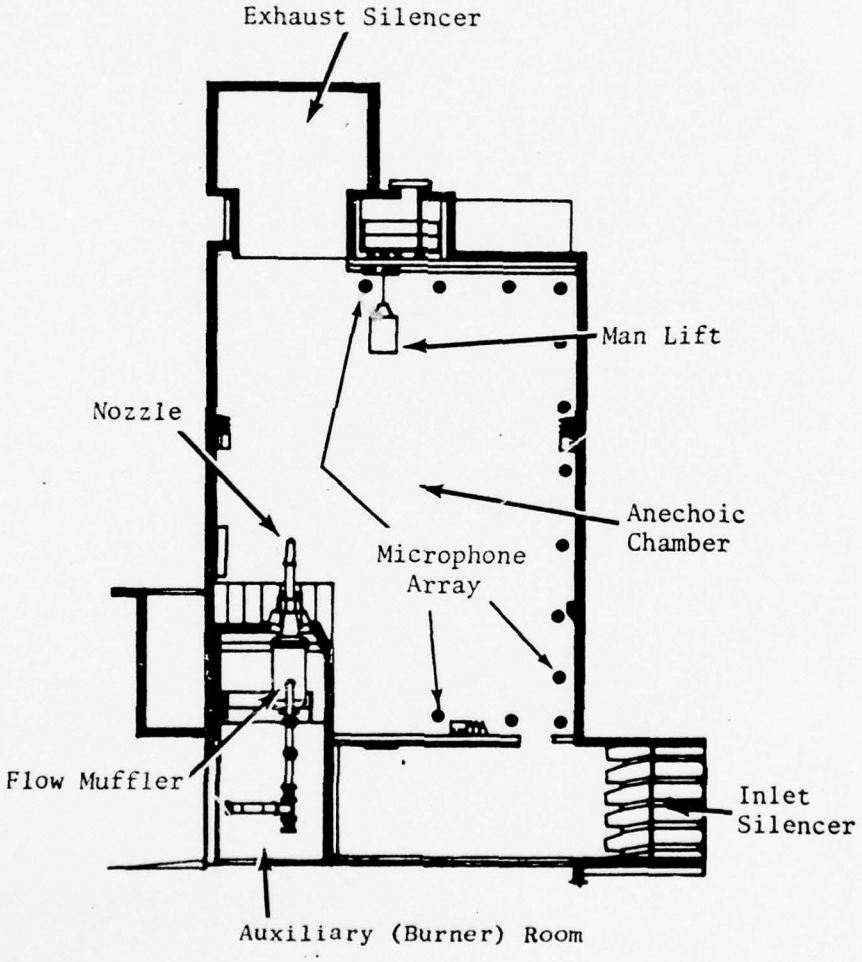

Figure 2-4. General Electric Anechoic Test Chamber Schematic.

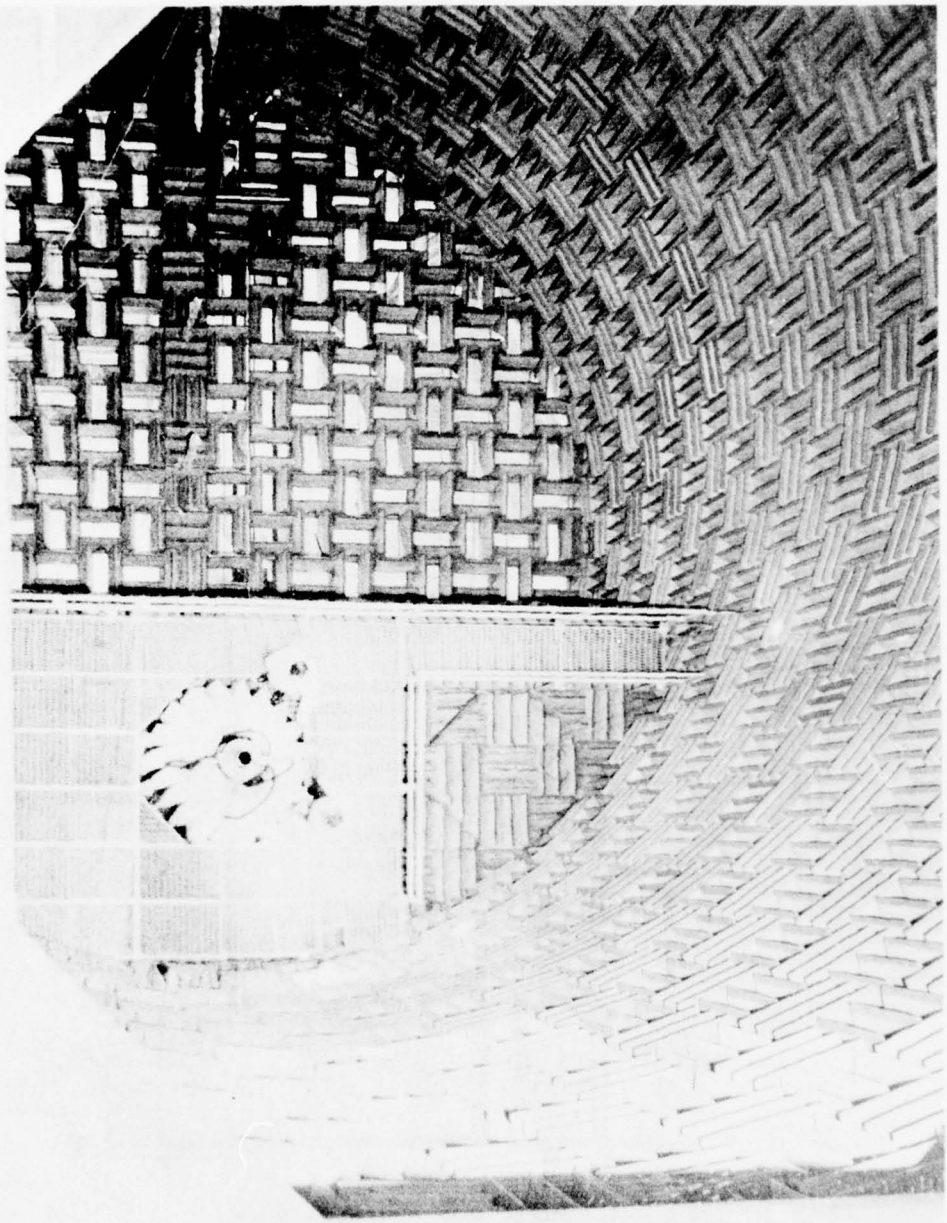

Figure 2-5. Overhead View of the General Electric Anechoic Jet Noise Test Facility Interior.

chamber during operation from passing down through the false floor and being reflected back into the chamber.

The auxiliary room, located on the west side of the chamber, is used to house the in-line acoustic muffler, primary and secondary stream burners, fuel control systems, and lower access rails for the laser velocimeter (LV) and ellipsoidal mirror (EM) cart. The auxiliary room is pneumatically sealed from the test chamber to prevent unsuppressed piping and burner noises from entering the test chamber.

The test chamber itself is shown on Figure 2-6, along with a typical single-flow nozzle installation. Surfaces within the chamber are covered with either anechoic wedges or wrapped with fiberglass to maintain their anechoic properties. Access to the test chamber area is achieved through a doorway opening onto the roof on the west wall of the chamber. Access to the nozzle is provided by means of expanded aluminum flooring and railings, shown on Figure 2-6, which are removed from the chamber during acoustic testing as shown on Figure 2-7. The standard far-field microphones are arranged on the chamber false floor, walls, and ceiling as shown in Figure 2-4.

During operation, the jet plume is discharged through the "T-shaped" exhaust silencer mounted on the roof of the chamber. This silencer arrangement effectively reduces the emitted noise to levels in compliance with community noise standards, as discussed in Section 4.5.

Air is supplied from a central air system (discussed in Section 2.3.2) through a single pipe which penetrates the south wall of the cell (see Figure 2-8). Just inside the wall the air supply splits into two systems: the fan and core. The fan air is controlled by a single V-ball valve; however, the core air can be regulated by two V-ball valves either in combination with one acting as a bypass for fine tuning control, or with blank-off plates installed. Either valve can be used independently. The fan air flow rate is measured with sharp-edged orifice plates. The core air flow can be measured with either sharp-edged orifice plates or a system of orifice nozzles. The orifice nozzles provide the ability to measure low air flow rates which would simulate engine bleed flows. Rupture discs are located between the flow measurement section and the riser sections of the pipes. They constitute a safety feature which prevents over-pressurization of the facility. The fan and core combustors are located in their respective risers which feed into the acoustically treated plenum. The top side of the plenum feeds into a coannular dual-flow riser which terminates in the test arena. Test nozzles are attached at this point.

2.2 ACOUSTIC ARENA

2.2.1 Anechoic Wedge Specifications

The wedges used in the test chamber were fabricated from Owens Fiberglas "Intermediate Service Board" composed of fiberglass fibers bonded

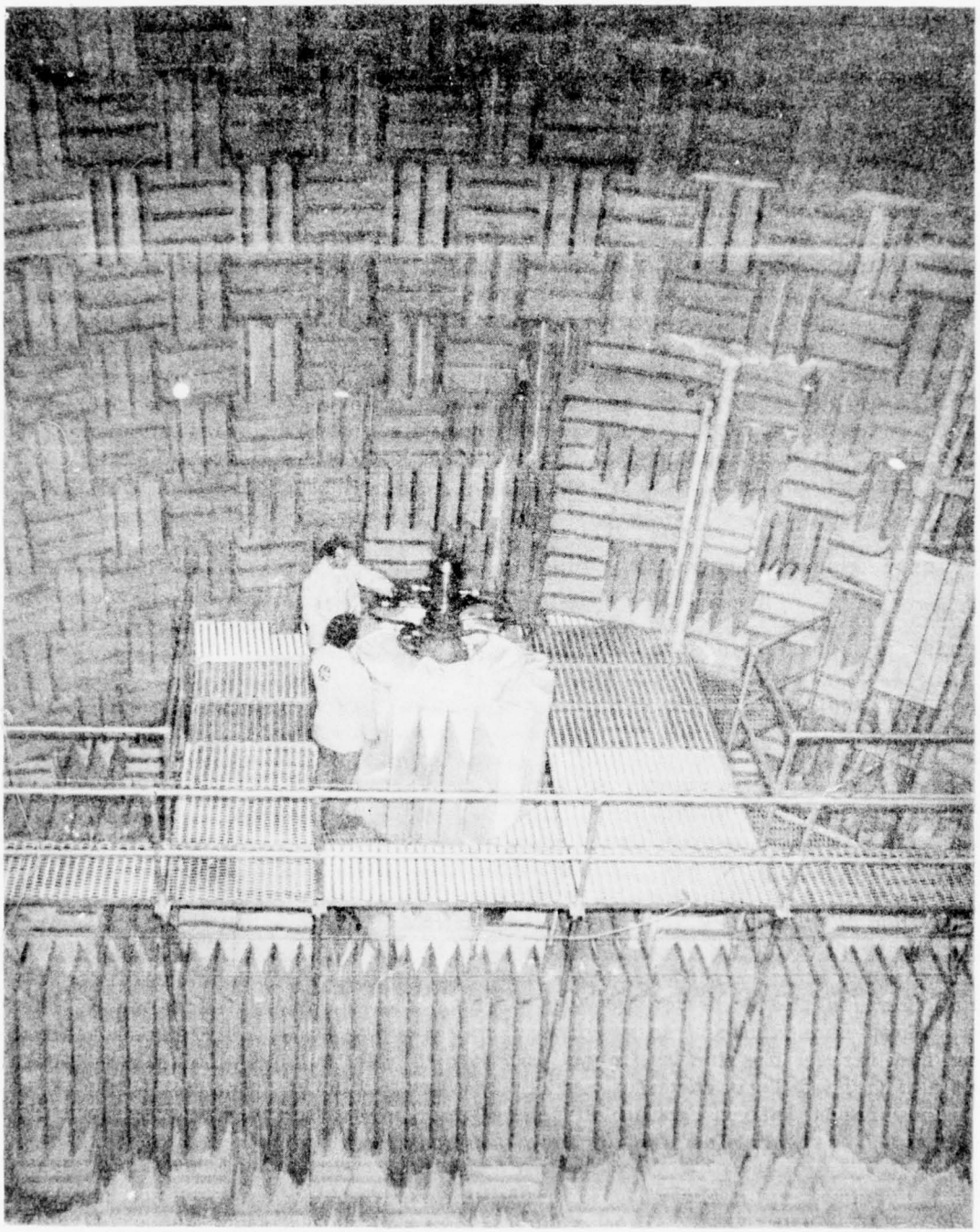

Figure 2-6. View of Test Arrangement in the General Electric Anechoic Jet Noise Test Facility.

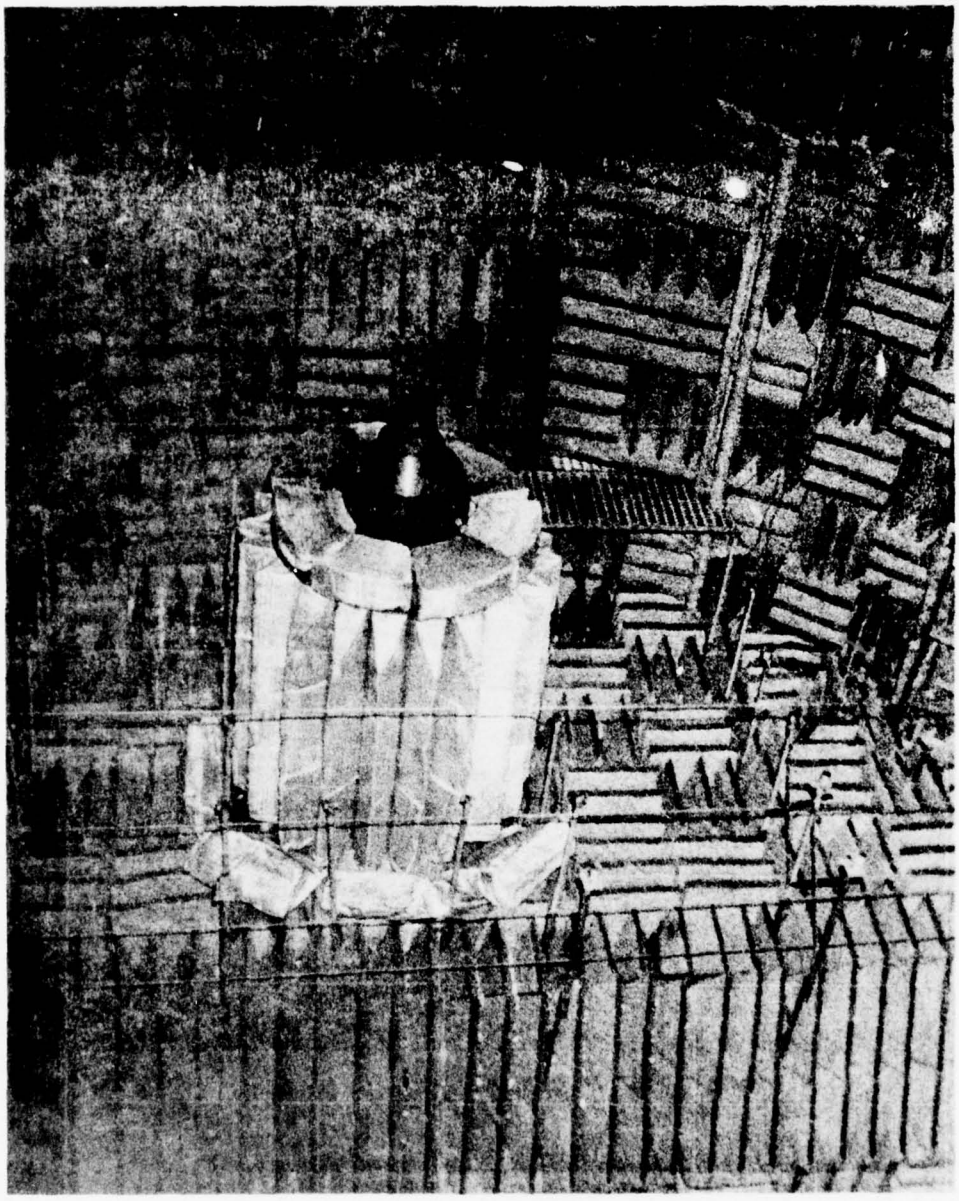

Figure 2-7. Internal View of the Test Arrangement During Operation with the Floor Removed.

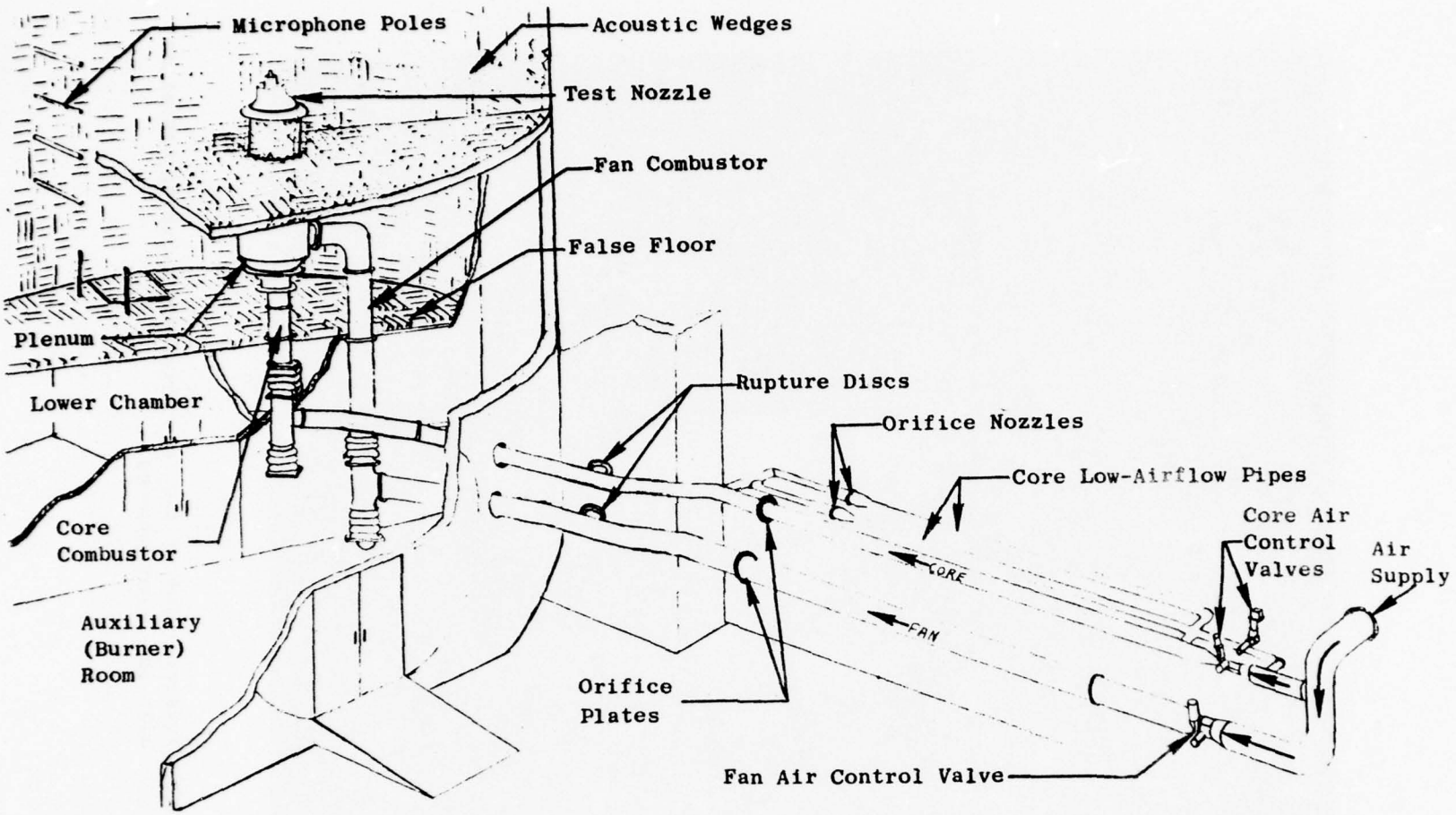

Figure 2-8. Cell 41 Anechoic Chamber Sketch.

together in a semirigid form with a binder rated for service at temperatures up to 455° C (850° F) with a material density of 48.05 kg/m^3 (3 lb/cu ft). The wedges are grouped three to a module as shown on Figure 2-9 with each module comprised of a 61-cm x 61-cm (2-ft x 2-ft) section. These modules are mounted on 0.46-cm thick (18-gage) steel base frames which, in turn, are mounted on steel tracks fastened to the concrete cell walls, with a 7.62-cm (3-inch) air space between the module base and the cell wall. The tapered surfaces of the wedges are covered with a wire mesh hardware cloth, and the wedge tips are covered with a strip of fine fiberglass cloth to prevent feathering.

In regions of the facility where the wedges may be subject to flow impingement and turbulence, the wedges are covered with a glass fiber cloth material to prevent degradation.

This wedge geometry and material were selected for meeting the facility requirements to a cutoff sound below a frequency of 220 Hz and absorption coefficient of better than 0.99 at frequencies above the cutoff frequency.

2.2.2 Microphone Locations

The stationary microphones used for far-field measurements within the chamber are located on the east wall, ceiling, and false floor in a vertical plane which includes the test nozzle. The microphones are positioned from 40° through 160° (re: jet exhaust angle = 180°) in 10° increments. They are mounted on standoff brackets such that each microphone is 1.52 m (5 ft) from the plane of the wedge tips, with the brackets wrapped with 5.08 cm (2 inches) of fiberglass material to prevent reflections from influencing the data, as shown in Figure 2-10, along with the man lift used for access to the microphone stations. During acoustic certification testing a microphone was traversed to within 0.43 m (1.4 ft) of the wedge tips and inverse square law characteristics were maintained, as shown in Figure 2-11, over the range of 160 Hz to 6300 Hz. The microphones themselves are held in a swivel mount and are oriented for normal incidence measurements relative to the sound-field center point, defined by the nozzle discharge plane and nozzle axis. The microphone positions for each angular location are presented on Table 2-I.

2.2.3 Traversing Microphone Capability

The capability exists for obtaining acoustic measurements within the same plane as the stationary far-field microphones by means of a remotely controlled traversing system. This system can be positioned within the bounds indicated on Figure 2-12. By adding an extension boom, data may be obtained closer to the nozzle with a corresponding decrease in the maximum distance attainable from the test nozzle. Operation and readout of vertical and horizontal position are achieved from the control console. The positioning readout is in terms of voltage, proportional to displacement, requiring calibration of the system prior to usage. In addition to acoustic measurements, this system can be used to transport temperature and humidity sensors for sampling profiles within the chamber during operation.

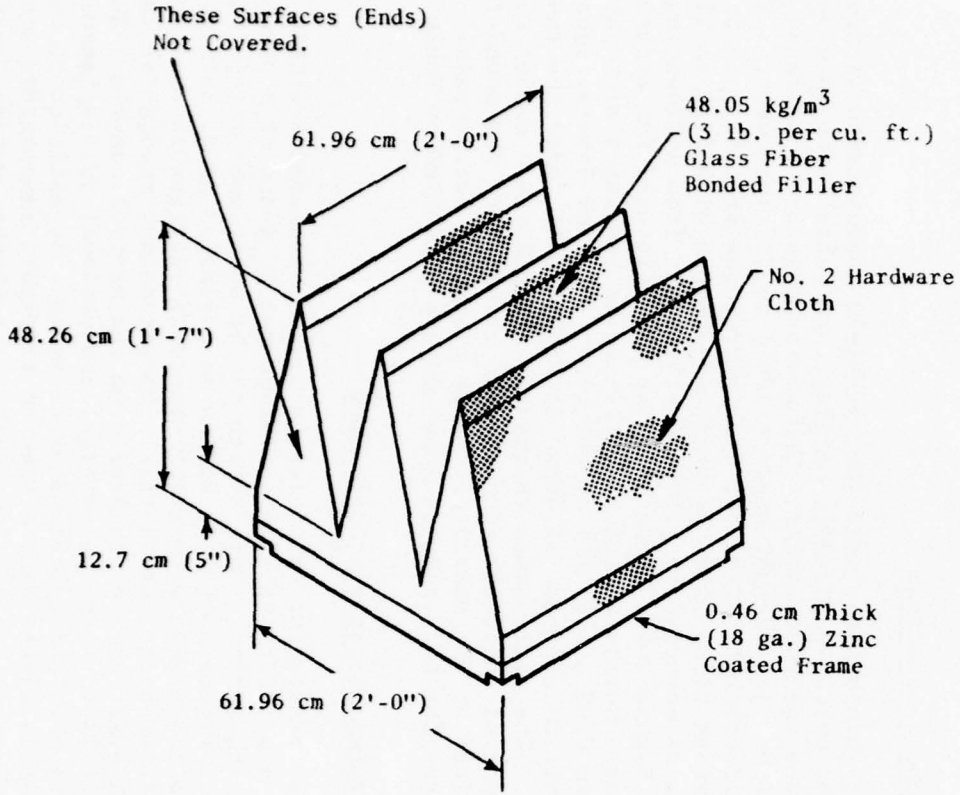

Typical Wedge Unit

Note: Wedges in Region of High Temperature, High Velocity Gas Flow Have Filler Covered With Glass Fiber Cloth, Prior to Hardware Cloth Cover.

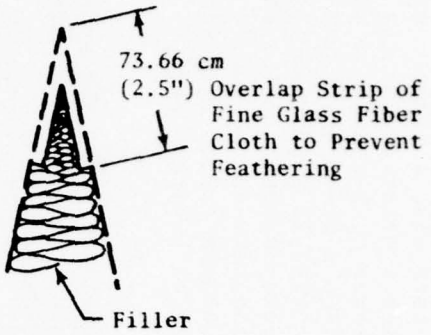

Wedge Tip Detail

Figure 2-9. General Electric Anechoic Facility Acoustic Wedge Details.

Figure 2-10. Internal View of the General Electric Anechoic Jet Noise Test Facility Demonstrating Man Lift Operation.

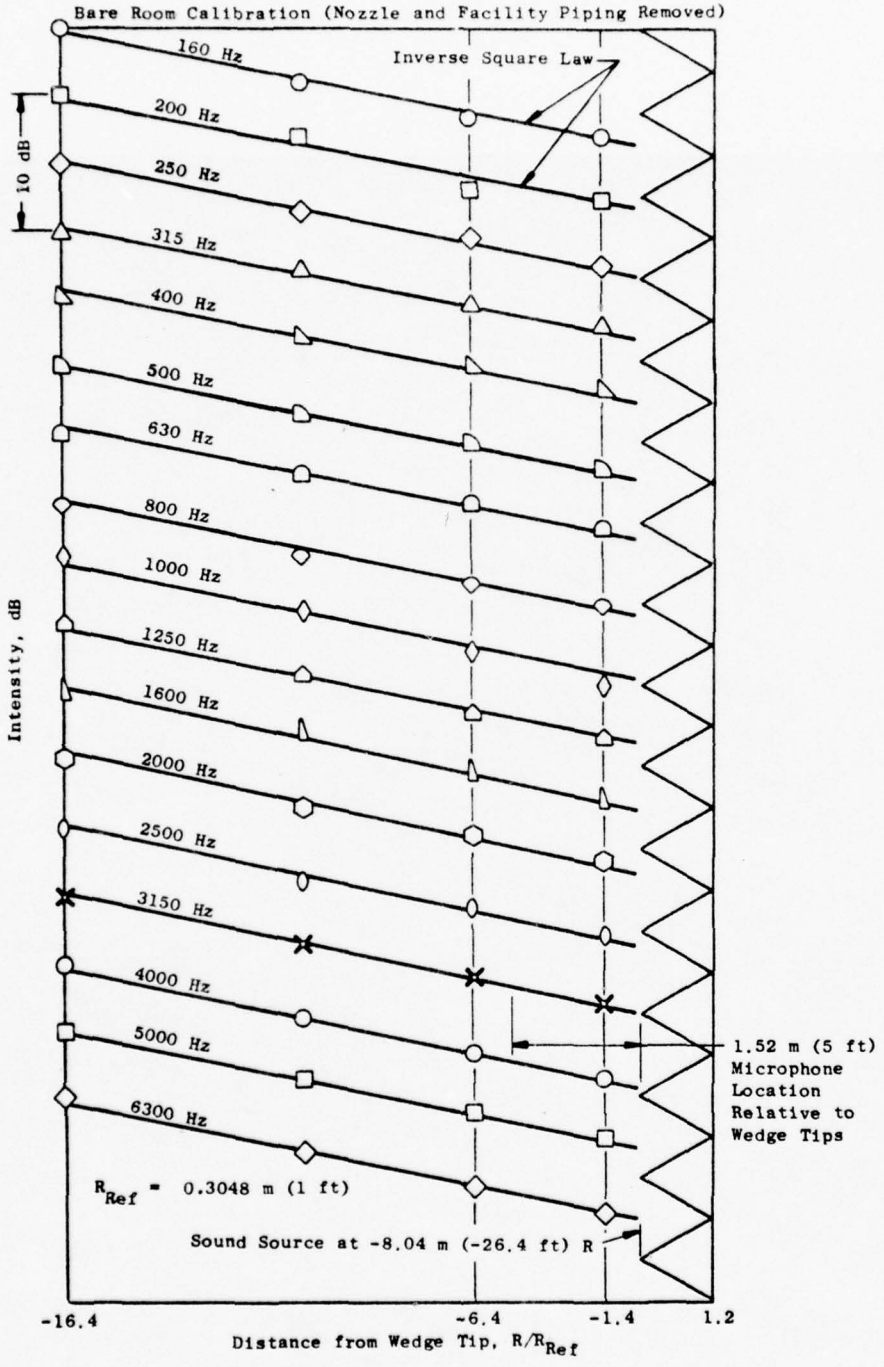

Figure 2-11. Acoustic Characteristics of the Anechoic Wedges.

Table 2-I. Far-Field Microphone Positions.

Angle (Degrees)	Radial Distance		X		Y	
	m	(ft)	m	(ft)	m	(ft)
40	6.91	(22.66)	4.44	(14.57)	-5.29	(-17.36)
50	8.23	(27.00)	6.3	(20.68)	-5.29	(-17.36)
60	9.50	(31.18)	8.23	(27.00)	-4.75	(-15.59)
70	8.76	(28.73)	8.23	(27.00)	-3.00	(- 9.83)
80	8.36	(27.42)	8.23	(27.00)	-1.45	(- 4.76)
90	8.23	(27.00)	8.23	(27.00)	0	(0)
100	8.36	(27.42)	8.23	(27.00)	1.45	(4.76)
110	8.76	(28.73)	8.23	(27.00)	3.00	(9.83)
120	9.5	(31.18)	8.23	(27.00)	4.75	(15.59)
130	10.74	(35.25)	8.23	(27.00)	6.91	(22.66)
140	10.09	(33.12)	6.49	(21.29)	7.73	(25.37)
150	8.93	(29.29)	4.46	(14.64)	7.73	(25.37)
160	8.23	(27.00)	2.81	(9.23)	7.73	(25.37)

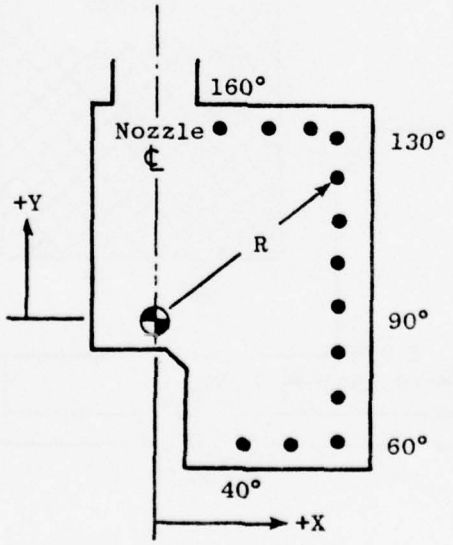

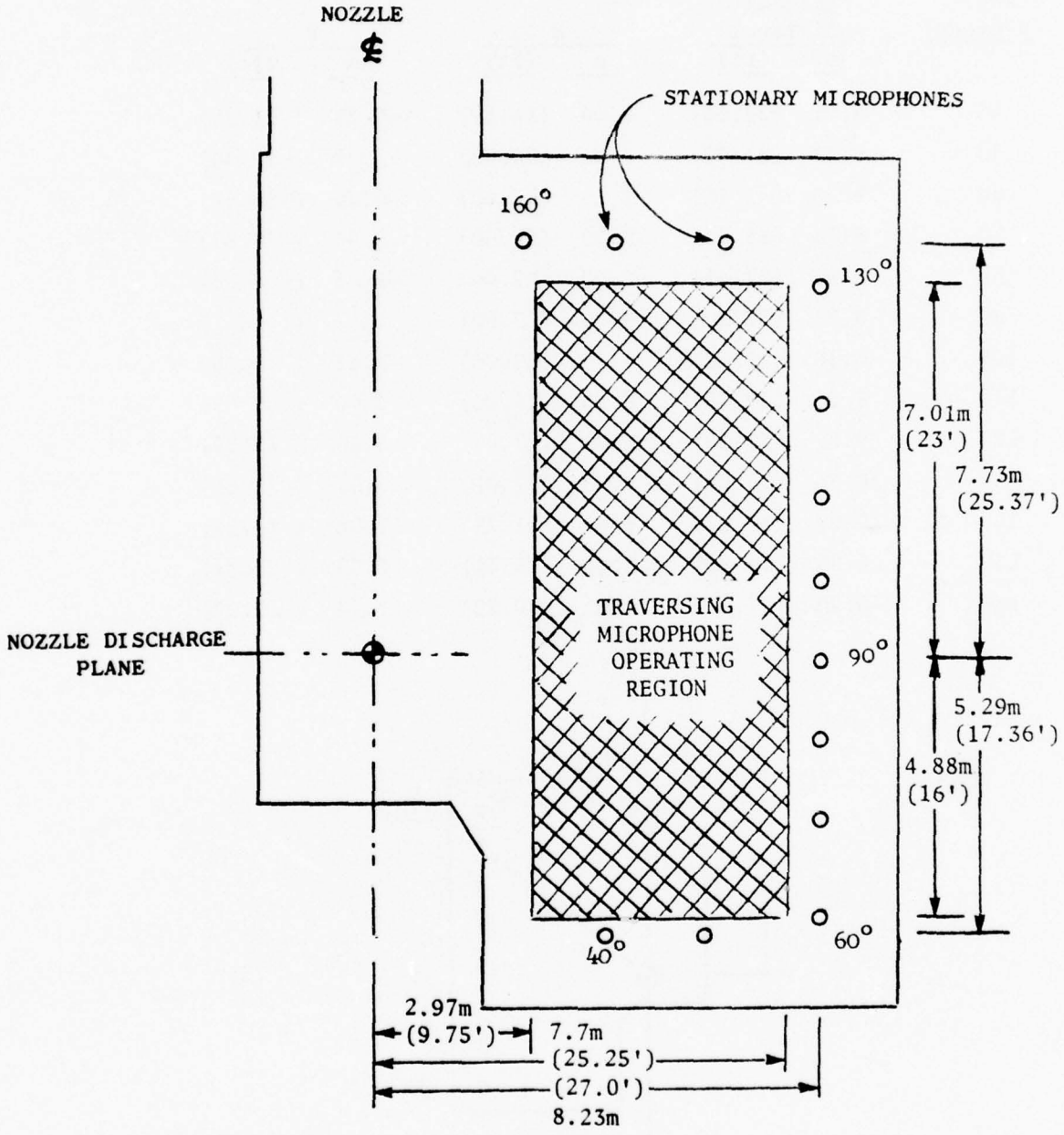

Figure 2-12. Traversing Microphone Physical Operational Limits.

2.2.4 Ellipsoidal Mirror and Laser Velocimeter Traversing System

An important feature of the facility is the system which permits aerodynamic and acoustic in-jet instrumentation to traverse parallel to the jet exhaust plume axis. This system normally is used to accept either the ellipsoidal mirror (EM) (see Figure 2-13), for noise source location measurements, or the laser velocimeter (LV) (see Figure 2-14), used for turbulent flow velocity measurements in the exhaust stream.

The track is located on the northwest side of the chamber at a position approximately 3.96 m (13 ft) from the nozzle axis. The traverse span ranges from approximately 61 m (2 ft) below the nozzle discharge plane to approximately 5.18 m (17 ft) above the nozzle discharge plane.

The cart and lift have a rated load capacity of 1633 kg (3600 lb). It rides on precision-aligned rails made of hardened steel for wear resistance and accurate positioning. The track extends through a sliding concrete hatch, via a hinged section of track, to the floor of the auxiliary room to permit interchanging the EM and LV systems as required. Traversing operation of the cart on the track can be accomplished from either the test chamber, auxiliary room, or the control console. Remote position indication is provided by means of a 10-turn potentiometer driven off the winch shaft, with readout at the control console; the ability to record the position signal on magnetic tape in conjunction with the acoustic data for subsequent correlation is provided.

2.3 FACILITY OPERATING CAPABILITY

2.3.1 Air Supply Sources

Several supply sources are available for providing airflow to the anechoic chamber at pressure and flow rates as required for the type testing being performed. The central air supply system in plant Building 401, Figure 2-15, is the basic air supply used throughout the various testing areas. This system is comprised of five multistage centrifugal compressors consisting of two first-stage units, two second-stage units, and one third-stage unit, driven by synchronous motors through speed-increasing gears. The flexibility exists for tandem and parallel combinations to meet required flow conditions up to 45.36 kg of air per second at 2.1 MN/m^2 pressure (100 lb/sec at 300 psig) as indicated on Figure 2-16.

Testing at lower flow conditions may be accomplished using the shop air supply system consisting of two compressors each having 2.72 kg/sec at 689 kN/m^2 (6 lb/sec at 100 psi) output. These units can be supplemented by the compressor boost (C/B) air which can provide an additional 1.81 kg/sec (4 lb/sec). A maximum of 7.26 kg/sec at 689 kN/m^2 (16 lb/sec at 100 psi) can be provided by this system. For lower flow rates the units may be run as indicated on Figure 2-17.

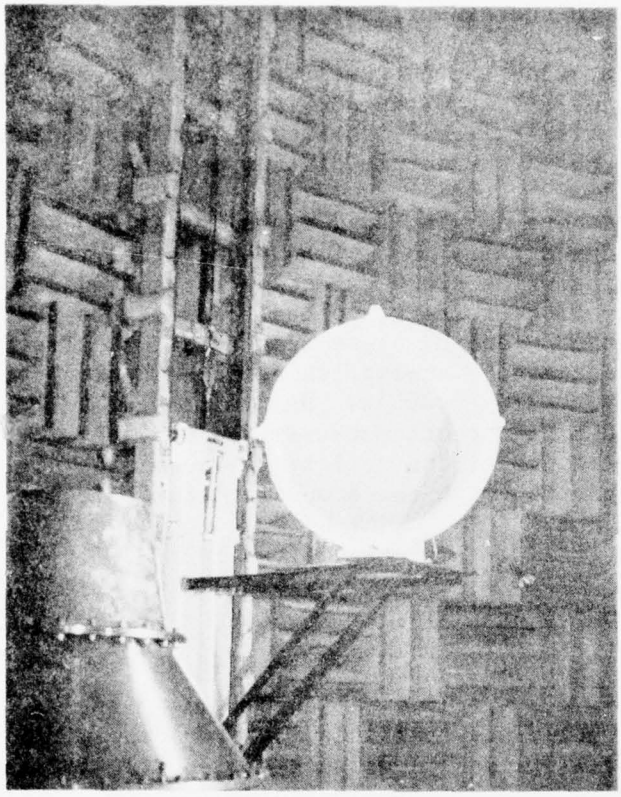

Figure 2-13. Ellipsoidal Mirror Traverse System.

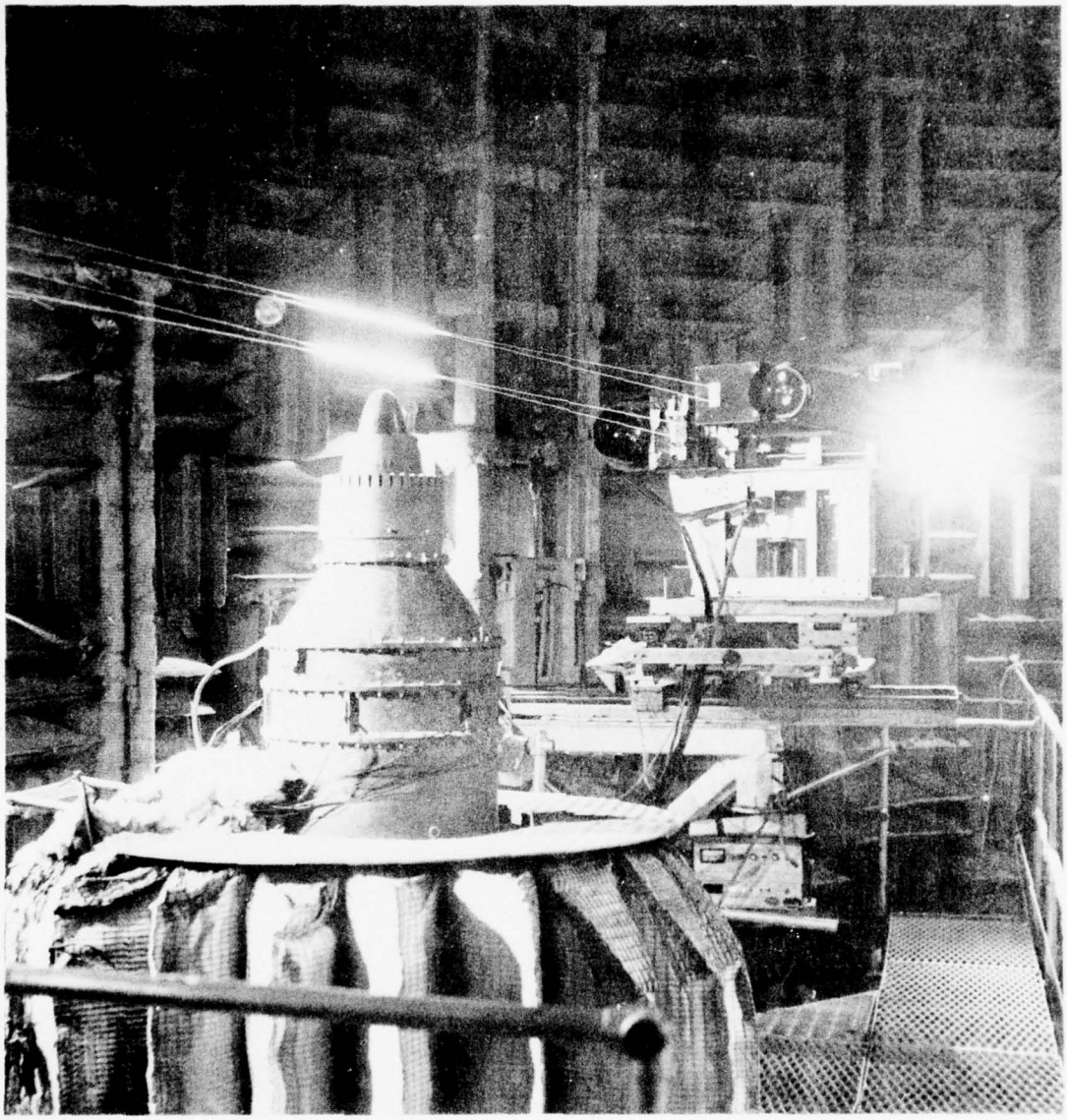

Figure 2-14. Laser Velocimeter Traverse Test.

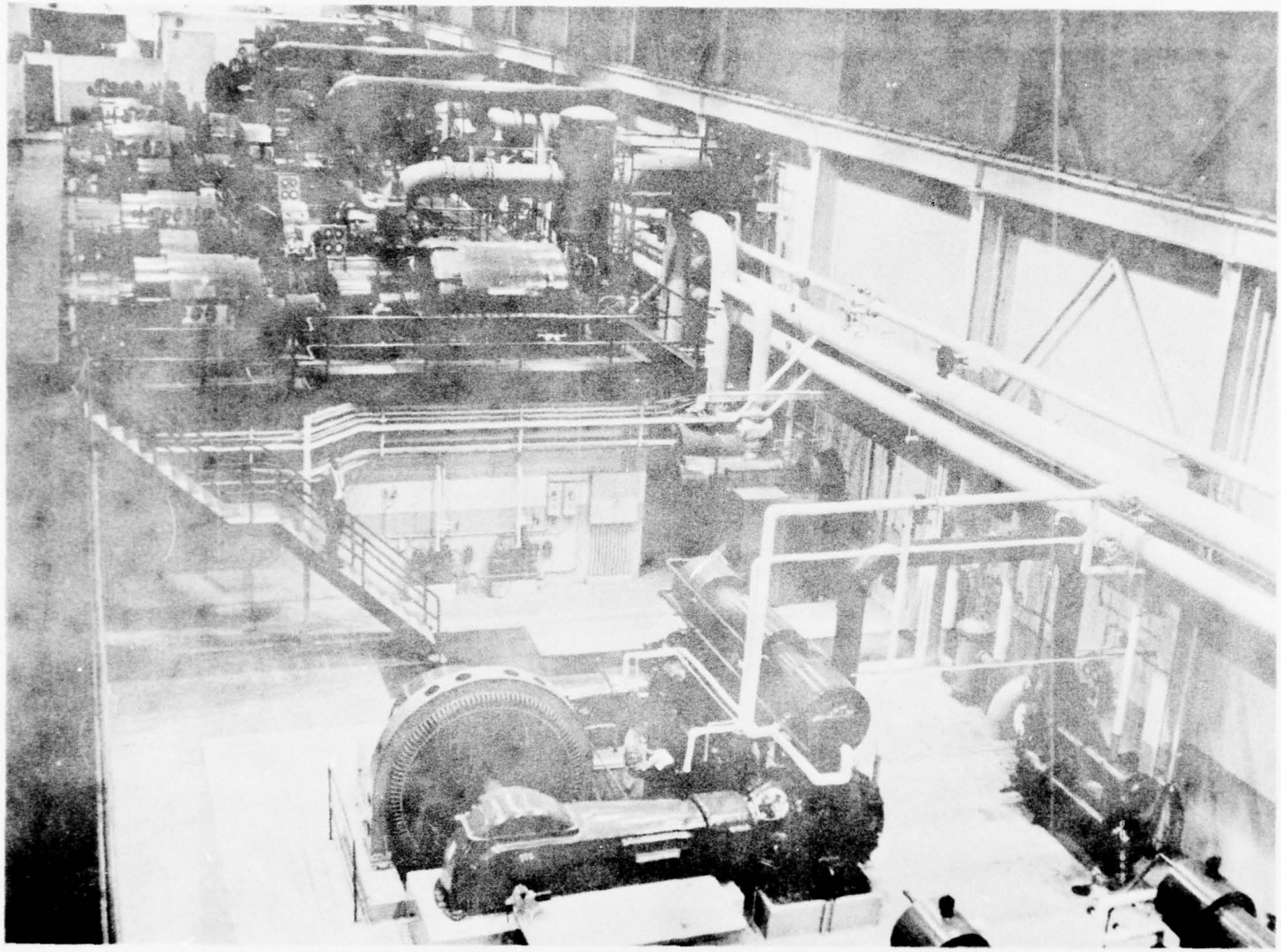

Figure 2-15. Central Air Supply System - Building 401.

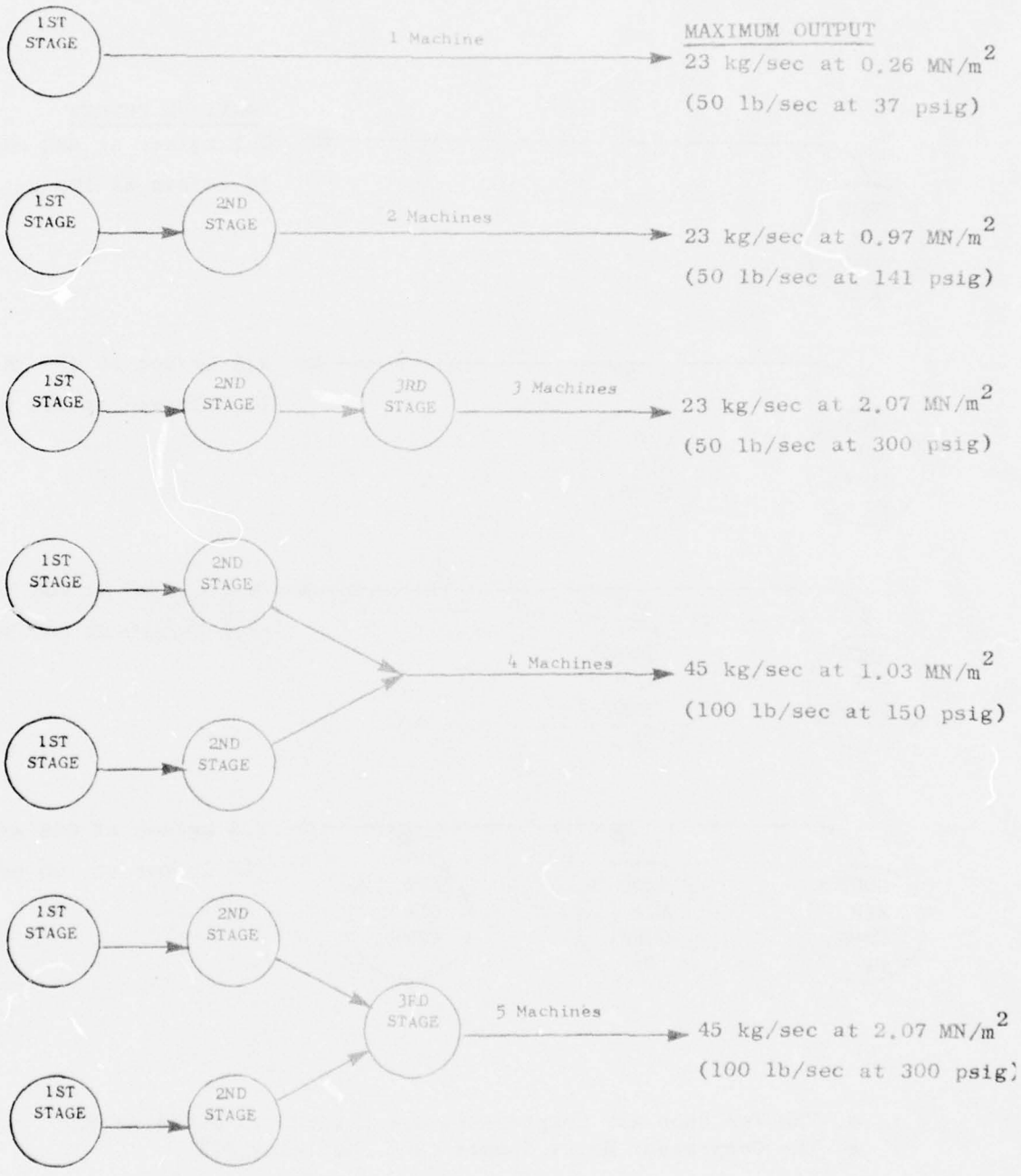

Figure 2-16. Central Air Supply System (Building 401) Compressor Staging and Output.

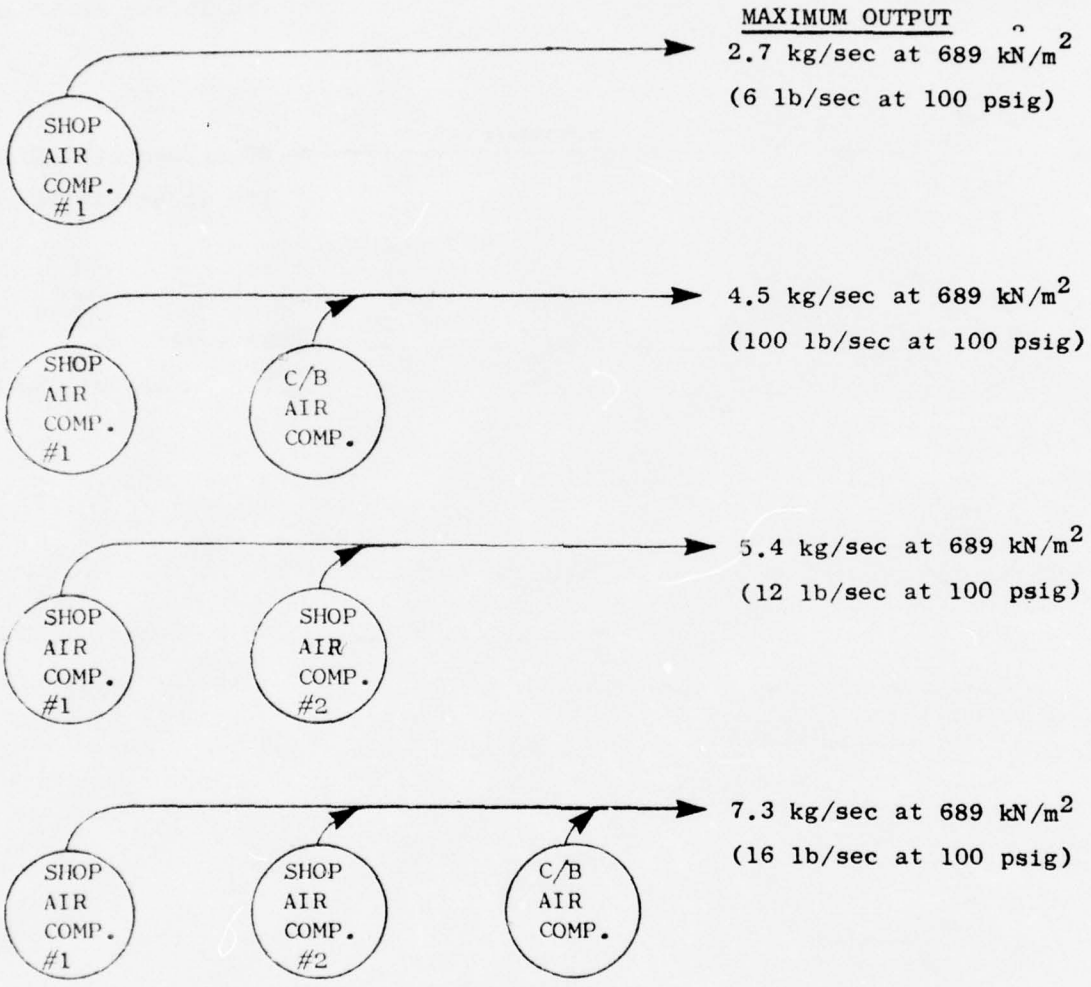

- The Two Shop Air Compressors are Located in Building 401
- The Compressor Boost Supply is in Building 302

Figure 2-17. Shop and Compressor Boost Air Supply System.

Shop air also is available in limited quantities normally ranging from 0.45 to 2.67 kg/sec (1 to 5 lb/sec) from the south boiler house, with the available quantities depending on the demand of other users. The south boiler house has a total of nine electric motor-driven compressors and three steam driven compressors (see Figure 2-18). All 12 compressors feed into the same supply pipe. The total 12-compressor capacity is 13.8 kg/sec at 689 kN/m^2 (30.4 lb/sec at 100 psig). As this system is used extensively throughout the manufacturing areas, extreme caution is required when using this air source, as accidental dumping of this header could cause serious equipment operational problems throughout the plant.

2.3.2 Air Supply System

The air is supplied to the nozzles by a 40.64-cm (16-inch) pipe from Building 401. A 30.48-cm (12-inch) branch line connects to the 40.64-cm (16-inch) pipe just outside the Cell 41 test cell. This branch line includes a 25.4-cm (10-inch) pressure-reducing valve (PRV-1) which will control to a maximum pressure of 1.0 MN/m^2 (150 psig) with remote setting control operated from the facility control console. Piping in this section is protected against overpressurization by means of a 5.08-cm (2-inch) pressure relief valve to allow for any valve leakage and a 30.48-cm (12-inch) rupture disc rated to rupture at 0.9 to 1.2 MN/m^2 gage (135 to 173 psig). Both shop air sources are connected via a 15.24-cm (6-inch) branch line tied in downstream of PRV-1. To prevent backflow through the shop air system during Building 401 air operation, a line-sized check valve is installed in the 15.24-cm (6-inch) supply line.

The flow then is split into a primary and secondary stream, providing air supply to the test model core and fan ducts, respectively. The primary stream is supplied through a 30.48-cm (12-inch) supply line with downstream pressure maintained by a remotely operated 15.24-cm (6-inch) V-ball control valve (PCV-1) with shutoff capability. The secondary stream uses a 40.64-cm (16-inch) supply line with control provided by a 25.4-cm (10-inch) V-ball control valve (PCV-2). These valves are used to set desired test points and are controlled remotely from the control console.

Airflow measurements are determined on both primary and secondary streams using line-size orifice plates. Three sizes of orifice plates are available for each stream corresponding to beta ratios of 0.4, 0.6, and 0.8 for the primary stream and beta ratios of 0.4, 0.5, and 0.6 on the secondary stream where beta ratio is defined as the ratio of orifice hole size to the internal pipe diameter. Table 2-II shows the approximate operational airflow range based on sensitivity of the control system at the low flow to choking at the high flow. The flow system was designed for a maximum 27 kg/sec (57 lb/sec) capacity.

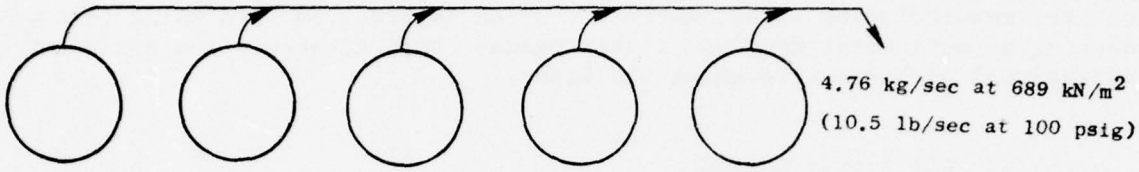

Five 0.952-kg/sec (2.1-lb/sec) Electric Motor Driven Compressors (Building 417) Normal Plant Air Supply

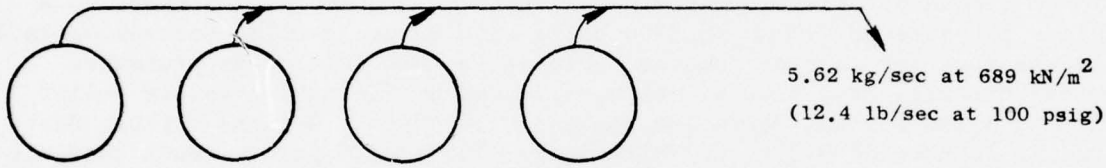

Four 1.405-kg/sec (3.1-lb/sec) Electric Motor Driven Compressors (Building 421) Used to Supplement the Normal Plant Air Supply

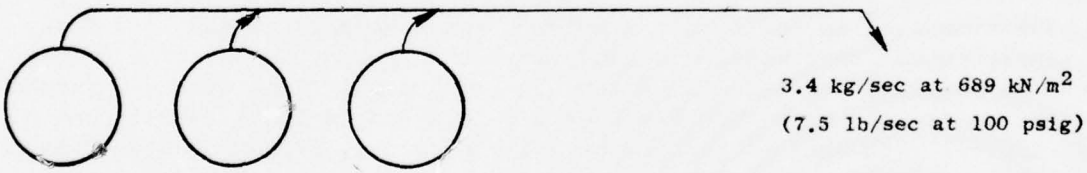

Three 1.133-kg/sec (2.5-lb/sec) Steam Driven Compressors (Building 421) Normally Not Operated, are Available on Request

Figure 2-18. South Boiler House Air Capability.

Table 2-II. Airflow Orifice Plates Operation Range.

$P_{upstream}$ = 5.27 kg/cm^2 (75 psi); ΔP = 0.007 kg/cm^2 (0.1 psi)

		Hole Diameter		Approximate Weight Flow Range	
	β	cm	(in.)	kg/sec	(lb/sec)
Primary Flow	0.4	12.192	(4.8)	0.5 to 10.9	(1 to 23)
30.48-cm (12-inch) Diameter Pipe	0.6	18.29	(7.2)	1.7 to 28.4	(3.6 to 60)
	0.8	23.04	(9.6)	Above 38	(Above 8)
Secondary Flow	0.4	14.61	(6.1)	1.2 to 19.9	(2.5 to 42)
40.64-cm (16-inch) Diameter Pipe	0.5	18.29	(7.625)	Above 1.9	(Above 4)
	0.6	23.1	(9.15)	Above 3.1	(Above 6.5)

- Accuracy within 10%

Both the primary and secondary stream piping, as well as the burners and coannular plenum sections, are protected against overpressurization by rupture discs (RD-2 and RD-3), located downstream of the orifice plates, rated to rupture between 517 to 655 kN/m^2 gage pressure (75 to 95 psig). A schematic of this system is shown on Figure 2-19.

2.3.3 Burner Systems

Three independent burners were designed for use in the facility, but only two at a time can be operated simultaneously. These are:

No. 1 Afterburner - for turbojet configuration only

No. 2 Core or Primary Burner - for turbofan configuration

No. 3 Fan or Secondary Burner - for turbofan or turbojet configurations

All burners and their fuel supply systems were designed to operate on either JP-4 or natural gas; however, due to the questionable availability of natural gas, the JP-4 system has become the prime operating mode for all burner systems. The general positioning of these burner systems within the facility are illustrated schematically on Figure 2-20.

All burners are equipped with a high-flow and low-flow fuel dispersion system with their use dictated by the required temperature rise and airflow rates.

Burners Nos. 2 and 3 are located upstream of the plenum/silencer section and are used for the dual-flow turbofan and duct-burning applications. Both burners utilize a combustor can and spray nozzle arrangement and are capable of providing output temperatures of approximately 1111 K (2000° R) over a wide range of flow conditions.

For simulation of a turbojet with afterburner (A/B) operation, burners Nos. 1 and 3 are employed. Burner No. 1 is located downstream of the plenum/silencer at a position approximately 2.44 meters (8 ft) upstream of the nozzle discharge plane. This burner consists of a pilot burner, V-gutter, and spraybar arrangement. During operation, a temperature rise of up to 538° C (1000° F) is taken across Burner No. 3 and the remaining rise taken up on the A/B unit using the spraybars and/or pilot burner, depending on the required temperature rise and airflow rate.

Ignition of all burners is achieved through the use of a hydrogen torch igniter. For this system, gaseous hydrogen is ignited by a spark discharge and, in turn, ignites the JP-4/air mixture.

Burner discharge temperature is set by controlling the fuel pressure to the high- and low-fuel-flow nozzles of each burner individually.

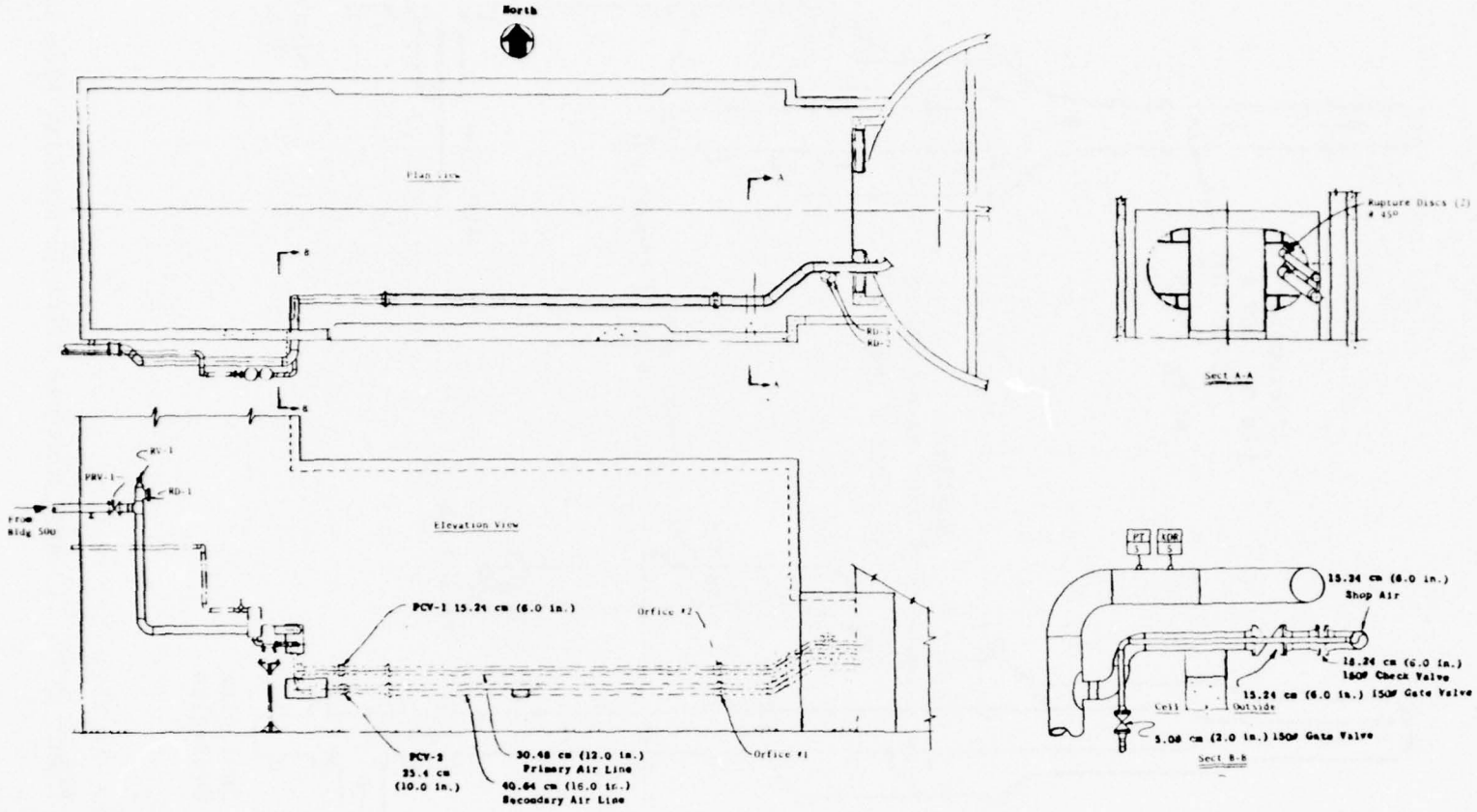

Figure 2-19. General Electric Anechoic Facility Air Supply Piping.

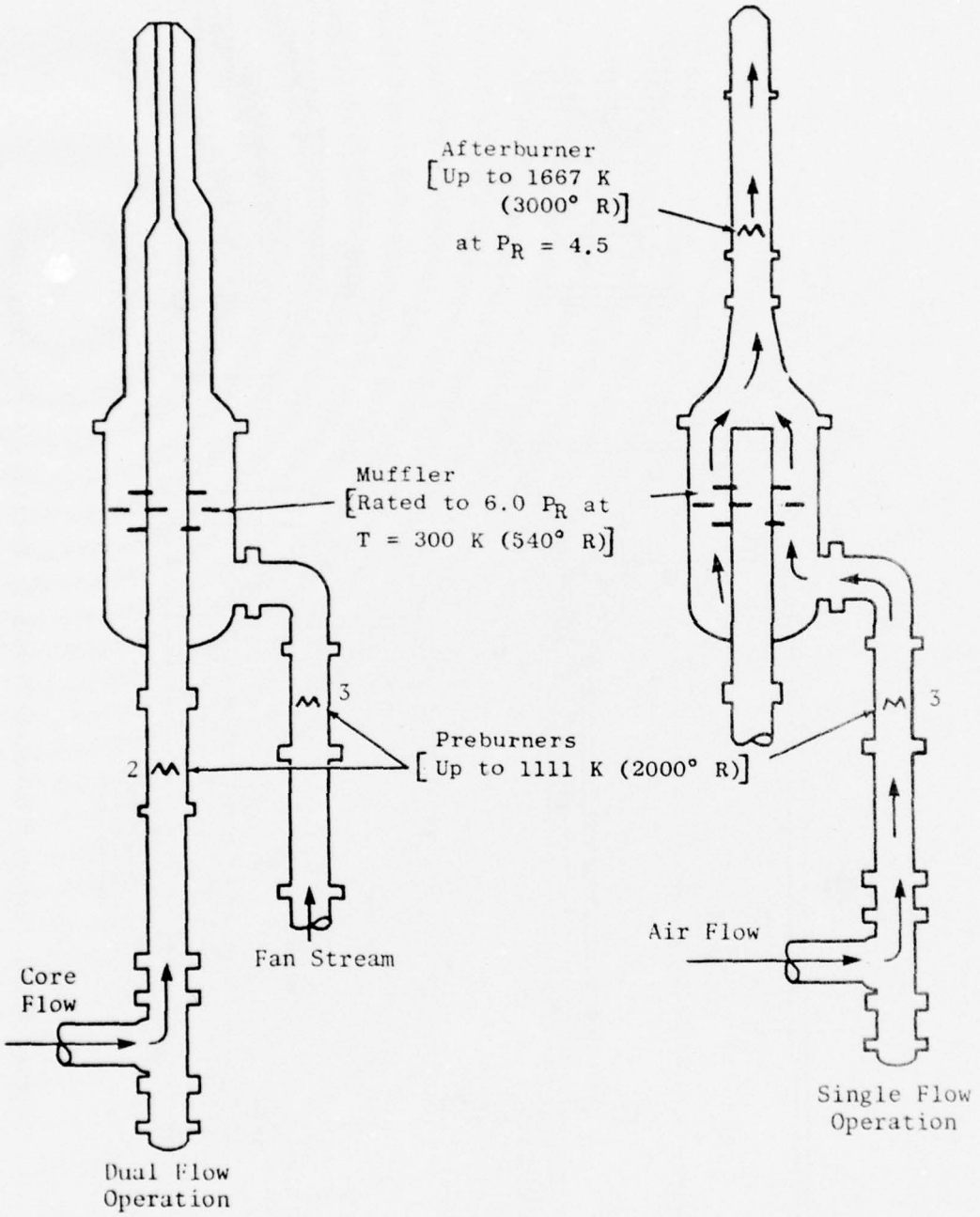

Figure 2-20. General Electric Anechoic Facility Flow System.

Numerous safety interlocks and trip-outs have been built into these burner systems to protect against improper fire-up sequencing, flameouts, and overtemperature conditions.

2.3.4 Plenum/Silencer System

The primary and secondary streams pass through a coannular plenum which includes acoustically treated walls and internal baffles, as shown on Figure 2-20. This device was designed for suppression of flow noise resulting from valves, orifices, etc., which is radiated through the flow system, as well as for suppression of burner noise from the primary and secondary stream burners.

This system was designed for operation with gas stream temperatures up to 1111 K (2000° R) on either stream at an operating pressure of 517 kN/m^2 (75 psig). Those surfaces which are subjected to the 1111 K (2000° R) temperatures are constructed of Hastelloy material, while the plenum shell is thermally insulated from the gas streams and designed for lower operating temperatures.

Support of the plenum chamber from the structural members of the roof of the auxiliary room establishes the anchor plane in regard to thermal growth. Expansion of the plenum chamber, burners, and piping is accommodated by balanced tees located at the lower entry point of the primary and secondary piping to the plenum chamber. Support of the secondary burner, insulated elbow, and secondary air riser piping by a spring hanger support at the centerline minimizes the eccentric loading resulting from differential growths in the plenum chamber between the anchor plane and the entry of the secondary air piping.

During testing of dual-flow configurations, all hardware downstream of the coannular plenum is constructed of Hastelloy X material and is designed for the 1111 K (2000° R) gas temperatures. For the turbojet with afterburner configurations, the ducting between the coannular plenum and the afterburner is constructed of stainless steel with approximately 833 K (1500° R) capability. The flame tunnel sections downstream of the afterburner are water-cooled in order to withstand the operating temperatures to 1667 K (3000° R).

2.3.5 Automatic Temperature and Pressure Control Systems

An automatic control system provides closed-loop setting of key parameters in the anechoic chamber air supply system. These key parameters are the primary and secondary stream temperatures and pressures. This automatic control system is designed to maintain the stable temperature and pressure output required without drifting off the desired test conditions while test data are being obtained. A block diagram of this system is shown on Figure 2-21. The pressure reducing valve (PRV-1) sets and regulates the pressure upstream of the main pressure control valves by sensing the upstream pressure upstream. The main pressure control valves (PCV-1 and PCV-2) are used

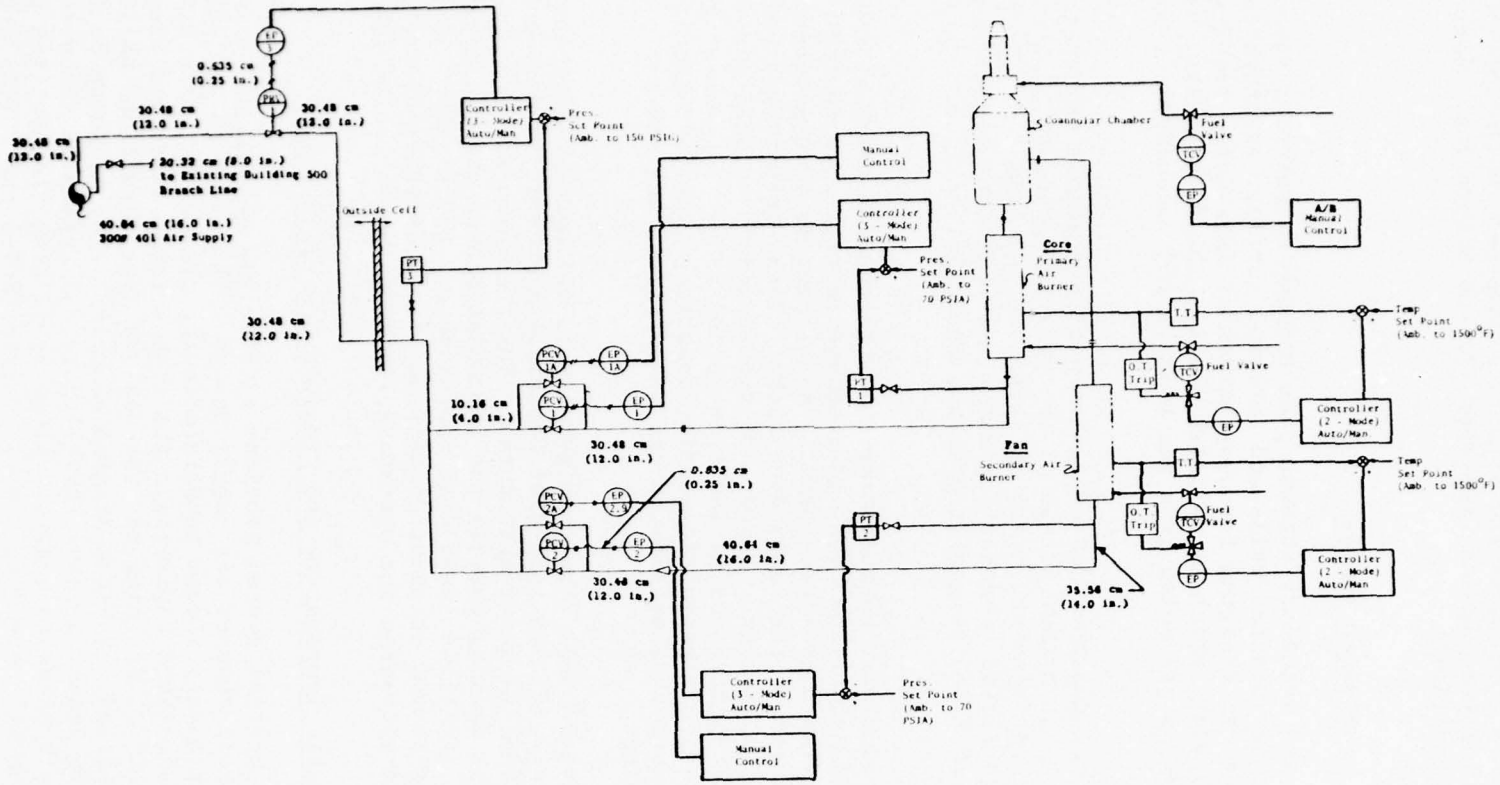

Figure 2-21. General Electric Anechoic Facility Control System Schematic.

to control the flow rate and split between the primary and secondary streams and to maintain the set pressure by sensing pressure upstream of the primary and secondary burner sections.

Temperature is set by controlling fuel flow to both the primary and secondary stream burners using a closed-loop control system sensing burner discharge temperature. Overtemperature protection is provided on both primary and secondary burners, automatically shutting off the fuel when prescribed limits are exceeded.

2.3.6 Domestic Water System

Domestic water supply is available in the test chamber at approximately 414 kN/m^2 (60 psi) pressure from a 10.16 cm (4 in.) supply line to water cool necessary hardware and instrumentation.

2.3.7 Facility Operating Domain

The design intent of this facility was to provide the capabilities to test over a wide range of temperatures and pressures that would be representative of existing and future engine exhaust systems. It has the capability for performing parametric variations of temperature and pressure including high temperature/low pressure and low temperature/high pressure conditions of both the fan and core streams, respectively, within the facility design operating envelope.

The design operating envelope is based on the nozzle pressure ratio capability of 6:1 with cold flow and a maximum pressure ratio of 4.5 at the temperature limits of 1667 K (3000° R) in the turbojet/afterburner mode and 977 K (1760° R) on either stream in the dual-flow mode. Single-flow testing without the afterburner can be conducted with either the fan or the core piping. The fan has the advantage of a higher available air flow rate, while the core can be set to a slightly higher temperature.

The air supply system has the capability of delivering up to 45.4 kg/sec (100 lb/sec) of air at a back pressure of 2.1 MN/m^2 (300 psi). Figure 2-22 shows this limit as a function of the air supply pressure and the valve exit pressure for both the fan and the core valves. Airflow at a given valve exit pressure can only be obtained at values below the indicated lines for a given supply pressure. Another limit on airflow is that value which will exceed a Mach number of 0.3 at the nozzle entrance flange where the aero instrumentation is located. These limitations in terms of nozzle pressure ratio and total temperature are shown for the core and fan in Figure 2-23. With a limiting Mach number of 0.3 at the nozzle entrance, nozzles up to 10.67 cm (4.2 in.) in diameter with the core alone, 17.55 cm (6.91 in.) with the fan alone, and 20.54 cm (8.09 in.) with the fan and core combined can be accommodated without acoustic considerations. Acoustically, studies of the proximity of the microphones to the near-field noise levels, discussed

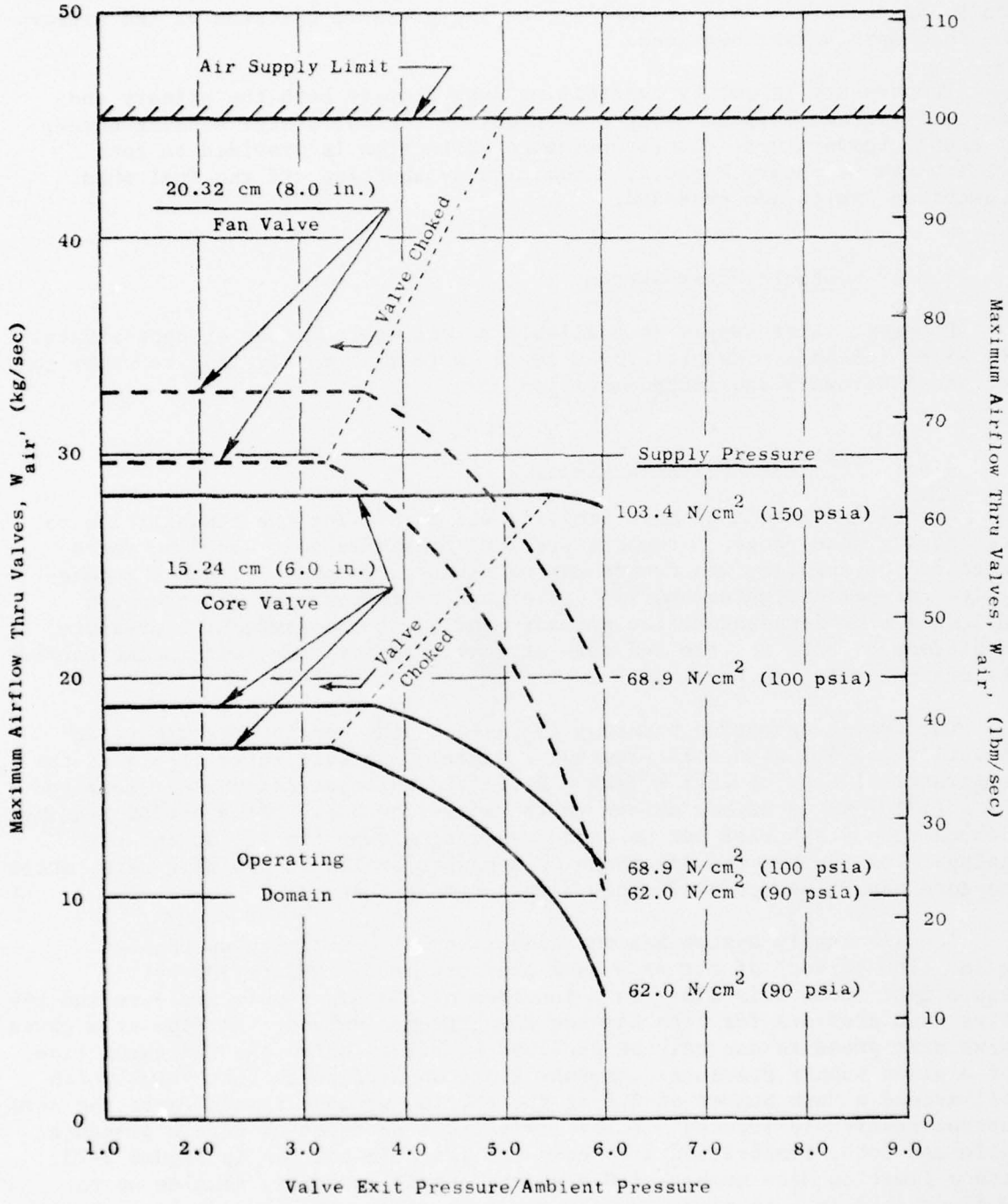

Figure 2-22. Airflow Limits through the Air Control Valves with Combustors Removed.

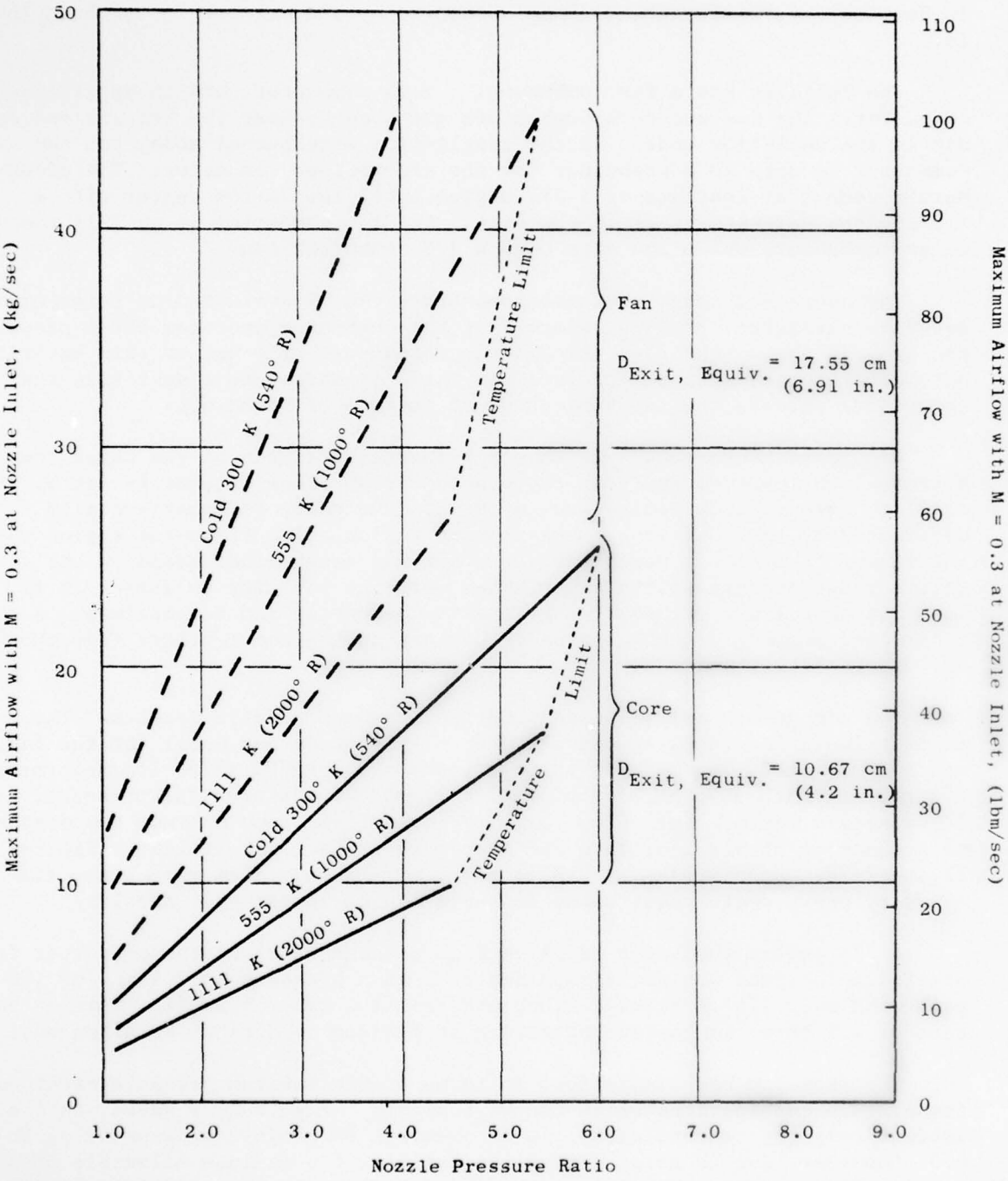

Figure 2-23. Airflow Limits to Restrict the Mach Number at the Test Nozzle Entrance to M < 0.3.

in Section 3.4, limits the maximum effective nozzle diameter to 15.8 cm (6.23 in.).

The facility has a fan combustor, a core combustor, and an afterburner combustor. The fan and core combustors are used to heat the fan air and core air in the dual-flow mode. In the single-flow afterburner mode, the fan combustor is used as a preburner for the afterburner combustor. The afterburner combustor consists of a J97 engine swirl cup in the center with a flameholder surrounding it in the duct; the fan combustor is an X211 coannular combustor, while the core uses a J73 combustor can.

The operating range of these combustors can be evaluated in terms of a severity parameter, $P^2/\dot{W}_{Air}$, where P is the combustor upstream total pressure and $\dot{W}_{Air}$ is the weight flow through the combustor. The use of this severity parameter plotted against the fuel air ratio (temperature rise across the combustor) permits the identification of regions of flame out.

Figures 2-24 through 2-26 show the operating domain of the three combustors. The maximum fuel-air ratio boundary on these figures is set by the facility temperatures limits, while the minimum value is experimentally determined by the lean-fuel flame-blowout region. The flame-out region where the values of severity parameter are small was established based on the entire range of data points experienced with the facility to date. It is possible that lower values of the severity parameter can be obtained. A controlled mapping of this region is planned during the tertiary flow checkout of the facility.

The combustors are supplied with fuel through simplex nozzles. The maximum fuel flow rates are 657.7 kg/hr (1450 pounds per hour) for the fan, 453.6 kg/hr (1000 lbm/hr) for the core, and 798.3 kg/hr (1760 lbm/hr) for the afterburner with 3.45 MN/m^2 (500 psi) fuel nozzle differential pressure. These nozzle maximum fuel flow rates are translated into maximum temperatures as a function of air flow rate and presented as facility limits in Figures 2-27 and 2-28. Acquisition of a data point with an air flow rate above the boundary curve would require the installation of larger fuel nozzles.

A J79 engine fuel pump supplies high pressure fuel to the combustor fuel nozzles. The pump nominally supplies fuel at a pressure of 3.45 MN/m^2 (500 psi) with over 7257.5 kg/hr (16,000 lbm/hr) flow rate. This flow rate exceeds that of all three combustors operating at maximum conditions simultaneously.

The facility has limitations in terms of the maximum pressure ratio and temperature combinations which can be achieved. Figure 2-29 shows, that at ambient temperature conditions, it is possible to achieve a pressure ratio of 6.0. However, due to metal stress limitations, the maximum allowable pressure ratio decreases to 4.5:1 at the maximum temperature conditions for the skin and burner discharge. The maximum allowable skin temperature for the coannular plenum and the fan elbow is 867 K (1560° R). Both the fan and core burner maximum gas stream discharge temperature is 1089 K (1960° R). Both

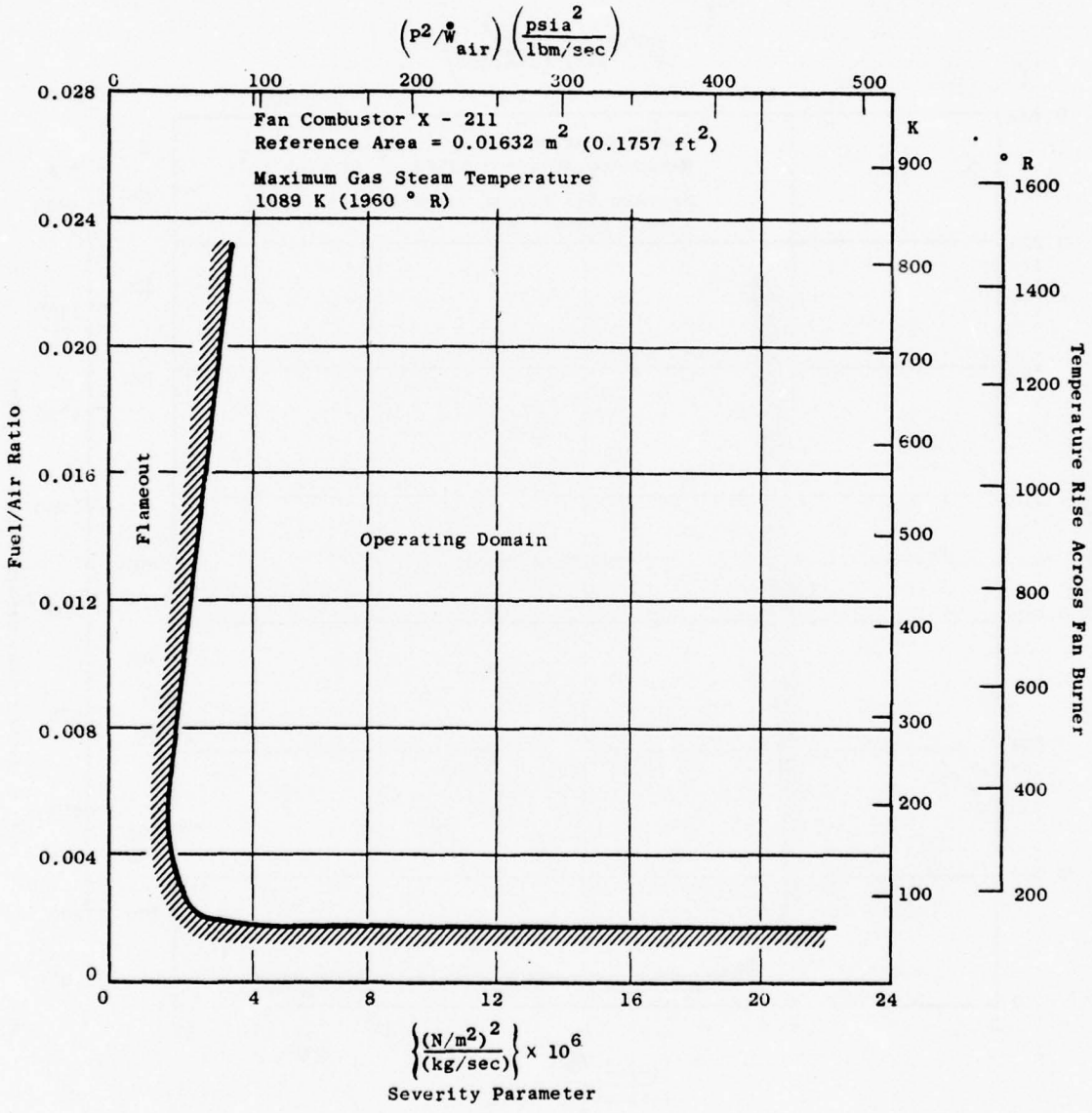

Figure 2-24. Fan Combustor Operating Domain.

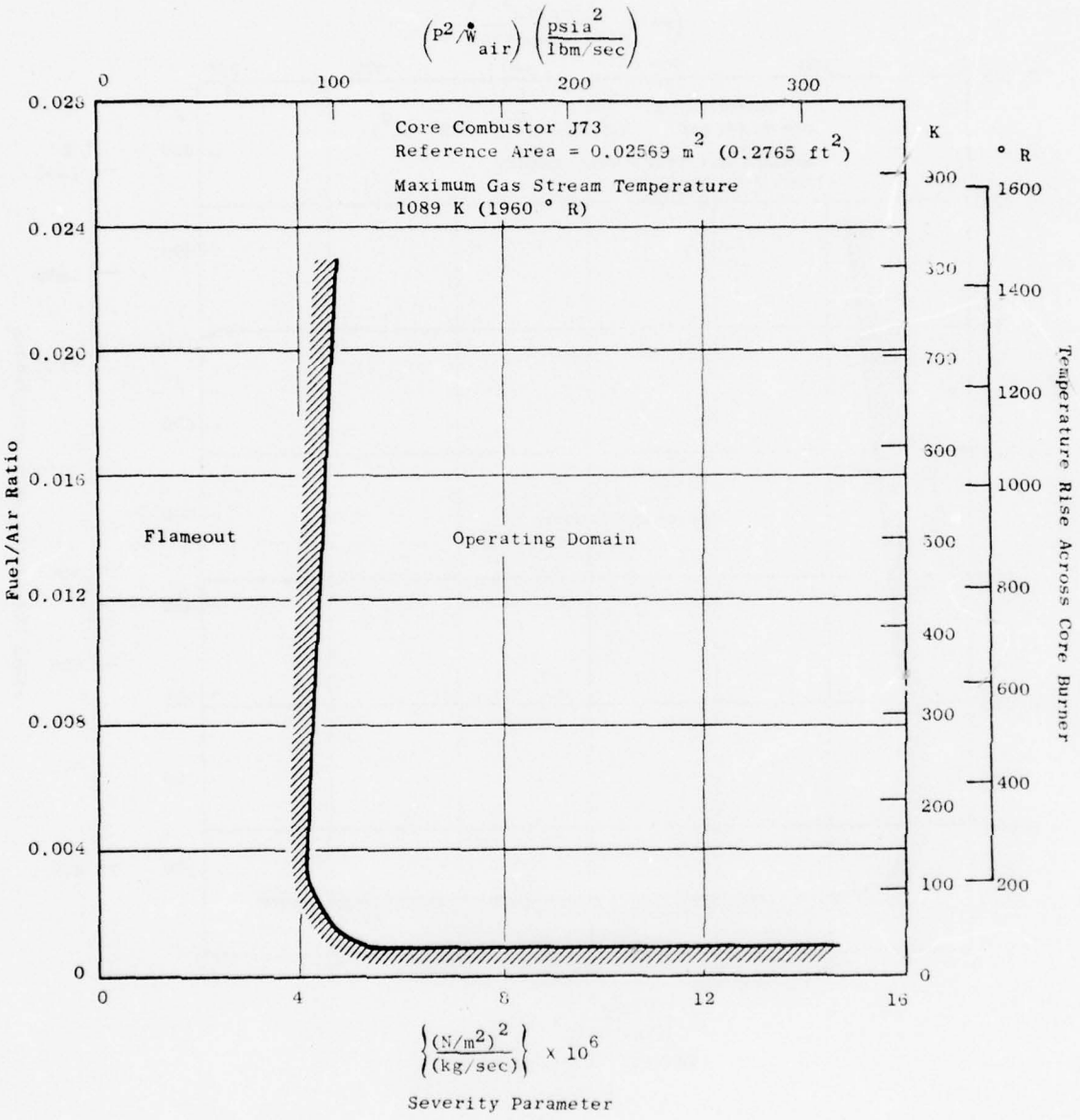

Figure 2-25. Core Combustor Operating Domain.

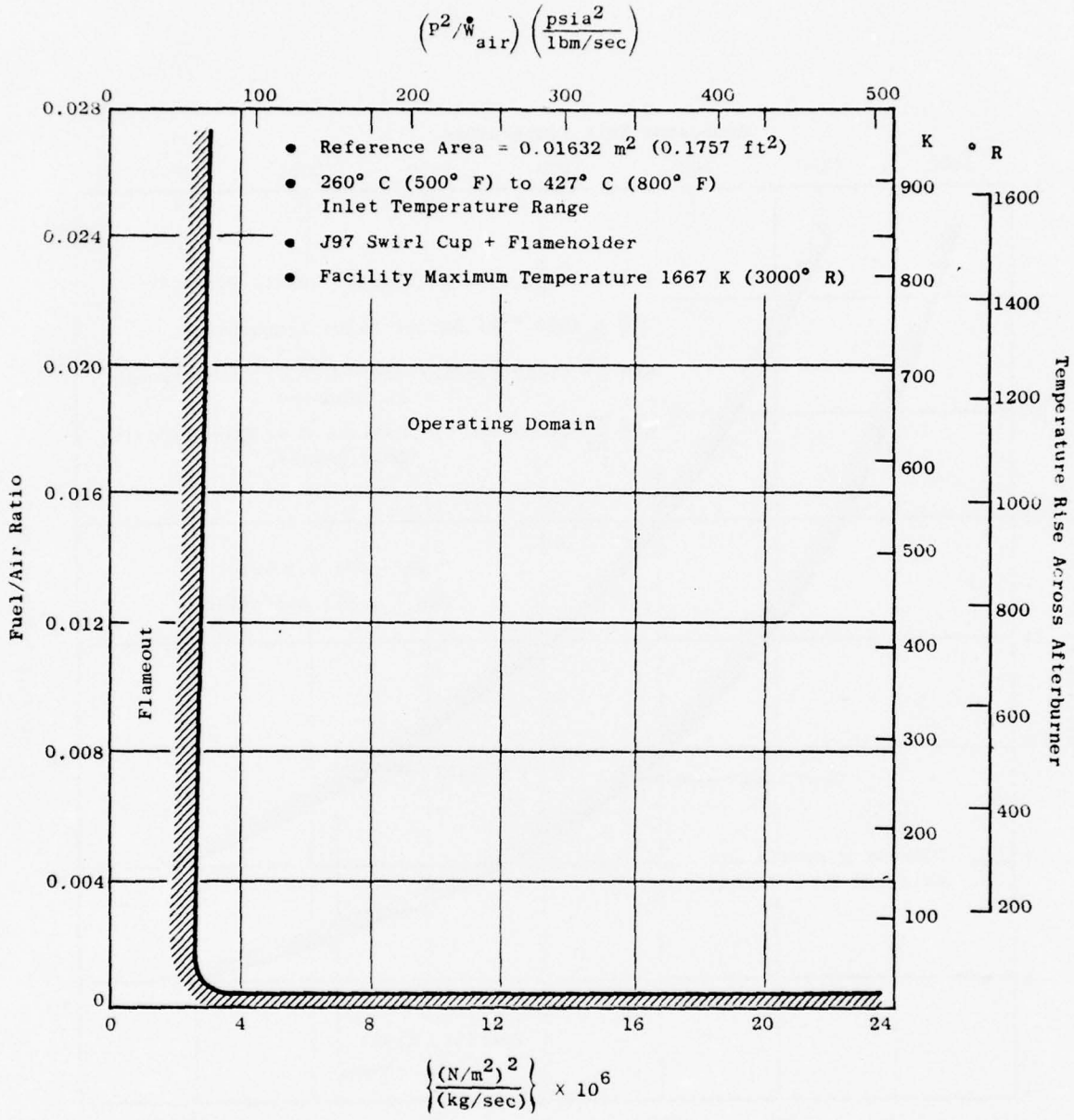

Figure 2-26. Afterburner Combustor Operating Domain.

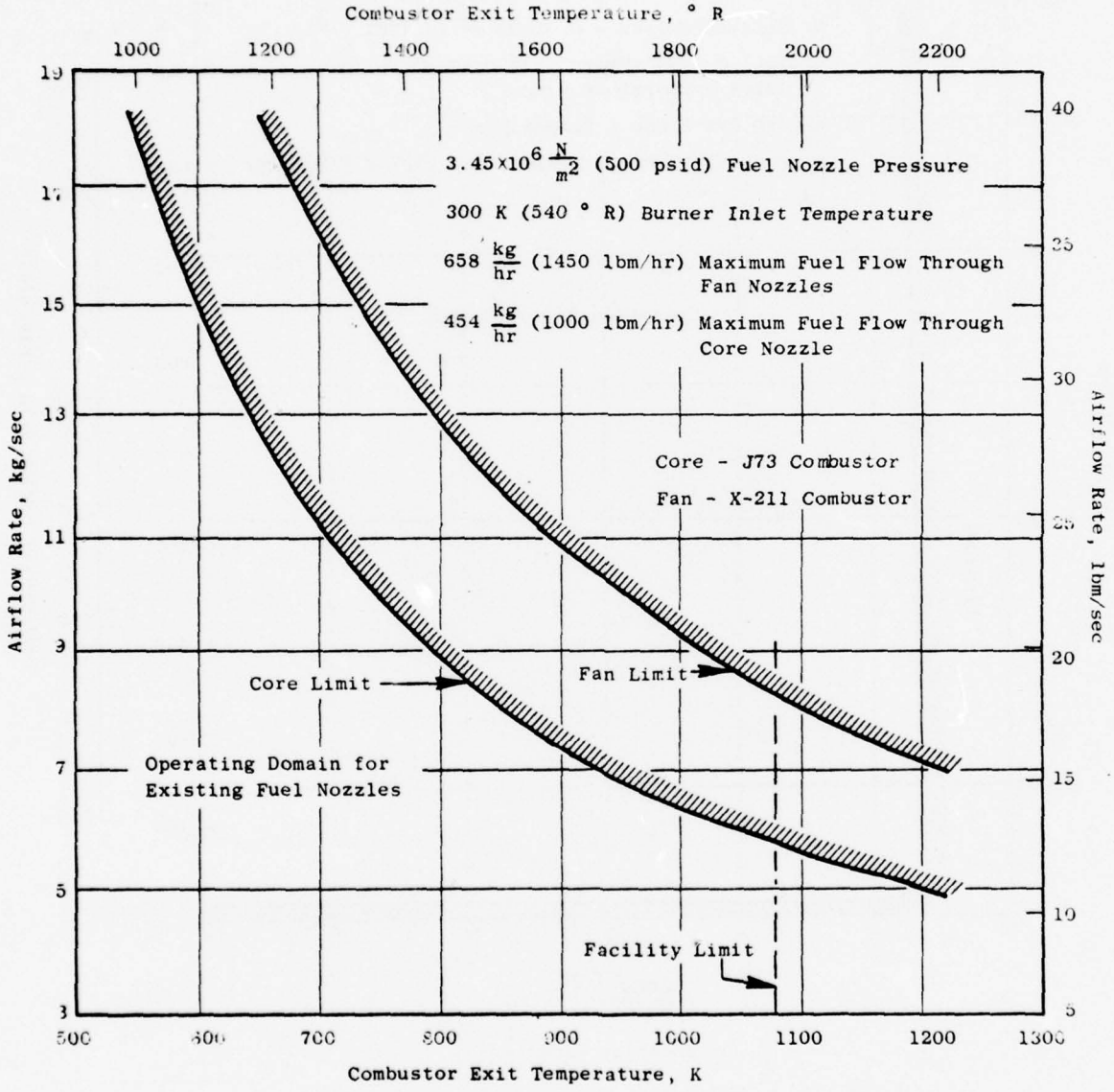

Figure 2-27. Effect of Fuel Nozzles Maximum Fuel Flow on Fan and Core Combustors.

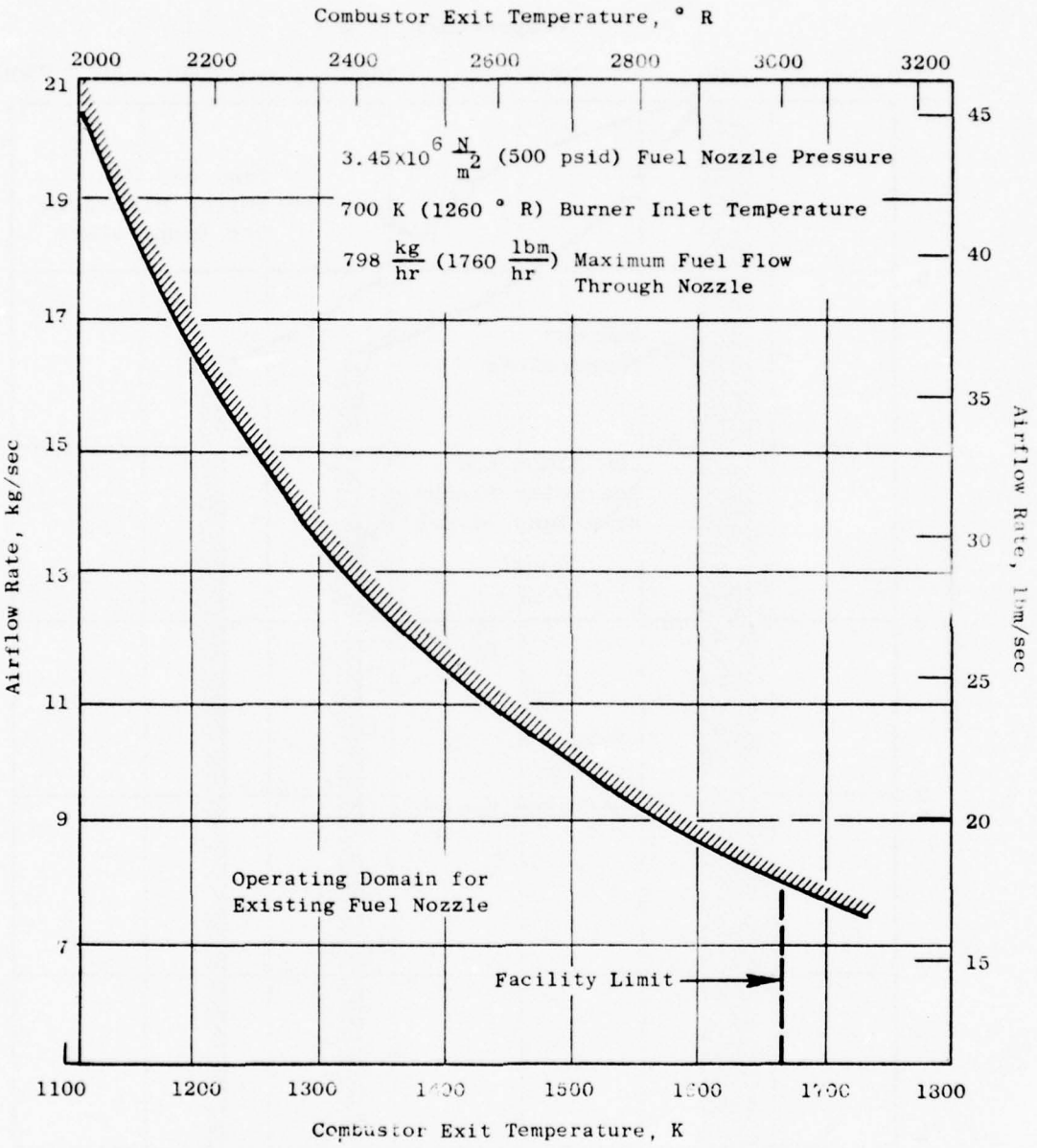

Figure 2-28. Effect of Fuel Nozzle Maximum Fuel Flow on Afterburner Combustor.

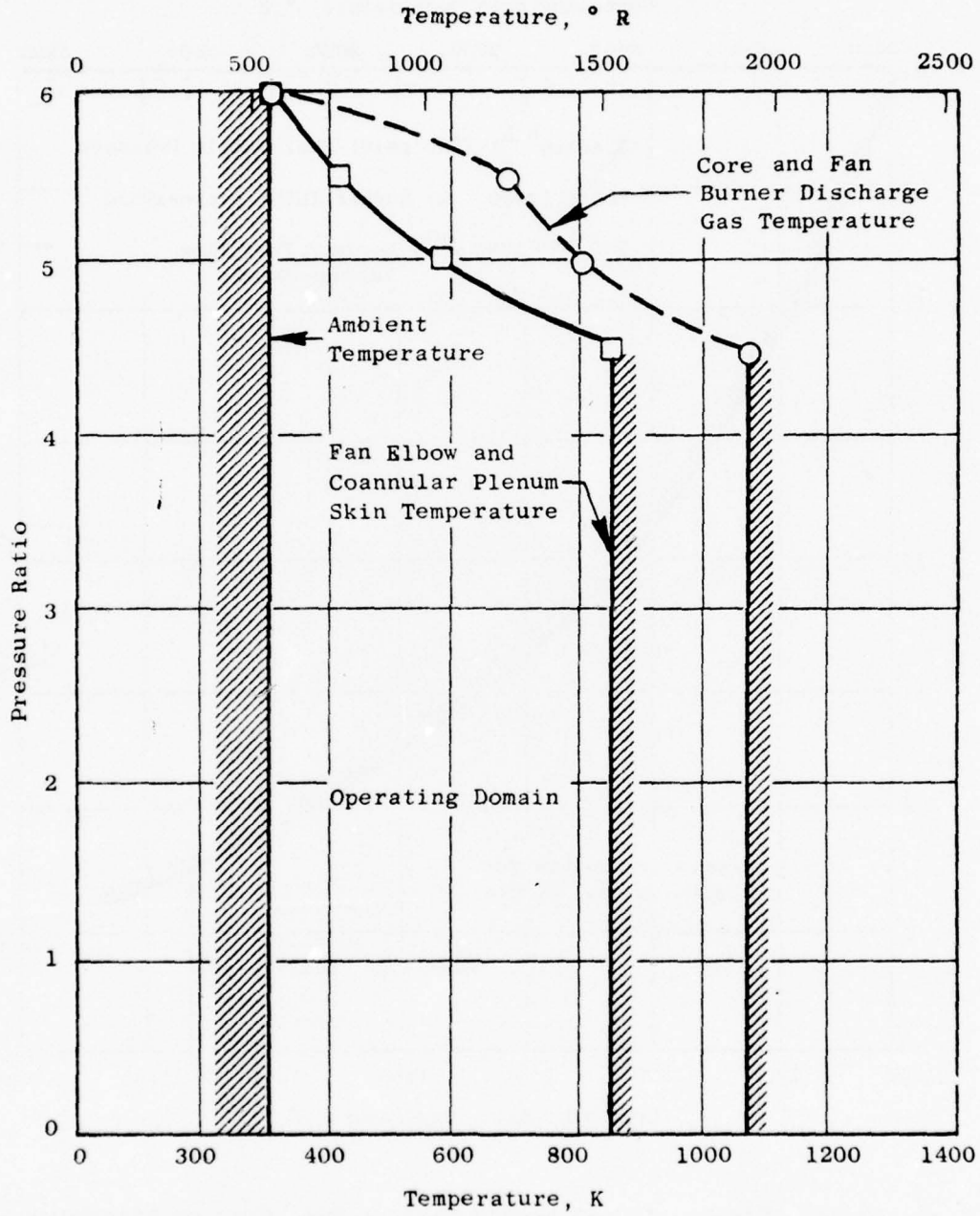

Figure 2-29. Effect of Pressure on Facility Temperature Limits.

the outer skin temperature and the inside gas temperature limits are established to maintain acceptable stress across the heated hardware. For the dual-flow mode these four critical temperatures were related to the fan and core nozzle gas stream total temperatures. Figure 2-30 shows that the plenum skin temperature is at its limit when the fan nozzle exhaust temperature reaches 975 K (1760° R). This plenum skin temperature was the limiting temperature for the test points to date. The fan elbow skin temperature limit shown in Figure 2-31 does not present a problem in attaining exhaust temperatures of 1089 K (1960° R). Inherent heat loss between the combustor and the nozzle, however, limit the maximum fan nozzle exit temperature to 925 K (1760° R) (see Figure 2-32). This condition will not change with the addition of tertiary flow. In the core, the nozzle exit temperature was within 10% of the core combustor discharge temperature (see Figure 2-33). This means that in some cases the core nozzle exhaust temperature may be limited to 975 K (1760° R); therefore, within the limits of the facility, the maximum temperature that either the fan or core nozzle exit can be set to is 975 K (1760° R).

The afterburner hardware consists of a stainless steel transition pipe from the plenum to the afterburner which has a skin temperature limit of 867 K (1560° R). This piping is not insulated; thus, the inlet gas temperatures to the afterburner from the fan preburner are also limited to 867 K (1560° R). Higher pressure ratios at temperatures below 867 K (1560° R) can be achieved by operating the fan burner only as shown in Figure 2-34 up to a pressure ratio of 6.0 (with cold flow). The water-cooled afterburner jacket is designed to withstand 1667 K (3000° R) at a pressure ratio of 4.5. High pressures at temperatures between 867 K (1560° R) and 1667 K (3000° R) are not achievable because of the minor effect of reduced temperature on the heat transfer drop across the water coils.

2.4 AERO DATA SYSTEM

During facility operation, there are two main classifications of aerodynamic data: (1) facility operating parameters used for safety monitoring and setting test point conditions, and (2) nozzle performance data used for determination of nozzle operating characteristics such as weight flow, Mach number, velocity, etc. A system schematic is shown on Figure 2-35.

2.4.1 Facility Operating Parameters

The facility operating parameters are monitored during testing at the control console to ensure that prescribed facility limits are not exceeded and for setting test point conditions.

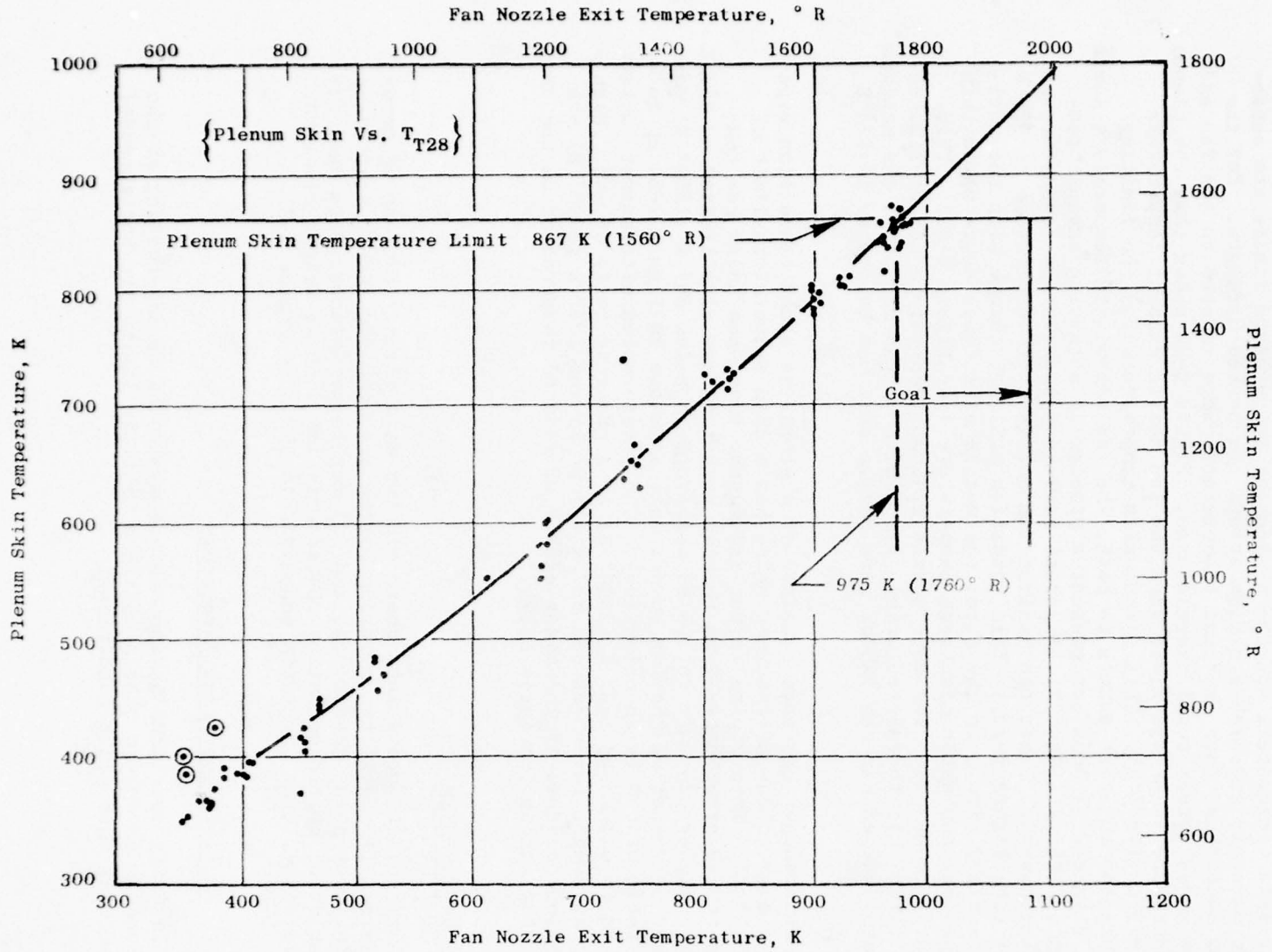

Figure 2-30. Relationship of Coannular Plenum Skin Temperature to Fan Nozzle Exit Temperature, T_{T28}.

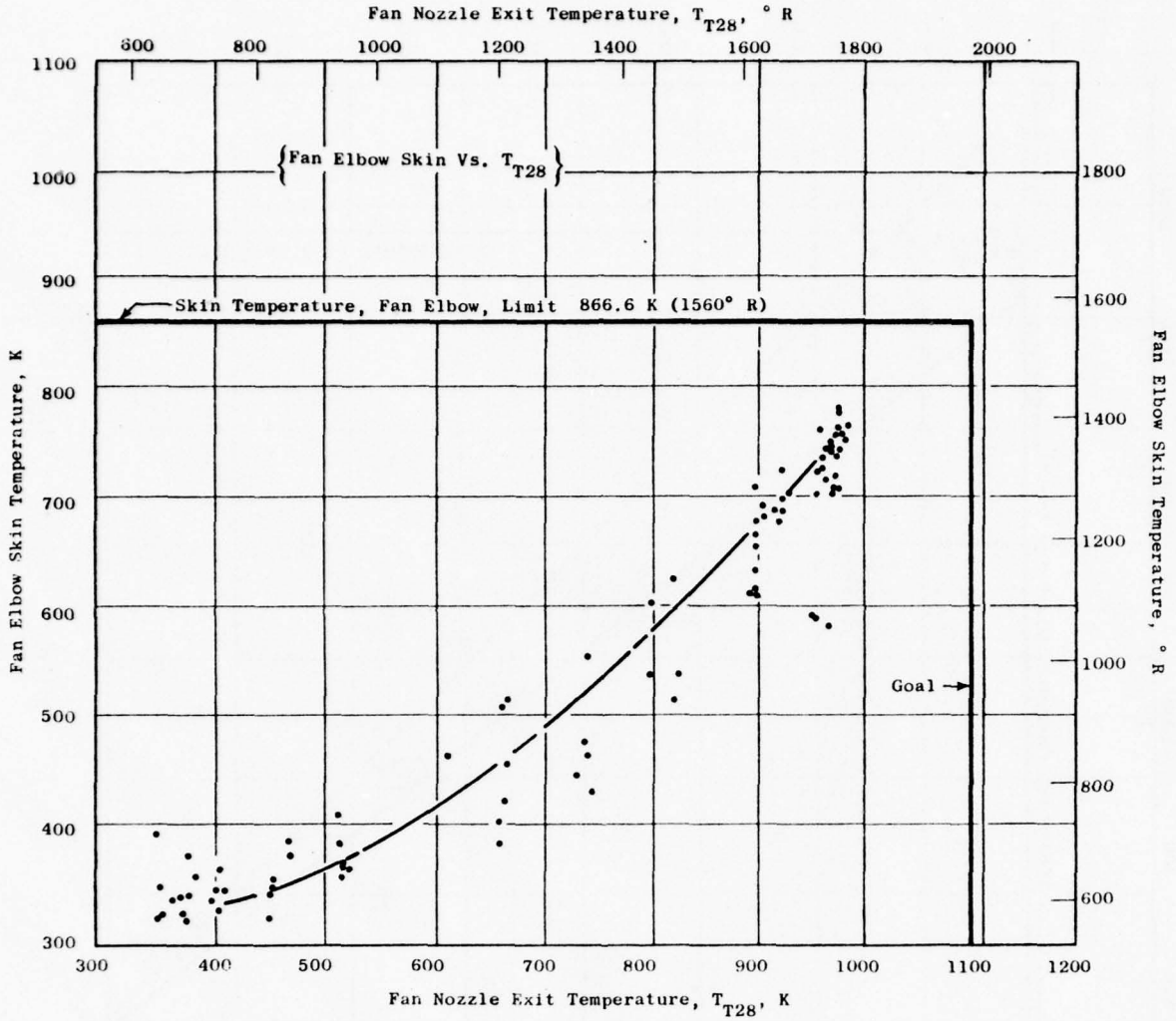

Figure 2-31. Relationship of Fan Elbow Skin Temperature to Fan Nozzle Exit Temperature, T_{T28}.

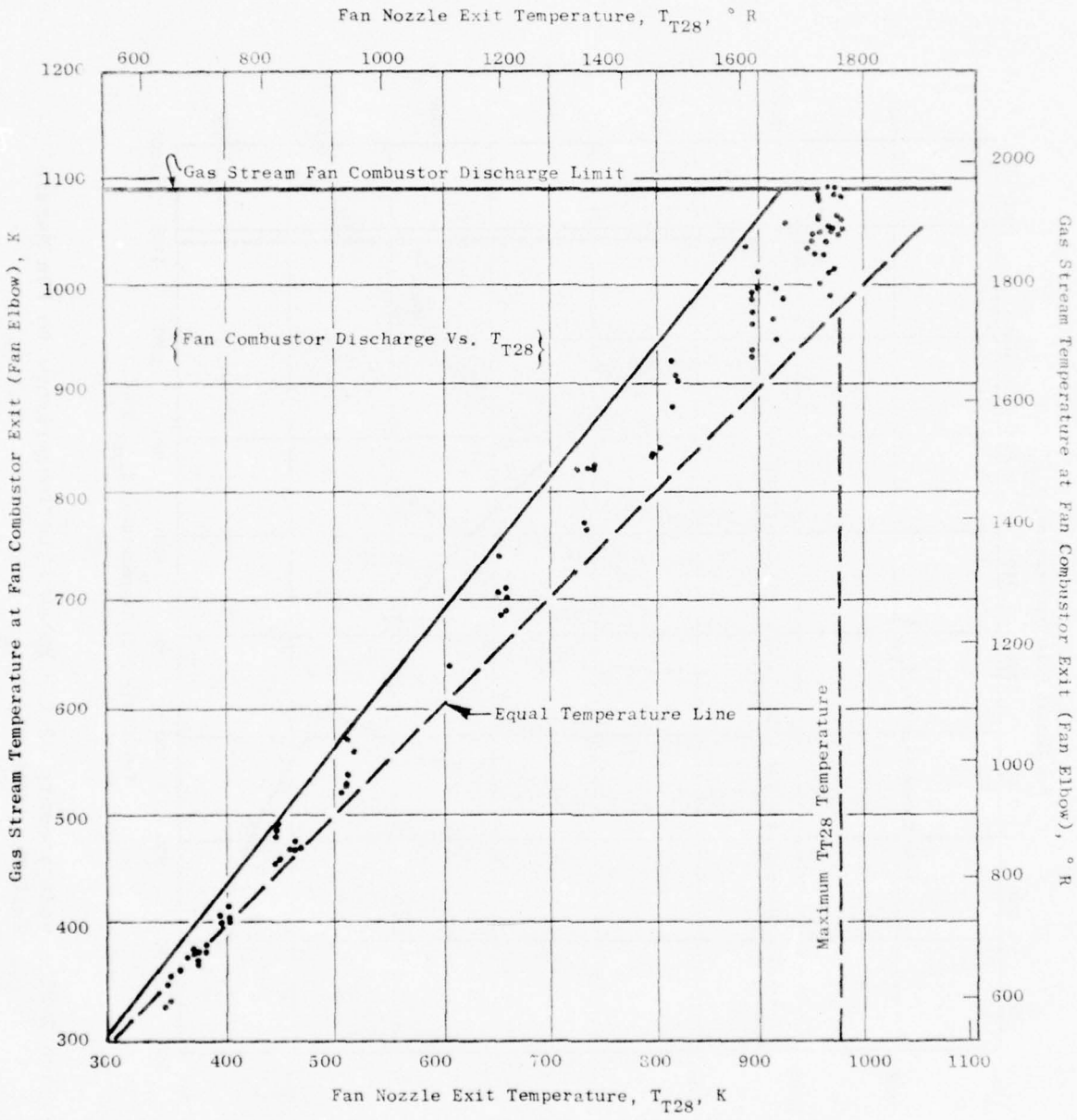

Figure 2-32. Fan Combustor Discharge Temperature Compared to Fan Nozzle Exit Temperature, T_{T28}.

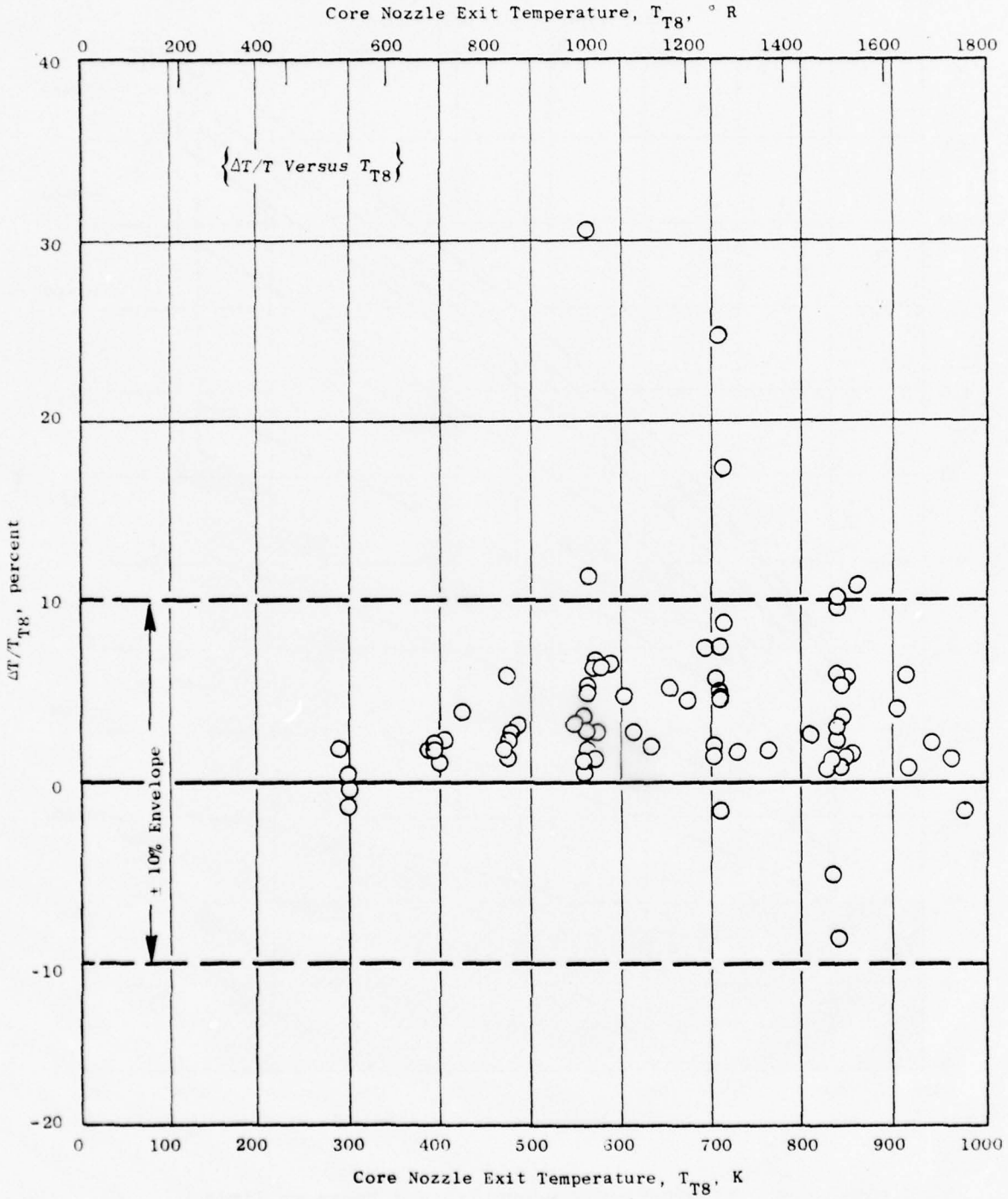

Figure 2-33. Effect of Temperature Drop from Core Combustor Discharge to the Core Nozzle Exit Temperature, T_{T28}.

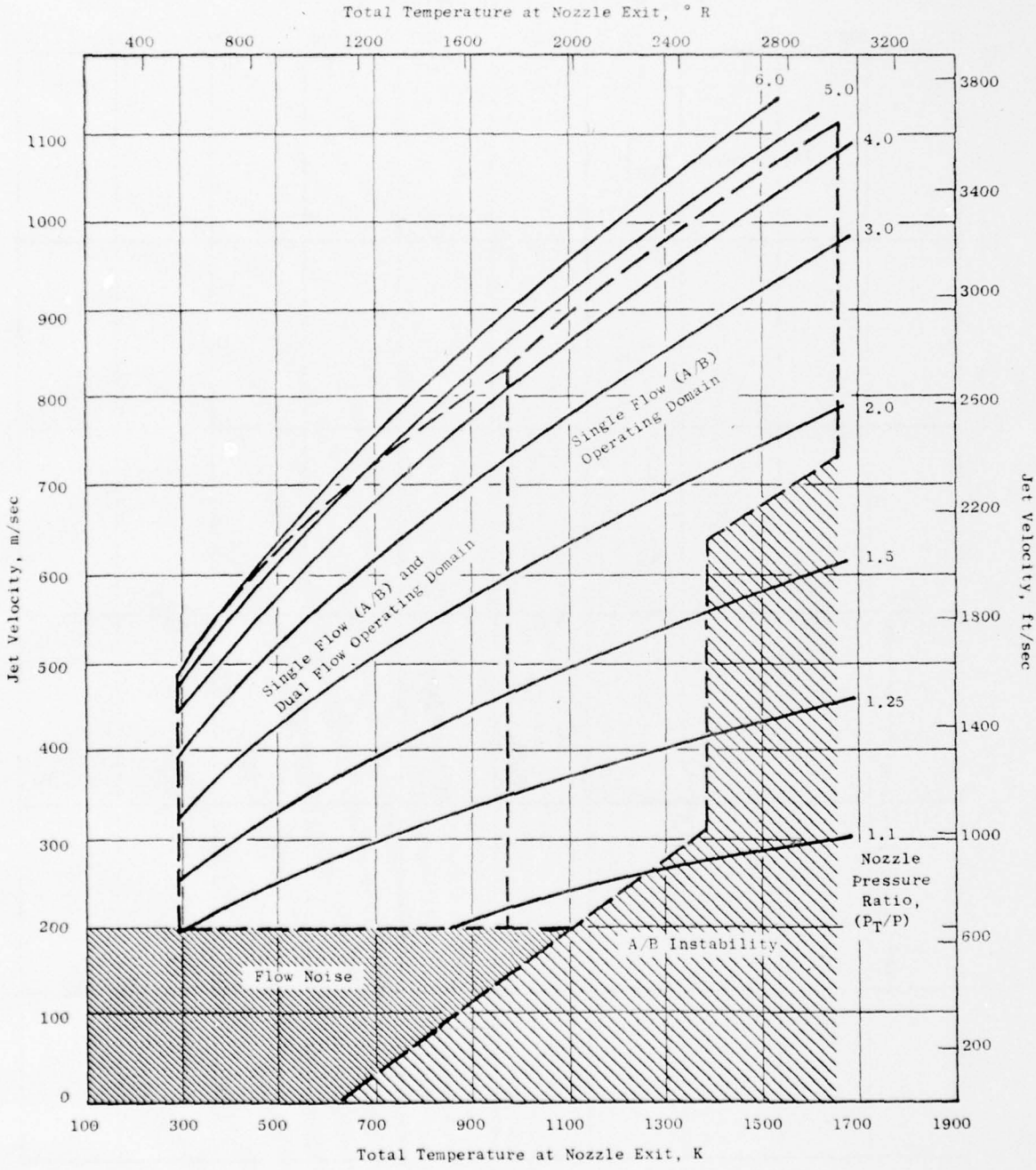

Figure 2-34. Afterburner Temperature and Pressure Limit.

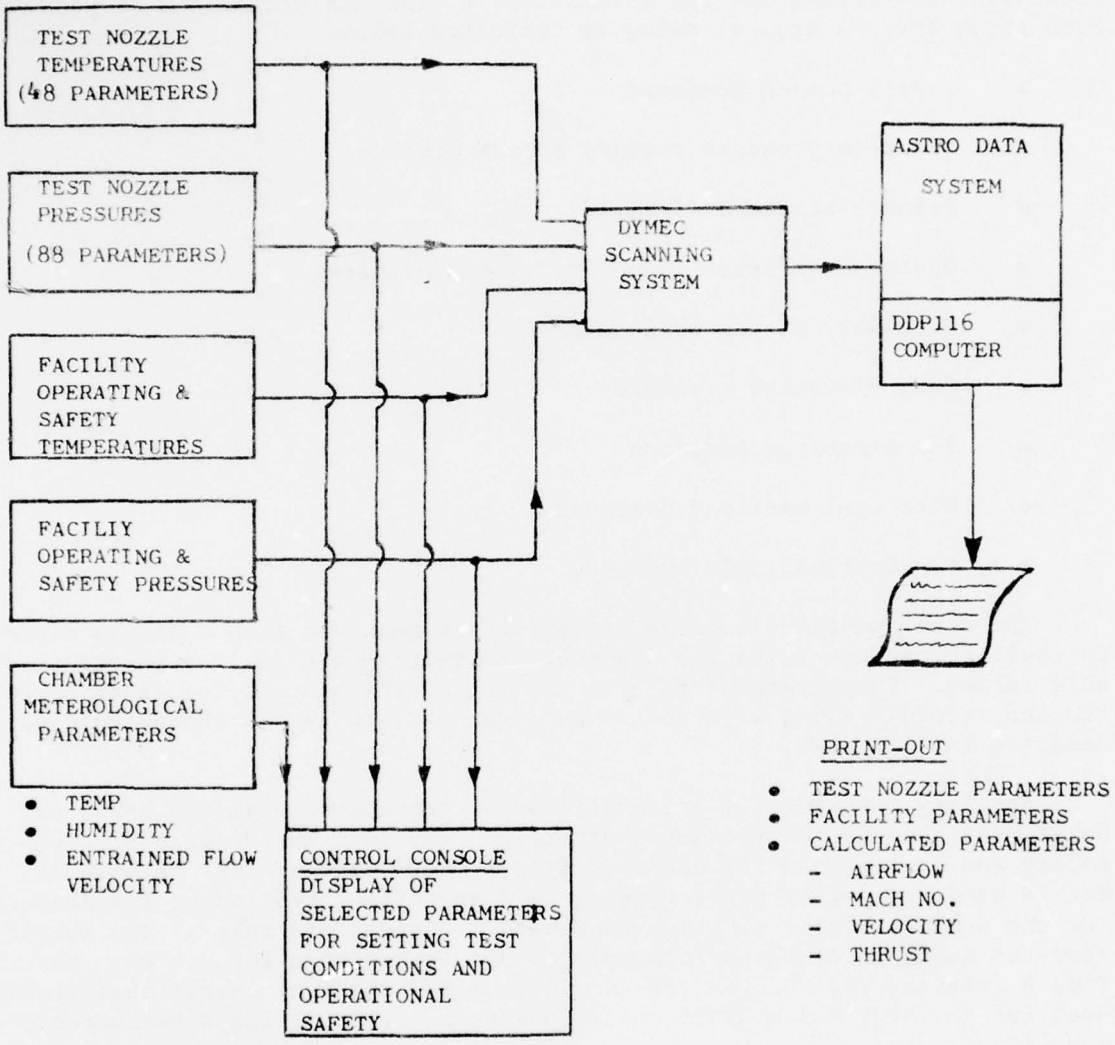

Figure 2-35. General Electric Anechoic Chamber Aerodynamic Data Processing System.

Control console display capability exists for monitoring nine air and fuel pressures during testing activities; a separate transducer is used for each parameter. A typical setup is indicated below.

- Supply header pressure
- Upstream pressure primary stream orifice
- Primary stream orifice ΔP
- Upstream pressure secondary stream orifice
- Secondary stream orifice ΔP
- Core discharge pressure
- Fan discharge pressure
- Core fuel manifold pressure
- Fan fuel manifold pressure

The core and fan discharge pressures are measured from a single element on their respective rakes and are used for setting the desired nozzle pressure ratios. These parameters also are routed through a Dymec scanning system and recorded along with nozzle performance data by the aerodynamic data handling (ADH) system.

Facility temperatures are monitored at the control console using two Doric multichannel temperature indicators. One unit has 24-channel capability and is designed for use with Type K thermocouples (chromel-alumel) and is used for safety monitoring as well as setting test point temperatures for the dual-flow system, which uses Type K temperature rakes. The second read-out unit has 12-channel capability and is designed for use with the Type B (platinum/6% rhodium versus platinum/30% rhodium) thermocouple rakes used for the high temperature conditions encountered during afterburner operation.

2.4.2 Nozzle Pressure and Temperature Measurements

A critical parameter used in evaluating acoustic test results is nozzle exhaust velocity. Determination of this velocity depends on an accurate determination of the exhaust temperature and pressure which, in turn, depend on adequate sampling across the stream to account for profile effects. Special multielement rakes have been designed for use on the single- and dual-flow systems.

The dual-flow system uses four rakes, two on each stream, each having three pressure and three temperature elements with spacing of the elements corresponding to centers of six equal-area annular segments of the flow stream. These rakes use shielded Type K thermocouples (chromel-alumel) and have a recovery factor very close to unity.

The single-flow system uses two water-cooled rakes, with each rake containing three pressure and three temperature elements with spacing of the elements such that a total temperature and a total pressure are measured at six equal-area segments of the flow annulus. Because of the high temperature ranges (1667 K or 3000° R) to which this rake is subjected, shielded Type B (platinum/6% rhodium versus platinum/30% rhodium) thermocouples are used. In order to prevent clogging and aspiration, the temperature elements require purging with shop air during operating periods when aerodynamic data are not being acquired. A vacuum pump is used for this purpose during periods when data are being obtained.

Estimated accuracies for the temperature measurement of both dual- and single-flow rakes are indicated on Figure 2-36. Pressure measurement accuracy is controlled by the accuracy of the transducer used for the measurement. The scanivalve transducers used for nozzle performance measurements are rated at 0.1% of full-scale range. For the chamber certification, 448-kN/m^2 (65-psia) transducers were used in order to accommodate 4.0 pressure-ratio conditions. These tolerances are expressed in terms of velocity error as shown on Figure 2-37.

2.4.3 Aerodynamic Performance Data Acquisition Systems

The Dymec system used for data acquisition in the anechoic chamber is a 200-channel automatic data scanning system controlled remotely by the central digital data system in the Instrument Data Room (IDR).

The present Dymec system can be configured with up to eight pressure scanners, each having 12 pressure ports. However, one port on each transducer is vented to atmospheric pressure as a zero reference, reducing the number of useable pressure-measuring channels to 88. Different ranges and types of transducers are available for either absolute, relative, or differential pressure measurements as necessary for meeting test objectives. The transducers are calibrated periodically and certified by the Calibration Laboratory. Calibration factors determined over the transducer operating range are incorporated into the data system to account for any nonlinearity in the transducer.

The chromel-alumel (CA) thermocouple (Type K) temperature inputs to the Dymec system are accomplished using a mini-CATS block reference in conjunction with a J.P. Kaye ice-point reference. Provision exists for 48 Type K thermocouples, hard-wired into the Dymec system, with 24 originating from the burner deck and 24 from the auxiliary room. In addition to CA thermocouples, provision exists for reading six Type B (platinum-rhodium)

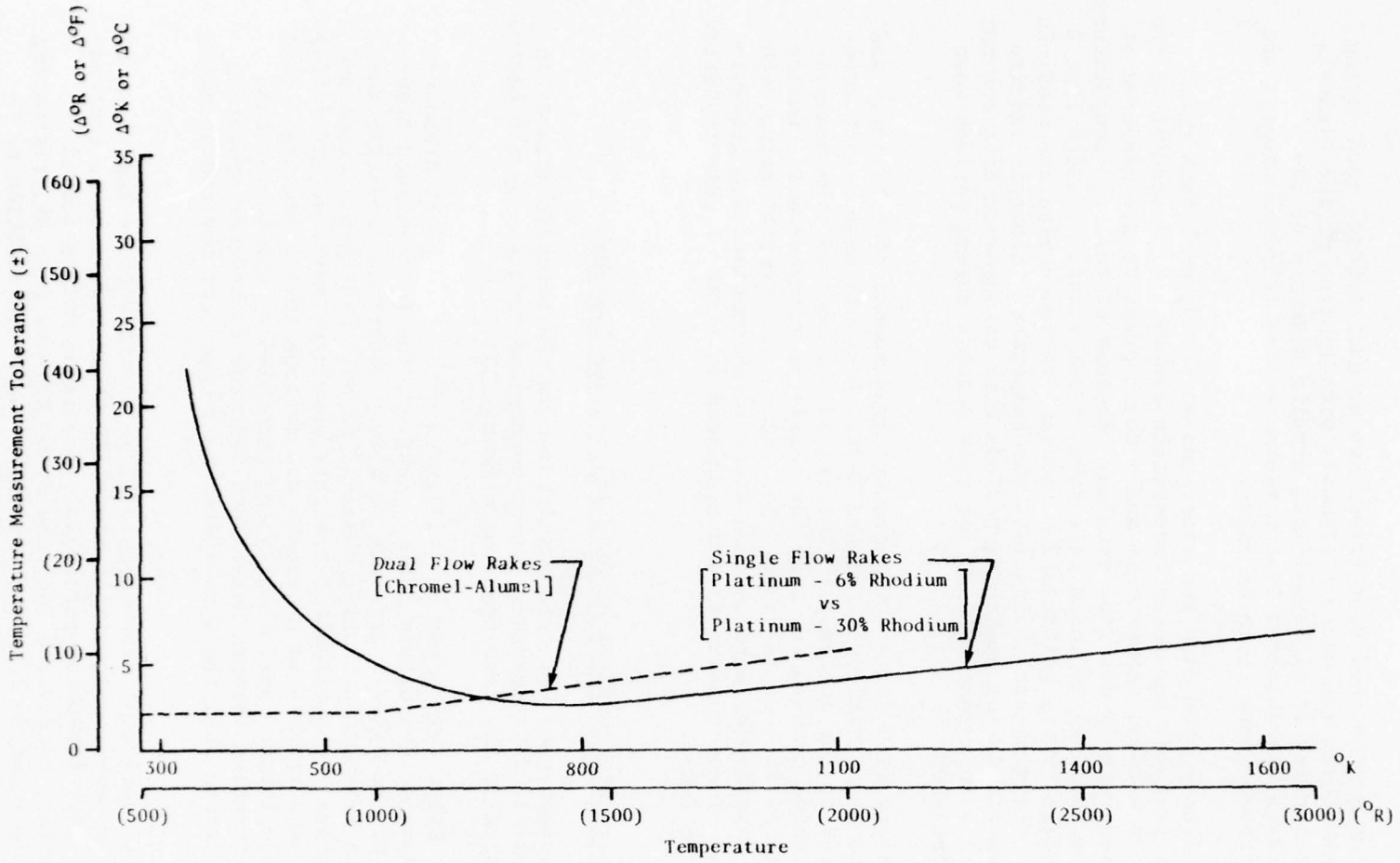

Figure 2-36. General Electric Anechoic Facility Temperature Measurement Tolerances.

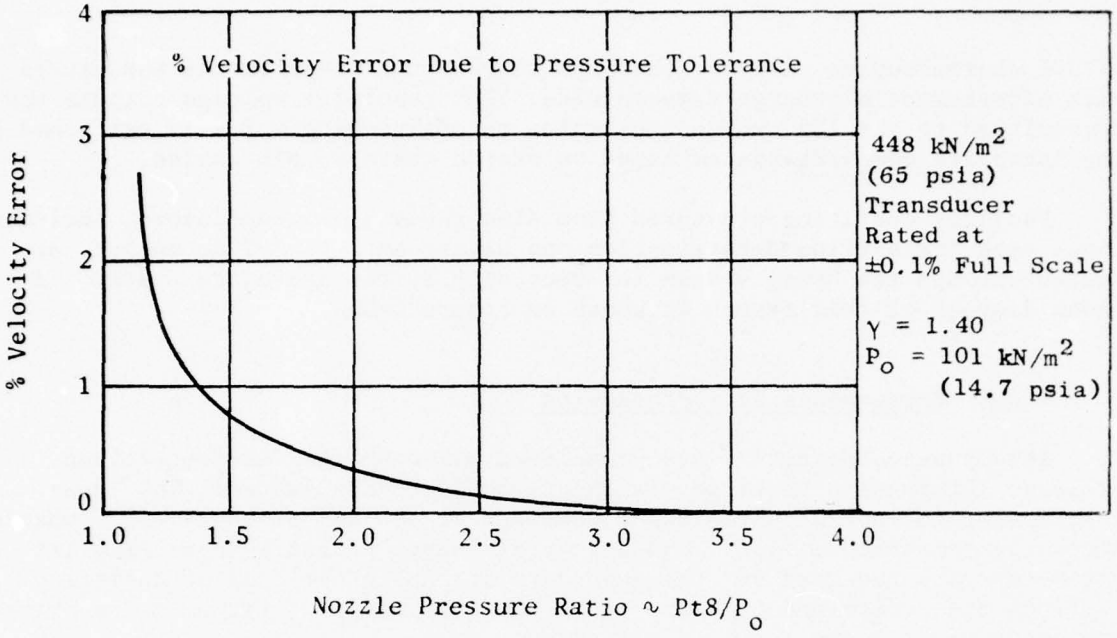

(a)

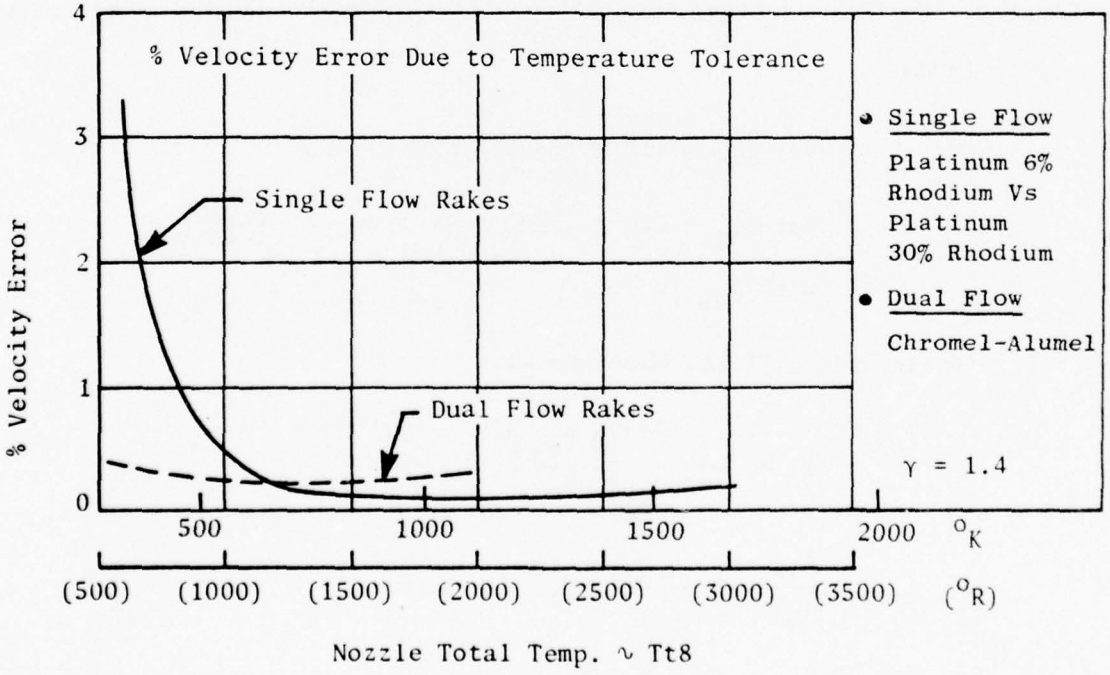

(b)

Figure 2-37. Velocity Error Due to Aerodynamic Measuring Tolerances.

6%/30% thermocouples used for the high temperature measurements associated with afterburner discharge temperatures. The resulting voltage outputs are transmitted to the IDR, where conversion to engineering units is performed by the Astrodata computer system based on stored thermocouple tables.

Facility operating pressures from nine individual transducers, including those used for airflow determination and having an 0 to 5-V dc output, are routed through the Dymec system for recording by the Astrodata system. A block diagram of this system is shown on Figure 2-38.

2.4.4 Performance Data Processing

Aerodynamic parameters are calculated based on the temperature and pressure information acquired via the Dymec/Astrodata system. The input information for nozzle performance consists of ambient pressure (P_o), nozzle discharge temperature (T_{T8}), and nozzle discharge pressure (P_{T8}). Similar parameters are required for the secondary stream in the case of dual-flow. Airflows are determined by means of Meriam instrument orifices in the primary and secondary streams.

Output of the processing program consists of tabulations of the individual input parameters with their identification, averages of similar parameters (i.e., P_T rake average), and calculated parameters as indicated below.

1. Gamma

For $T_{S8} \leq 440$ K (788.3° R); $\gamma = 1.4$

For $T_{S8} > 440$ K (788.3° R); $\gamma = \dfrac{2.23708}{\left(T_{S8}\right)^{0.070271}}$

with T_{S8} in ° R

2. Isentropic or Ideal Mach number

$$M_8 = \frac{2}{\gamma-1}^{1/2}\left[\left(\frac{P_{T8}}{P_o}\right)^{\gamma-1/\gamma} - 1\right]^{1/2}$$

$$\frac{T_{T8}}{T_{S8}} = 1 + \left(\frac{\gamma-1}{2}\right) M_8^{\,2}$$

$$T_{S8} = T_{T8} \Big/ \left(T_{T8}/T_{S8}\right)$$

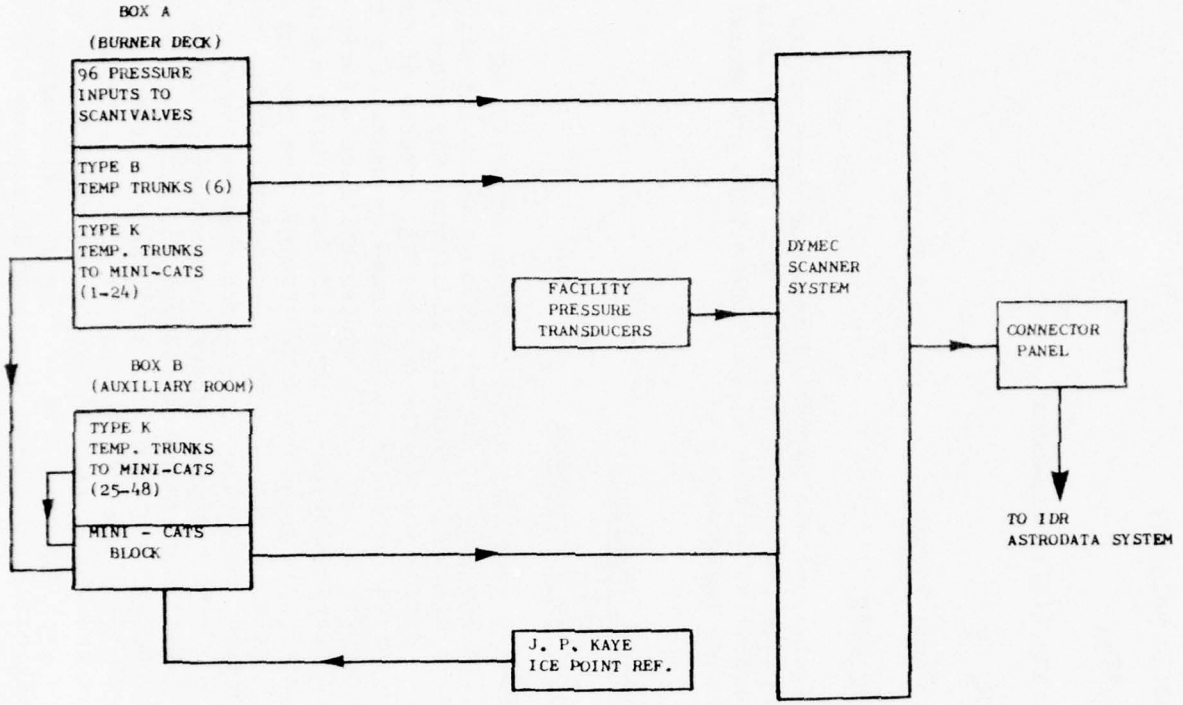

Figure 2-38. Aerodynamic Data Acquisition System Used in the General Electric Anechoic Facility.

where T_{S8} is initially assumed equal to T_{T8}. Starting with the gamma calculation, the above calibrations are repeated by an iteration procedure until the difference in T_{S8} between iterations is less than one degree.

3. Local Acoustic Velocity

$$C_8 = \gamma RT_{S8}$$

4. Ideal Velocity (fully expanded)

$$V_8 = M_8 C_8$$

5. Calculated Ideal Thrust

$$F_8 = V_8 W_i/g$$

6. Airflow calculations are performed based on measurements of orifice upstream temperature and pressure, and differential pressure across the orifice in accordance with procedures of ASME Power Test Code (Reference 1).

2.4.5 Meteorological Parameters

2.4.5.1 Humidity Measurement

One of the parameters necessary for correcting acoustic data for atmospheric absorption is the humidity of the air through which the signal is propagating. Since varying nozzle operating conditions may cause changes in the chamber environment during the course of testing, a means of remote humidity readout is required. This is accomplished by means of a Hygrometrix Model 8501 Relative Humidity System. This system utilizes a Xeritron sensor that is an assembly of hygromechanical crystallite structures and piezoresistive silicon strain gages on a common substrate. The sensing element responds to changes in relative humidity by a dimensional change reflected in the strain gage resistance; resistance is proportional to the relative humidity. Temperature at the humidity sensor location is measured using a Type K thermocouple. Readout of both temperature and relative humidity is provided at the cell control panel and is logged for each test point. Provision exists for humidity readout from any of the microphone positions; however, the sensor is mounted at the 40° microphone position, as this location represented a good approximation of mean chamber conditions as determined from the environmental survey discussed in Section 3.3.

The manufacturer's stated accuracy for this system is ± 2% over the range of -40° C (-40° F) to 125° C (257° F). A detailed description of the sensor and signal-conditioning, readout, and calibration procedures may be found in the vendor's operation manual.

2.4.5.2 Wind Speed Measurement

To ensure that the requirement of an entrained airflow velocity not exceeding 2.13 m/sec (7 ft/sec) was met, an anemometer system has been provided for use in this test chamber. This system can be affixed to any of the far-field microphone stations with remote digital readout at the control console. This unit is a Climet 011-1 wind speed transmitter, a research grade sensor using a 3-cup anemometer assembly, and a light beam chopper producing a square wave output whose frequency is directly proportional to rotational speed. The velocity threshold of this instrument is 0.27 m/sec (0.88 ft/sec). Over the range from the threshold to 4.57 m/sec (15 ft/sec) the rated accuracy is ± 0.067 m/sec (± 0.22 ft/sec).

Based on results of the ambient survey conducted during chamber checkout, mounting the sensor at the 40° position was chosen as being representative of the chamber conditions.

2.5 ACOUSTIC DATA SYSTEMS

2.5.1 Acoustic Data Acquisition System

A schematic of the microphone data acquisition system used to obtain acoustic data during testing in the chamber is shown on Figure 2-39. This system has been optimized for obtaining the acoustic data up through the 80 kHz 1/3-octave center frequency, the design operating range of the facility.

The prime microphone type used to obtain 80 kHz data is the B&K 4135 0.64 cm (1/4 in.) condenser microphone for far-field measurements and the B&K 4136 0.64 cm (1/4 in.) condenser microphone for near-field measurements. All testing is conducted with microphone grid caps removed to obtain the best frequency response. For testing where the data requirements are only through the 40 kHz 1/3-octave band, and of relatively lower amplitude, increased sensitivity is obtained using B&K 4133 or 4134 1.27 cm (1/2 in.) microphones for far-field and near-field measurements, respectively. For special near-field measurements, B&K 4138 0.32-cm (1/8-in.) condenser microphones are sometimes used.

The cathode followers used in the chamber are transistorized B&K 2619's for optimum frequency response and lower inherent system noise characteristics relative to the 2615 cathode follower. During the original system checkout, it was observed that these preamplifiers were sensitive to case vibrations transmitted through the mounting arrangement. B&K representatives recommended modifying the transistor by adding a 51-ohm, 1/4-watt, carbon resistor in series with the signal output lead to obtain improved signal stability.

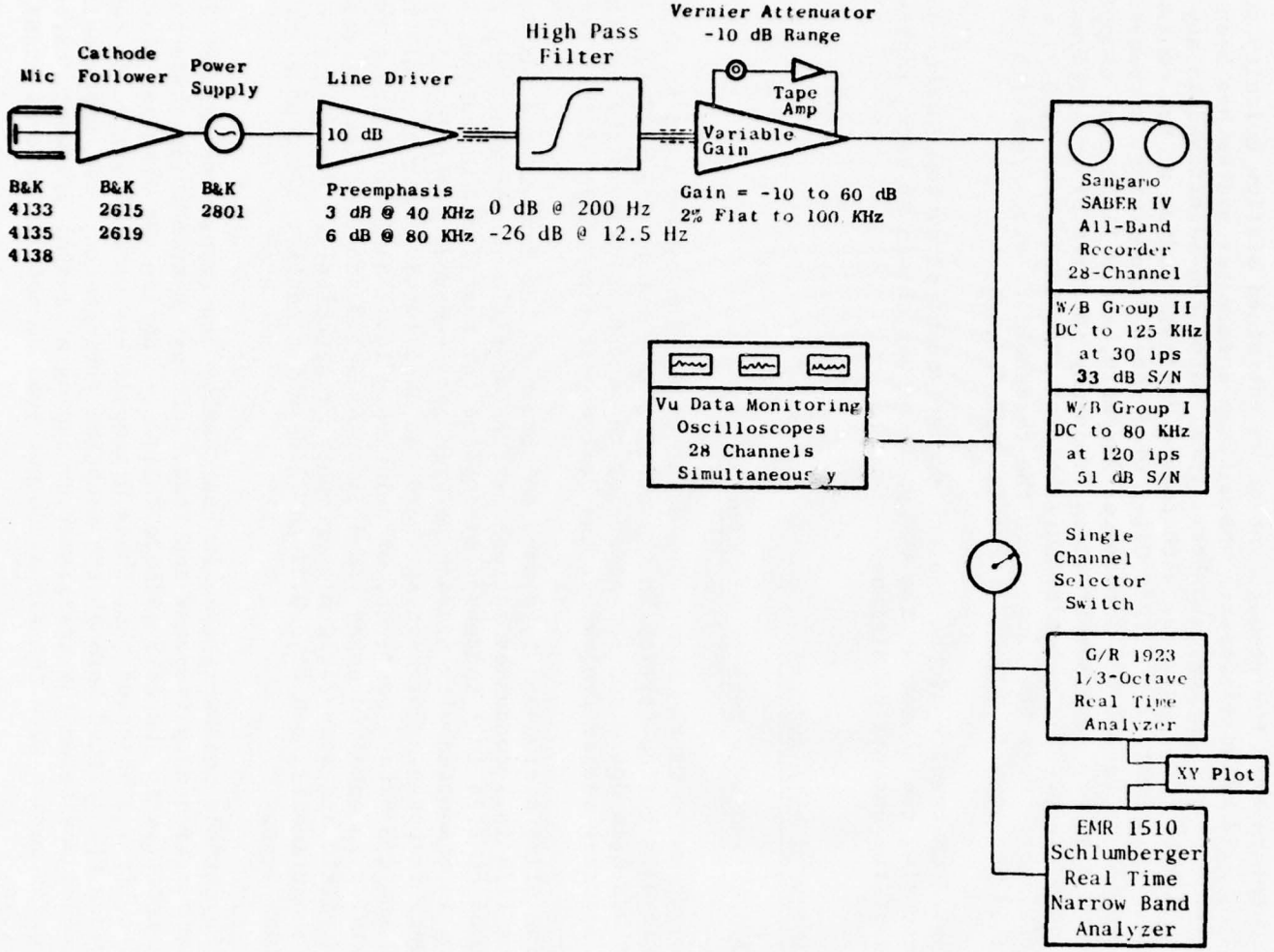

Figure 2-39. General Electric Anechoic Facility Acoustic Data Acquisition System.

All systems utilize the B&K 2801 power supply operated in the direct mode, avoiding the sensitivity loss associated with the optional 50-ohm and 200-ohm transformer outputs.

The output of the power supply is connected to a line driver adding 10 dB of amplification to the signal as well as adding "preemphasis" to the high frequency portion of the spectrum. These amplifiers were designed by General Electric (AEG Electronic Instrumentation Group) and built by Random Electronics of Cincinnati. The net effect of this amplifier is a 10 dB gain at all frequencies, plus an additional 3 dB at 40 kHz and 6 dB at 80 kHz due to "preemphasis", increasing the ability to measure low amplitude high frequency data.

During system checkout, it was found that low frequency noise levels attributable to operation of adjacent engine test cells were being detected by the microphones within the test chamber. While the frequencies (less than 20 Hz) were below the range of interest, the amplitude was limiting the amount of amplification that could be used when recording the microphone signal, resulting in noise floor problems at higher frequencies. In order to remove this low frequency noise, high-pass filters with attenuations of approximately 26 dB at 12.5 Hz decreasing to 0 dB at 200 Hz, were installed in the system.

The tape recorder amplifiers were designed by General Electric and built by Random Electronics. They have a variable gain from -10 dB to +60 dB in 10-dB steps and a gain-trim capability for normalizing incoming signals. The prime system used for recording acoustic data is a Sangamo/Sabre IV, 28-track FM recorder. Initially, the system was set up for IRIG (Inner-Band Instrumentation Group) Wideband Group II operation, which would provide the required response at a tape speed of 30 ips. However, the signal-to-noise ratio attainable in this operating mode was found to be insufficient for obtaining low amplitude/high frequency data. Evaluation of the optional operational modes indicated that an improvement of 18 dB in signal-to-noise could be obtained by operating in Wideband Group I (intermediate band double extended) at 120 ips tape speed. While this high tape speed is unattractive because four times as much tape is used during a test, it does provide the improved dynamic range necessary for obtaining the high frequency/low amplitude portion of the acoustic signal. The tape recorder is set up for ± 40% carrier deviation with a recording level of 8 V peak-to-peak. During recording, the signal is displayed on a calibrated master oscilloscope, and signal gain is adjusted to maximum without exceeding the 8-V peak-to-peak level.

Individual monitor scopes are used for observing signal characteristics during operation. On-line data monitoring is available via a Schlumberger EMR 1510 Analyzer or a General Radio 1921 1/3-Octave Analyzer with their outputs on display scopes or hard copy via an x-y plotter.

2.5.2 Acoustic Data Reduction System

During testing, on-line monitoring of the microphone signals is provided by means of wave-form presentation via an oscilloscope. In addition, on-line data analysis may be performed in 1/3-octave bands using a GR 1921 Spectrum Analyzer or by narrowband analysis using a Schlumberger EMR 1510 Spectrum Analyzer, with the results of either type of analysis displayed on an x-y plotter.

Off-line reduction of the recorded data is performed using the Automated 1/3-Octave Reduction System, shown schematically on Figure 2-40 and located in the IDR. The recorded data are played back on a CEC 3700 B, 28-track system, with electronics capable of reproducing IRIG Wideband Groups I and II and Intermediate band data.

In the automatic operating mode, control of the system is provided by means of the GEPAC-30 computer and operator-provided information. The data to be sampled are located by means of a time code reader, indexing from the time code signal recorded on the data tape. This tape-shuttling is continued for each data channel, with sampling performed over the same time increment, until all channels of a particular reading have been processed. The system then advances to the next data point, based on the operator-supplied time reference, and repeats the shuttling process.

After the processing information (including reading identification, reading time, attenuation changes, etc.) has been set up by the operator, the system will run without further operator assistance until a magnetic tape change is required.

All 1/3-octave analyses are performed using a General Radio 1921 1/3-Octave Analyzer. A normal integration time of 16 seconds is used to provide adequate sampling of the low frequency portion of the data signal. The frequency range of processing is optional, with lower and upper limits of 12.5 Hz and 125 kHz, respectively, based on the filter set capability of the analyzer; however, data are normally acquired to 80 kHz because of acquisition system limitations. The analyzer has a rated accuracy of ± 0.5 DB with a 0.25 dB resolution capability in each band.

Each data channel is passed through an interface to the GEPAC 30 computer, where data are corrected for frequency response of the acquisition and reduction system and for microphone-head response. A "quick-look" display of results is provided by means of a Terminet 300 console with data transferred and stored in the Honeywell 6000 system via a direct time-sharing link. An alternate to this method provides these data on punched paper tape for subsequent input to the 6000 system, allowing 1/3-octave processing during periods when the 6000 system is unaccessible. Processing in the 6000 system is performed via the Full-Scale Data Reduction (FSDR) program, where calculations are performed correcting data for atmospheric attenuation in accordance with SAE ARP 866 (References 2 and 3) extended for frequencies greater than 10,000 Hz, with all data output corrected to a

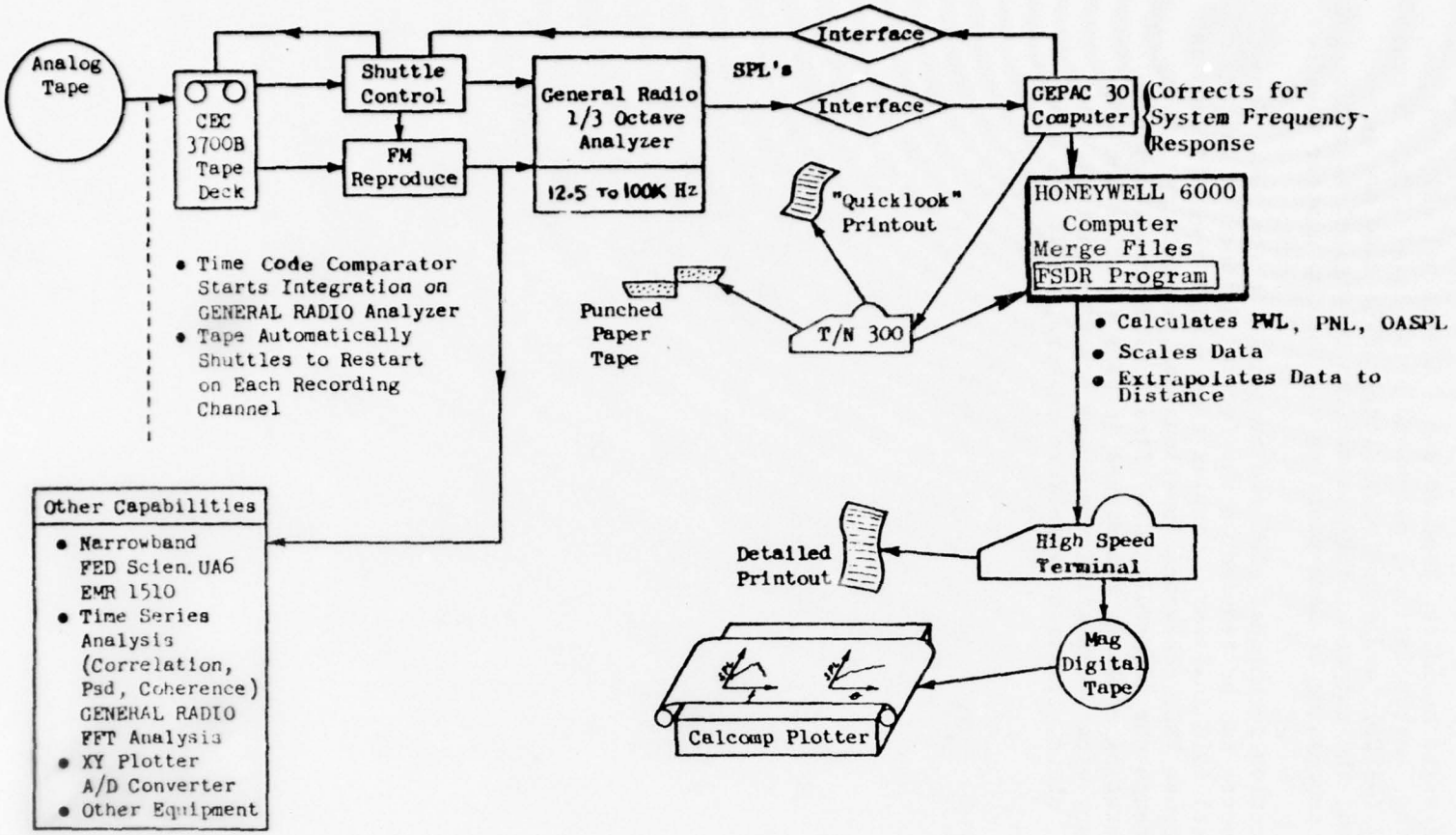

Figure 2-40. General Electric Acoustic Data Reduction System.

15° C (59° F)/70% relative humidity standard day. Additional calculations, including data scaling, extrapolations, perceived noise level (PNL), overall sound pressure level (OASPL), and sound power level (PWL) also are performed. As an option, the output of FSDR is written to digital magnetic tape for subsequent processing or data plotting via Calcomp plotter routines.

Other data reduction techniques also are available in the IDR. Constant narrowband spectra can be reduced on the Federal Scientific UA6 or the EMR (Schlumberger) 1510 Analyzer. Complex time series analysis such as cross correlation, cross PSD, coherence functions and probability density can be processed through the (General Radio) Time Data System (computer-based system incorporating analysis techniques in both the time and frequency domains). Many other capabilities such as tracking filters, high speed "fiber optics" plots, transient wave form capture, etc., are also available.

3.0 ANECHOIC QUALITY AND FAR-FIELD REGION OF THE TEST ROOM

3.1 INTRODUCTION

The anechoic room was required to deliver effective free-field data over a 220 Hz to 80 kHz frequency region of interest. This means that the acoustic data must be free of reflections and reverberations, such that the sound decays as the inverse square law with distance away from a noise source.

In general, one can divide the variation of sound inside a large enclosure into a near-field and a far-field region, both being a function of distance away from the sound source as shown in Figure 3-1. This figure indicates that the sound level may vary in any fashion near the source but, ideally, the sound level should decrease 6 dB for each doubling of the distance (inverse square law) far away from the source. Furthermore, in the presence of large reflecting surfaces (such as the concrete walls of a test chamber), a reverberant sound field generally will be set up in which the sound level remains virtually constant with increasing distance. The more common situation, however, is that only a few reflections occur, such that the sound level decays in an oscillator fashion about an ideal, 6 dB, doubling-of-distance line. The purpose of an anechoic chamber is to eliminate these reflections and reverberations which may influence the data.

General Electric's anechoic chamber was designed to deliver free-field data by employing wedges covered with a fiberglass-type material on all the walls, such that reflections could be eliminated and certain specified acoustic performance could be achieved. The acoustic material conformed to the following specifications:

- A 220 Hz anechoic cutoff frequency
- A 0.99 or greater sound absorption coefficient above the cutoff frequency

With these wedges installed, and with a minimum measurement station of 1.52 m (5 feet) away from the wedge tip, Eckels Industries was required to design the wedges to be within ± 1.5 dB of inverse square law over the frequency range from 220 Hz to 10 kHz and within ±3 dB over the range from 10 kHz to 80 kHz. These specifications were set using appropriate air-absorption corrections for a distance of 1.68 m (5.5 feet) from the noise source to within 1.52 m (5 feet) from any wall, ceiling, floor, or wedge tip.

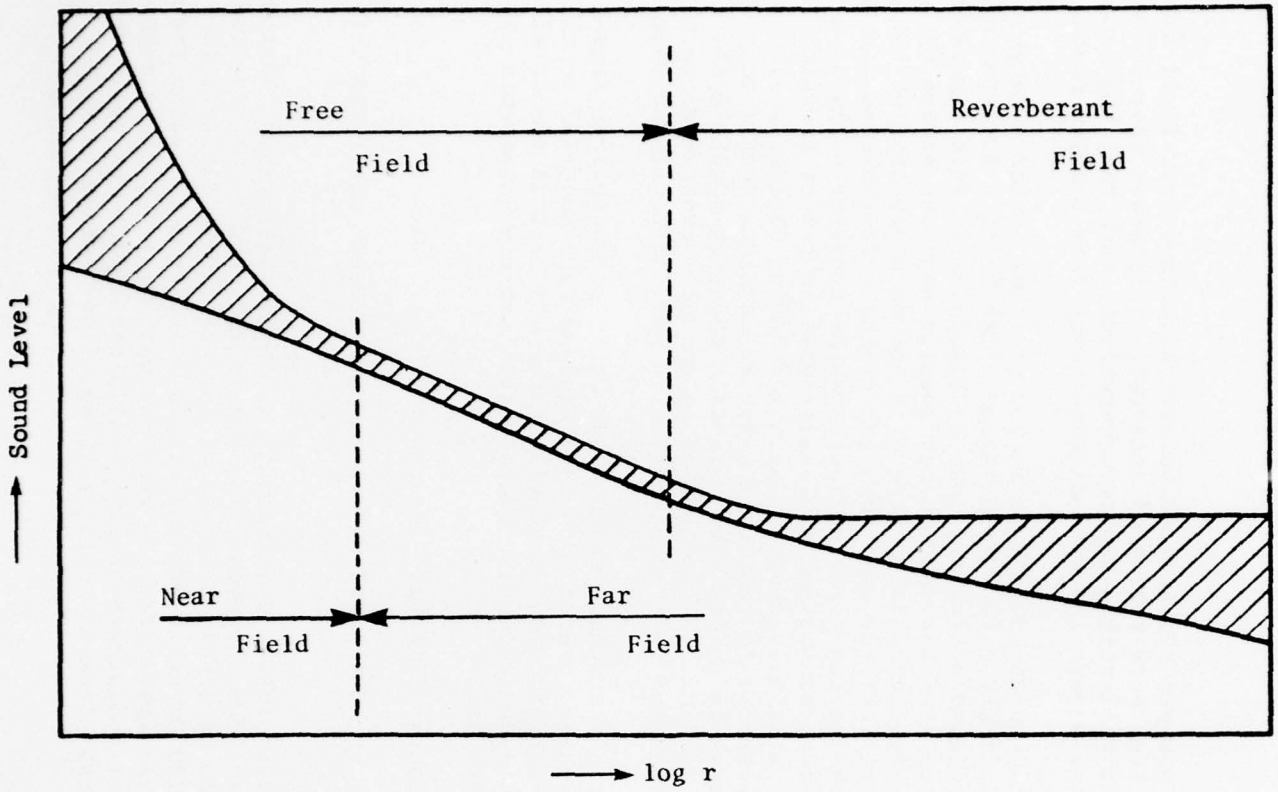

Figure 3-1. General Behavior of Sound with Distance from a Source.

3.2 ANECHOIC QUALITY OF THE ROOM

The anechoic quality of the room was investigated by conducting spherical divergence tests with the aid of a 30.48-cm (12-inch) diameter Altech speaker (shown in Figure 3-2) for radiating a pink-noise-like signature for the 125 Hz to 800 Hz frequency region and with an omnidirectional white-noise sound source called an "air ball" (shown in Figure 3-3) for examining the 1 kHz to 80 kHz high frequency region of the noise spectrum. The air ball was borrowed from the Boeing Aircraft Company where it was used to certify the high frequency regime in their chamber. The design consisted of a 15.24-cm (6-inch) diameter sphere having 500 tiny holes, each being 0.79 mm (0.31 inch) in diameter, through which high pressure air was blown to generate tiny sonic jets.

The spectrum characteristics for both the speaker and air ball noise sources are shown in Figures 3-4 and 3-5. An unshaped pink-noise signal was input to the speaker yielding the spectral shape in Figure 3-4 designated as "spectrum shaper off". The Altech 9860A Active Equalizer spectrum shaper is a 26-channel, active, 1/3-octave band, rejection filter bank which provides up to 15 dB attenuation at the center frequencies. While observing the real-time output of a 1/3-octave analyzer, each band was attenuated by the shaper to give the nearly flat output shown as "spectrum shaper on" in Figure 3-4. A flat response was achieved up to 5 kHz, but only data below 800 Hz was used for analysis. The airball was used for the 1/3-octave frequencies from 1 kHz to 100 kHz.

In order to obtain the sound pressure levels of the source as a function of distance, a stationary and a traversing microphone system were set up as shown in Figure 3-2. The stationary microphone was located 1.52 m (5 feet) away from the source where the sound intensity is high and air-absorption corrections are small. This microphone acted as a reference station yielding the level of the sound source itself. The traversing microphone was attached to a cable and pulley system on which it could travel away from the noise source to the microphone station under investigation. Microphone traverses were made for the 40°, 90°, 130°, and 160° angles from the inlet as shown in Figure 3-6 and the laser upper and lower track stations as shown in Figure 3-7. The latter two positions were investigated because the laser track and cart are used in conjunction with the ellipsoidal mirror as well as a laser velocimeter during detailed noise source investigations of a jet plume. The only part of the track not wrapped with fiberglass is that part where the cart makes contact with the rails. Since possible reflections could occur from the bare rail, it was judged advisable to investigate these stations. Both noise source spectrum levels and traversing microphone levels were recorded real time and on magnetic tape during the traverse from the noise source to the microphone station of interest. The data were played back from the tape through a General Radio 1923 1/3-Octave Analyzer for each position to check the inverse square law spherical divergence relationship.

Figure 3-8 shows the results of the 90° tests using the speaker noise source for some typical low frequencies (125 to 800 Hz), while Figures 3-9

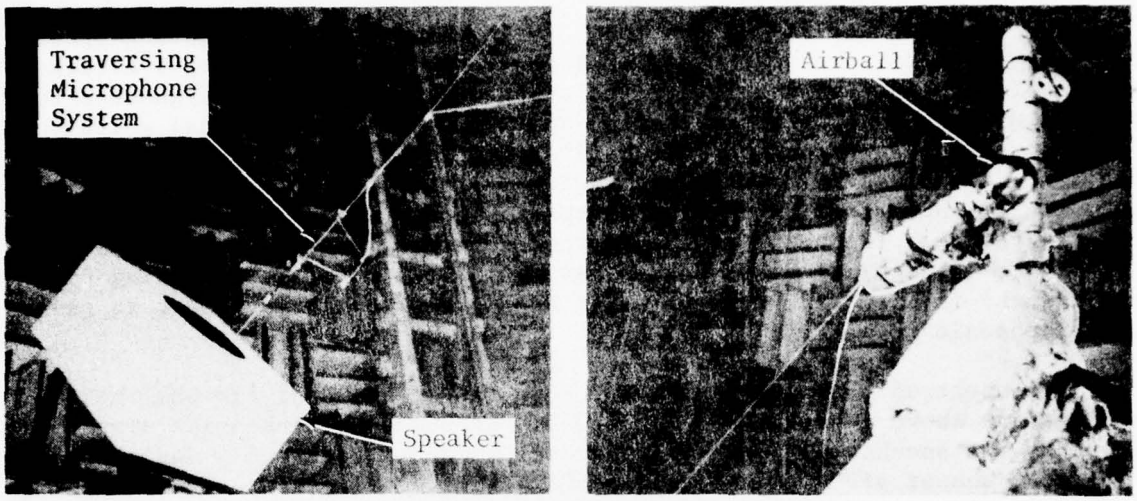

Figure 3-2. Setup of Speaker, Air Ball, and Traversing Microphone System.

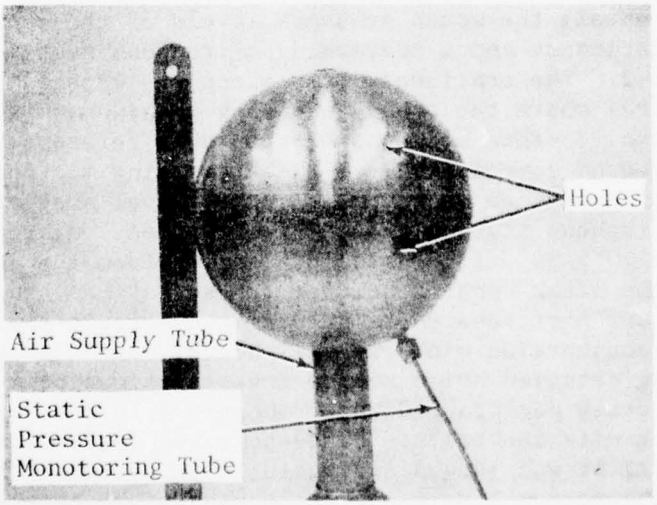

Figure 3-3. Closeup of the Air Ball Noise Source.

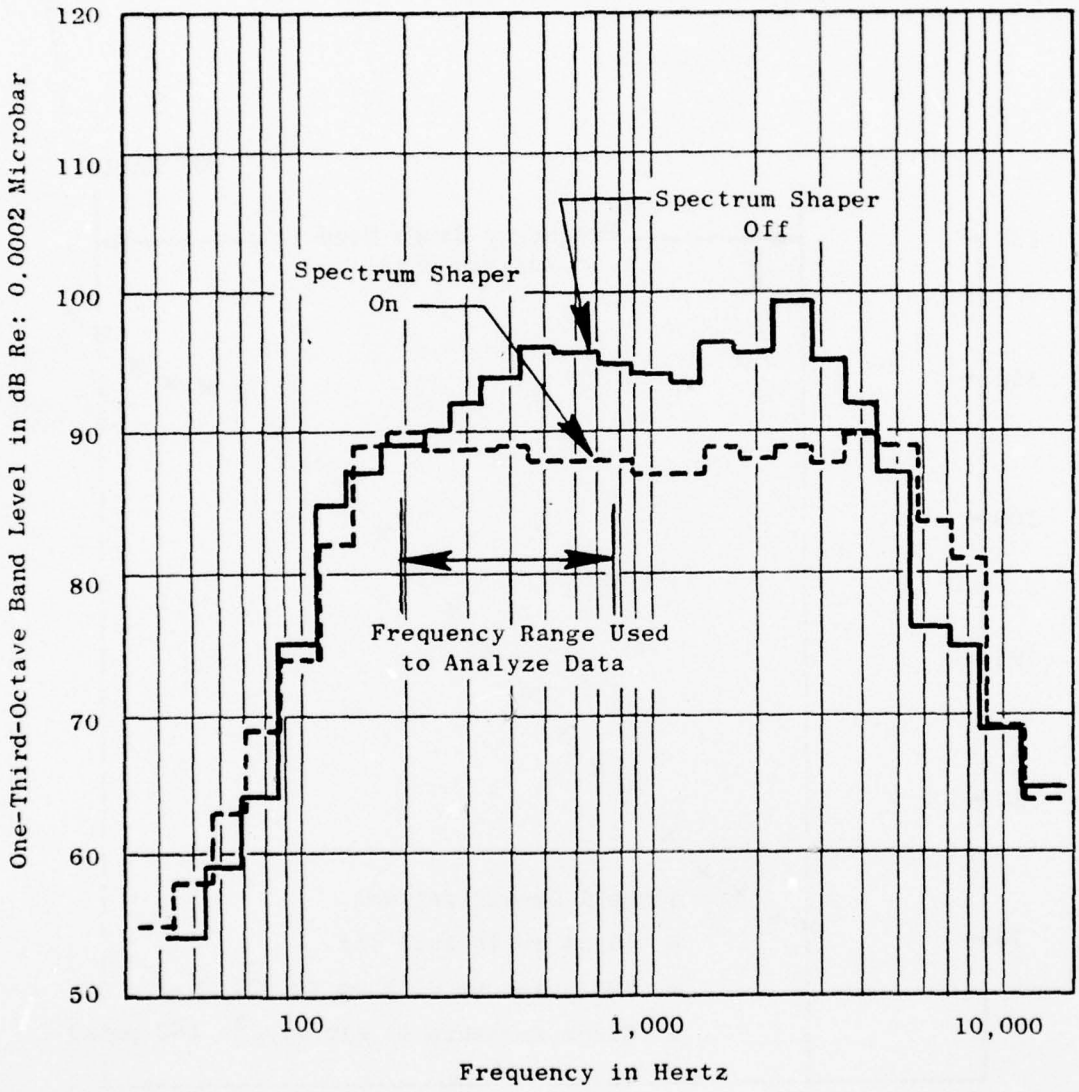

Figure 3-4. Speaker Noise Spectrum at 1.52 m (5 ft) Radius with 30.5 cm (12 in.) Diameter Altech Speaker and Altech Active Equalizer Spectrum Shaper.

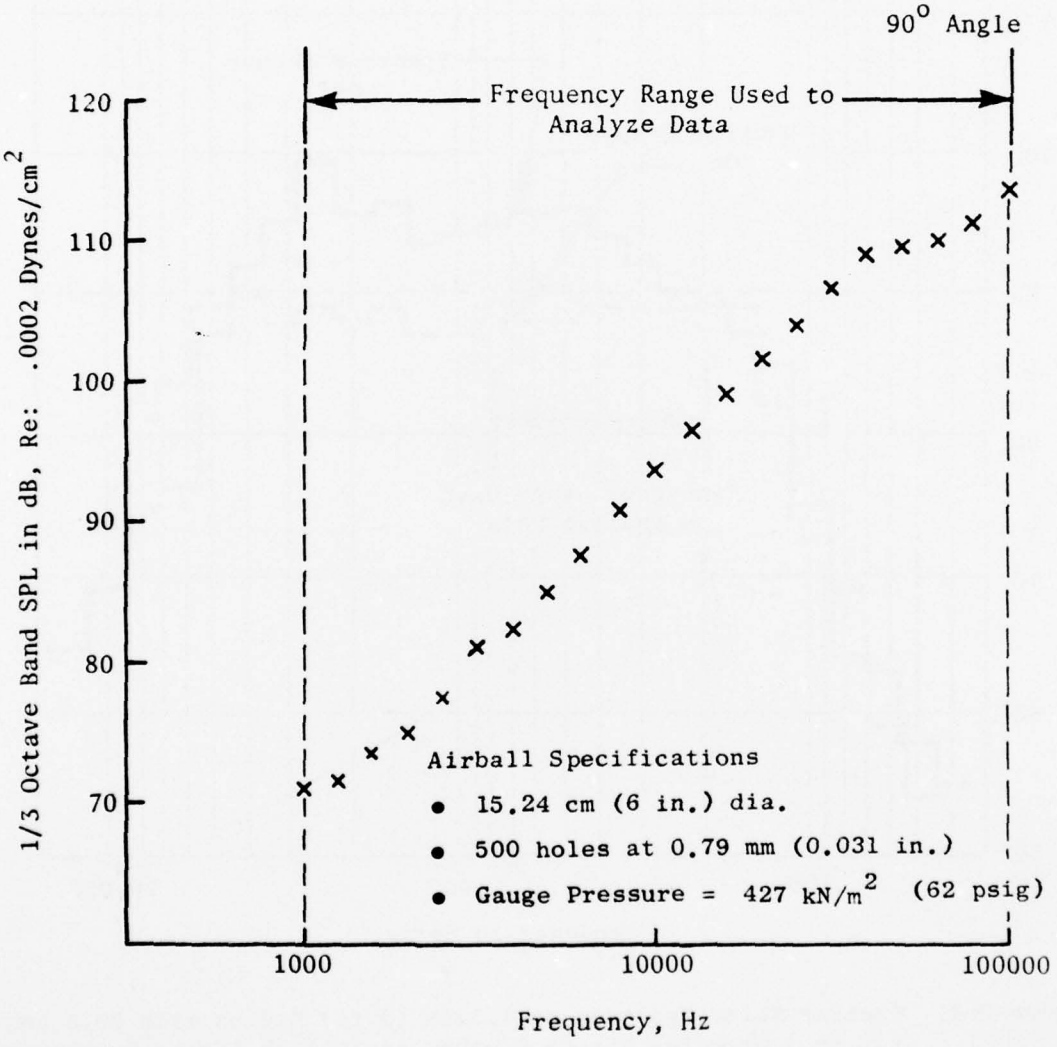

Figure 3-5. Air Ball Noise Spectrum at 1.52 m (5 ft) Radius.

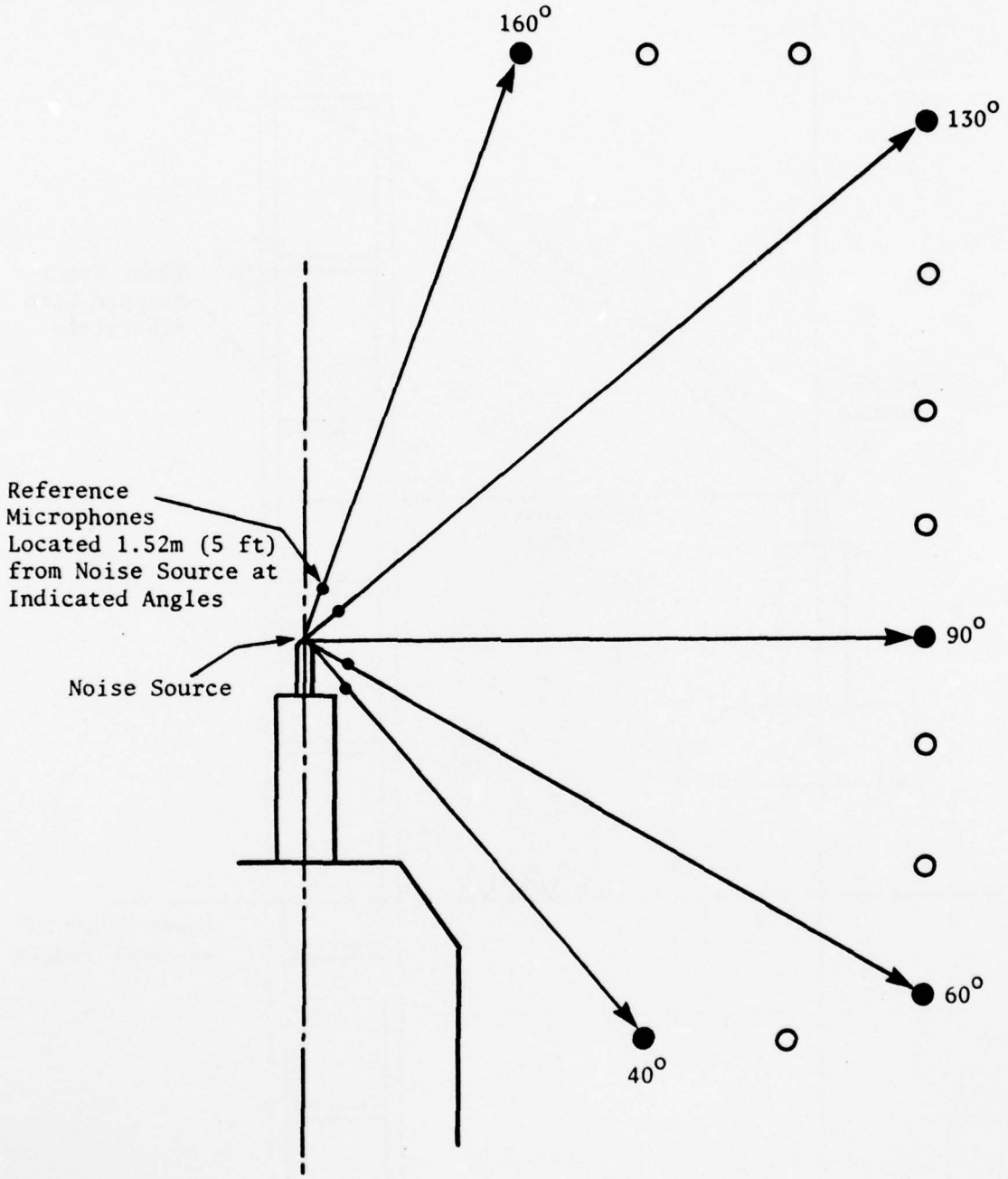

Figure 3-6. Traversing Positions in the Plane of the Microphones.

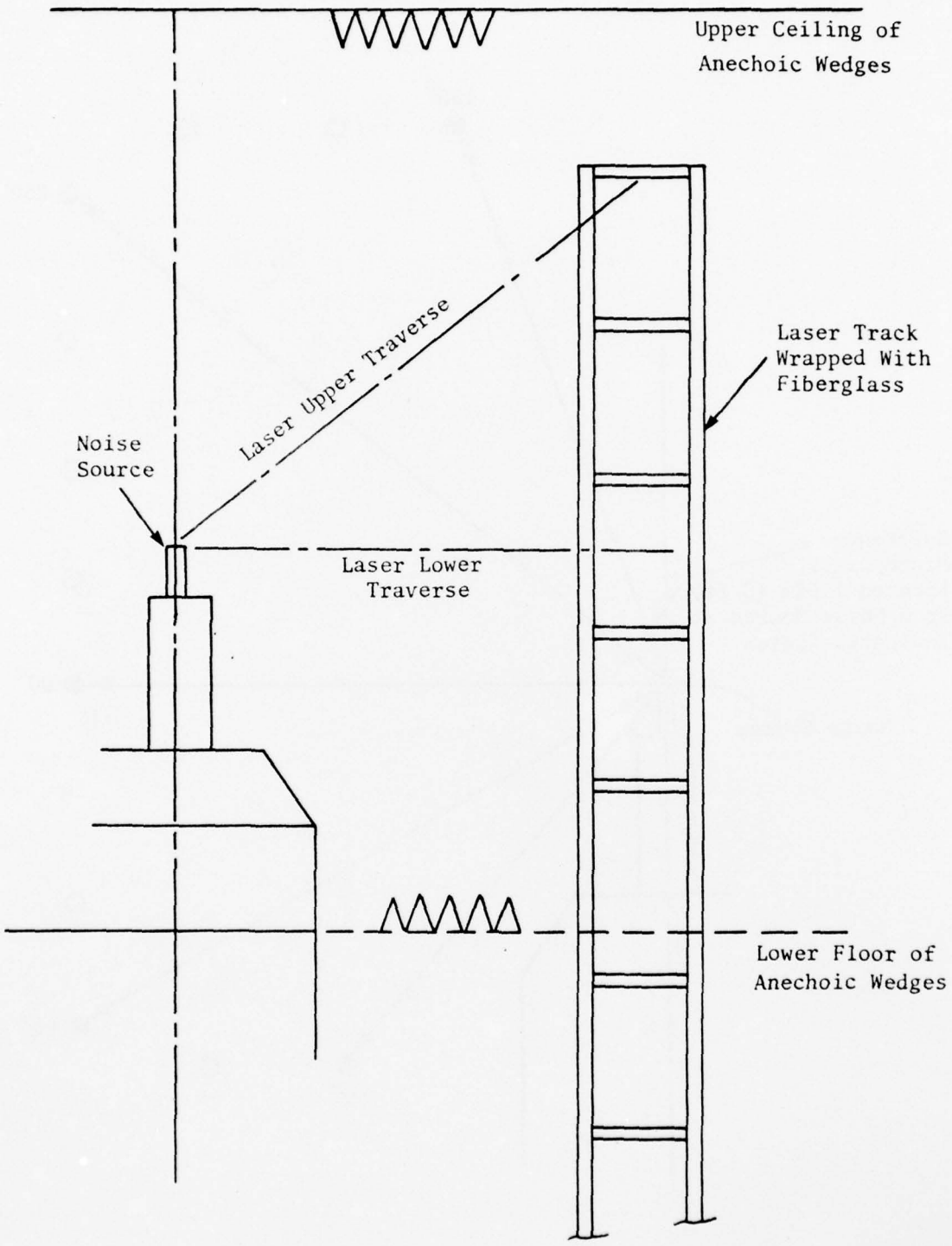

Figure 3-7. Traversing Positions in the Plane of the Laser Track.

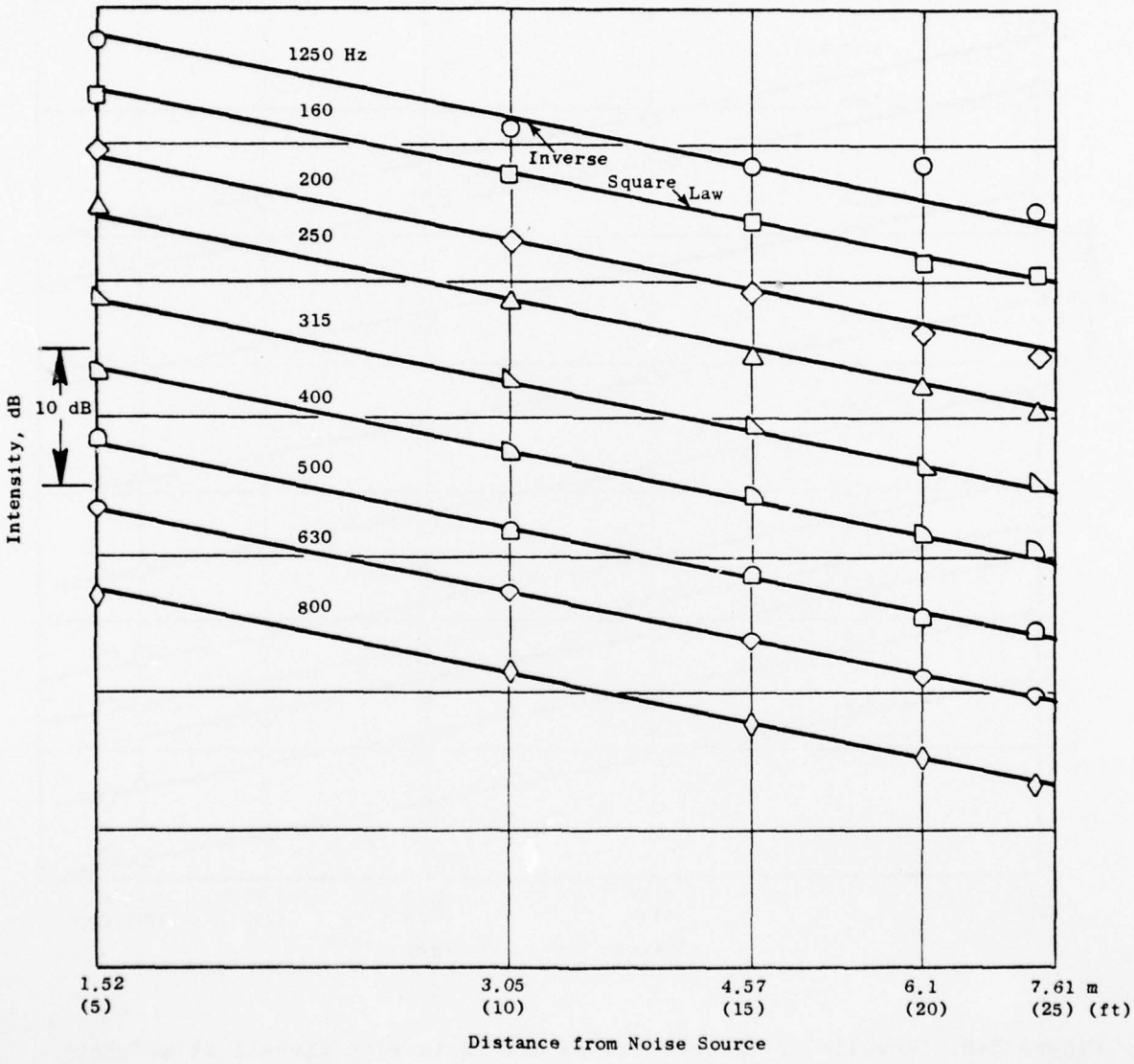

Figure 3-8. Results of Inverse Square Law Tests with Speaker at 90° for Low Frequency.

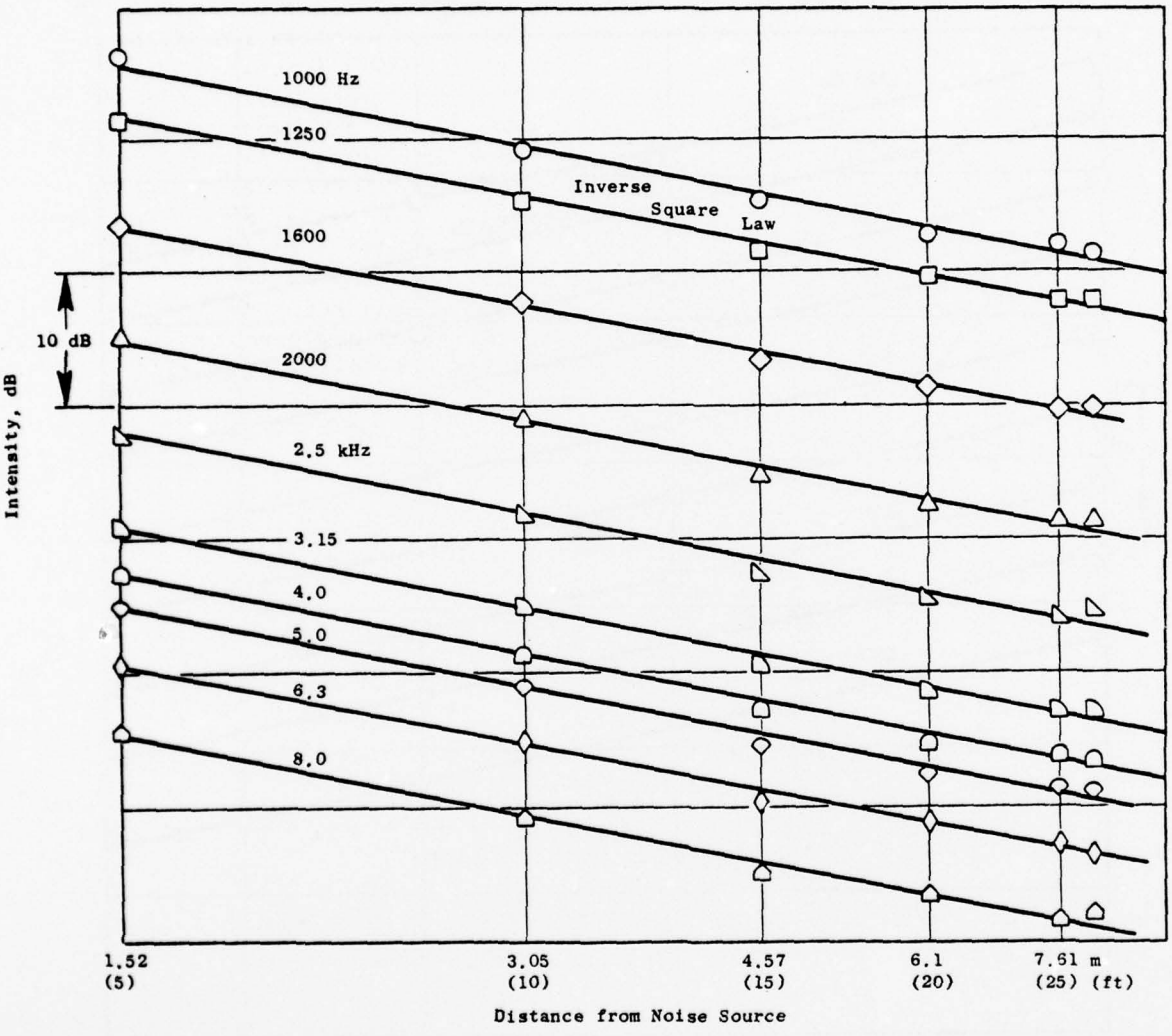

Figure 3-9. Results of Inverse Square Law Tests with Airball at 90° for Intermediate Frequency.

and 3-10 show the results with the "air ball" noise source for each 1/3-octave band starting at 1 kHz to 100 kHz. The high frequency traces on Figure 3-10 contain the measured 1/3-octave band sound data (represented by open symbols) as well as the data corrected for air attenuation. The air attenuation equations by Bass, Bauer, and Evans (Reference 4) were used with the center frequency of the band to represent the average 1/3-octave value. Air attenuation corrections were applied only for those frequencies for which the magnitude was 0.5 dB or more. These are shown with closed symbols on the plots. All of the data, with the exception of the 160° microphone station, were taken within the range of temperatures specified by the Bass, Bauer, and Evans report (20° C ±5° or 68° F ±9°) as shown on Figure 3-11. A best-fit, 6-dB per doubling of distance line was drawn through these data points representing the $1/r^2$ spherical divergence criteria. It can be seen from the results that the anechoic room meets these criteria within 1 dB or less for the 200 Hz to 10 kHz region and within 2 dB or less for the 10 kHz to 80 kHz region. The standard deviation about the $1/r^2$ mean value for each frequency band was calculated by normalizing the data to the reference position (1.52 m = 5 feet in distance). This was accomplished using the following equations:

$$SPLC_i = SPL_i - 20 \log_{10} (R_i/5) - \alpha(R_i - 5)/1000_j ; R_i \text{ in feet}$$

where:

$SPLC_i$ = Normalized, corrected sound pressure levels (dB) for

i = 1 to N (N being the number of samples)

SPL_i = Measured sound pressure levels (dB) as a function of distance away from the source

R_i = Measurement radius

α = Air attenuation correction (dB) over a 304.8 m (1000 ft) distance using the Bass, Bauer, and Evans equations

The mean of the corrected sound pressure levels $\overline{SPLC}_i$ normalized to the 1.52 m (5 ft) position was obtained using:

$$\overline{SPLC} = \sum_{i=1}^{N} \frac{SPLC_i}{N}$$

Next, the standard deviation σ of the corrected data was tabulated using:

$$\sigma = \left[\sum_{i=1}^{N} \frac{(SPLC_i - \overline{SPLC})^2}{N} \right]^{1/2}$$

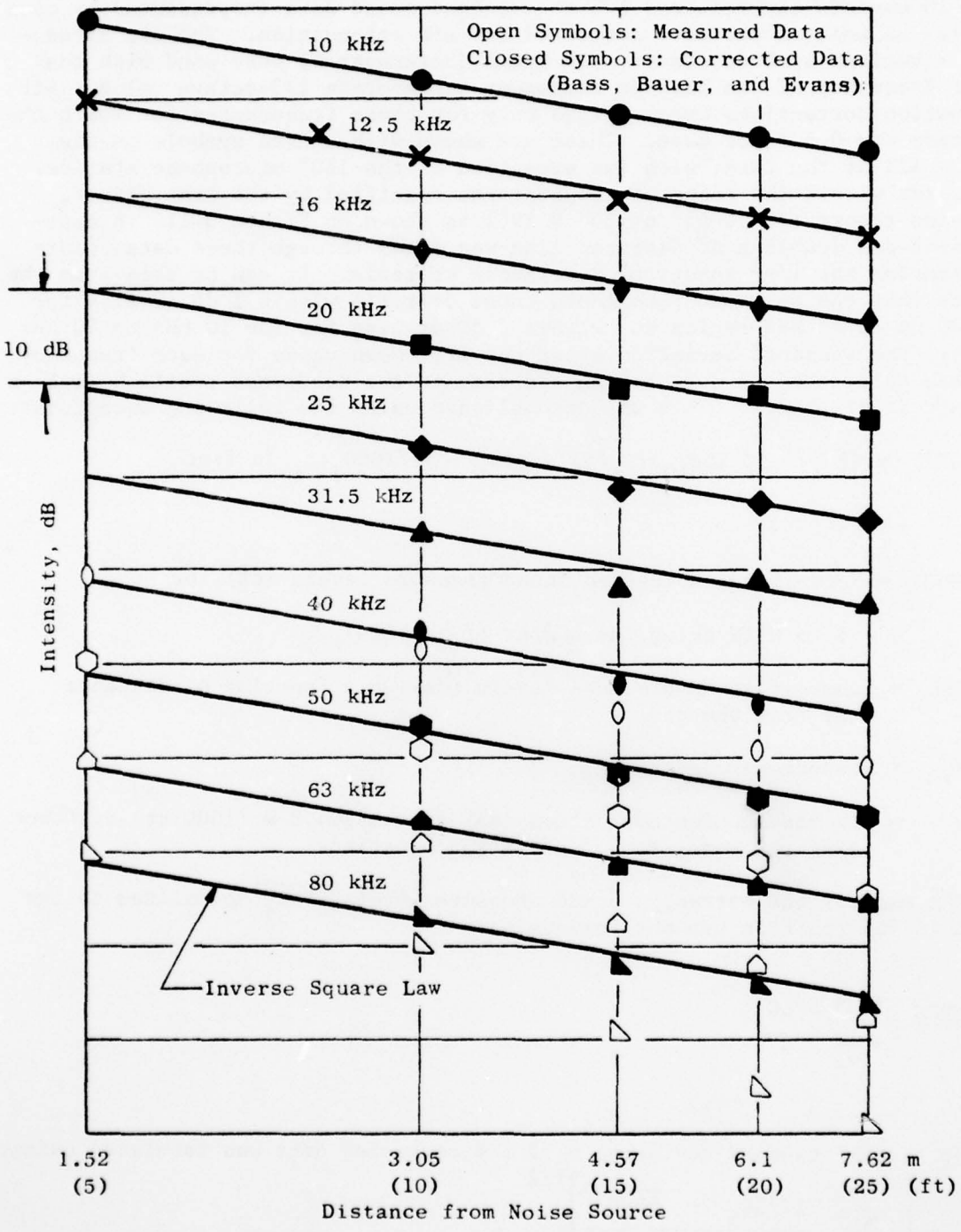

Figure 3-10. Results of Inverse Square Law Tests with Airball at 90° for High Frequency.

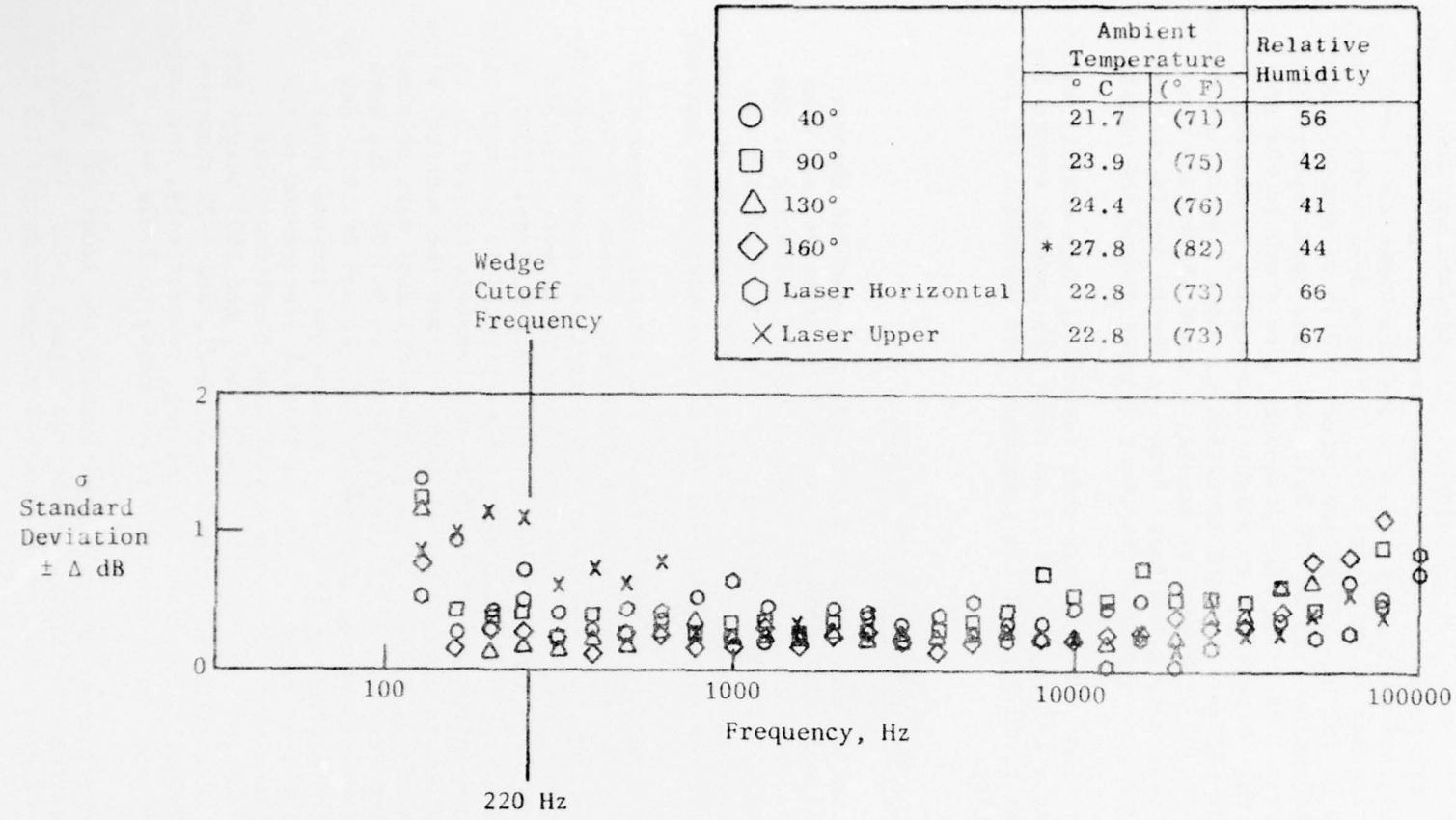

* Temperature outside the limits of the Bass, Bauer, and Evans Analysis Range.

Figure 3-11. Standard Deviation of Inverse Square Law Tests.

This step-by-step procedure for calculating the standard deviation is shown in the sketch of Figure 3-12. The standard deviation was calculated for each of the investigated microphone stations and the upper and lower laser track positions and are shown graphically in Figure 3-11. The results show that the majority of the data is of the order of 0.25 dB standard deviation. At the low frequencies (125 to 250 Hz), the laser upper section is seen to fluctuate to over 1 dB. The high frequency data above 10 kHz are seen to swing upward, most likely due to slight inaccuracies in the air attenuation model. The highest standard deviation at these frequencies occurs at 40°, which is believed to be biased by excessive sound absorption when the microphone was closer than 3.05 m (10 feet) from the nozzle due to the nearness of the microphone to the acoustic treatment wrapped around the nozzle.

These results show that the anechoic test room is of high quality and far exceeds the present specification of ±1 dB about the inverse square law criteria for the 220 Hz to 10 kHz and the targeted ±3 dB deviation for the 12.5 kHz to 80 kHz region.

3.3 AMBIENT AND TEMPERATURE ENVIRONMENTAL SURVEY

An environmental survey was carried out inside the anechoic chamber encompassing the measurements of humidity, dry bulb temperature, and wind velocity statically and with the 5.7-inch conical nozzle operating at the conditions given in Table 3-I. This work was performed to establish the severity of any environmental gradients that might exist along the acoustic propagation path between the nozzle exit and the various microphone stations.

Figure 3-13 shows a sketch of the inside of the anechoic chamber with the microphone stations, 40° to 160°, five of which were chosen for this survey (60°, 90°, 130°, 140°, and 160°), forming a vertical plane inside the anechoic chamber. Data along each of the five chosen radii were obtained through the use of a Xeritron humidity sensor (Hygrometrix, Model 8501), a Climet anemometer, and a Type K thermocouple probe attached to the near-field microphone system (shown in Figure 3-14), which was remotely controlled to move up and down and sideways along a set of cables to map the vertical plane of interest. In Figure 3-13, all of the positions where data were obtained are shown, starting with Position No. 1 through Position No. 29. The data were obtained over a four-day period (October 22, 23, 24 and 28/1975) due to having to extend the traversing arm in order to reach the extreme inner radii. To interpret the test results, a normalization (referenced to the outside ambient conditions with the exception of wind conditions) was used. The resulting data for the 60°, 90°, 130°, 140°, and 160° survey are shown in Figures 3-15 through 3-19. Figures 3-20, 3-21, and 3-22 show the variation along the chamber false floor and ceiling, respectively, for both jet nozzle stream "off" and "on" operation set according to Table 3-I.

There are no temperature or humidity gradients in the front 60° angle over the range of operating conditions, as seen in Figure 3-15. The high velocity points 5 and 42 give a uniform wind speed of approximately 1.5 m/sec

AD-A042 327 GENERAL ELECTRIC CO CINCINNATI OHIO AIRCRAFT ENGINE GROUP F/G 14/2
HIGH VELOCITY JET NOISE SOURCE LOCATION AND REDUCTION. TASK 1. --ETC(U)
FEB 77 C T SAVELL, E J STRINGAS DOT-OS-30034
UNCLASSIFIED R77AEG188 FAA-RD-76-79-1A NL

2 OF 3
ADA042327

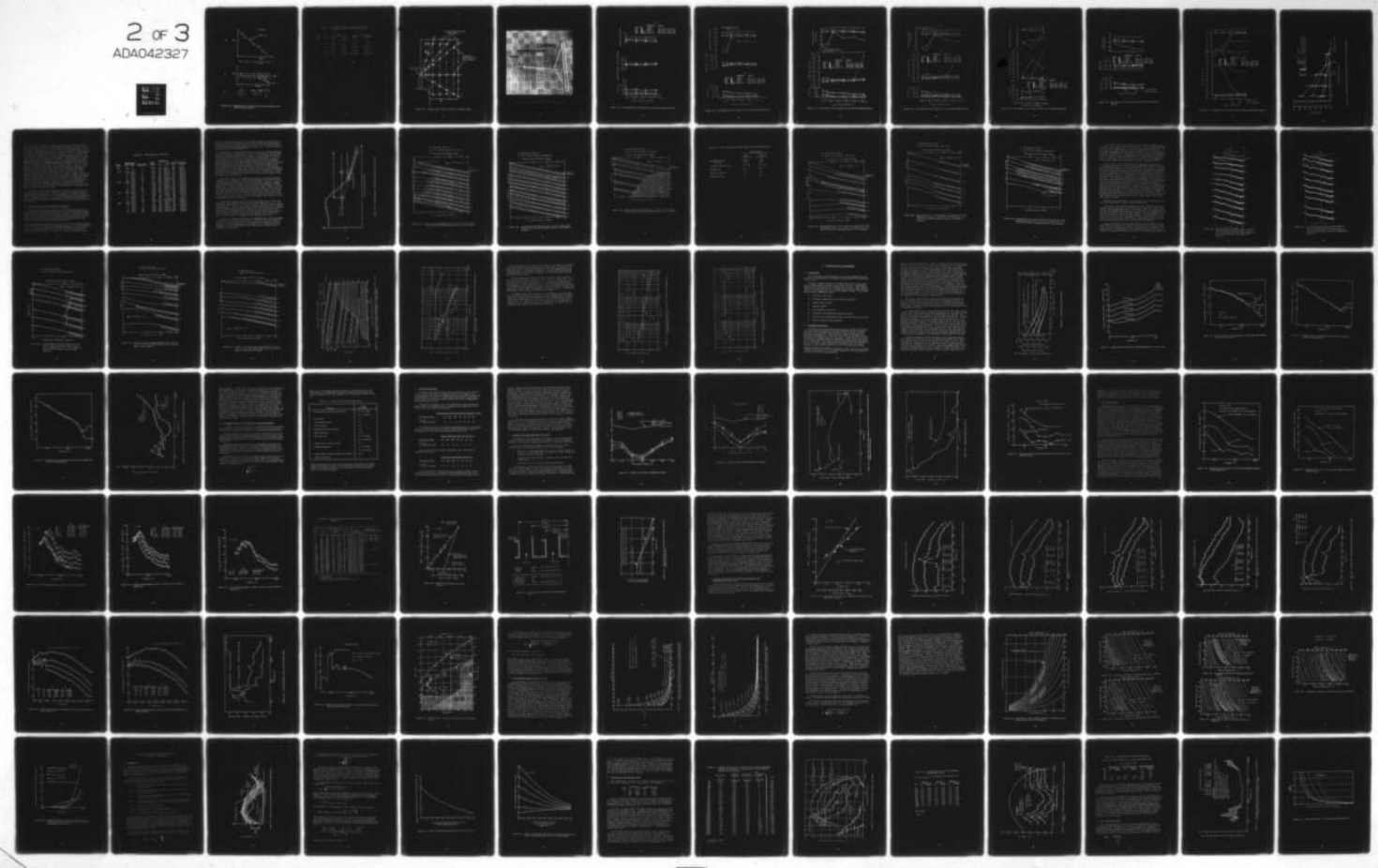

(a)

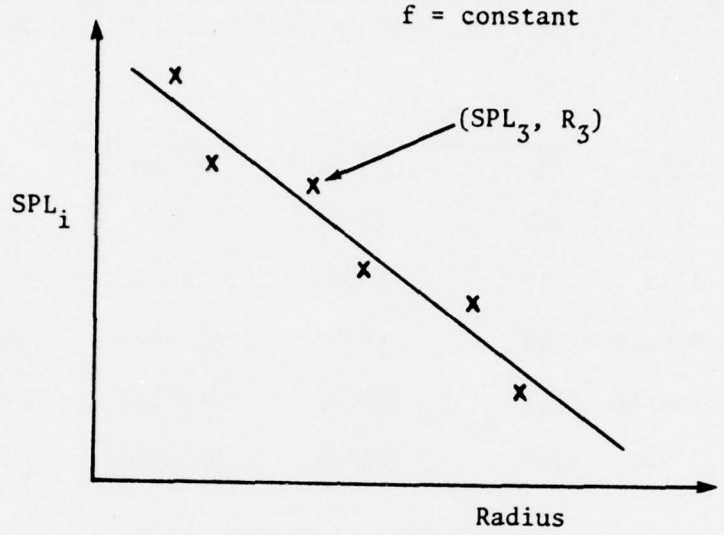

$$SPLC_i = SPL_i - 20 \log_{10}\left(\frac{R_i}{5}\right) - \alpha\,(R_i - 5)$$

(b)

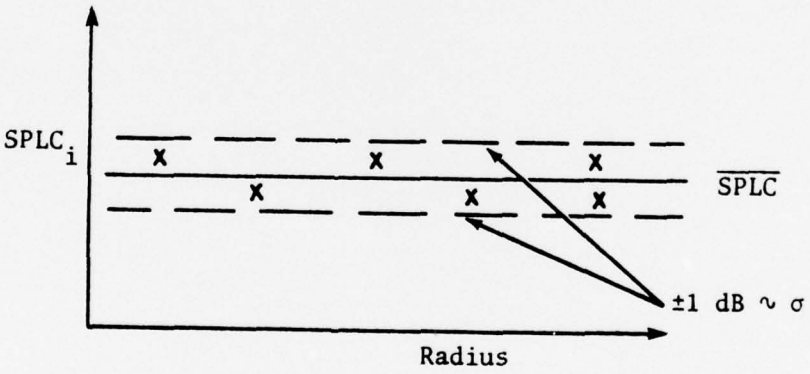

(c)

$$\sigma = \left[\sum_{i=1}^{N} \frac{(SPLC_i - \overline{SPLC})^2}{N} \right]^{\frac{1}{2}}$$

Figure 3-12. Representation of Standard Deviation Calculation from Inverse Square Law Data.

Table 3-I. Environmental Survey, Aerodynamic Points for the 14.48 cm (5.7 inch) Conical Nozzle

Test Point	PR	T_T		V_j	
		K	(° R)	m/sec	(Ft/sec)
0	0	300	(530)	0	(0)
2	1.15	300	(530)	152	(500)
5	3.9-4.13	300	(530)	433-442	(1420-1450)
37	1.1-1.12	1111	(2000)	244-259	(899-850)
42	3.7-3.8	1389	(2500)	945-960	(3100-3150)

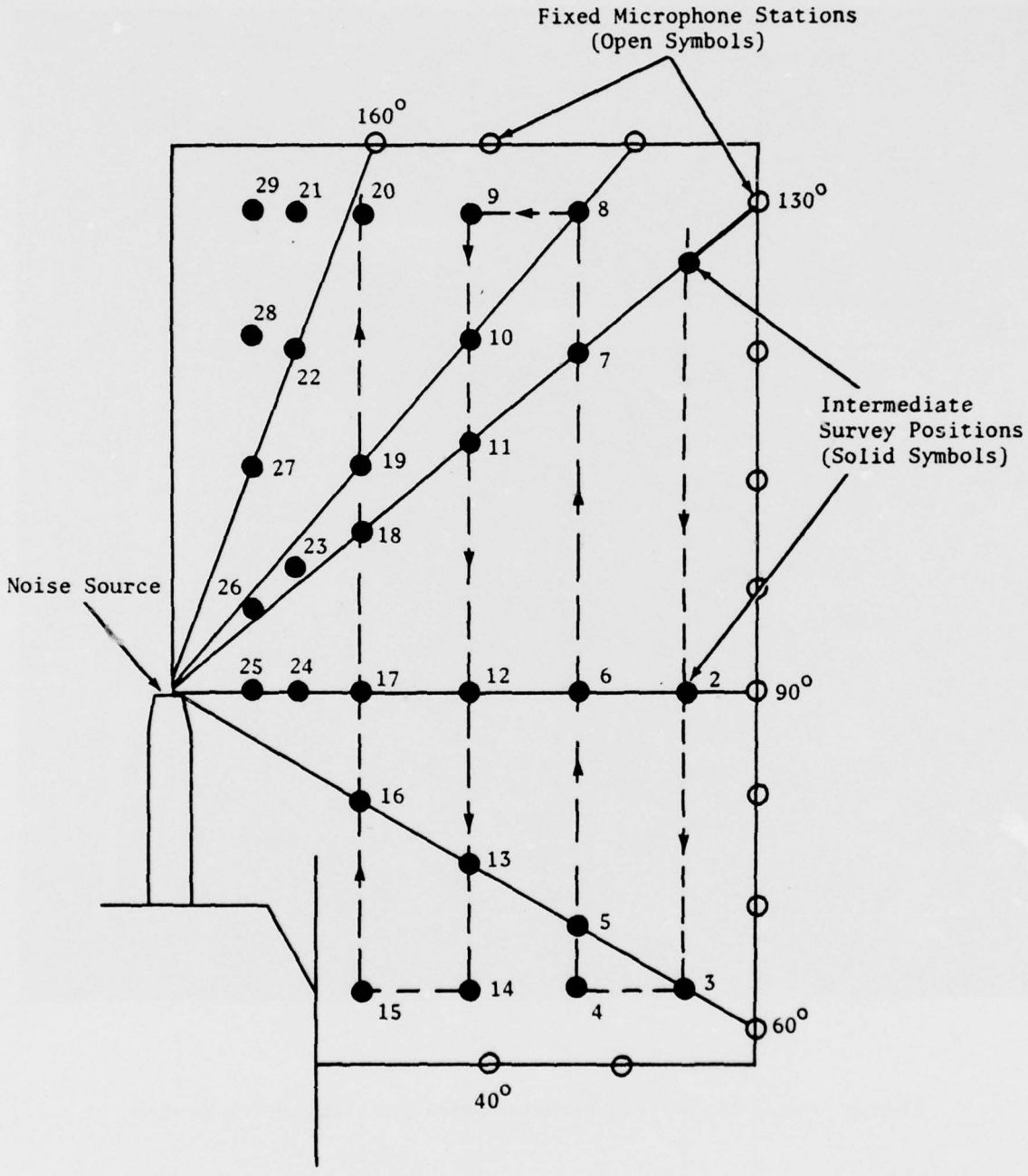

Figure 3-13. Ambient Survey Locations Inside the Anechoic Room.

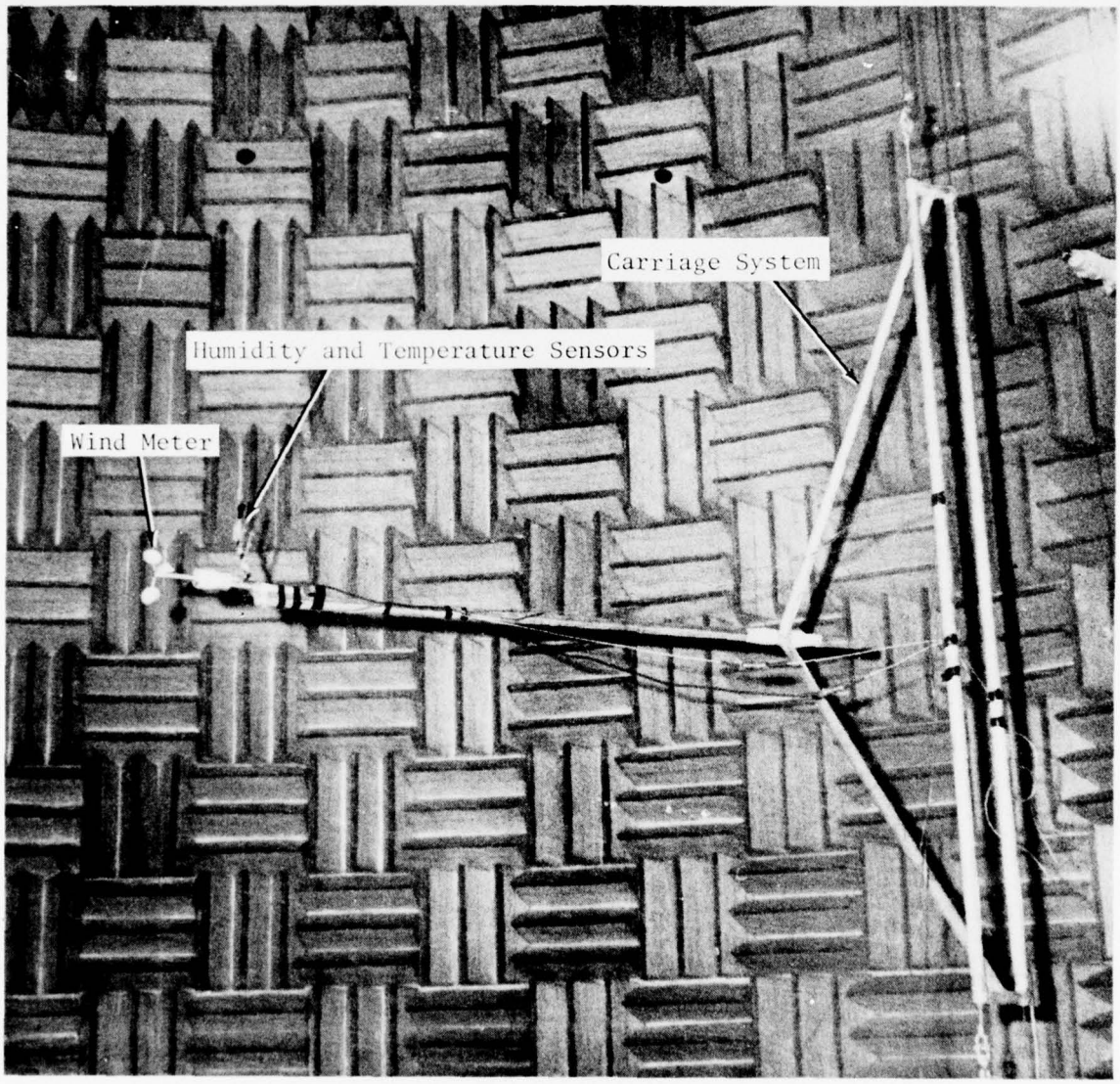

Figure 3-14. Near-Field Environmental Data Gathering System.

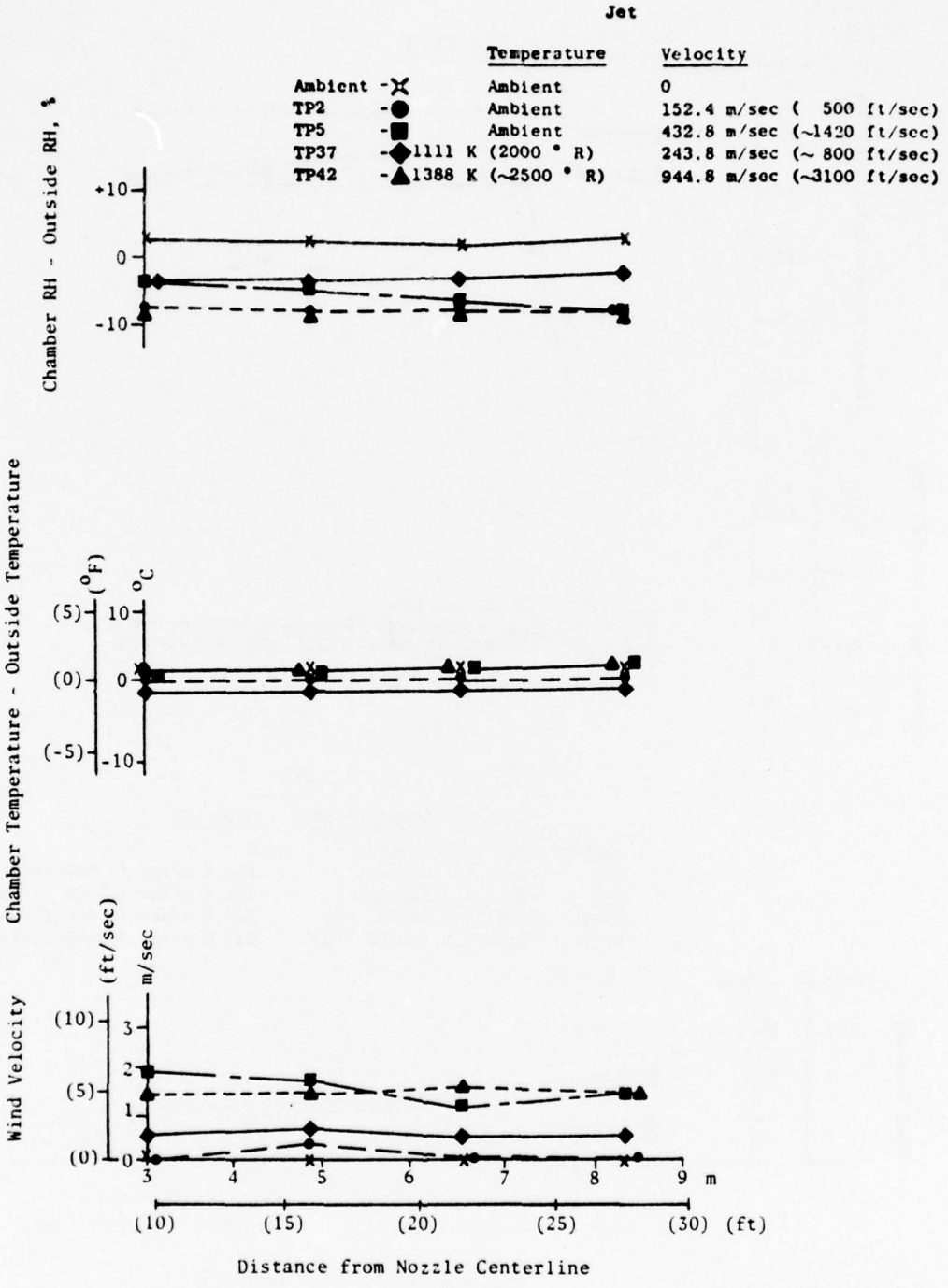

Figure 3-15. Environmental Survey Results for the 60° Microphone Station.

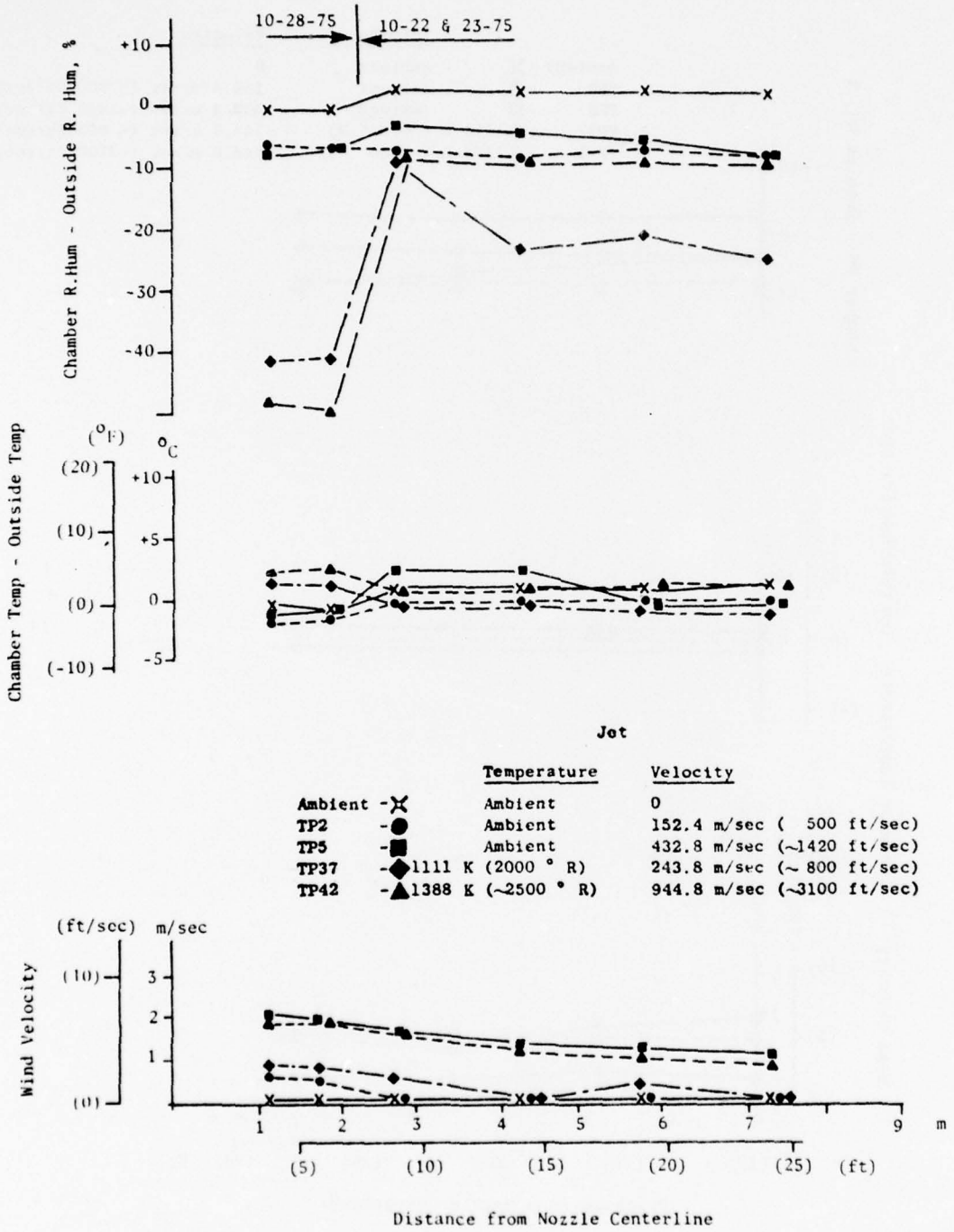

Figure 3-16. Environmental Survey Results for the 90° Microphone Station.

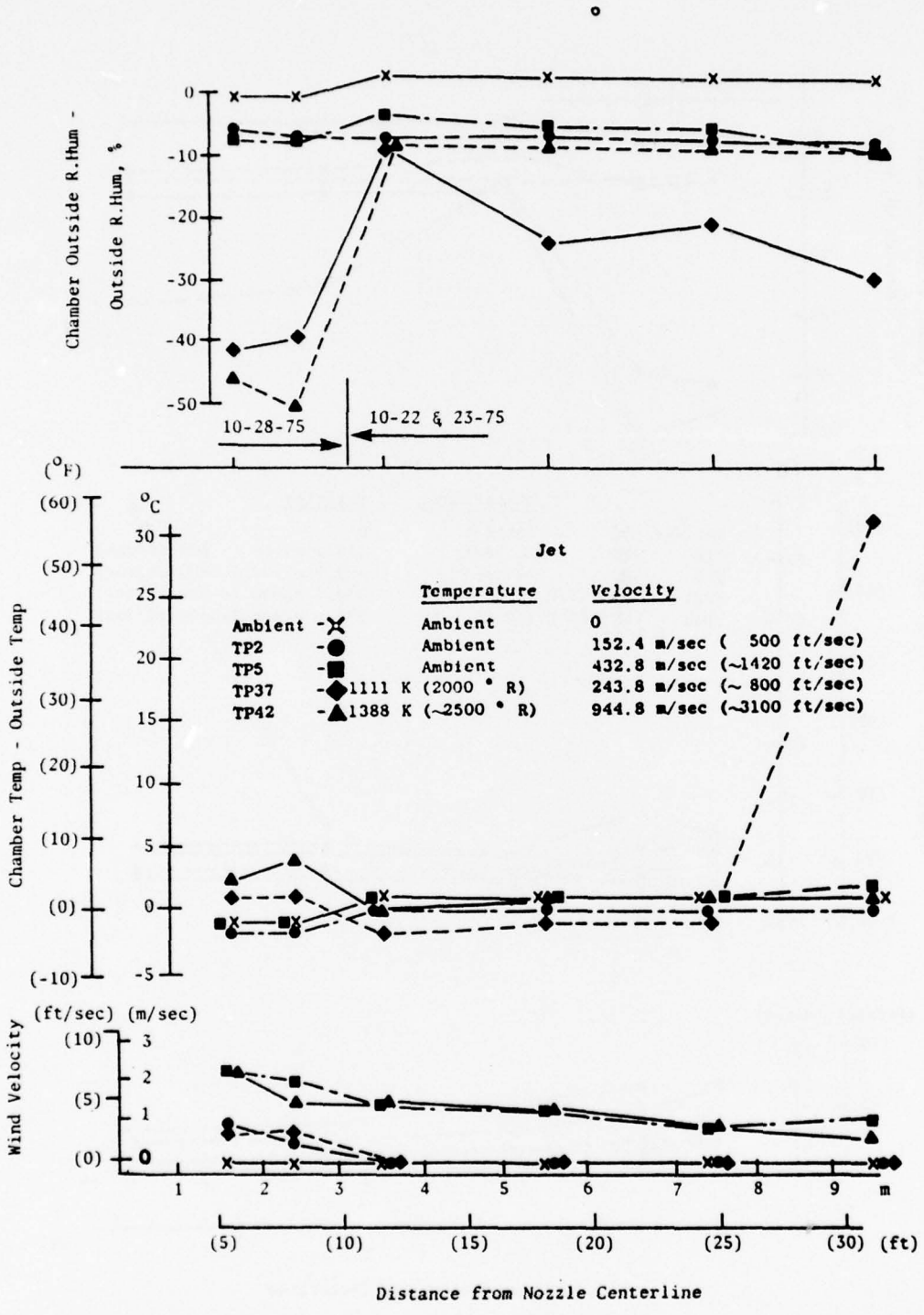

Figure 3-17. Environmental Survey Results for the 130° Microphone Station.

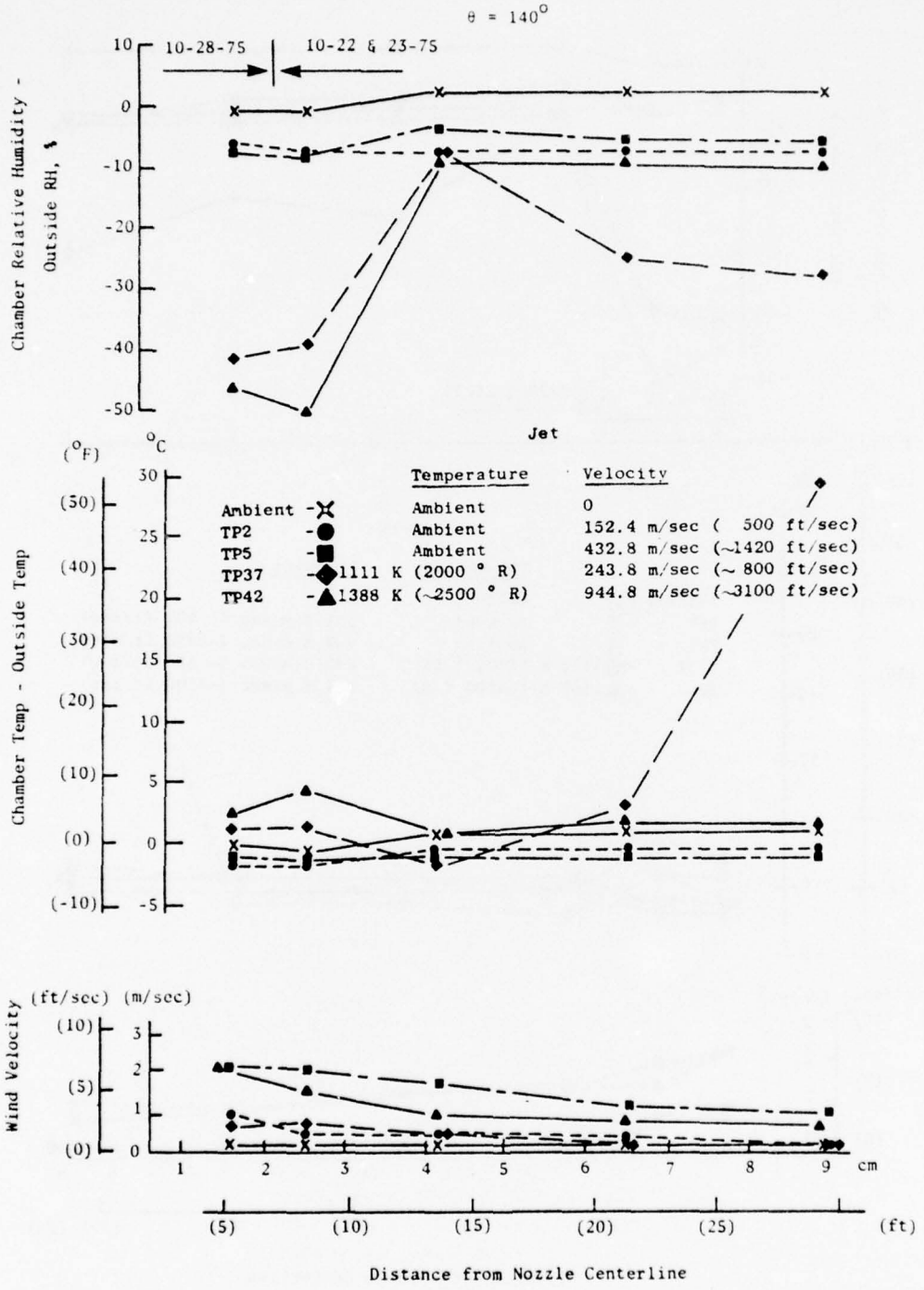

Figure 3-18. Environmental Survey Results for the 140° Microphone Station.

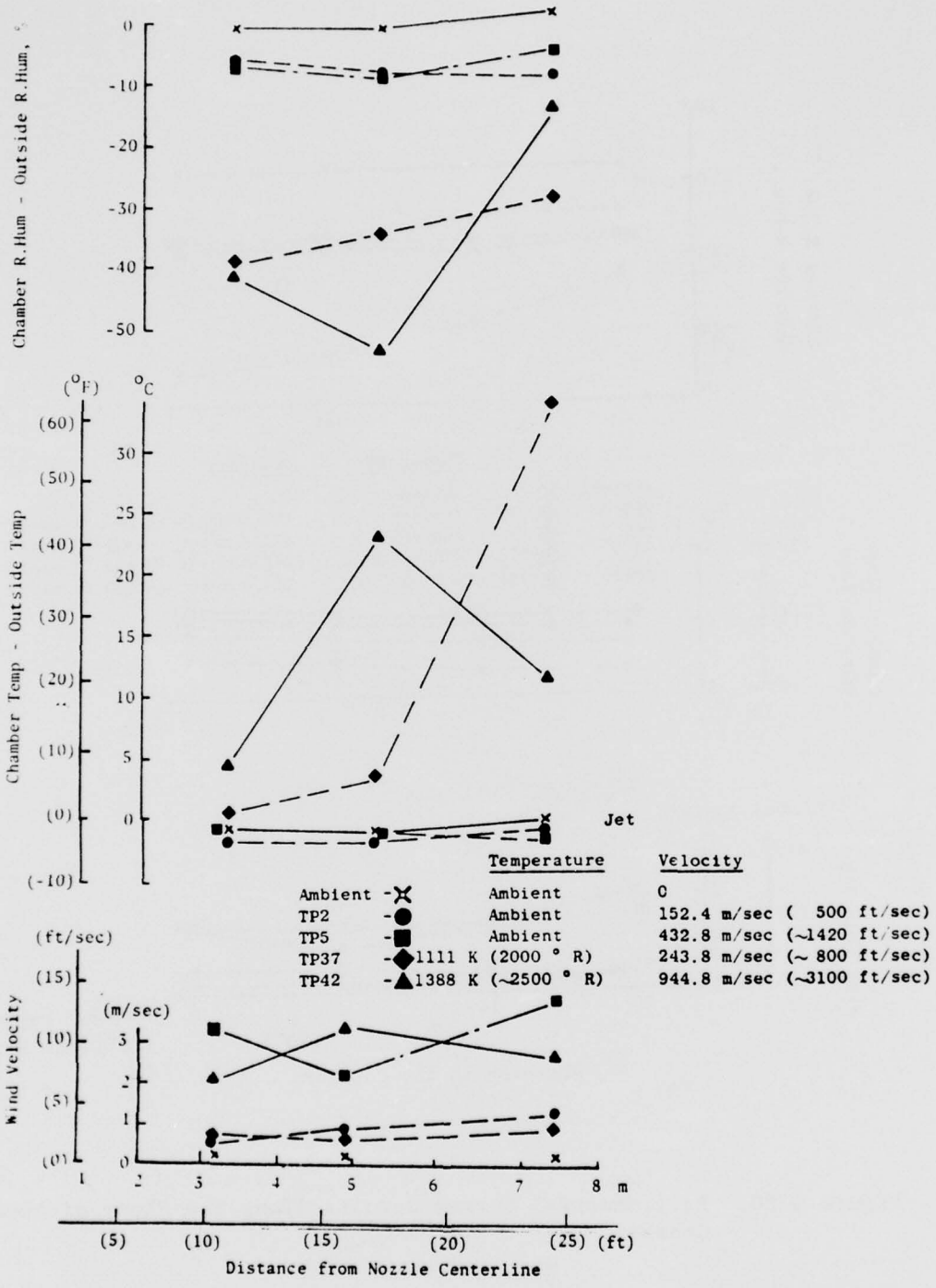

Figure 3-19. Environmental Survey Results for the 160° Microphone Station.

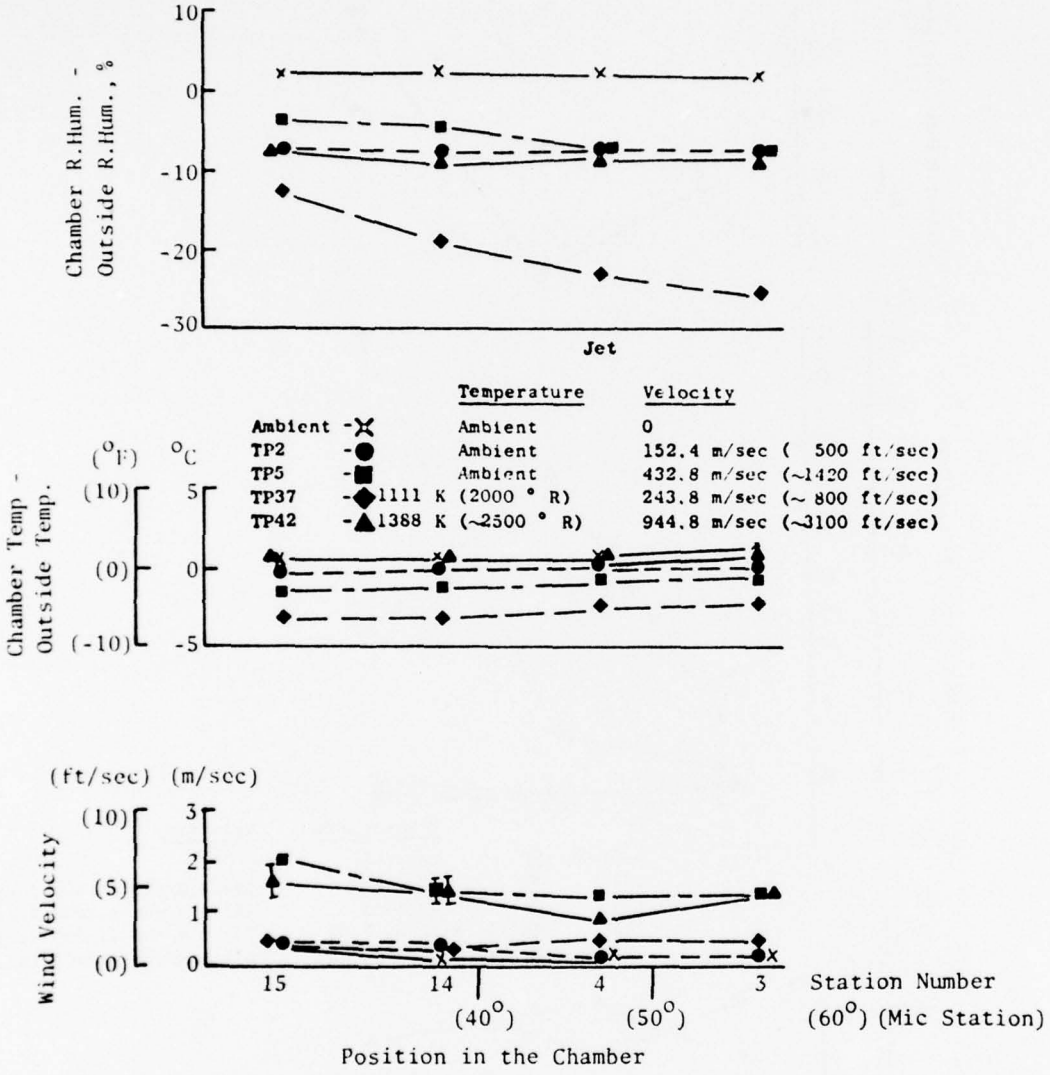

Figure 3-20. Environmental Survey Results Along the Floor of Anechoic Chamber.

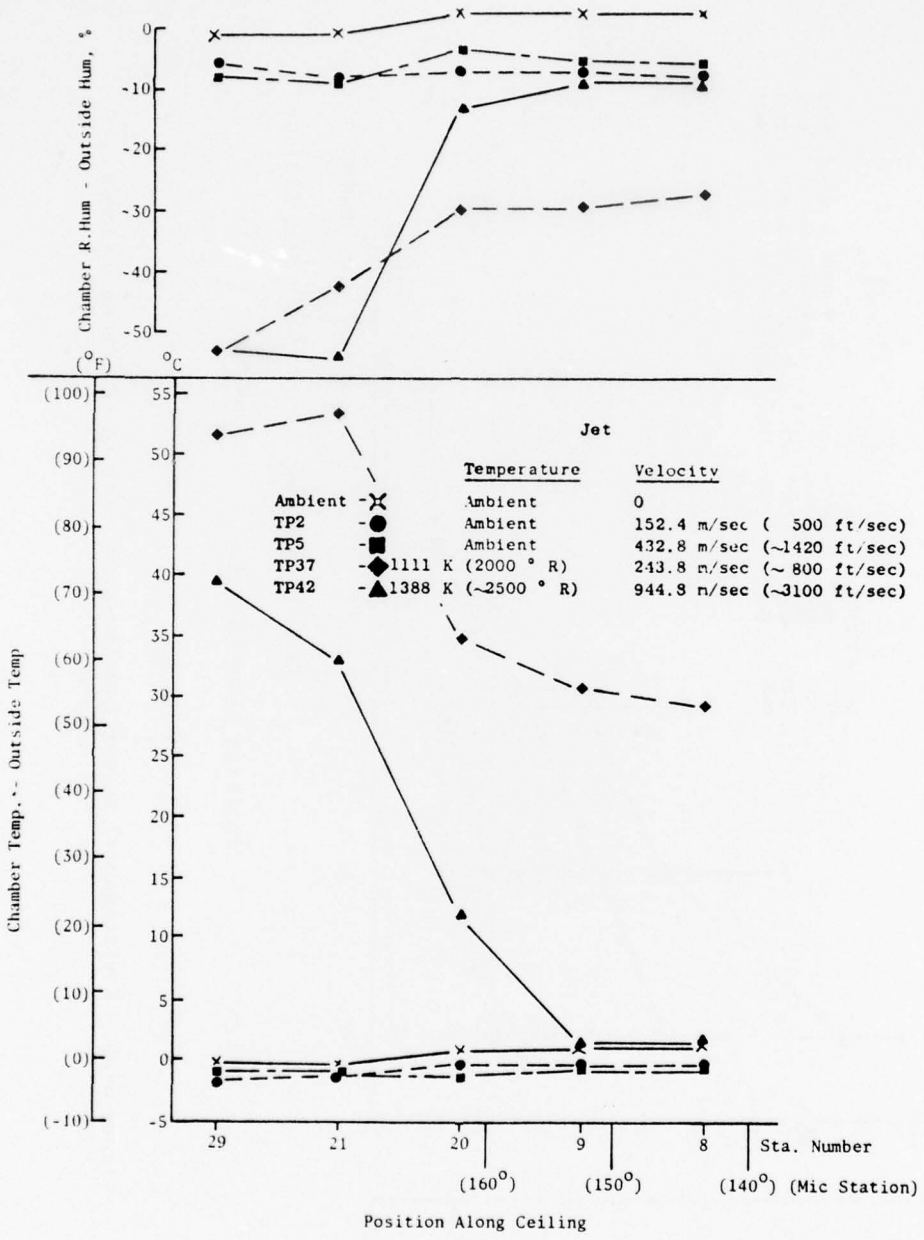

Figure 3-21. Environmental Survey Results Along Ceiling of Anechoic Chamber.

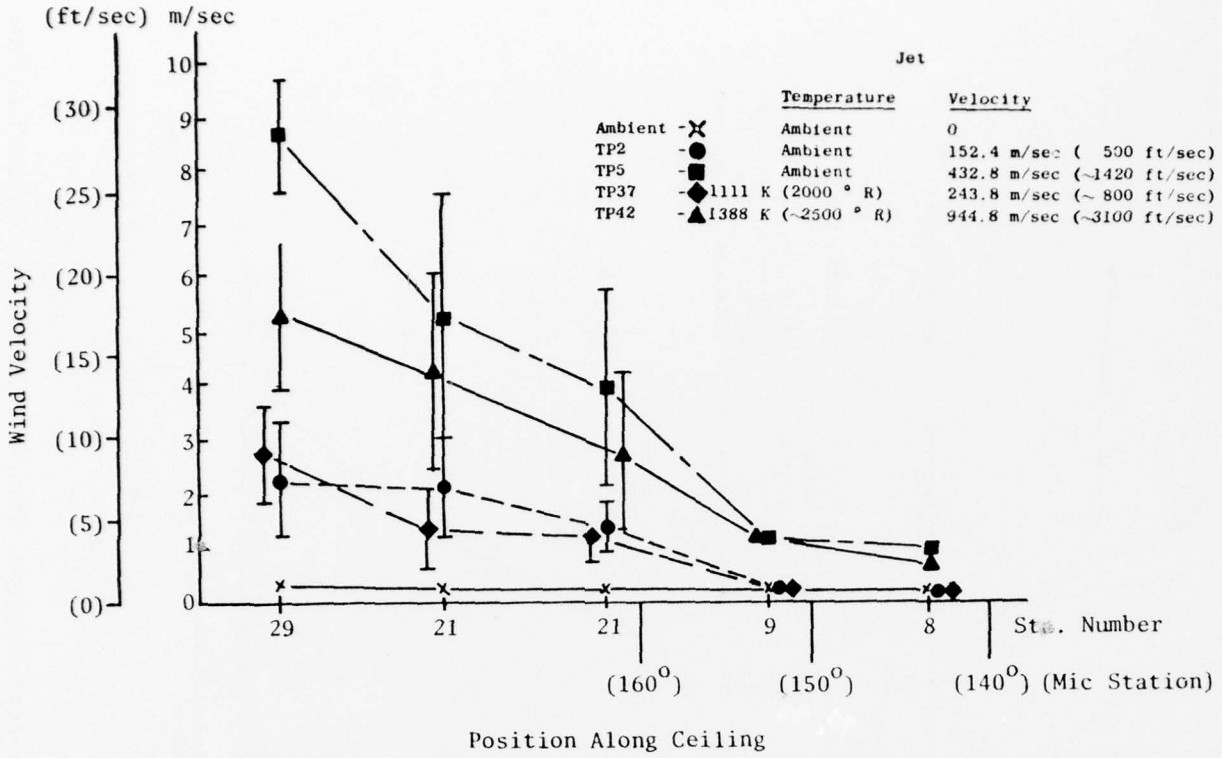

Figure 3-22. Environmental Survey Results Along Ceiling of Anechoic Chamber.

(5 ft/sec) along the traverse. Similar conditions are observed at 90° in Figure 3-16 with the exception that the relative humidity very near the jet has dropped significantly (40 to 50% RH) for the two hot-jet points. The minor rise in temperature of 2.5° C (4.5° F) can only account for about a 15% RH change, assuming a constant moisture content in the air. These extremely dry conditions occurring over the first 2 meters (7.1 ft) of traverse are probably due to some type of local mass exchange between the hot, dry, jet exhaust and the entrained flow in the chamber. The results at 130° and 140° are similar as seen in Figures 3-17 and 3-18. At the low-velocity, high-temperature point 37, a layer of hot air becomes trapped along the ceiling and in the corner of the chamber resulting in a dramatic 30° C (55° F) increase in temperature over the last 1.52 meters (5 feet). The local wind speed has increased to around 2.5 m/sec (7 ft/sec) at these angles. Along the edge of the jet plume at 160°, substantial temperature and humidity gradients occur for hot jet conditions, as seen in Figure 3-19. The entrained wind velocity varies between 2.5 m/sec (7 ft/sec) and 5 m/sec (14 ft/sec) along the ray to the far-field microphone. Uniform profiles are obtained along the false floor and along the ceiling (at ambient jet temperature) in Figures 3-20, 3-21, and 3-22, respectively. The rapid increase in the ambient temperature as the plume is approached at hot operating conditions is observed in Figures 3-21 and 3-22. Inside the 160° microphone, a 58.5 K (105° R) rise in ambient temperature is observed at the 1389 K (2500° R) jet point. High entrainment velocities between 7.6 to 9.75 m/sec (25 to 32 ft/sec) also are recorded in the neighborhood of the exhaust cowling at the cold, high velocity point.

The existence of gradients in humidity, temperature, and wind velocity obviously have an effect on the refraction of sound, the ambient speed of sound, and the air attenuation. With the exception of the low jet-velocity, high temperature conditions, all of the gradients along the sound propagation path are considered acceptable. The impact of these small environmental fluctuations on the precision of the air attenuation corrections is discussed in Section 4.8.

3.4 NEAR- AND FAR-FIELD REGIONS DURING JET OPERATION

In order to determine the transition of the near-field regions to far-field regions of an extended sound source, spherical divergence measurements were made using the pulley system described in Section 3.2 with the jet operating. Such testing establishes the largest size nozzle that can be tested in the far-field region of the noise field with the microphone stations as currently set up. The distances from the jet exhaust centerline to the respective microphone stations are given in Table 2-I.

Measurements were obtained with both a 5.08-cm (2-inch) diameter nozzle operating at ambient temperature and pressure ratios of 1.89 and 4.0 and with a 14.48-cm (5.7-inch) diameter nozzle operating at ambient and elevated temperatures at pressure ratios of 1.2 and 4.0. The actual test matrix for both of these nozzles is given in Table 3-II. Data were collected using a

Table 3-II. Test Matrix of Jet Nozzles.

Angle	Nozzle Size cm	Nozzle Size (in.)	Data Point	Press. Ratio	Temperature K	Temperature (°R)	V_j m/sec	V_j (ft/sec)
160°	5.08	2	4	1.89	303	(577)	488	(1077)
		2	5	4.1	307	(585.5)	691	(1524)
90°	14.49	(5.7)	2	1.12	301	(575.9)	213	(470.2)
	↓	(5.7)	4	1.87	237	(459.7)	430	(950.2)
		(5.7)	5	3.9	304	(579.8)	680	(1501.8)
		(5.7)	37	1.04	956	(1753)	335	(740.1)
		(5.7)	42	3.8	1529	(2782.8)	1501	(3310.5)
		(5.7)	42A	2.6	1274	(2324.6)	1151	(2626.1)
130°	14.49	(5.7)	2	1.13	301	(575.0)	223	(492.6)
	↓	(5.7)	4	1.89	301	(575.4)	487	(1074.4)
		(5.7)	5	4.03	301	(575.9)	683	(1507.8)
		(5.7)	37	1.09	907	(1664.2)	311	(687.8)
		(5.7)	42	4.08	1262	(2663.4)	1498	(3304.6)
		(5.7)	42A	2.89	1163	(2123)	1182	(2608.4)
140°	14.49	(5.7)	2	1.15	303	(577.6)	238	(525.3)
	↓	(5.7)	4	1.98	311	(593.3)	509	(1123.3)
		(5.7)	5	3.92	310	(590.1)	686	(1513.0)
		(5.7)	37	N/A	N/A	N/A	N/A	N/A
		(5.7)	42	4.09	1377	(2504.6)	1452	(3202.2)
		(5.7)	42A	2.85	1190	(2174.2)	1190	(2624.1)
160°	14.49	(5.7)	2	1.13	304	(578.7)	220	(486.8)
	↓	(5.7)	4	1.8	304	(579.5)	473	(1043.5)
		(5.7)	5	3.85	304	(578.1)	675	(1490.6)
		(5.7)	37	1.08	820	(1507.7)	293	(647.1)
		(5.7)	42	3.94	1498	(2727.4)	1501	(3310.8)
		(5.7)	42A	2.78	1250	(2281.1)	1207	(2662.4)

reference microphone 1.52 meters (5 feet) away from the jet noise source to monitor the source intensity and along the path between the reference microphone and the room microphone station of interest. The traverse was made using the cable/pulley system, described in Section 3.2, to guide the roving microphone along its designated path.

An example of a typical noise field as a function of distance away from the nozzle is shown in Figure 3-23 to clarify the methodology used in determining the near- and far-field noise regions. This figure depicts that the source sound pressure level in the flow field is high and more or less of constant amplitude. This region is dominated by pseudosound fluctuations that frequently are hydrodynamic in nature and are explored by pressure-sensitive devices such as acoustic probes and Kulites. Further away from the source, the geometric near field of the jet is maintained because of the source distribution which finally transitions into the far-field acoustic region where the inverse square law is obeyed. Because of these phenomena, a tolerance band of ±1 dB is drawn about the ideal $1/r^2$; all the data contained within this band are defined to be in the far field. A departure by 1 dB of the ideal $1/r^2$ is defined as the onset of the far-field noise region, shown by an asterisk in Figure 3-23.

The acoustic data of the traverses was reduced in 1/3-octave bands and corrected for air attenuation using the relationships from the Bass, Bauer, and Evans equations (Reference 4) with the front-edge, 1/3-octave filter frequency representing the average 1/3-octave value as recommended in ARP866A (Reference 3). These corrections were applied when they amounted to 0.5 dB or more, which occurred around the 20 kHz frequency region. Next, a best-fit $1/r^2$ dahed line was drawn through these data favoring the data from the last microphone positions (those farthest away from the jet nozzle), since those were most likely to be in the far-field acoustic region. The extent of the traverse for the 5.8 cm (2 in.) jet was 30 to 150 X/D (where X/D is the ratio of the distance from the nozzle to the nozzle diameter) and an X/D of 10.5 to 52.6 for the 14.5 cm (5.7 in.) jet.

Figures 3-24 through 3-26 show the 160°-angle results for a 2-inch jet nozzle operating at ambient temperatures and a pressure ratio of ∿4.0. For frequencies above 2000 Hz, the far field generally extends beyond 30 diameters from the nozzle. The electronic noise floor was encountered in the 40 kHz to 100 kHz frequency region as seen in Figure 3-26. These data were recorded on tape using the IRIG Wideband Group II mode at 30 ips, which has a 33 dB dynamic range (see Table 3-III). To alleviate this problem during certification, the tape recorder was changed to IRIG Wideband Group I at 120 ips, where the noise floor is 51 dB down from the maximum overall level.

Figures 3-27 through 3-29 show the 160° angle data at a jet total temperature of 321 K (578° R) and jet velocity of 455 m/sec (1490 ft/sec) with a 14.5-cm (5.7-inch) conical nozzle. For frequencies from 400 Hz to 5000 Hz, the onset of the far-field region occurs about 32 to 42 diameters from the jet nozzle. At high frequencies, the far-field region extends beyond 10 diameters from the nozzle.

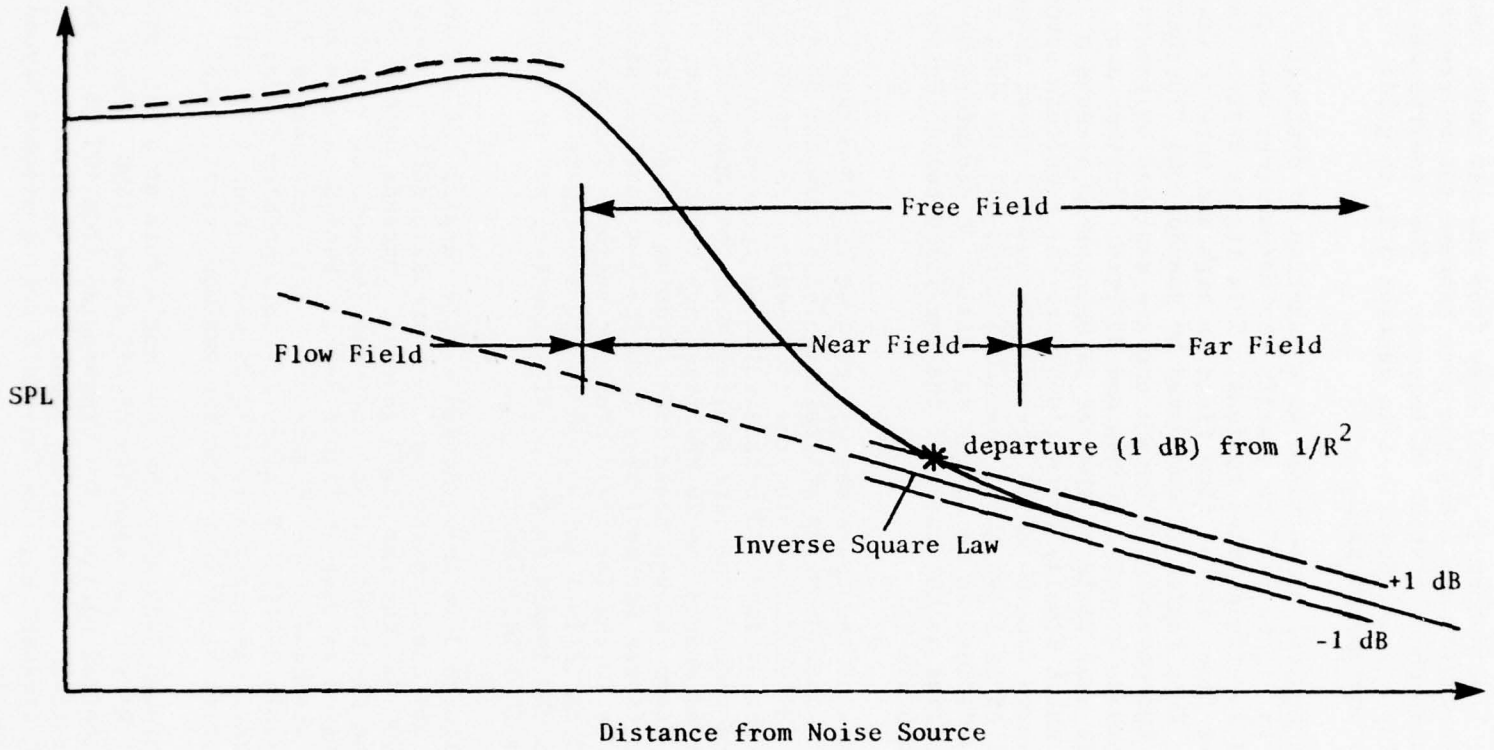

Figure 3-23. Typical Behavior of Sound with Distance from a Source.

- 47% Relative Humidity
- 13.3° C (56° F) Ambient Temperature

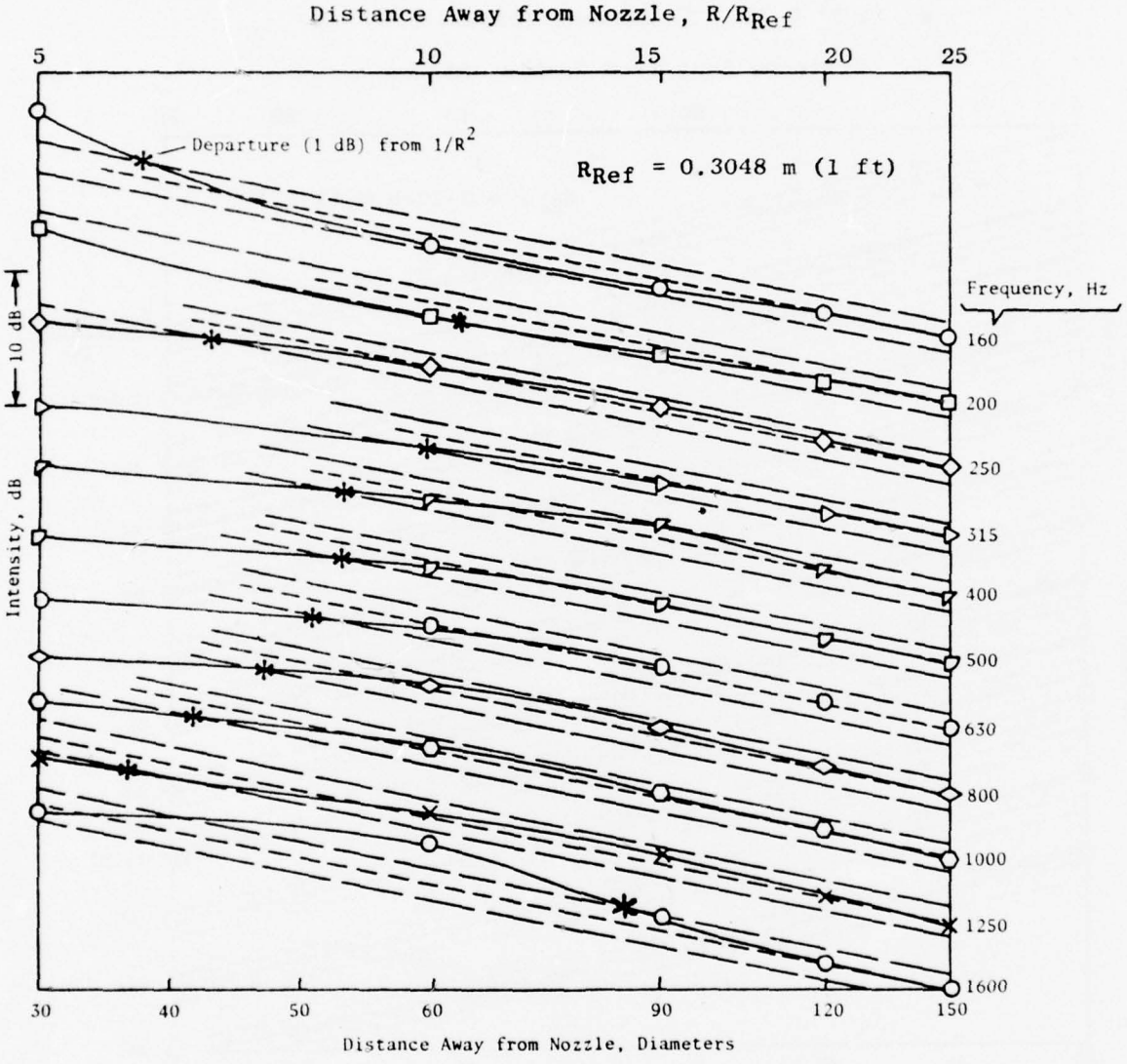

Figure 3-24. Inverse Square Law Tests with a 5 cm (2 in.) Nozzle (PR = 4.0 Cold) for the 160° Microphone Station at Low Frequency.

- 47% Relative Humidity
- 13.3° C (56° F) Ambient Temperature

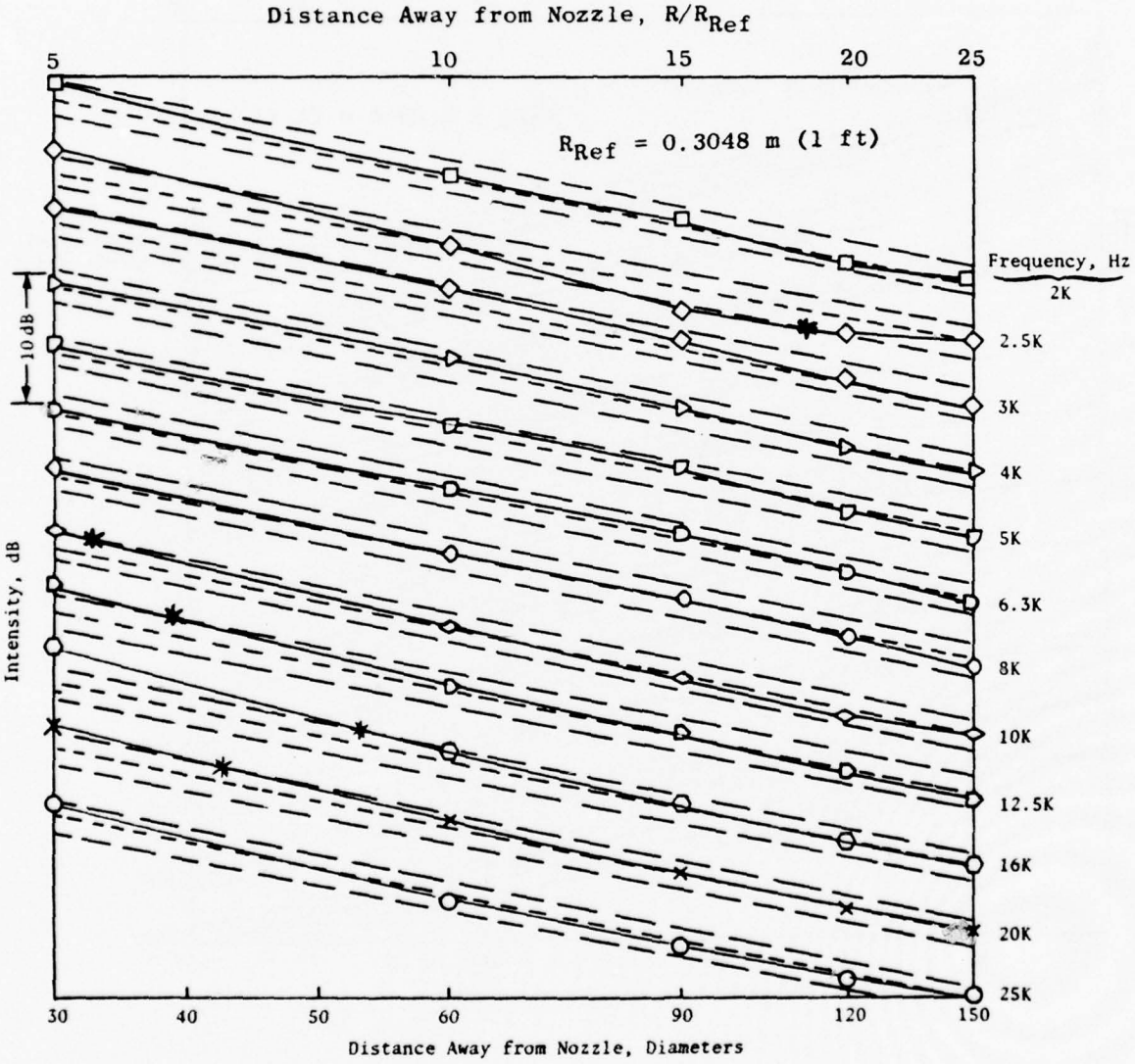

Figure 3-25. Inverse Square Law Tests with a 5 cm (2 in.) Nozzle (PR = 4.0 Cold) for the 160° Microphone Station at Intermediate Frequency.

- 47% Relative Humidity
- 13.3° C (56° F) Ambient Temperature

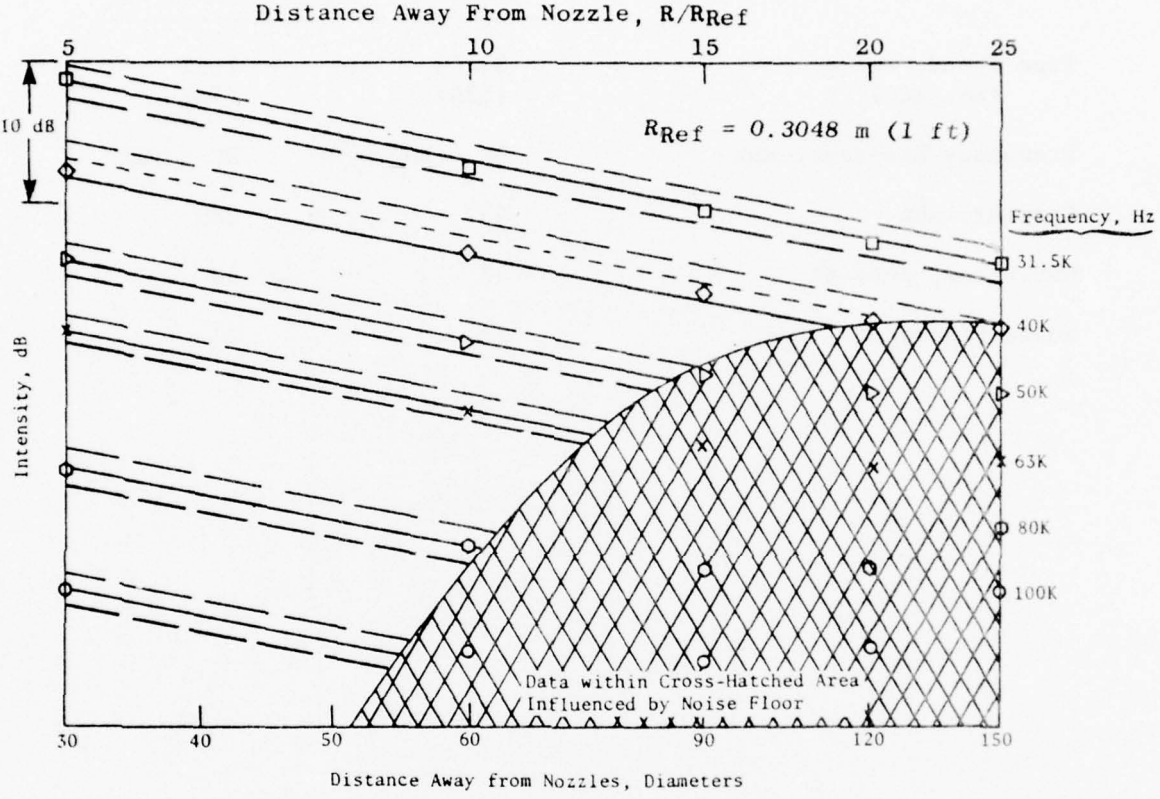

Figure 3-26. Inverse Square Law Tests with a 5 cm (2 in.) Nozzle (PR = 4.0 Cold) for the 160° Microphone Station at High Frequency.

Table 3-III. FM Tape Recorder Wideband Group I and II Specifications

	FM TAPE MODE	
	GROUP I	GROUP II
Tape Speed, cm/sec (in./sec)	30.48 (120)	7.62 (30)
Frequency Response, kHz	DC - 80	DC - 125
Carrier, kHz	432	225
Deviation, percent	40	40
Noise Floor, dB	51	33

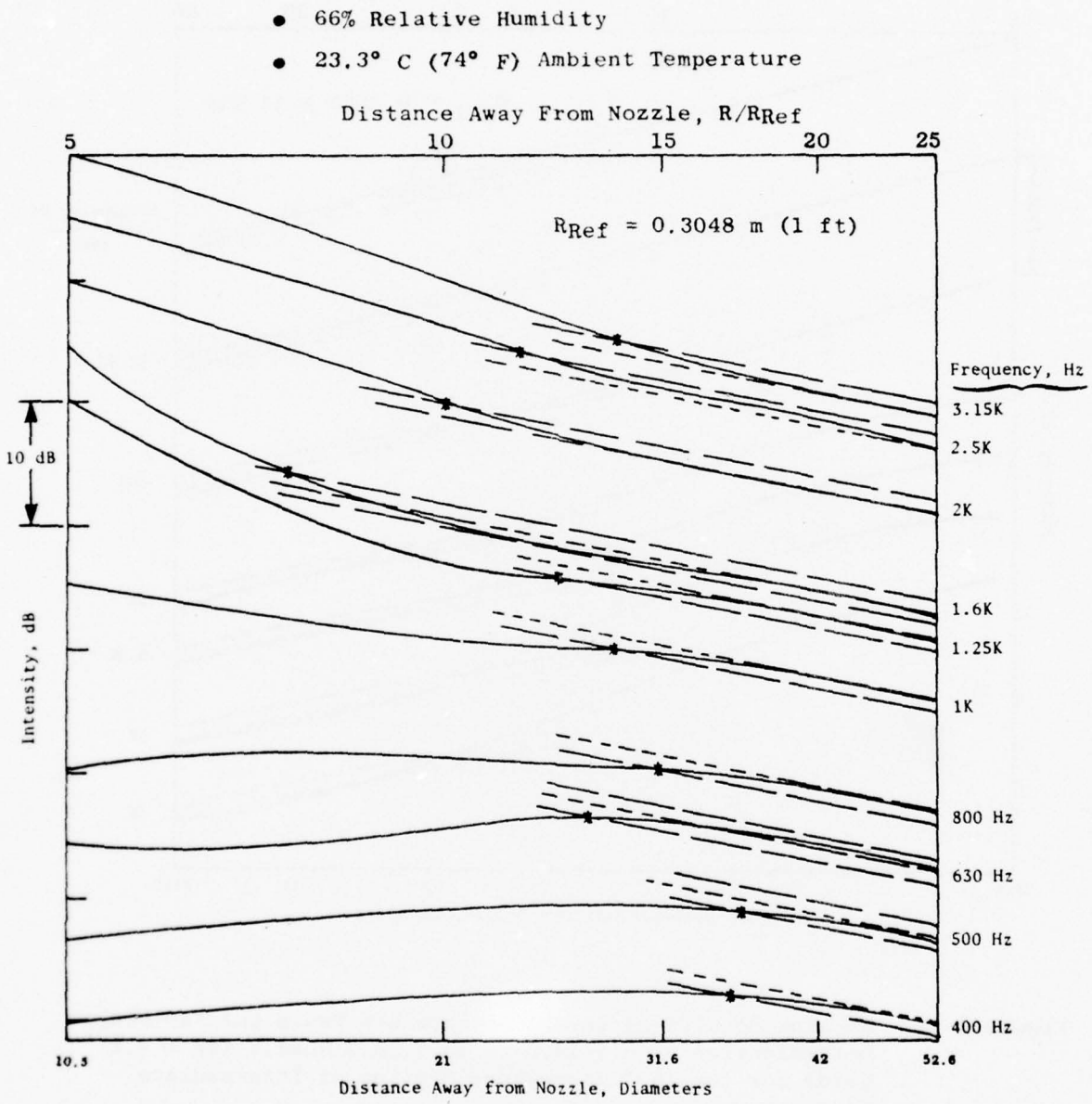

Figure 3-27. On-Line Results of Inverse Square Law Tests and Far-Field Determination with a 14.5 cm (5.7 in.) Nozzle (PR = 4.0 Cold) for the 160° Microphone Station at Low Frequency.

- 66% Relative Humidity
- 23.3° C (74° F) Ambient Temperature

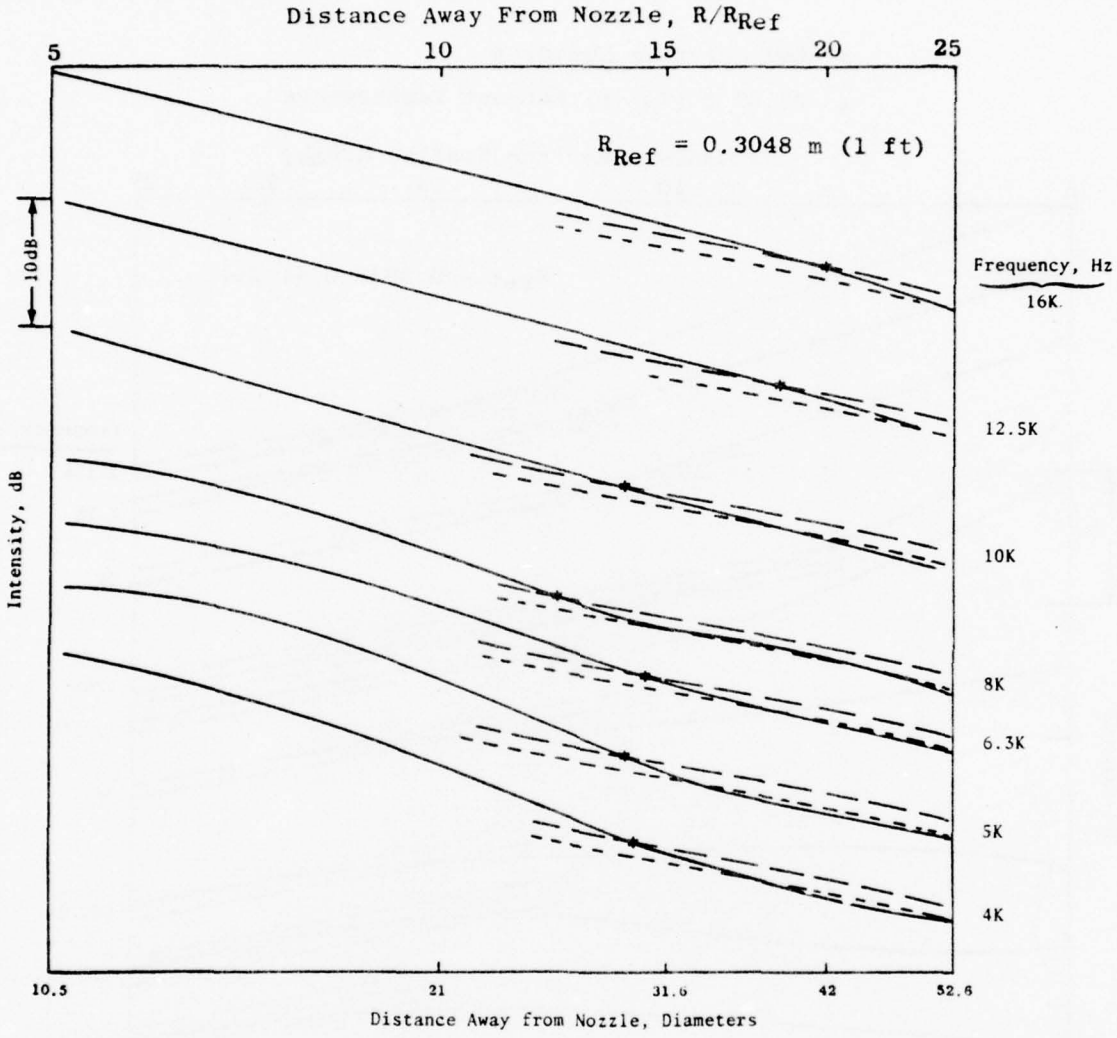

Figure 3-28. On-Line Results of Inverse Square Law Tests and Far-Field Determination with a 14.5 cm (5.7 in.) Nozzle (PR = 4.0 Cold) for the 160° Microphone Station at Intermediate Frequency.

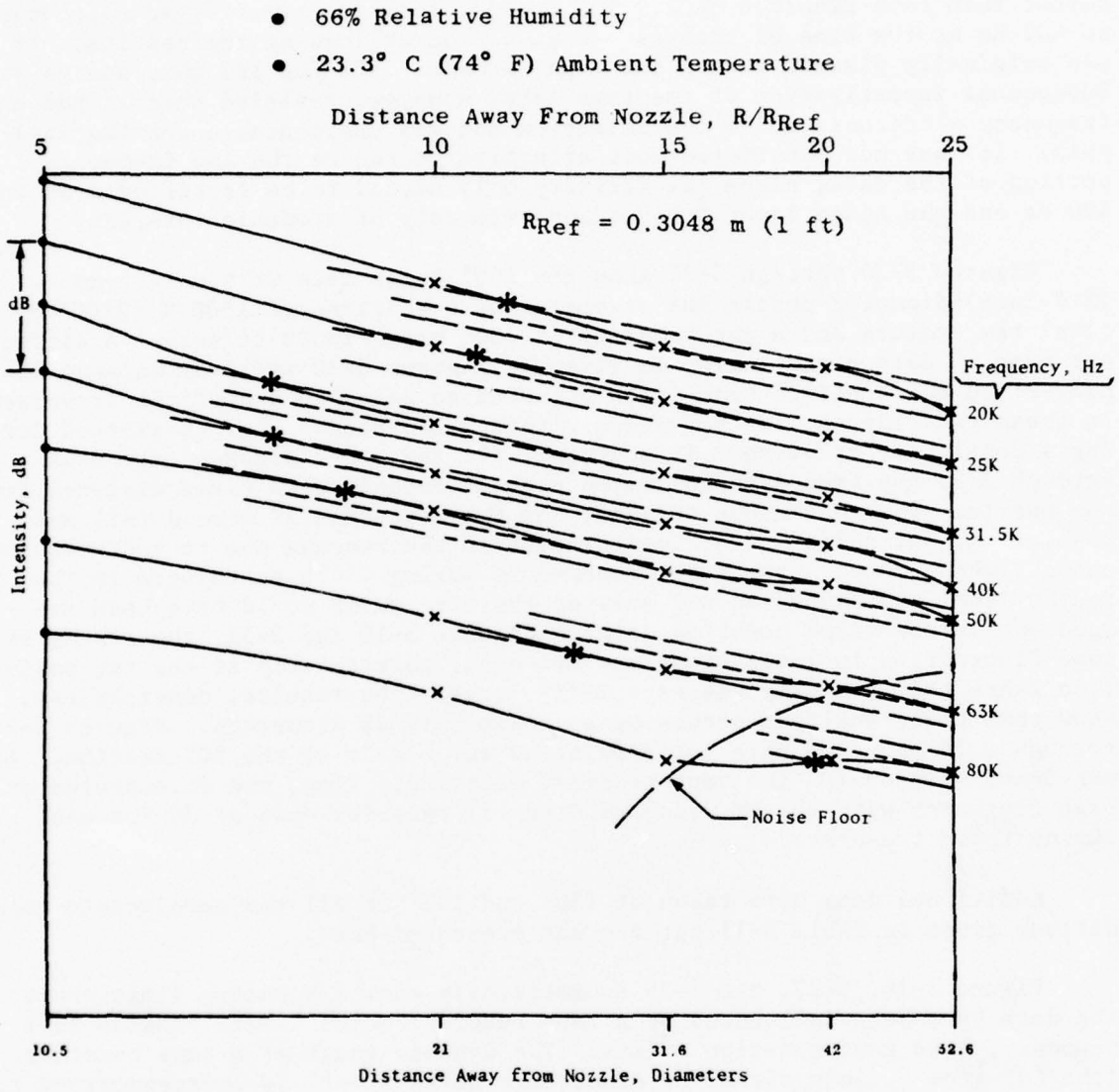

Figure 3-29. On-Line Results of Inverse Square Law Tests and Far-Field Determination with a 14.5 cm (5.7 in.) Nozzle (PR = 4.0 Cold) for the 160° Microphone Station at High Frequency.

Lower frequency data (less than 400 Hz) are missing from some of the 14.5 cm (5.7 in.) nozzle plots because "on-line" 1/3-octave spectra were used rather than tape recorded data. The on-line spectra were plotted only down to 400 Hz at the time of the test to give a quick look at the results. It was originally planned to use the tape recorded data for all this analysis. Subsequent investigation of the tape data, however, revealed that it had high frequency electronic noise contamination and was unacceptable for the analysis. It was not considered cost effective to reduce the low frequency portion of the data, since the facility only needed to be certified down to 400 Hz and the added lower frequencies were only of academic interest.

Figures 3-30 through 3-32 show the 160° angle data with a 14.5-cm (5.7-inch)-diameter nozzle but at operating conditions of 1500 K (2700° R) total temperature and a jet velocity of 1006 m/sec (3300 ft/sec). A different type of data presentation is given in Figures 3-30 and 3-31 because the near-field to far-field transition occurred so near the end of the traverse. In these two figures, the variation within a 1/3-octave band is plotted during a continuous traverse. In contrast, all the other figures from 3-24 through 3-35 are from data collected over 32 seconds at a fixed distance from the nozzle. The continuous traverse has the advantage of more detail and resolution, but suffers from inaccuracies in the average due to instantaneous changes which occur when the microphone is moving (such as changes in the source level and vibration and sway of the wire which would have been averaged out in the fixed position data). Figures 3-10 and 3-31, therefore, show some fluctuation in level along the traverse, particularly at the far position where the wire sway was especially large. The results, nevertheless, show that the transition occurs at approximately 48 diameters. Figures 3-34 through 3-35 show the same jet conditions and nozzle at the 90° station. As mentioned previously, the tape recorder electronic floor was encountered at high frequency with the FM wideband Group II recorder mode at 30 ips used during these traverses.

Additional data were taken at 130° and 140° at all the aerodynamic conditions given in Table 3-II but are not presented here.

Figure 3-26, 3-29, and 3-35 schematically show a boundary limit where the data have been influenced by a tape recorder noise floor. Inside this boundary, data contamination exists. The dynamic range of a tape recorder (the ΔdB from maximum signal to electronic noise floor) is independent of the microphone location or jet conditions. Because of air attentuation, the jet spectra falls off more rapidly at high frequency. Since the amount of air attenuation of the jet noise increases with distance from the jet, the jet noise spectra intercepts the noise floor at lower frequency when the microphone is further away from the jet as indicated in the figures.

Figure 3-36 shows the onset of the far-field acoustic region (as measured at 90°) of the anechoic chamber, for the 14.5-cm (5.7-inch) jet operating cold at a pressure ratio of 1.89 as indicated by the asterisk on the earlier figures. In addition, data from Lockheed (Reference 5) and the University of Southern California (Reference 6) are presented for comparison.

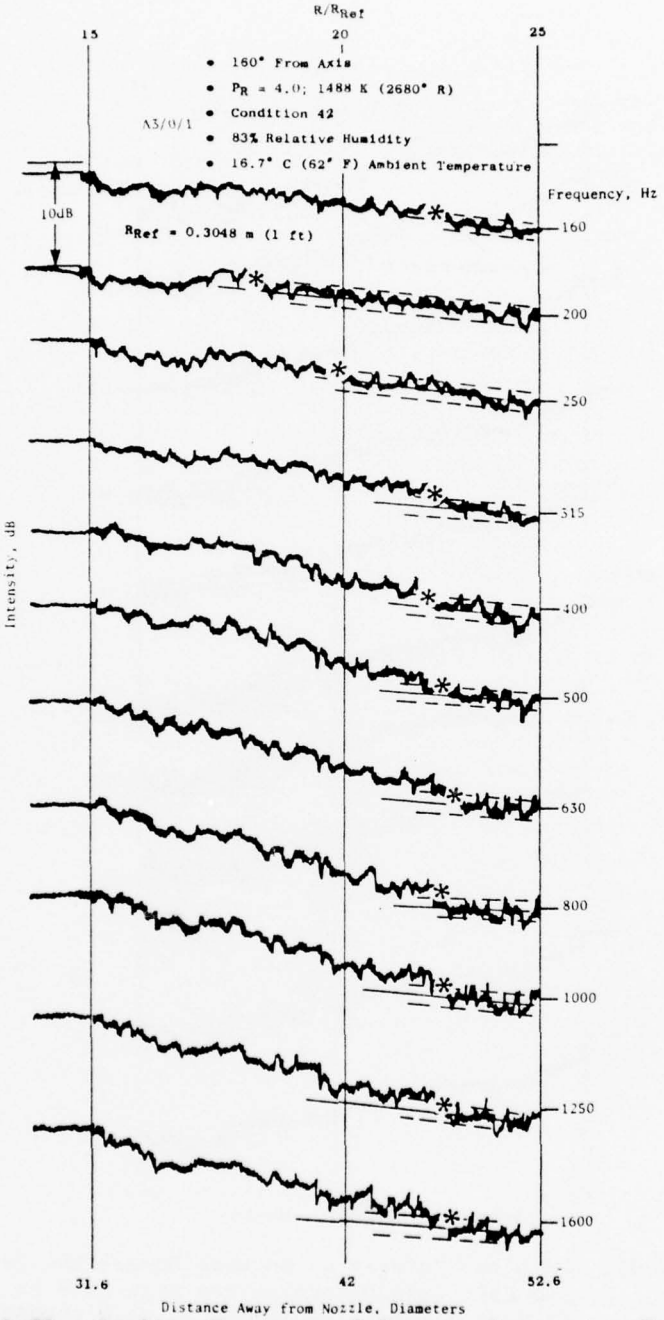

Figure 3-30. On-Line Traverse of Inverse Square Law Tests and Far-Field Determination with 14.5 cm (5.7 in.) Nozzle [PR = 4.0, 1488 K (2680° R)] for the 160° Microphone Station at Low Frequency.

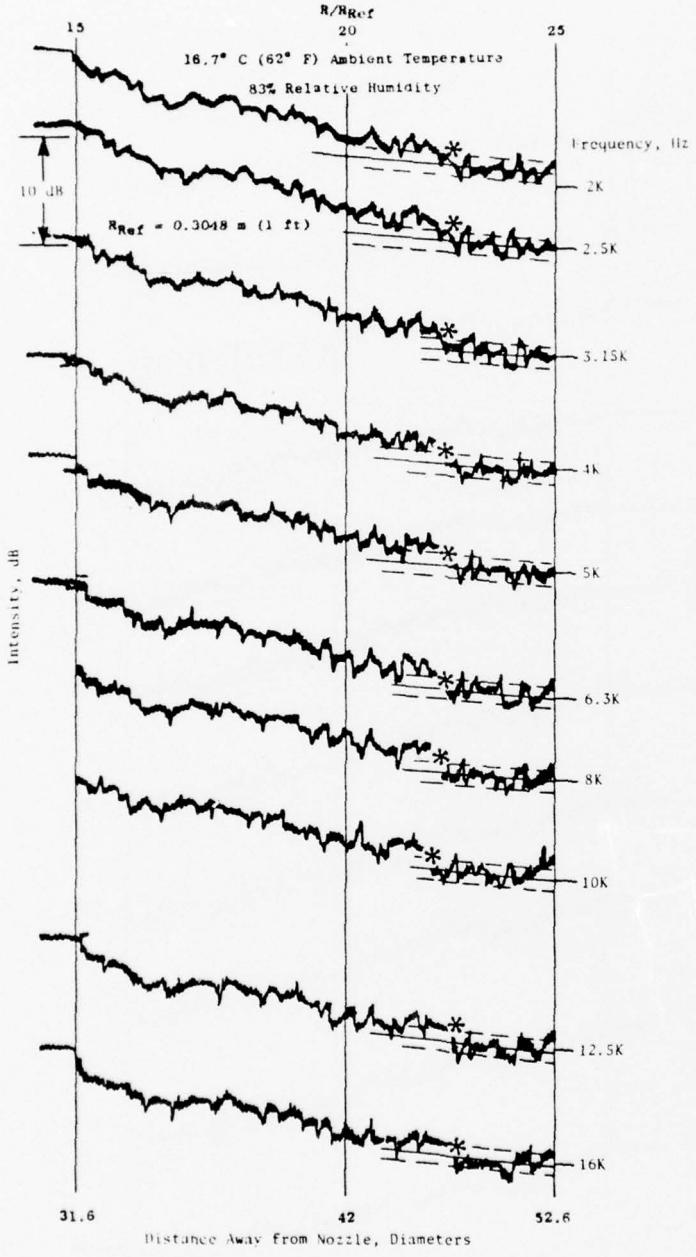

Figure 3-31. On-Line Traverse of Inverse Square Law Tests and Far-Field Determination with 14.5 cm (5.7 in.) Nozzle [PR = 4.0, 1488 K (2680° R)] for the 160° Microphone Station at Intermediate Frequency.

- 83% Relative Humidity
- 16.7° C (62° F) Ambient Temperature

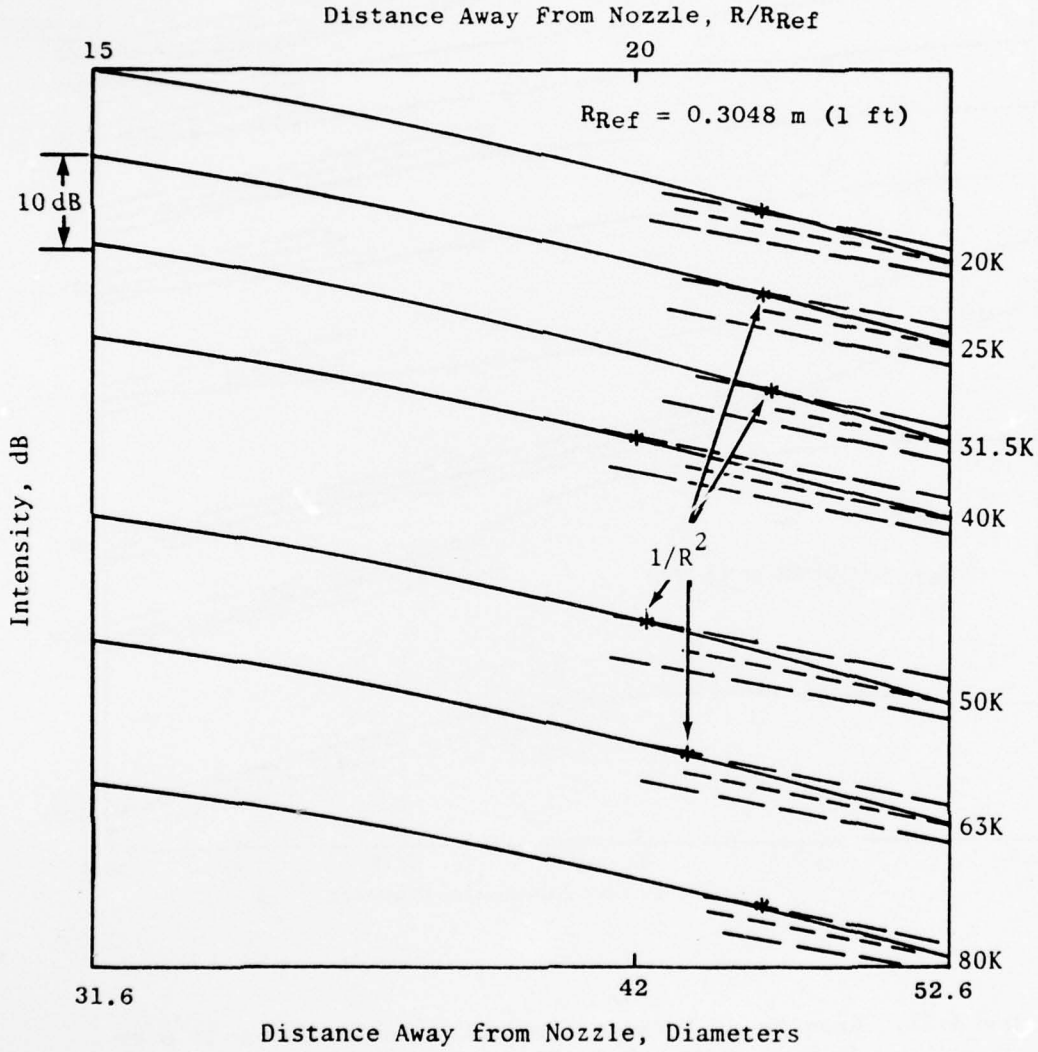

Figure 3-32. On-Line Results of Inverse Square Law Tests and Far-Field Determination with 14.5 cm (5.7 in.) Nozzle [PR = 4.0, 1488 K (2680° R)] for the 160° Microphone Station at High Frequency.

- 65% Relative Humidity
- 23.3° C (74° F) Ambient Temperature

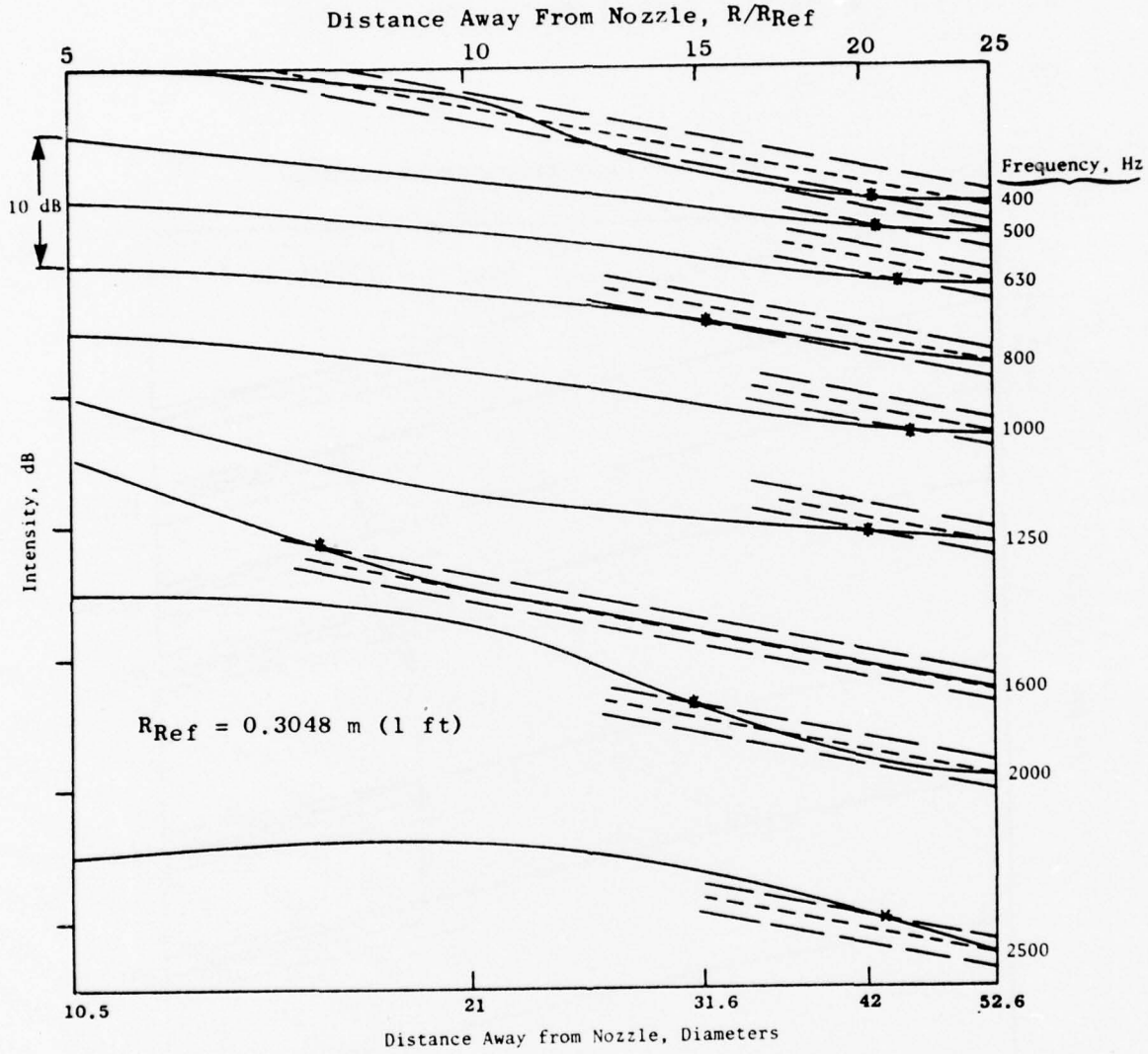

Figure 3-33. Results of Inverse Square Law Tests with a 14.5 cm (5.7 in.) PR = 3.8, 1546 K (2783° R) Jet for the 90° Angle at Low Frequency.

- 65% Relative Humidity
- 23.3° C (74° F) Ambient Temperature

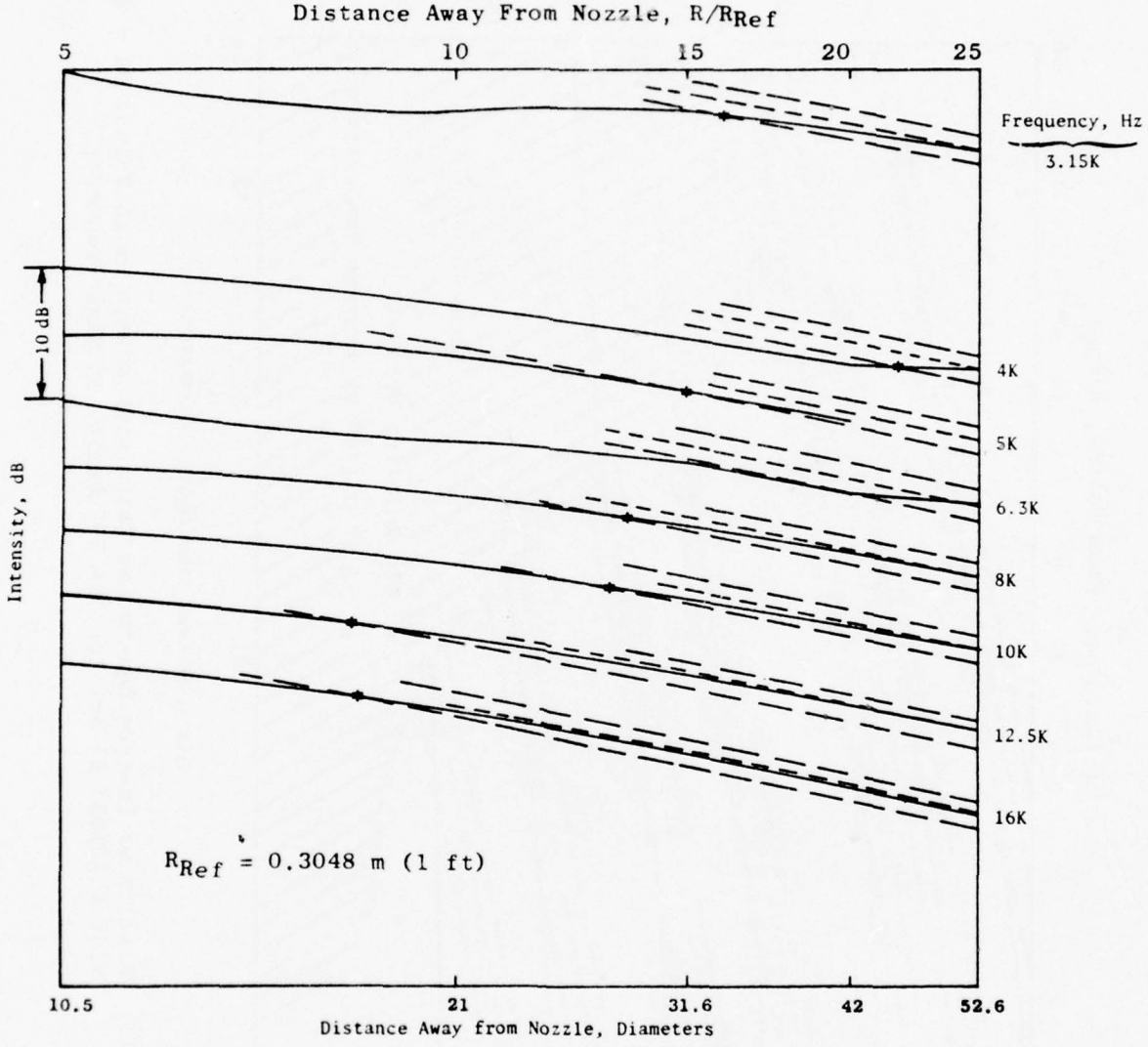

Figure 3-34. Results of Inverse Square Law Tests with a 14.5 cm (5.7 in.) PR = 3.8, 1546 K (2783° R) Jet for the 90° Angle at Intermediate Frequency.

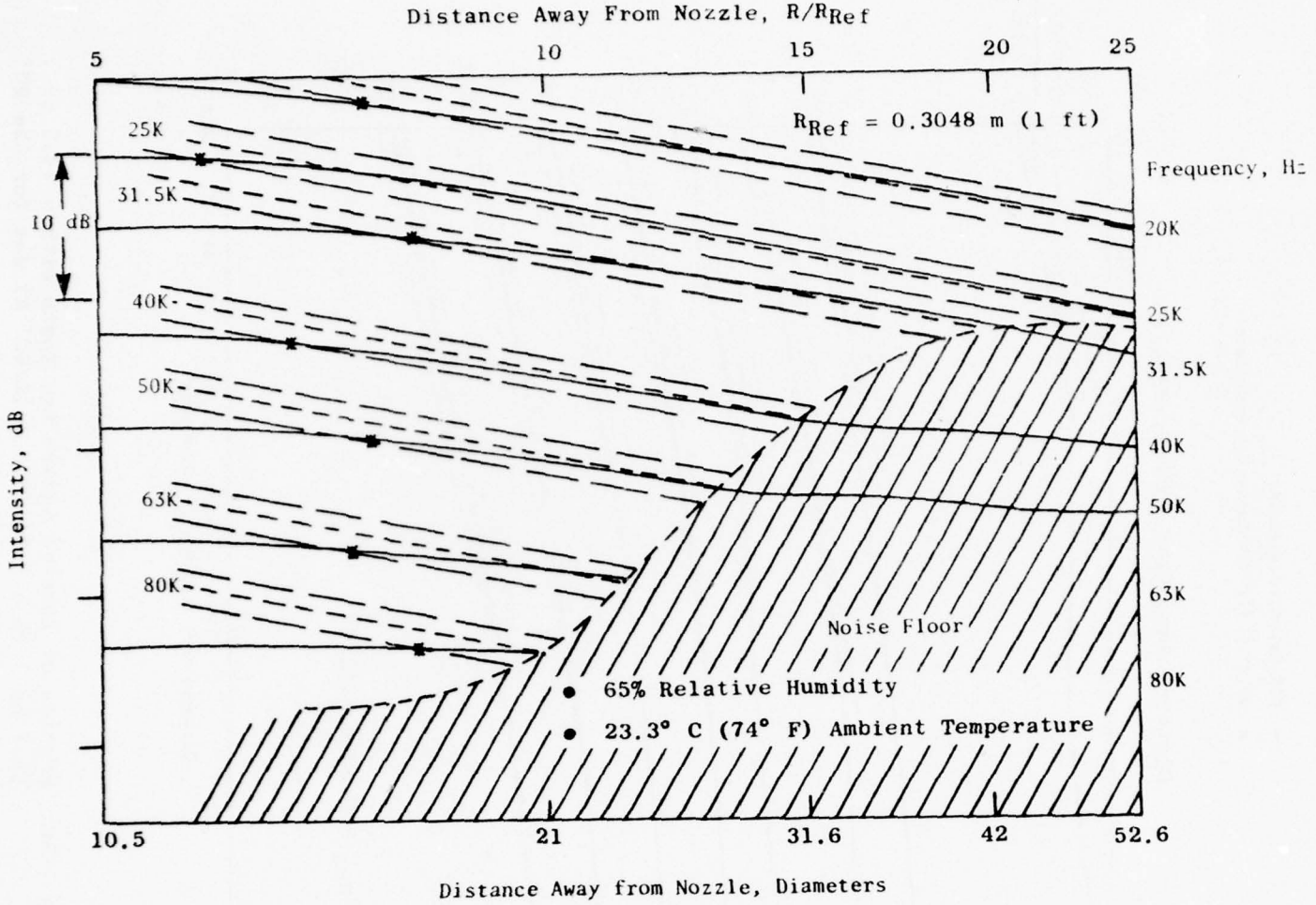

Figure 3-35. Results of Inverse Square Law Tests with a 14.5 cm (5.7 in.) PR = 3.8, 1546 K (2783° R) Jet for the 90° Angle, at High Frequency.

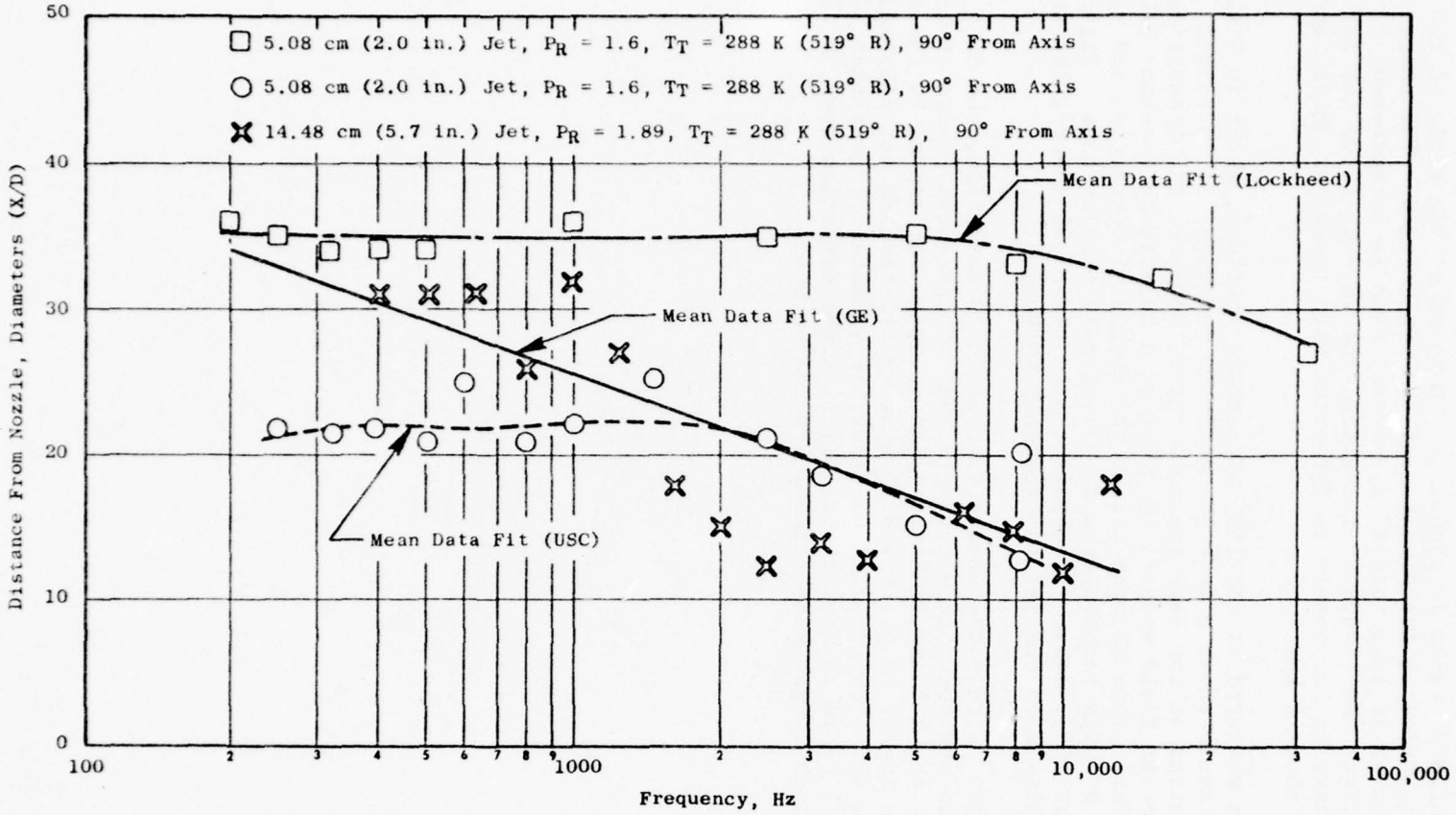

Figure 3-36. Location of Near Field to Far Field as a Function of Frequency for Cold Jets at 90°.

The far-field region is pinpointed in terms of the ratio of the distance away from the source to the diameter of the nozzle used. The onset of the near-field occurs in less than 35 diameters; this is in agreement with the other facilities. As frequency increases, the GE data shows the far field occurring closer to the nozzle in agreement with classical theory and with the USC data above 2 kHz.

For data measured at the 160° microphone position, shown in Figure 3-37, the cold jet again shows a decreasing X/D as frequency is increased. For a hot jet operating at the same pressure ratio, however, the transition from near field to far field appears to occur at a relatively constant X/D at all frequencies. This is most likely the result of refraction and tunneling of the noise at high temperatures at angles near the jet axis. Figure 3-38 shows that (at 90°), again in agreement with classical theory, the transition point moves closer to the jet as frequency increases.

In summary, within the constraints of ±1 dB deviation, the data show that far-field and near-field criteria over the frequency range of interest can be met at the 90° and 160° microphones, which correspond to the shortest acoustic path length (e.g., R = 8.25 m or 27 ft) for X/D (or R/D) values ranging up to 48. Nozzles with an effective diameter of less than 17.3 cm (6.8 in.) will be in the far-field. If a larger deviation (say ±2 dB) is acceptable, much larger nozzle diameters can be used.

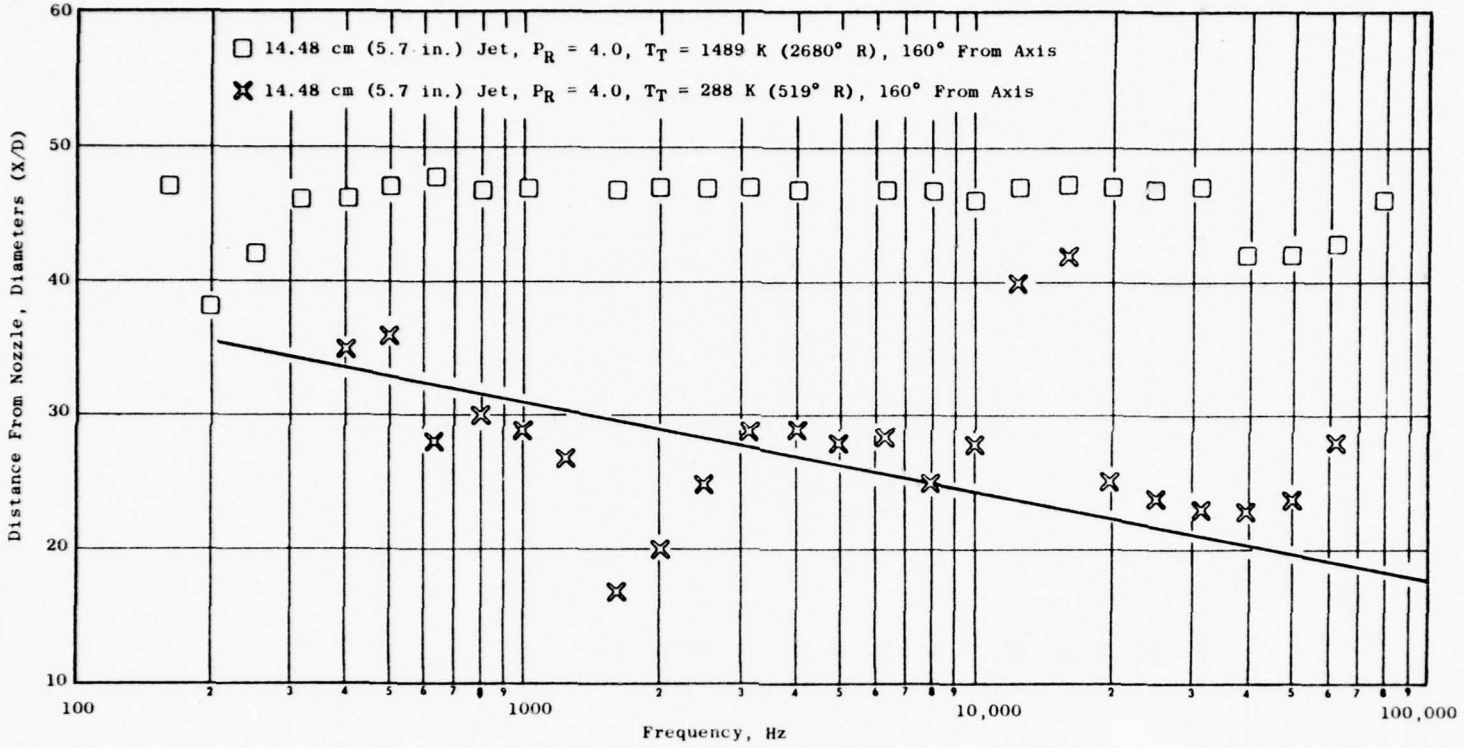

Figure 3-37. Location of Near Field to Far Field as a Function of Frequency for a Cold and Hot Jet at 160°.

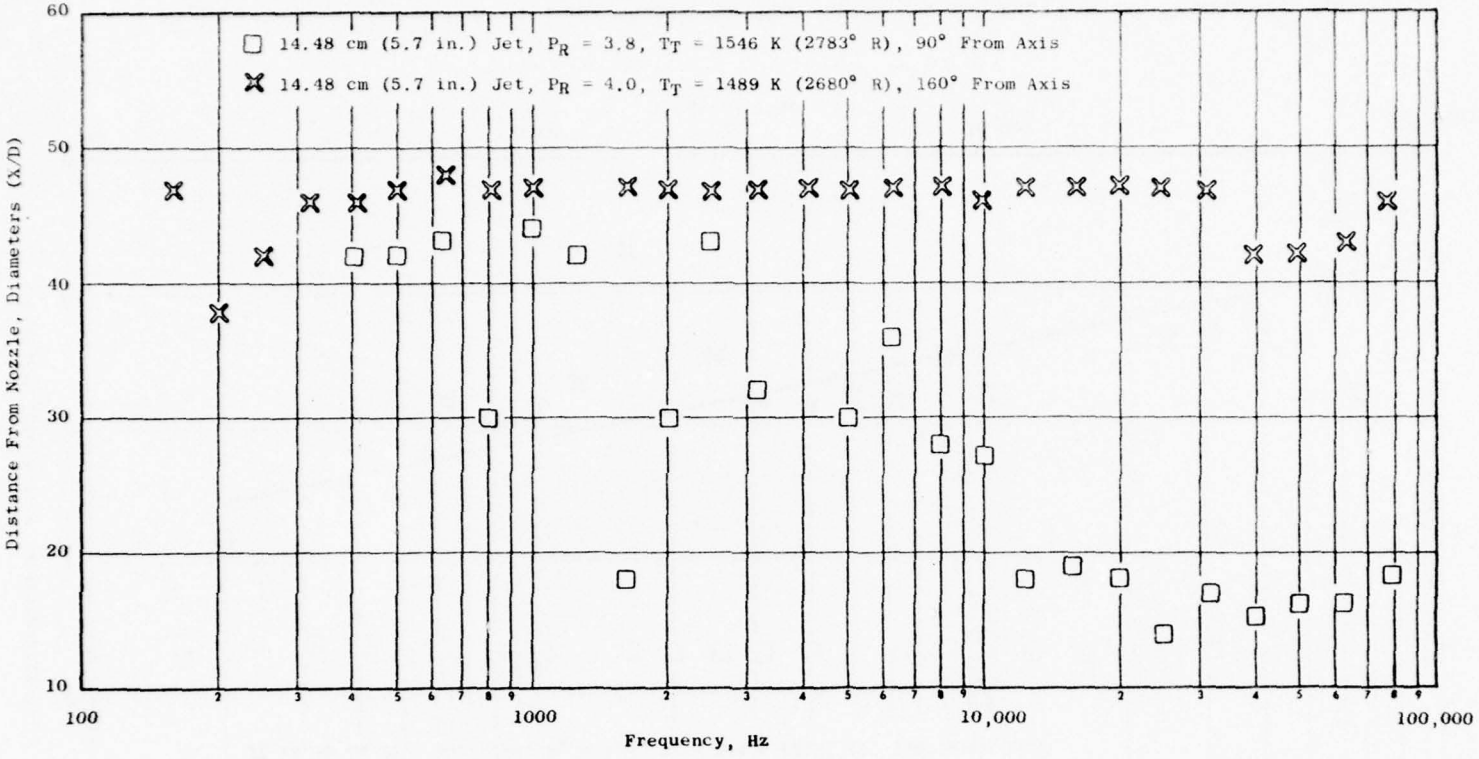

Figure 3-38. Location of Near Field to Far Field as a Function of Frequency for a Hot Jet 90° Vs. 160°.

4.0 CONTAMINATION OF THE MEASUREMENT

4.1 INTRODUCTION

One of the major tasks performed as a part of the chamber certification was the determination of the degree of contamination in the measured acoustic data.

A number of possible sources of contamination can occur which will cause the measurement to deviate from the pure jet noise. Individually, these sources can represent only a small source of error. When combined, however, this can often result in a significant loss in accuracy and precision to be considered for each test and analysis of data. Such biasing errors include contamination from:

- Electronic noise floor
- Microphone sensitivity and calibration variations
- Chamber ambient levels
- Community noise*
- Air attenuation variations
- Aerodynamic instrumentation measurement errors
- Facility noise from piping, valves, and obstructions in the flow
- Facility noise from the combustors

4.2 ELECTRONIC NOISE FLOOR

All electrical instrumentation generates small amounts of low-energy noise (even those with special low-noise components such as microphone cartridges, pre- and final-stage amplifiers, tape recorders, and data reduction instrumentation). This electrical signal is composed of all frequencies and appears in all data but is only noticeable where the spectrum has quite a large variation in amplitude. In jet noise, this occurs at the higher frequencies where the spectrum decreases and the electrical floor is increased. The acoustic data acquisition system was described in Section 2.5.1 and is shown schematically in Figure 2-39. The initial component in the system is the 0.64 cm (1/4 in.) Bruel-Kjaer condenser

*Community noise is not a factor in measured acoustic data but is included in this section because of its possible annoyance in the surrounding communities and adjacent company property.

microphone and FET preamplifier. Figure 4-1 depicts the self-noise analysis for the 0.64 cm (1/4 in.), 1.27 cm (1/2 in.), and 2.54 cm (1 in.) microphone systems. The noise is lowest in the 1 kHz to 10 kHz range. At higher frequencies the level is determined by random noise in the preamplifier. At lower frequencies, the level is determined by the capacitance of the microphone, commonly called 1/f noise in electrical terms. The smaller the microphone capacitance, the more the 1/f noise dominates the noise spectrum. In Figure 4-1, the anechoic chamber microphone systems exhibit a higher noise floor in the lower frequencies than the standard 0.64-cm (1/4-in.) system. The standard 6.35-mm (0.25-in.) microphone curve represents the floor with the latest model 2619 preamplifier. During the original system checkout of the acoustic data system in the anechoic chamber, it was observed that the model 2619 preamplifiers were very sensitive to case vibration coupled through their mounting arrangement. This problem was discussed with Bruel-Kjaer representatives, and they recommended installing a 51-ohm, 1/4-watt carbon resistor in series with the signal output lead (pin 4) in the connector housing. This was tried and found to be an effective fix. It is believed that the pressure of the 51-ohm resistor is responsible for the higher flow in the anechoic chamber systems.

The output of the microphone system is directly coupled through the Bruel-Kjaer power supply into a General Electric-designed and built line driver. The line drivers represent only a 3 μV electronic floor and are necessary to drive the long data-track lines to a central data recording area. They are basically noninverting amplifiers with 10 dB gain plus 6 dB of preemphasis at 80 kHz.

The last component in the data acquisition system is the tape recorder itself. To meet the frequency response requirements for the chamber required that the tape recorder be capable of recording data up to 100 kHz. Two types of electronics were available to satisfy these requirements: Wideband Group I at 120 ips, or Group II at 30 ips, as shown in Table 3-III. From an economic standpoint, less tape is used at 30 ips in the Group II mode; however, this choice results in a smaller dynamic range to the noise floor. Noise floor checks of the data acquisition system, with the recorder system in Group II, are given in Figure 4-2. The plot shows an increasing floor level ramp with increasing frequency. As the tape recorder gain setting is changed, the level shifts by a corresponding amount; thus, indicating the ramping to be in the tape recorder itself. Additional testing showed the ramping to shift in frequency with tape speed changes, suggesting the ramp to be an early anticipation of the FM carrier bleeding back into the data.

During the chamber free-field calibration tests, data were recorded both on-line (i.e., direct from the microphone into a General Radio real-time analyzer and then onto an x-y plotter) and on magnetic tape. Figure 4-3 shows the recorded data to be contaminated by the recorder ramping above 20 kHz. Subsequent tape recorder floor checks, comparing the Group I to Group II modes (Figures 4-4 and 4-5), showed the Wideband Group I to be the only acceptable choice for data acquisition. Figure 4-6 shows a comparison of the tape recorder floors in terms of dynamic range for the two

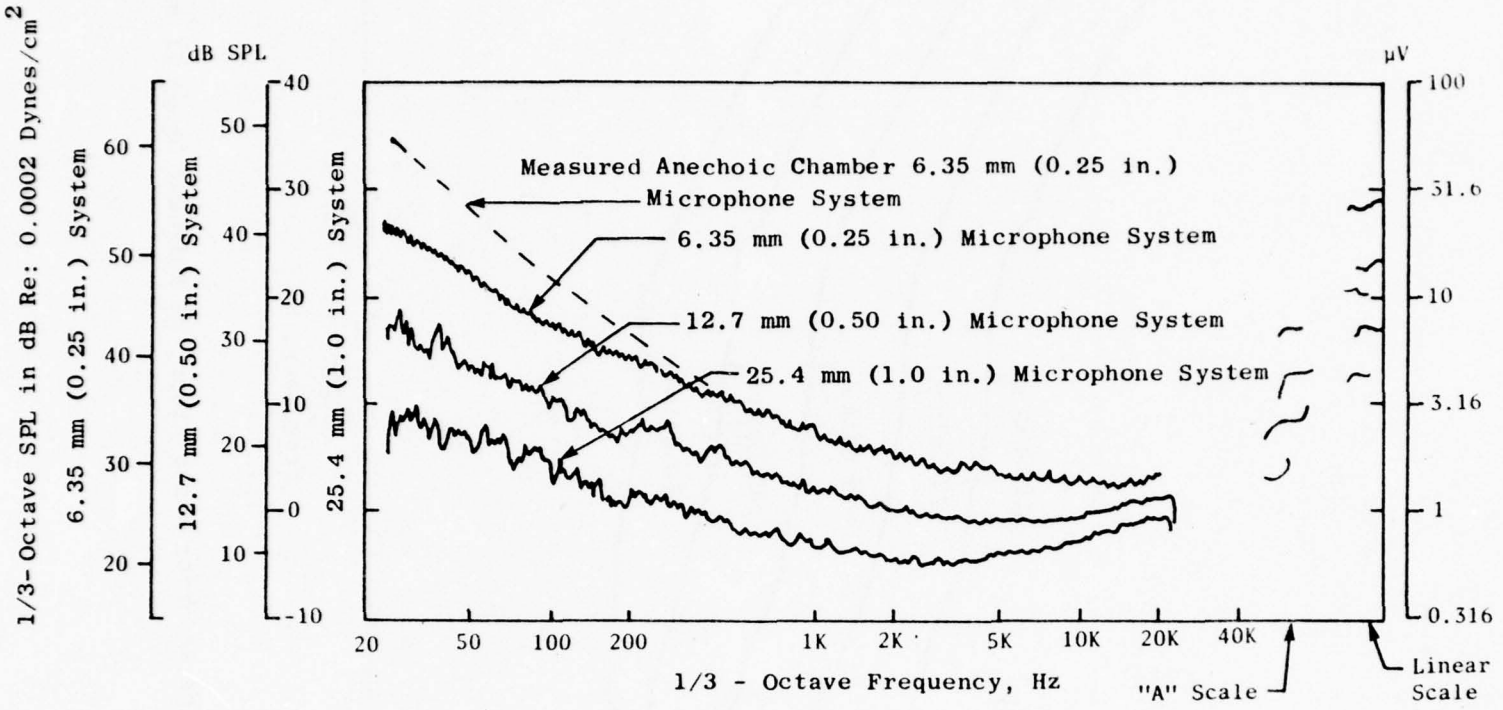

Figure 4-1. Microphone System Self-Noise.

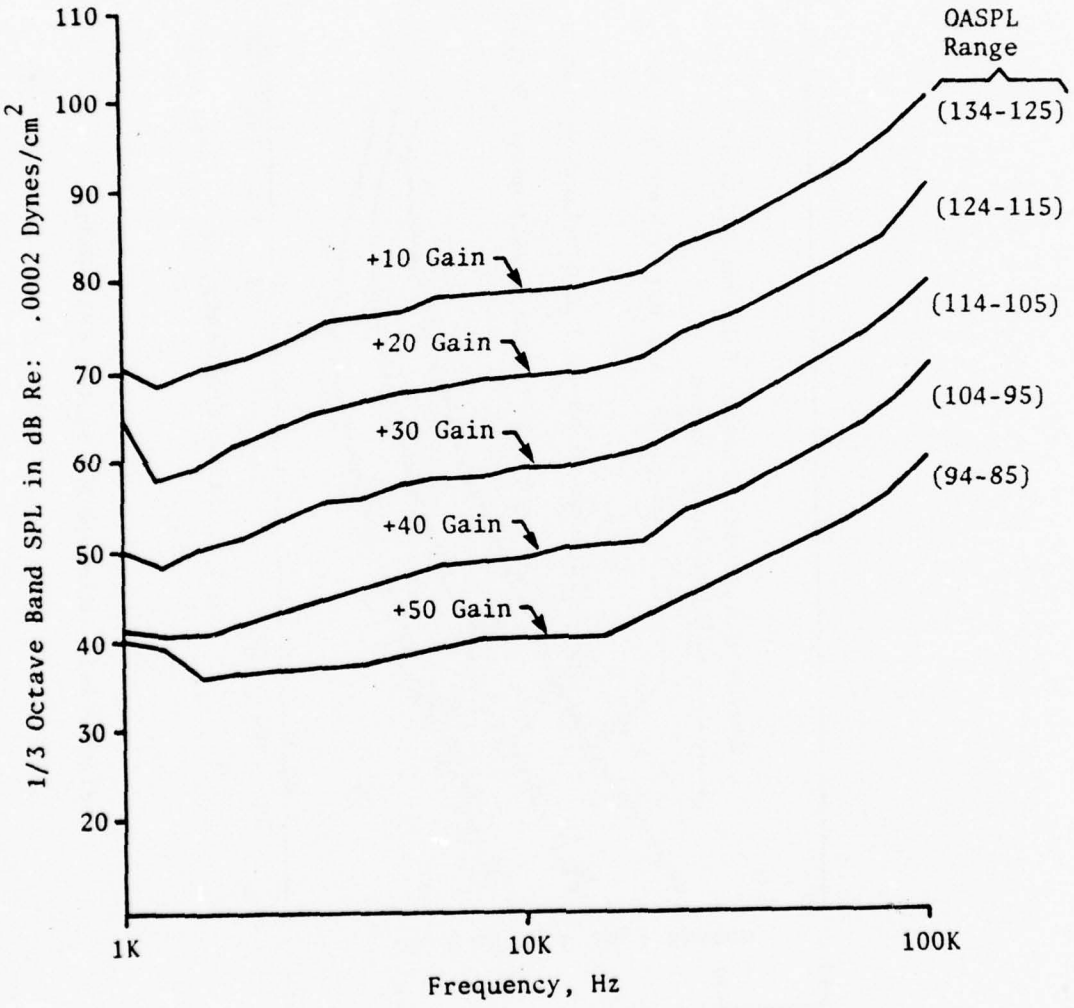

Figure 4-2. Tape Recorder Noise Floor, FM Wideband Group II at 30 in./sec.

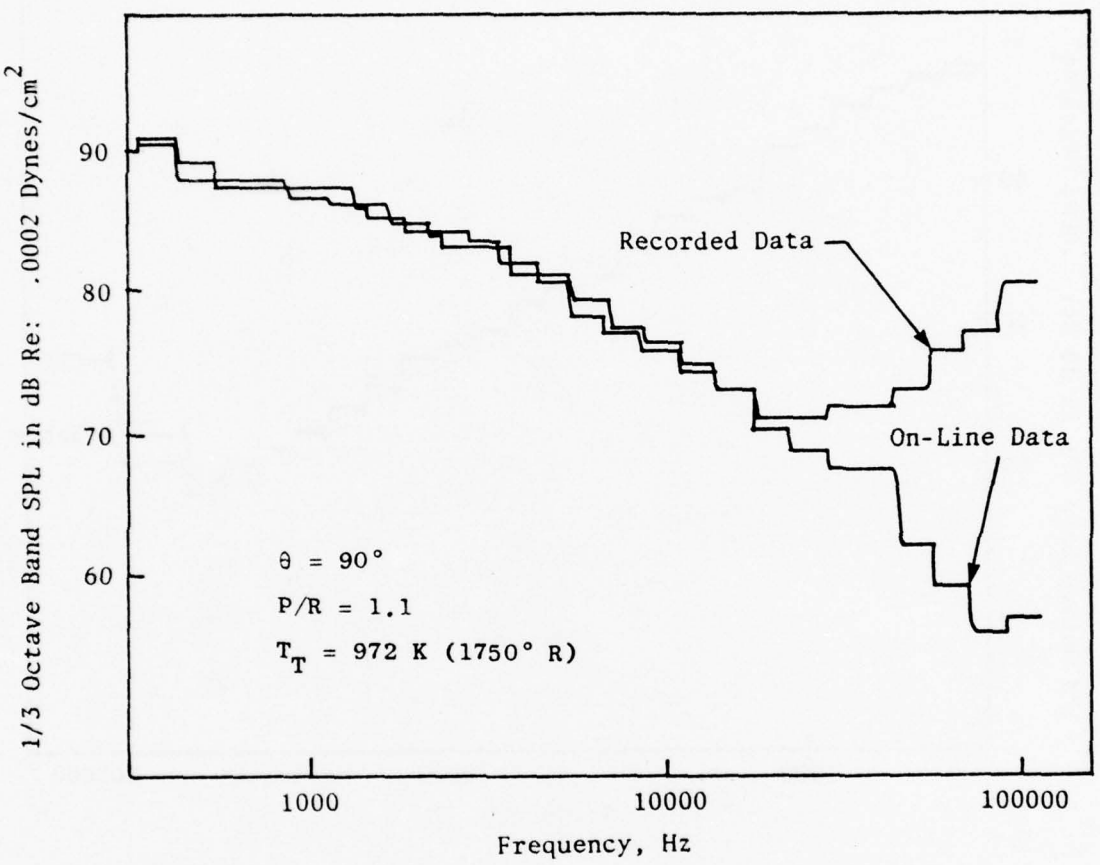

Figure 4-3. On-Line Recorded Data Versus Tape Recorder Data, FM Wideband Group II at 30 in./sec.

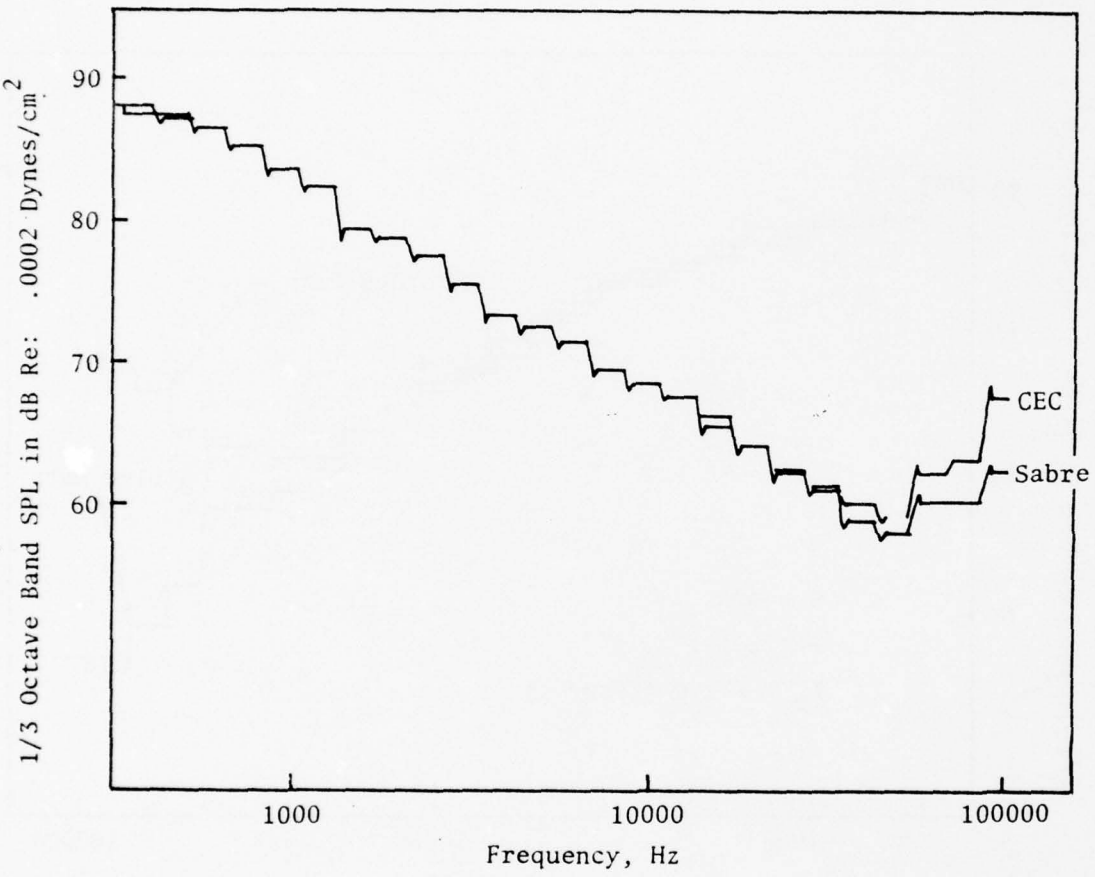

Figure 4-4. Wideband Group II Recorded Data Played Back through Two Different Discriminators.

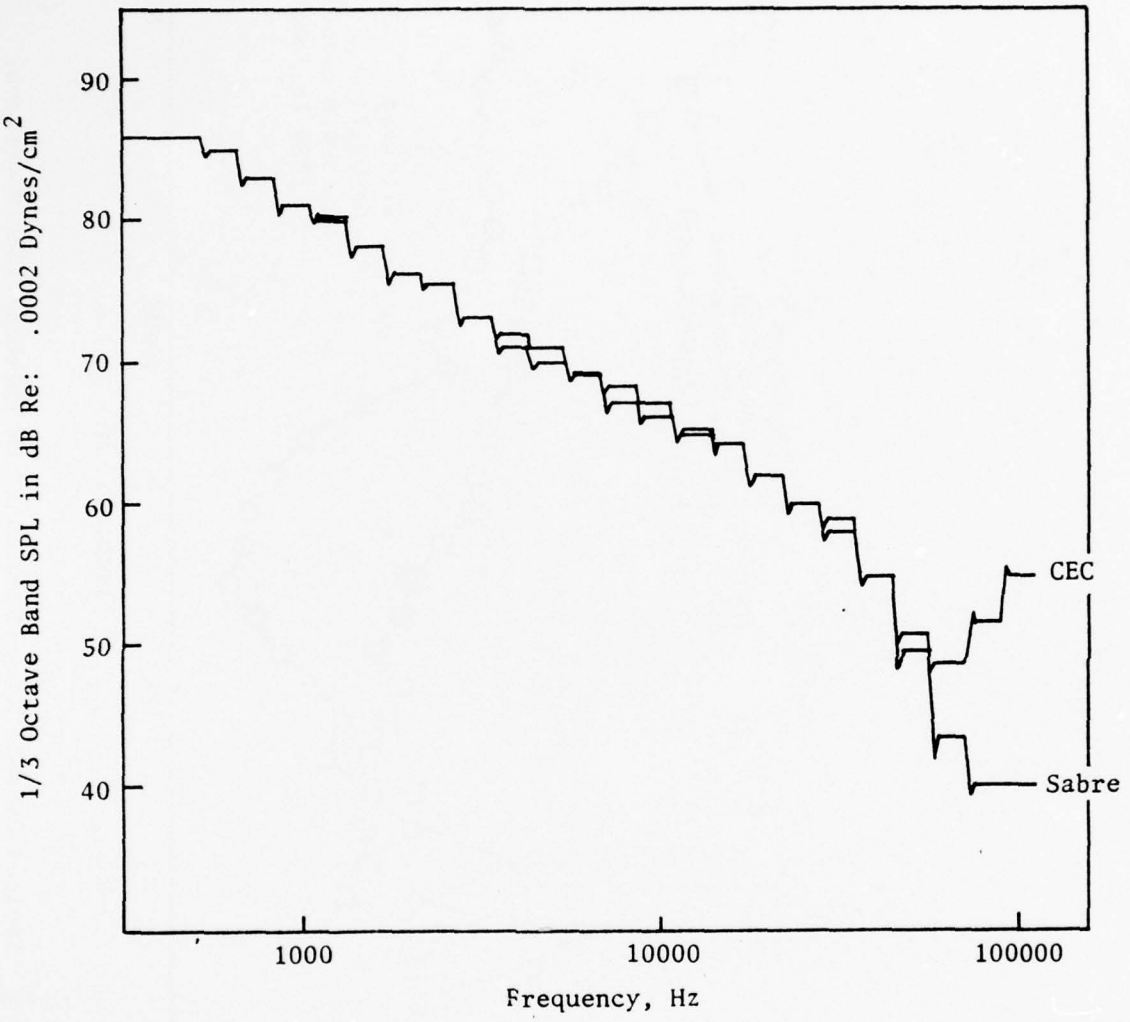

Figure 4-5. Wideband Group I Recorded Data Played Back through Two Different Discriminators.

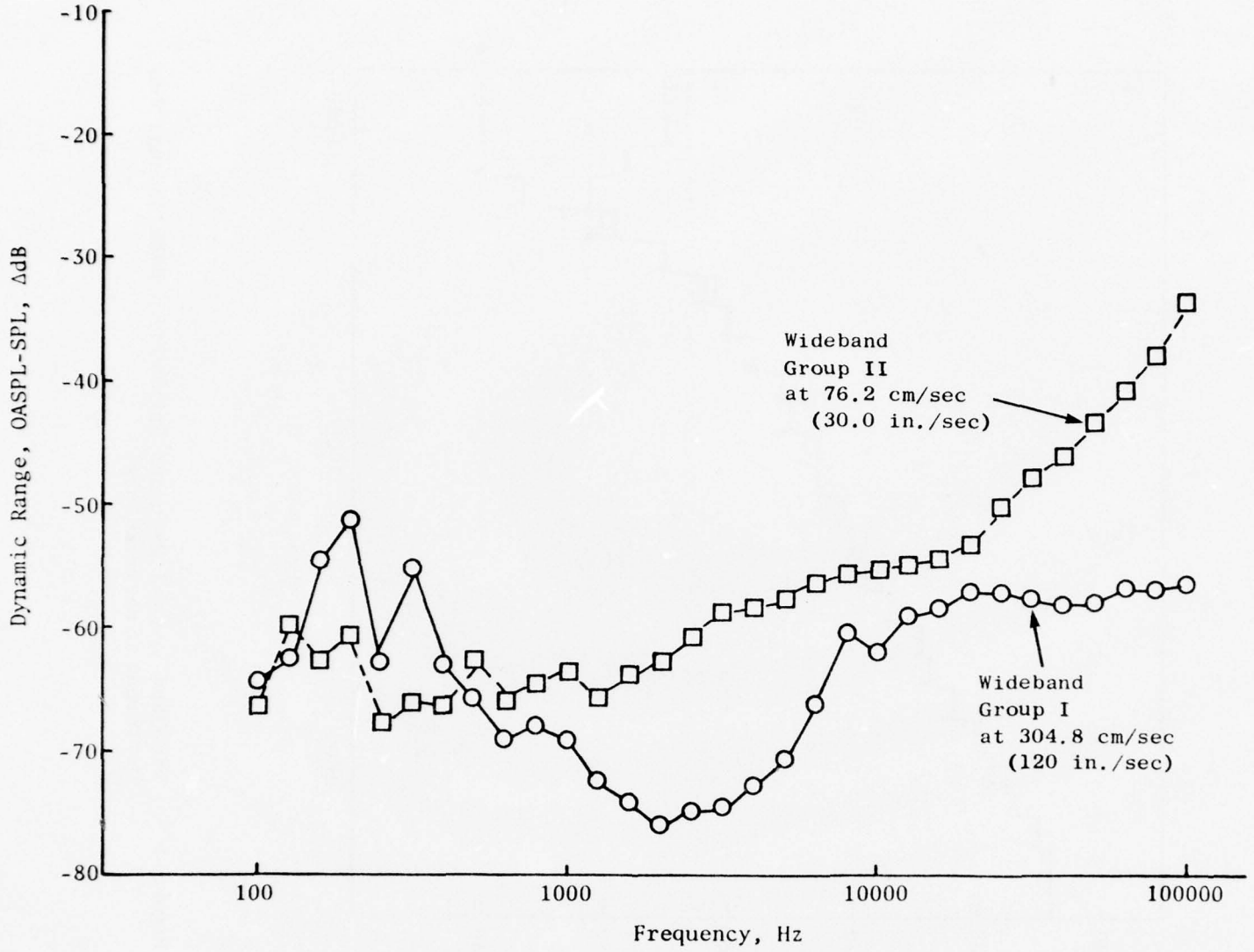

Figure 4-6. Typical Dynamic Range Spectra of FM Wideband Tape Recorders.

operating modes. A 60 dB range in any given 1/3-octave band is possible in the Wideband Group I setup under optimum gain conditions. This spectral level was found to be repeated to within a ± 3 dB standard deviation. Since fixed 10-dB gain amplifiers are used, any overall levels which fall slightly above the optimum setting (where the amplifier is saturated and signal clipping occurs) will require a 10-dB attenuation of the signal which, in turn, reduces the dynamic range by 10 dB as seen in Figure 4-2. The random nature of jet noise signals, particularly at angles near the jet, cause occasional clipping of signals which are significantly higher than the rms levels. In order to avoid this clipping, the tape operators often will attenuate the signal another 10 to 20 dB which, of course, results in an equivalent deterioration in the available dynamic range. It is important to avoid significant signal clipping, because it creates high frequency harmonics of the low frequency data which essentially gives a nonlinear frequency response and apparent increased levels at high frequency. The degree of acceptable clipping is still a question under study and will be a tradeoff between distortion of the frequency response and loss of dynamic range.

4.3 MICROPHONE SENSITIVITY AND FREQUENCY RESPONSE MEASUREMENTS

In general, the whole recording and reproduction process is calibrated by two methods: one is the insertion of a known level on the microphone cartridge, the second is the insertion of a calibrated pink-noise source.

Absolute calibration of the entire system is made prior to each test by the insertion of a 124-dB sound pressure level to the microphone cartridge using a Bruel-Kjaer Model 4220 pistonphone. Any microphone voltage output found to deviate more than ±1.5 dB from calibration specifications is replaced.

Frequency response characteristics are determined by removing the microphone head and connecting the output of the pink-noise generator to the cathode follower. The data are recorded on tape and processed like sound data. The resulting 1/3-octave spectra are normalized at the 250 Hz 1/3-octave level, and the resulting set of ΔdB's represent the system corrections.

The accuracy of the acoustic recording/processing system can be calculated from the tolerances of each independent component in the system. Since these tolerances are independent of each other, the estimated deviation of the system can be computed as the rms of the variances due to each component separately, using:

$$\sigma_{SL} = \sqrt{\sum_{i=1}^{N} \sigma_i^2}$$

where σ_{SL} = the estimated standard deviation in sound level due to variations in all of the independent components obtained or derived from the respective manufacturers, with specification (3σ tolerances) shown in Table 4-I.

Table 4-I. Accuracy of the Acoustic Data System.

Component	(± dB) Tolerances
B&K Microphone Cartridge Calibration	0.2 to 10 kHz
	0.5 to 100 kHz
Line Driver	0.1
B&K Cathode Follower	0.2
B&K Pistonphone	0.2
General Radio Noise Generator	0.5
B&K Power Supply	0.09
Tape Amplifier	0.1 to 50 kHz
	0.2 to 100 kHz
Sangamo Sabre IV Tape Recorder	0.5
Playback Amplifier	0.1 to 50 kHz
	0.2 to 100 kHz
General Radio 1/3-Octave Band (OB) Analyzer	0.25
GEPAC 300 Computer	0

Substituting the above values in the equation for the sound level variance yields an estimated 3σ tolerance of 0.85 dB below 10 kHz and 1.0 dB above 10 kHz for the sound level due to the acoustic data recording instrumentation in the anechoic chamber.

4.4 CHAMBER AMBIENT LEVEL

Synonymous with electronic noise floor is the subject of the anechoic chamber acoustic noise floor. Adjacent to the acoustic chamber is an Altitude Ram Test Facility (ATF) representing both a potential airborne and structure-borne noise source. Combined with the electrical floor, these ambient levels give the lowest sound pressure level that can meaningfully be measured in the chamber.

Recognizing the importance of a low ambient noise level early in the design stages of the chamber, strict requirements for permissible ambient levels inside the chamber were specified:

Design Specification for Permissible Ambient Levels

OB Frequency (Hz)	125	250	500	1K	2K	4K	8K
SPL (dB re 0.0002 dyne/cm^2)	54	46	43	40	40	40	40

To determine the amount of outside-to-inside suppression to be designed into the inlet mufflers in order to meet these specifications, numerous measurements were made outdoors during operation of the ATF:

Measured Outside Levels During ATF Run

OB Frequency (Hz)	125	250	500	1K	2K	4K	8K
SPL (dB re 0.0002 dyne/cm^2)	83	79	81	76	72	74	73

The required outside-to-inside transmission loss of the mufflers, therefore, was set at:

Outside-to-Inside-Design Suppression

OB Frequency (Hz)	125	250	500	1K	2K	4K	8K
SPL (dB re 0.0002 dyne/cm^2)	29	33	38	36	32	34	33

After installation of the mufflers in the acoustic chamber, acoustic measurements were made to determine the actual transmission loss across each inlet/exhaust baffle, as well as transmission loss measurements from

the baffle inner faces to four acoustic measurement stations within the chamber. Figures 4-7 and 4-8 show that both silencers exceeded specified acceptance levels. However, during the single-flow checkout, acoustic measurements recorded within the chamber during ATF operation showed quite high acoustic levels below the specification low frequency cutoff of 125 Hz. Even though this area of the spectrum is of no direct interest, the high ambient levels at low frequency do influence the electrical noise floor, forcing the tape system amplifier gain to be set at a lower position (see Figure 4-2). This creates noise floor problems at high frequency when trying to measure low-velocity, low-level jet noise signals. Figure 4-9 shows a typical spectrum measured in the chamber; a large tone in the 16 Hz, 1/3-octave band dominating the spectrum results in a loss in data above 50 kHz due to the electrical floor. To solve this problem, high-pass electronic filters were added to each measuring station microphone circuit. The filters lowered the spectrum low-frequency levels to the point that an additional 10-dB amplification could be applied allowing data to 100 kHz to be recorded.

With the ATF operating and the chamber jet nozzle shut down, chamber ambient levels were recorded using an on-line system (no electronic filters) and a 2.54-cm (1-in.) microphone to obtain true chamber ambient levels. Figure 4-10 shows that, within the spectrum range of interest (above 200 Hz), the levels are quite low; in fact, the levels were lower than the 20-dB noise floor level of the on-line GR analyzer. The high levels in the low frequencies remain, of course, since they are ATF-generated.

4.5 COMMUNITY AND SURROUNDING AREA NOISE LEVELS

The operation of any test facility generates a possible area of high acoustic levels in the near vicinity of the chamber as well as possible annoyance in the adjacent company property and any surrounding communities.

As a part of the Anechoic Chamber Acoustic Specifications, three distinct areas of chamber-generated noise levels were outlined:

1. Walsh Heely - OSHA requirements for personnel working outside in the near vicinity without ear protection, taking into account the projected reduction to 85 dBA.

2. Company property-line boundary - assumed as 500 feet from the sound source.

3. "Evendale Criteria" - one mile from the sound source.

During operation of the 14.5-cm (5.7-inch) conical nozzle at a temperature of 1667 K (3000° R) with a jet velocity of 1006 m/sec (3300 ft/sec), acoustic data were recorded at the exterior face of both the inlet and exhaust baffles. Figure 4-11 compares these data to the OSHA specifications for 8 hours of exposure without ear protection. No protection was

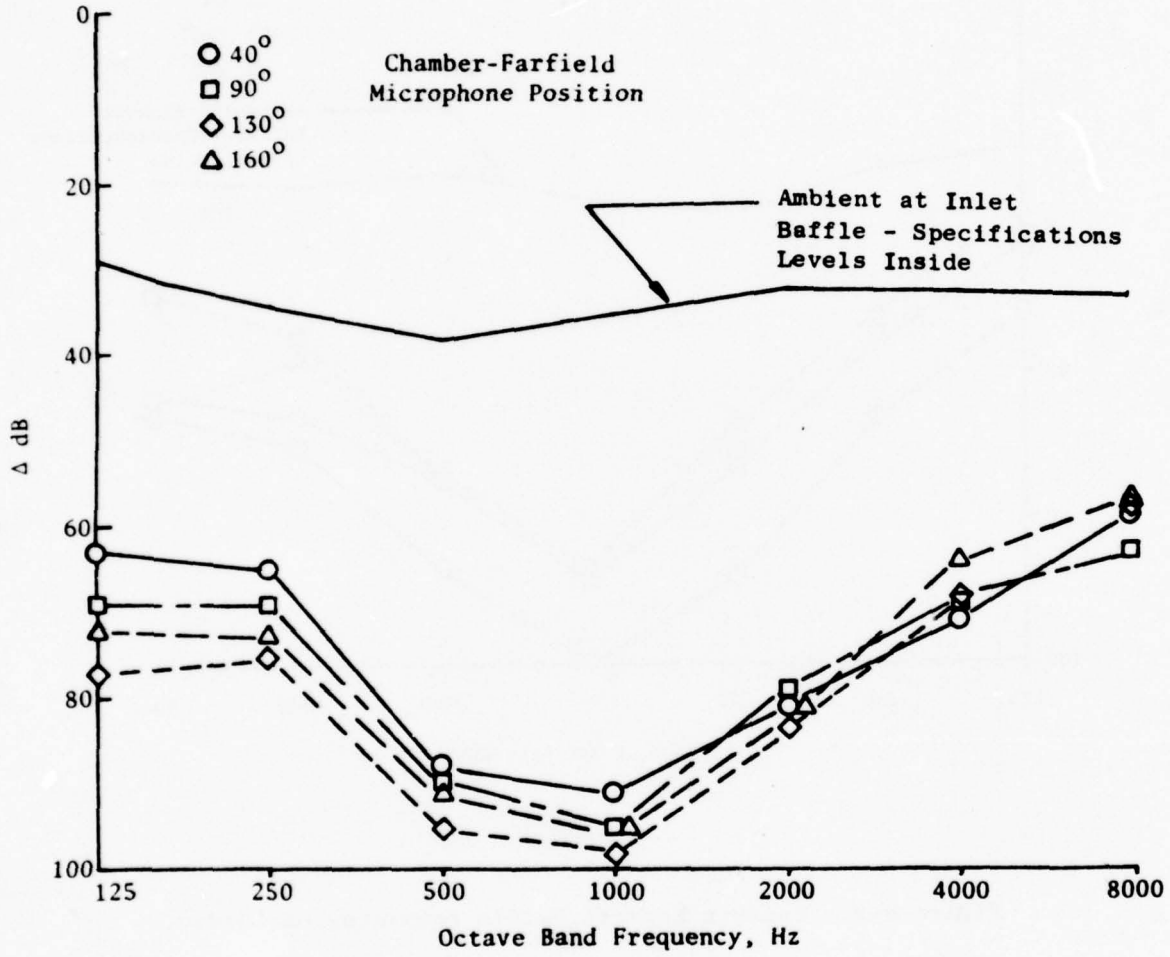

Figure 4-7. Chamber Inlet Baffle Transmission Losses.

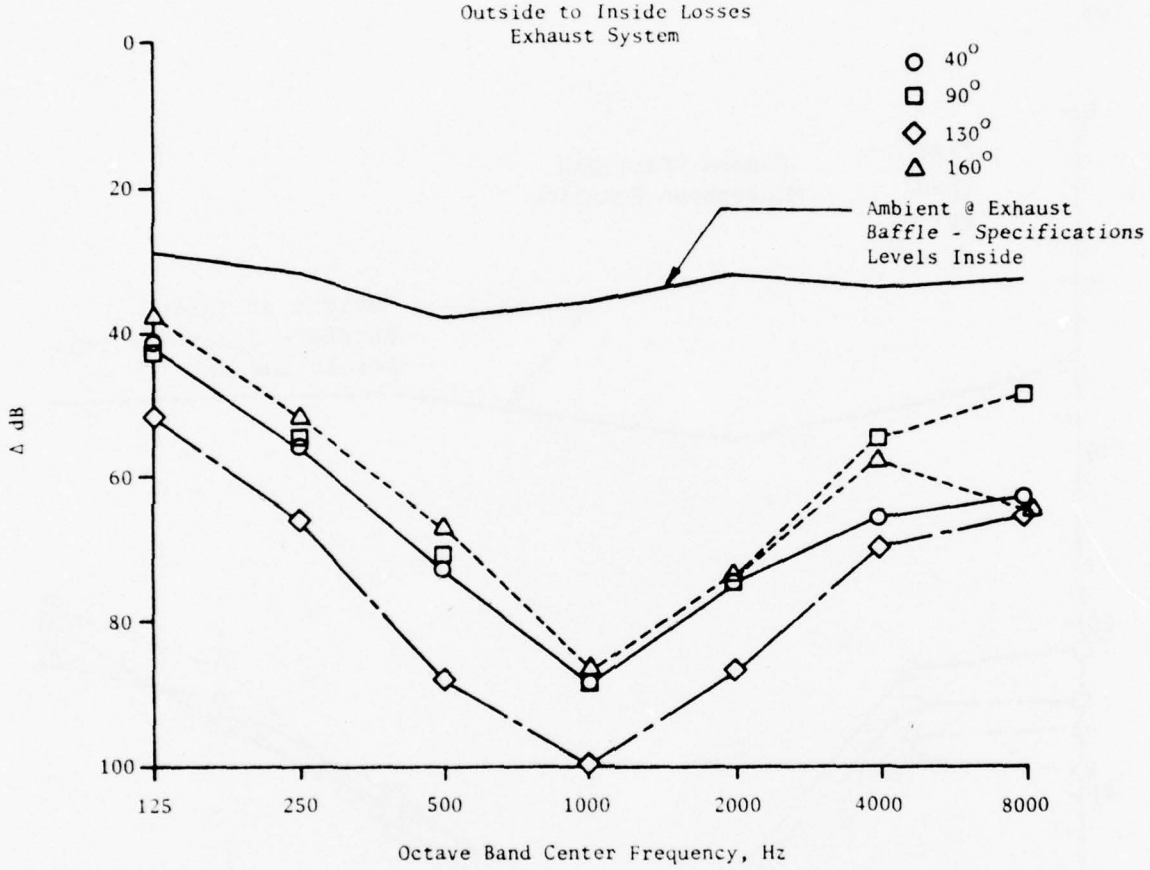

Figure 4-8. Chamber Exhaust Baffle Transmission Losses.

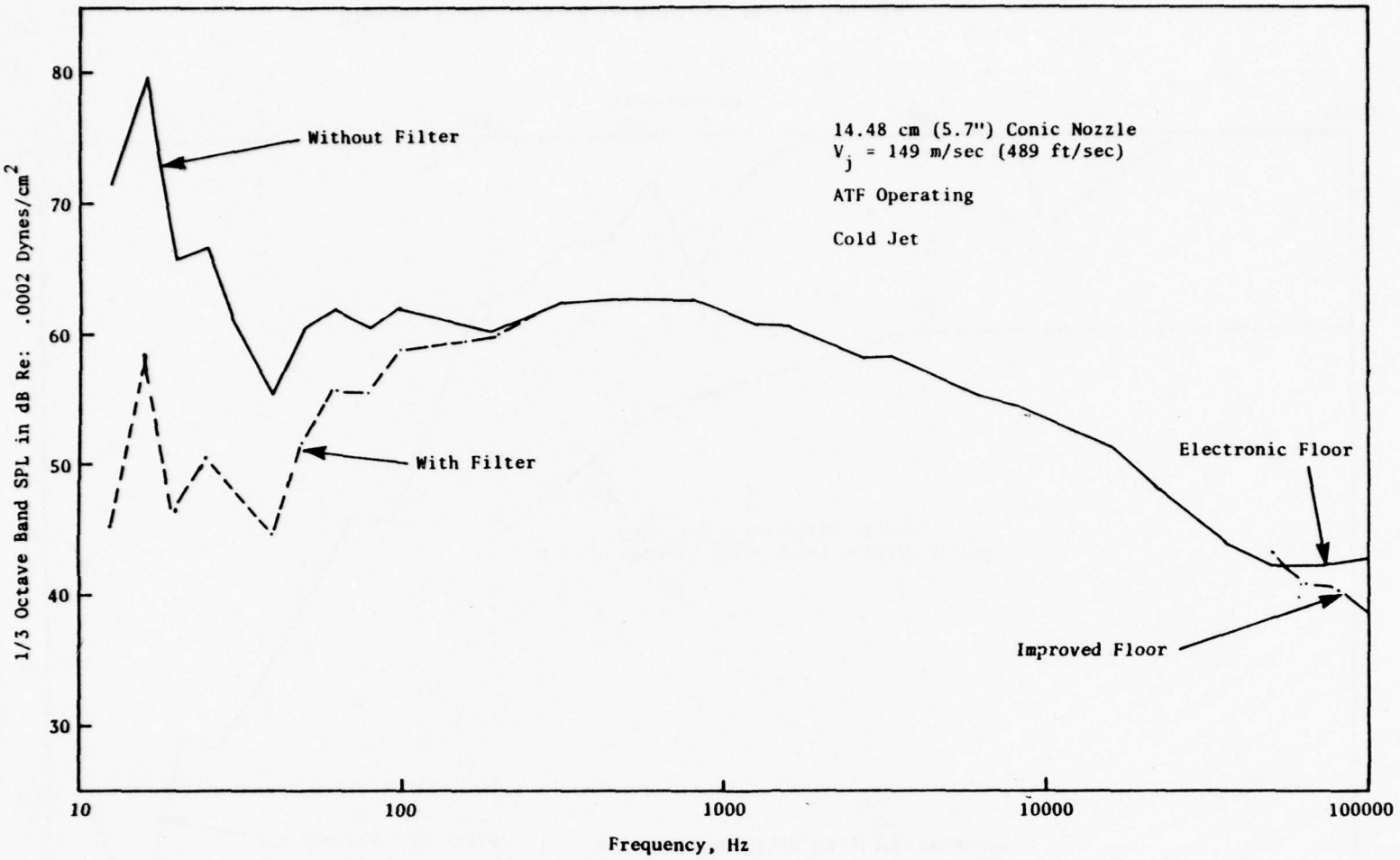

Figure 4-9. Chamber Noise Levels During RAM Test Facility Operation with and without Low Frequency Cutoff Filters.

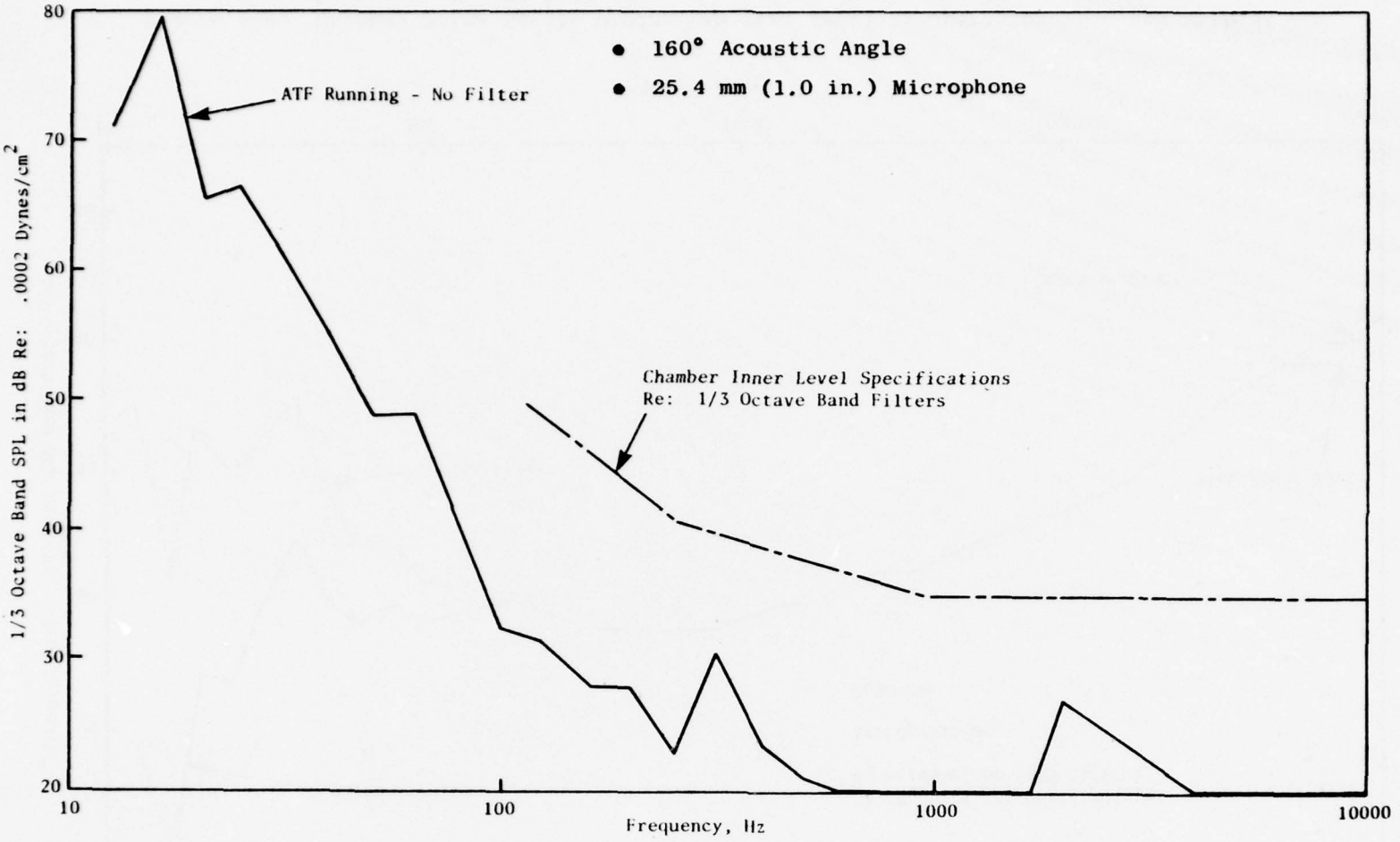

Figure 4-10. Chamber Ambient Noise Levels.

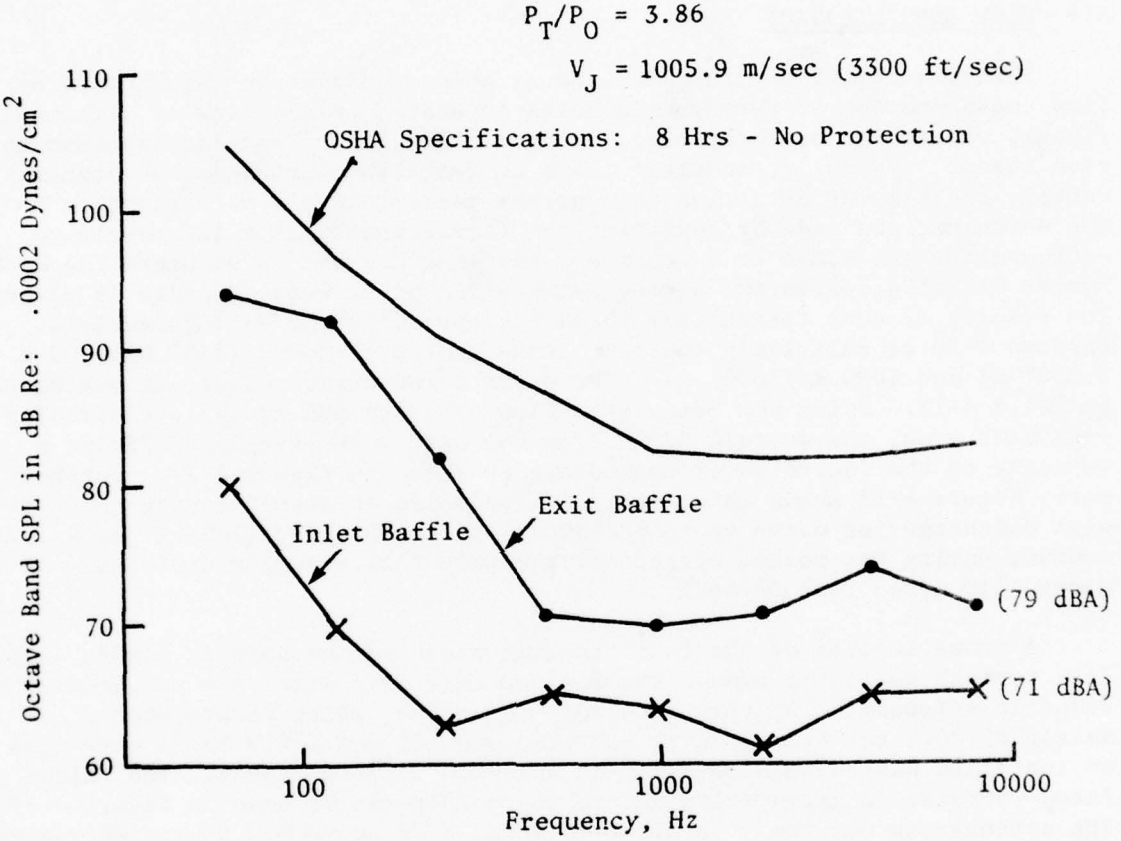

Figure 4-11. Chamber Exterior Noise Levels During Jet Operation Vs. OSHA Specifications.

required. For the 500 foot and 1 mile criteria (Figures 4-12 and 4-13), the data were extrapolated to each location using spherical divergence and atmospheric absorption for standard day conditions. All levels are well below the requirements. For the 1 mile criteria, air attenuation and spherical divergence losses were greater than the measured noise levels.

4.6 FLOW CONTAMINATION

The measurement of true jet exhaust noise can also be complicated by flow contamination or aerodynamic noise generated by the flow of air through piping, valves, combustors, etc., or over obstructions such as instrumentation rakes. Typically, acoustic tests to determine the amount of contamination, in terms of deviation from normal overall levels or distortion to the spectrum, are made by operating the facility without a jet nozzle to decrease the jet noise to a minimum. Airflows are set to simulate the Mach number distribution in the piping which would occur were a nozzle in place. The results of such testing are shown for the 90° angle in Figures 4-14 through 4-16 at relatively constant temperatures of 300 K (540° R), 700 K (1260° R) and 1000 K (1800° R). The exact aerodynamic points set are shown in Table 4-II. Using the calculated flow velocity and equivalent circular pipe exit area, the overall SPL's from the data were correlated giving a velocity to the fourth-power dependence as shown in Figure 4-17. Furthermore, Figure 4-17 shows this internal pipe noise is significantly above the pipe discharge jet noise up to a flow velocity 430 m/sec (1400 ft/sec). Of course, during jet nozzle operation, the pipe flow velocity would not exceed 150 m/sec (492 ft/sec).

A cross section of the facility exit plane can be seen in Figure 4-18. If a typical nozzle is added, the fan and core exit areas are reduced. The acoustic attenuation of this internal pipe noise, which occurs when a nozzle of 78.3 cm^2 (12.14 $in.^2$) fan area and 109 cm^2 (16.9 $in.^2$) core area is installed was calculated using an analysis in Reference 7. The calculated increase in attenuation due to the nozzle can be seen in Figure 4-19. The attenuation for the core alone is about 6 dB up to 400 Hz and decreases to zero at 4 kHz. The fan plus core attenuation is shown for comparison. Although it has a slightly higher attenuation, it decreases more rapidly. The net effect of either curve is expected to decrease the OASPL of the spectra in Figures 4-14 through 4-16 which peak at about 400 Hz by 6 dB.

Another estimate of the effects of flow noise can be made by comparing the piping noise OASPL with the jet noise which would occur with a typical nozzle installed. When the flow noise experiment without a nozzle was designed, the airflows used to set the data points were calculated using the ideal (isentropic) equations to represent the nozzle entrance conditions for a dual-flow nozzle with a core exit area of 109 cm^2 (16.9 $in.^2$) and fan exit area of 78.3 cm^2 (12.14 $in.^2$). During actual testing, however, a significant drop in the flow discharge coefficient occurred at the pipe exit with nozzle removed. As a result, a higher Mach number occurred at the pipe exit with the given airflow and total temperature. Many of these

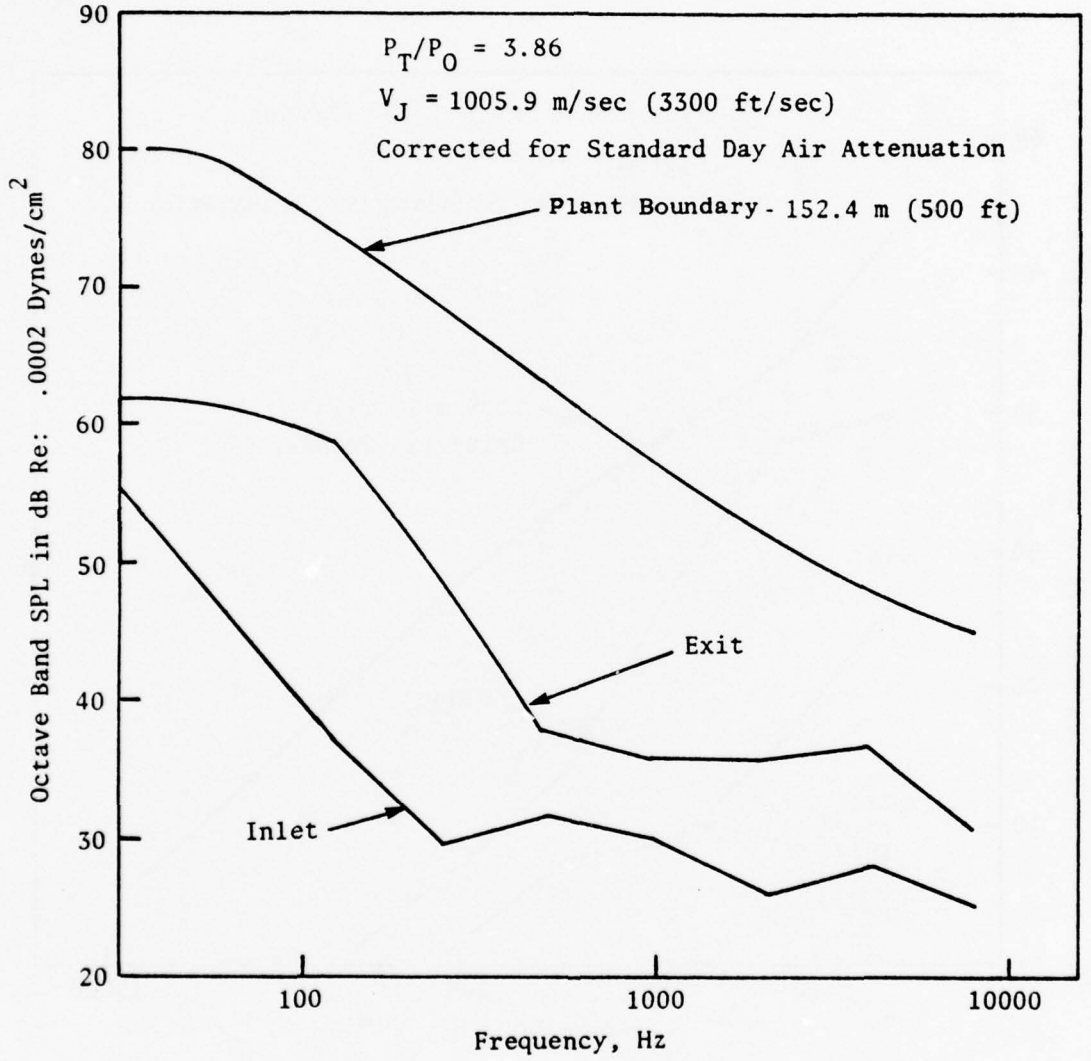

Figure 4-12. Company Property-Line Noise Levels During Chamber Operation Vs. Specifications.

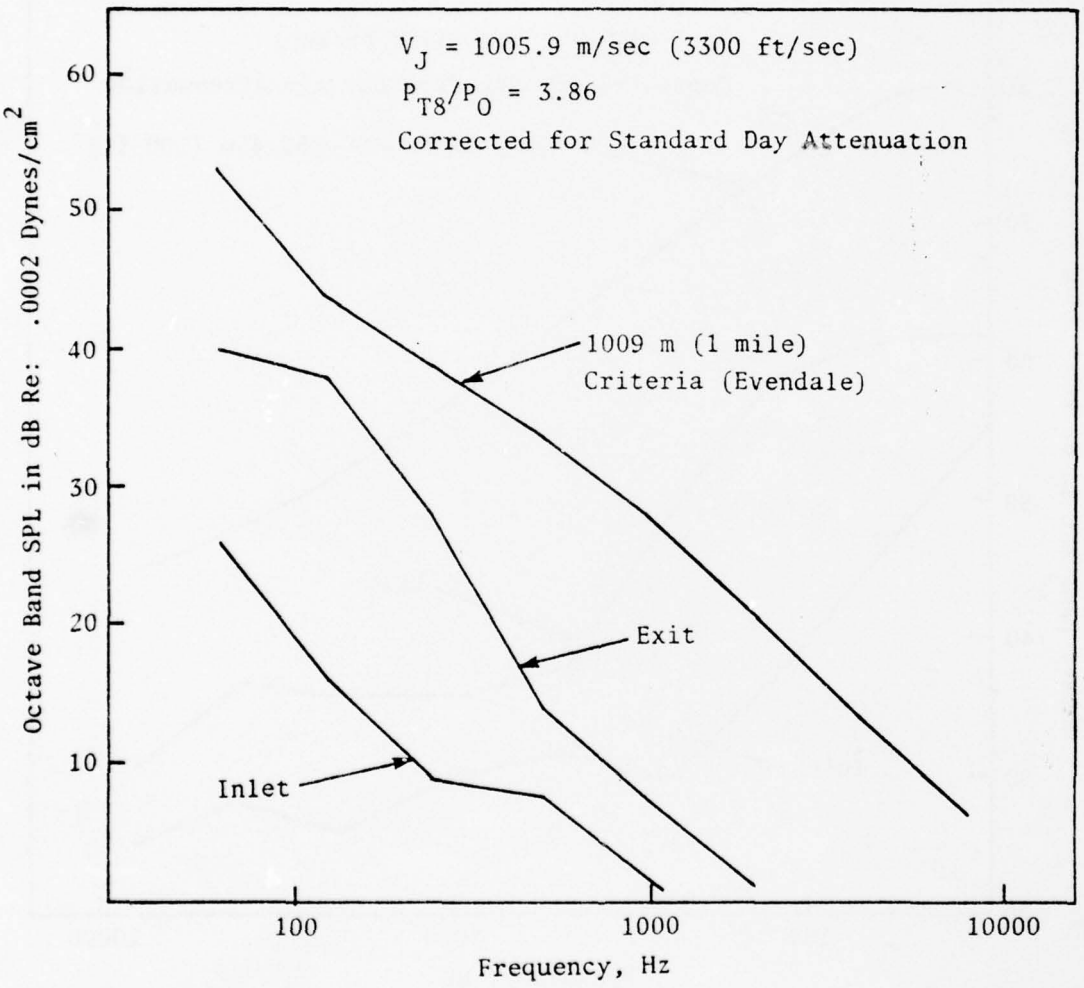

Figure 4-13. One-Mile Noise Level Criteria During Chamber Operation Vs. Specifications.

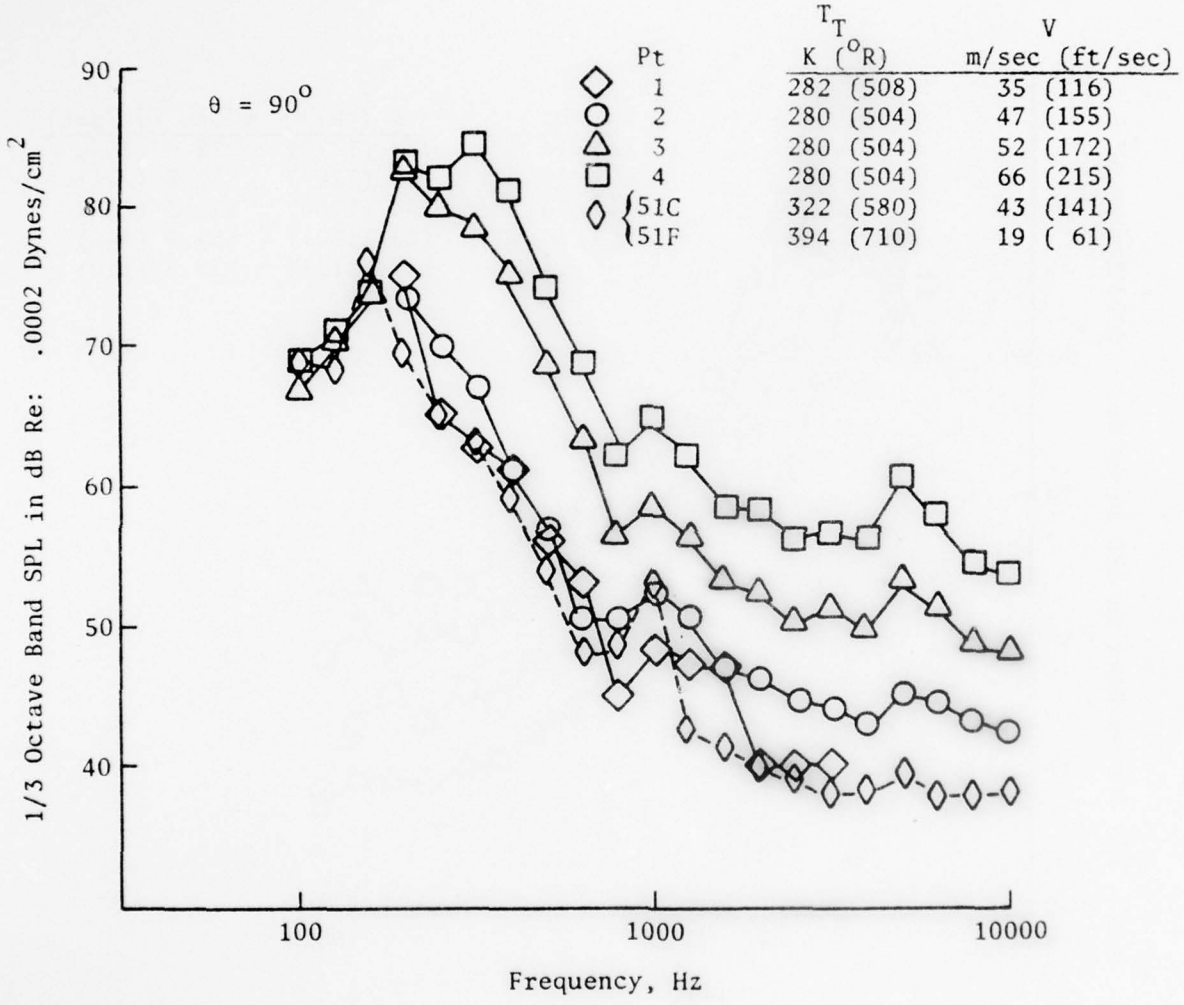

Figure 4-14. Flow Noise Measurements without a Nozzle with Cold Flow.

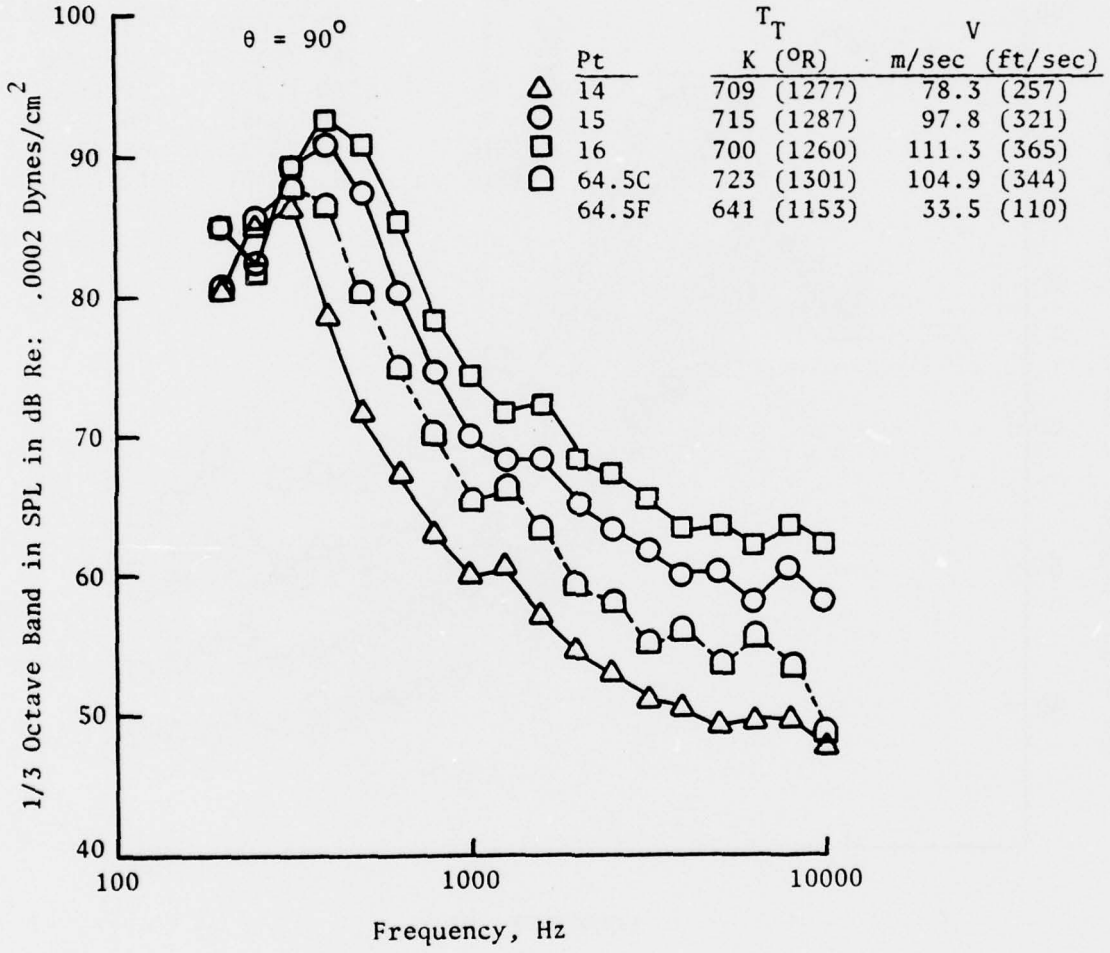

Figure 4-15. Flow Noise Measurements without a Nozzle at 700 K (1260° R) Temperature.

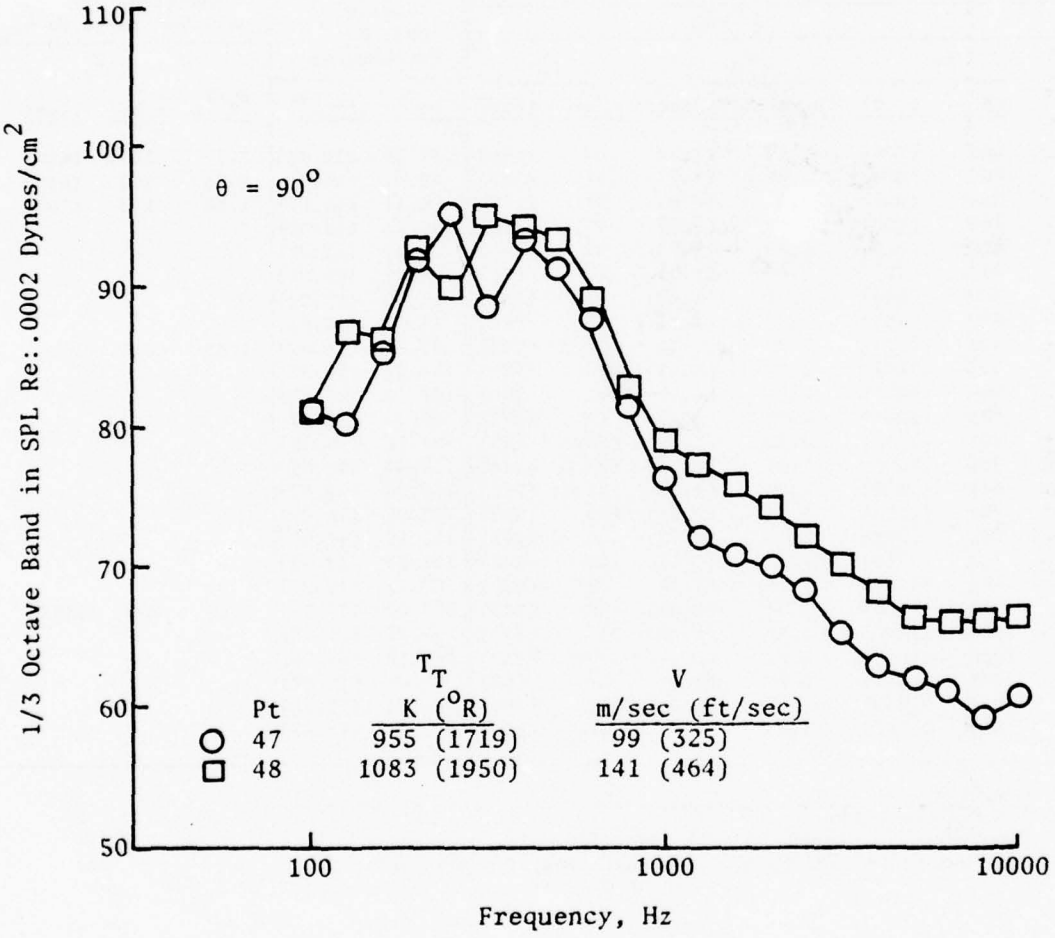

Figure 4-16. Flow Noise Measurements without a Nozzle at 1055 K (1900° R) Temperature.

Table 4-II. Aero Conditions Set for Flow Noise Testing without a Nozzle.

Pipe Conditions							Nozzle Exit Area For Choking		Conditions for D_j = 11.786 cm (4.64 in.)		
Actual											
	T_T		W_A		V_j					V_j	
PT	K	(° R)	kg/sec	(lb/sec)	m/sec	(fps)	cm^2	($in.^2$)	P_T/P_o	m/sec	(fps)
1	282	(508)	1.45	(3.2)	35	(116)	67.34	(10.44)	1.1	128	(420)
2	280	(504)	1.91	(4.2)	47	(155)	89.01	(13.8)	1.24	192	(630)
3	280	(504)	2.54	(5.6)	52	(172)	96.17	(14.91)	1.32	213	(700)
4	280	(504)	3.13	(6.9)	66	(215)	122.61	(19.01)			
51C	322	(580)	1.50	(3.3)	43	(141)	75.53	(11.71)			
51F	394	(710)	0.85	(1.9)	19	(61)	101.71	(15.77)			
52C	300	(540)	2.01	(4.43)	47	(154)	85.33	(13.23)			
52F	370	(667)	1.41	(3.1)	13	(44)	75.08	(11.64)			
14	709	(1277)	1.22	(2.7)	78.3	(257)	93.97	(14.57)	1.29	313	(1030)
15	715	(1287)	1.50	(3.3)	97.8	(321)	144.02	(22.33)			
16	700	(1260)	2.0	(4.4)	111.3	(365)	163.11	(25.29)			
64C	691	(1244)	0.70	(1.55)	84	(277)	128.35	(19.9)			
64F	601	(1082)	0.70	(1.55)	25	(85)	97.71	(15.15)			
64.5C	723	(1301)	1.84	(4.05)	104.9	(344)	122.87	(19.05)			
64.5F	641	(1153)	1.00	(2.2)	33.5	(110)	115.00	(17.83)			
65C	728	(1310)	0.94	(2.08)	103	(340)	121.06	(18.77)			
65F	551	(991)	0.78	(1.72)	30	(101)	113.19	(17.55)			
66C	731	(1316)	1.81	(4.0)	104	(342)	121.64	(18.86)			
66F	698	(1265)	1.18	(2.7)	39	(129)	127.77	(19.81)			
47	955	(1719)	1.38	(3.04)	99	(325)	103.00	(15.97)	1.53	471	(1550)
48	1083	(1950)	1.42	(3.13)	141	(464)	139.25	(21.59)			
97C	1050	(1890)	1.57	(3.47)	138	(453)	135.19	(20.96)			
97F	742	(1335)	0.95	(2.1)	25	(83)	83.65	(12.97)			
98C	1084	(1950)	1.81	(4.0)	151	(498)	145.64	(22.58)			
98F	851	(1532)	1.27	(2.8)	42	(139)	112.42	(17.43)			

C = Core Condition
F = Fan Condition
Test points 1 through 50 were core flow only.
Test points 51 through 100 were dual flow, fan plus core.

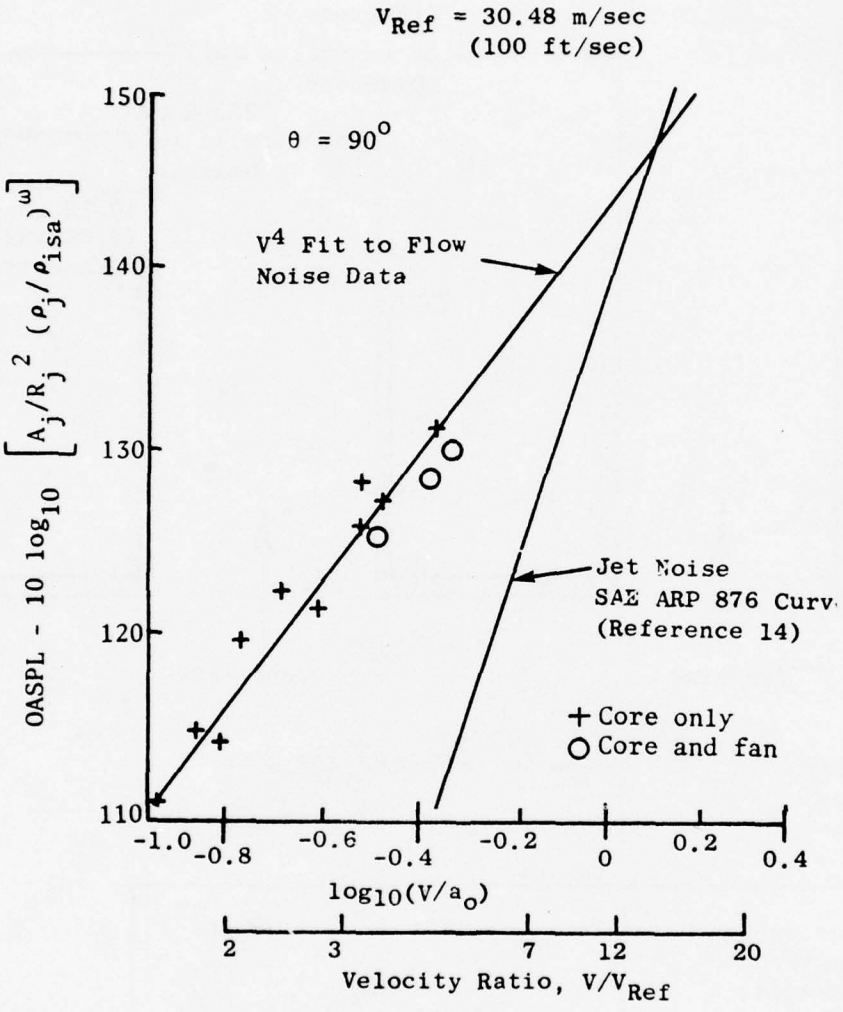

Figure 4-17. Flow Noise Correlation with Flow Velocity.

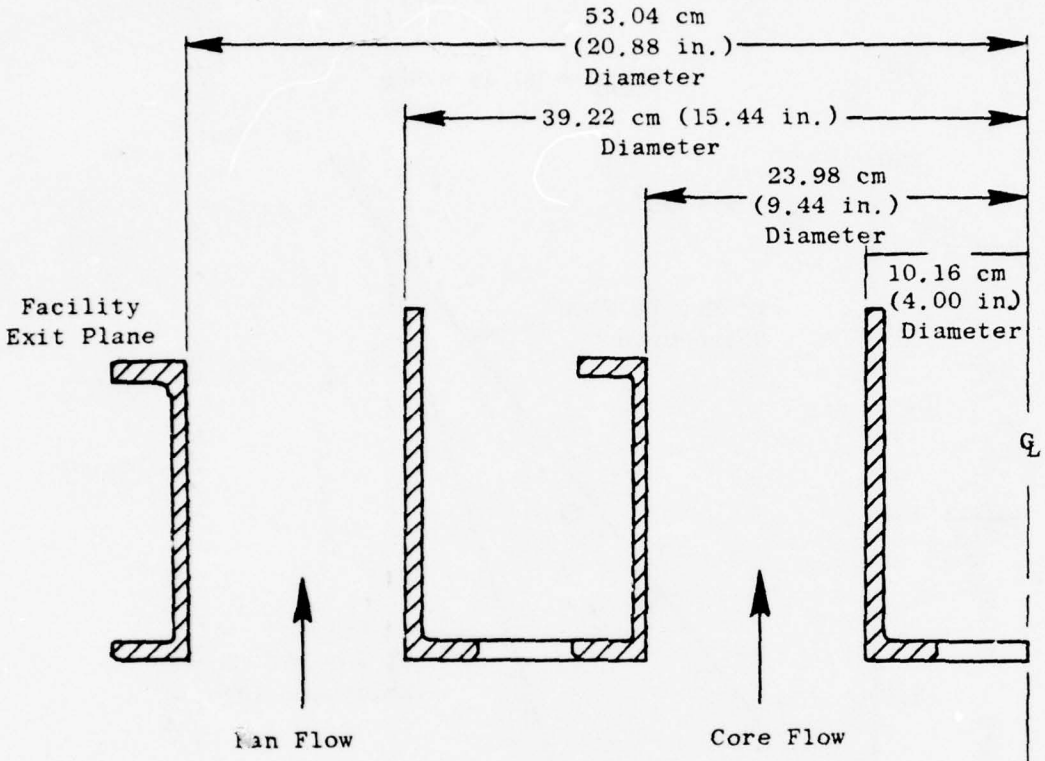

Facility Annulus Area	Core	= 370 cm^2 (57.4 $in.^2$)
	Fan	= 1001 cm^2 (155.2 $in.^2$)

Typical Exit Area with Test Nozzle Installed	Fan	= 78.3 cm^2 (12.14 $in.^2$)
	Core	= 109.0 cm^2 (16.9 $in.^2$)

Figure 4-18. Cross Section of Facility Exit Plane Annulus Area.

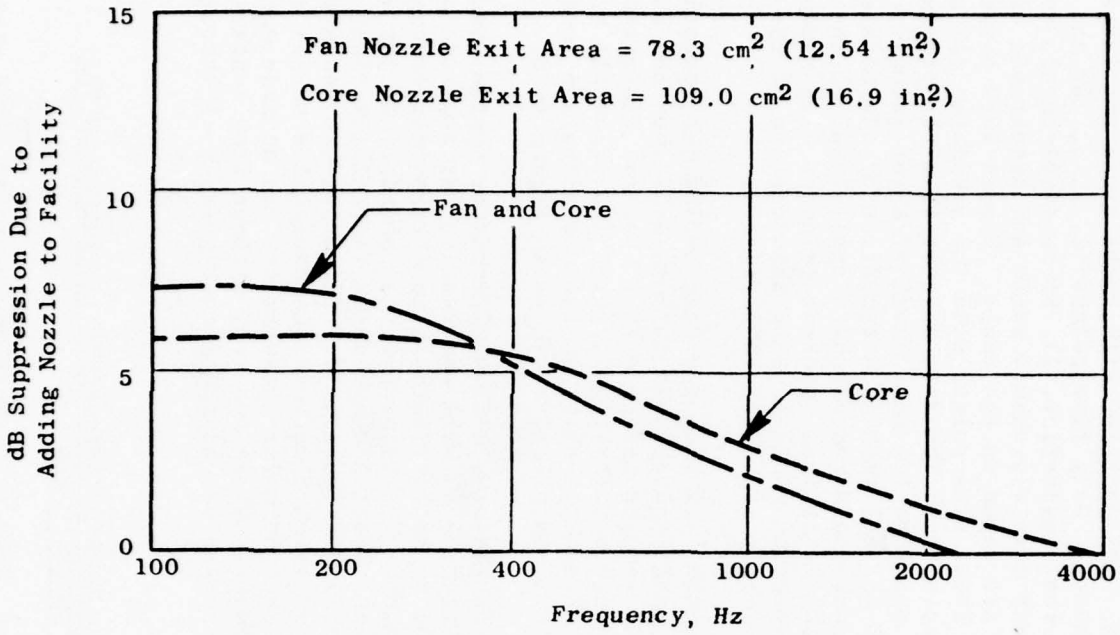

Figure 4-19. Attenuation Due to End Reflection Loss when a Nozzle is Added to the Facility.

Mach numbers exceeded the maximum which could be obtained with the intended nozzle. In Table 4-II, the required nozzle area to give choking at the exit with the same nozzle entrance Mach numbers measured with the nozzle removed are tabulated. Only nozzles with these areas and larger can achieve the measured Mach numbers. Only five points (1, 2, 3, 14, and 47) represent conditions with the single-flow, 11.786-cm (4.64-inch), core-only nozzle. The equivalent nozzle pressure ratio and isentropic exit velocity for these conditions are shown on the table. Figure 4-20 shows the measured flow noise OASPL for these five points with the predicted jet noise correlated against jet velocity. The data suggest that the piping noise and the nozzle jet noise would be the same level at a jet velocity of approximately 213 m/sec (700 ft/sec) with no attenuation by the nozzle. The nozzle transmission loss would reduce the overall level of the flow noise by something less than the maximum spectral value of 6 dB shown on Figure 4-19. A full 6 dB reduction would give an interception of the flow noise with the jet noise at about 152 m/sec (500 ft/sec).

Figures 4-21 through 4-24 show the single-flow jet acoustic spectra at various temperatures, and Figures 4-25 through 4-27 show the dual-flow spectra. Both sets of results indicate that spectral distortion due to flow noise does not occur until jet velocities are below 213 m/sec (700 ft/sec). An apparent frequency shift of the contamination tones also occurs when the nozzle is in place, as shown in Figure 4-28.

During checkout of the single-flow afterburner system, pure-tone components as shown in Figure 4-29 were observed in the acoustic spectrum. These tones were found to be attributable to afterburner combustion instability and rough burning. The mapping of the boundary of jet velocity and temperature combinations where A/B combustor instability first occurs is shown as the shaded area on Figure 4-30. The cross-hatched area on the figure is the region at which flow noise contamination occurs as per Figures 4-21 through 4-28. Good jet noise measurements can be made outside of these contamination zones. Clean spectra, without flow contamination, compared to referee spectra can be found on Figures 6-25 through 6-33 (see Section 6.3).

4.7 INFLUENCE OF AERODYNAMIC INSTRUMENTATION ERRORS ON THE INTERPRETED JET NOISE LEVELS

Another parameter which influences the measured sound pressure levels is the ability to accurately measure pressures and temperatures of the flow stream during jet nozzle operation. Errors in these parameters lead to misinterpretations of acoustic data and could cause disagreement when comparing levels on a test-to-test basis, as well as comparing levels measured from various other facilities.

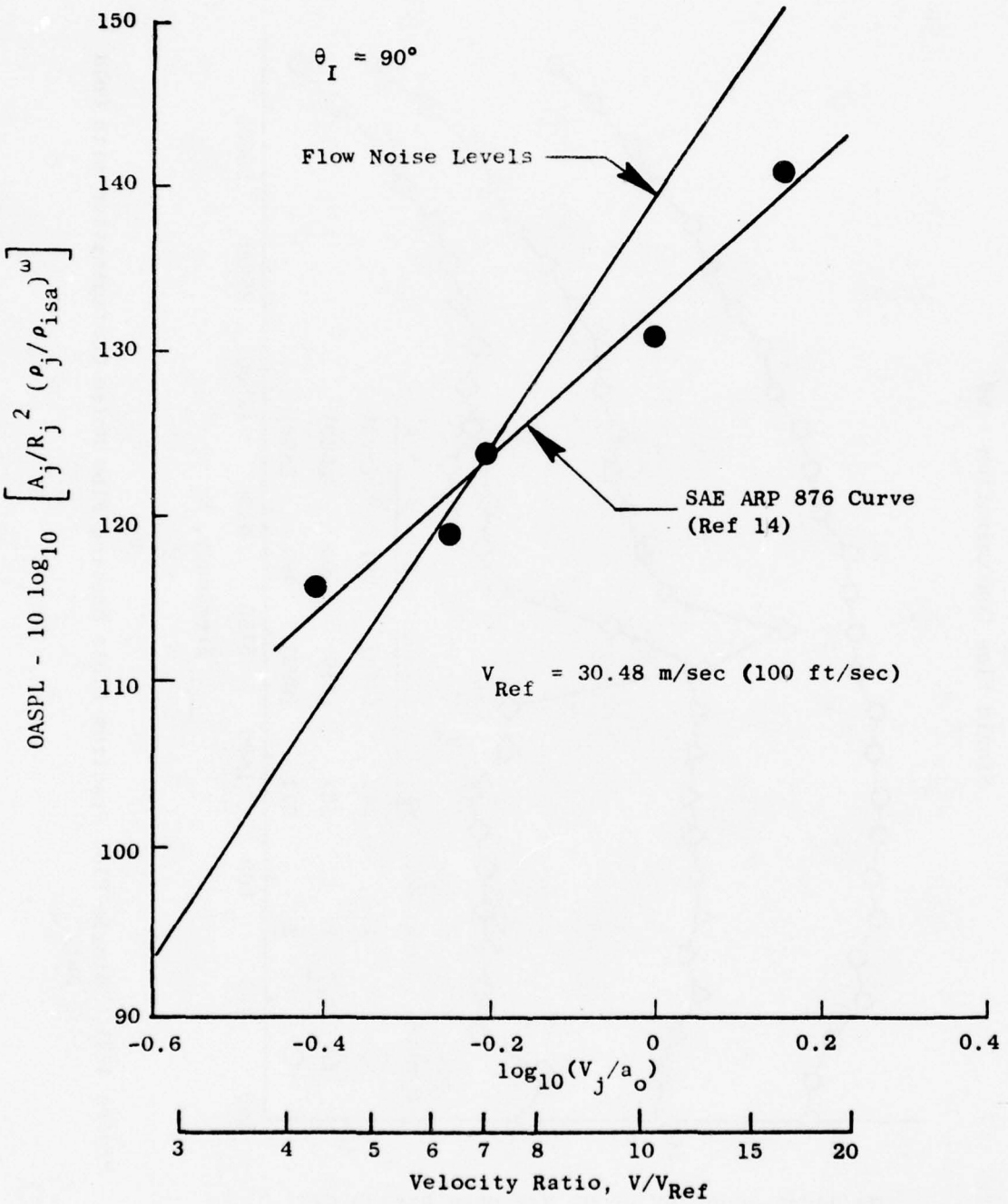

Figure 4-20. Flow Noise Correlation with Jet Exhaust Velocity if the Nozzle Were in Place.

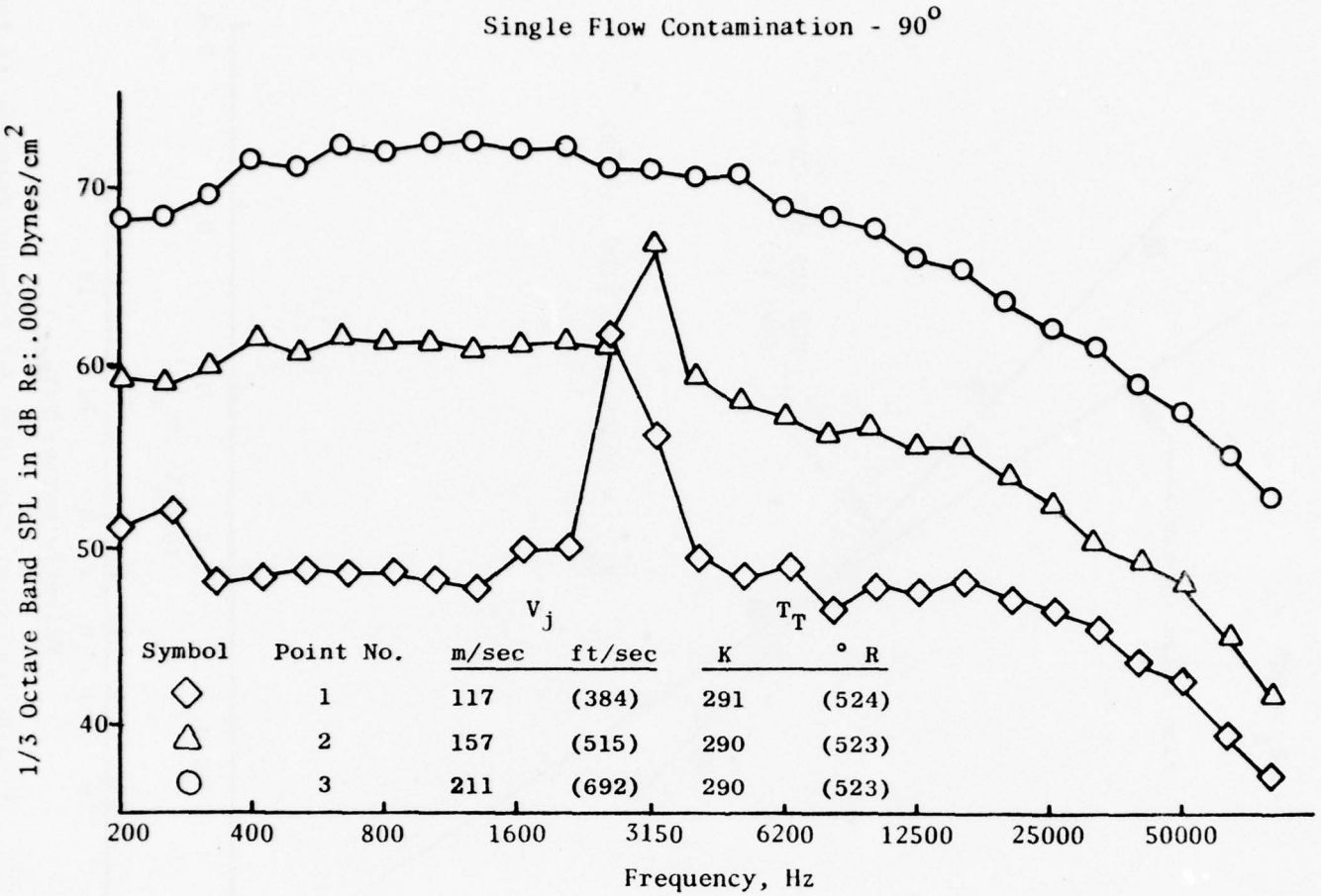

Figure 4-21. Single-Flow Spectrum Plots Showing Flow Noise Contamination with Cold Jet.

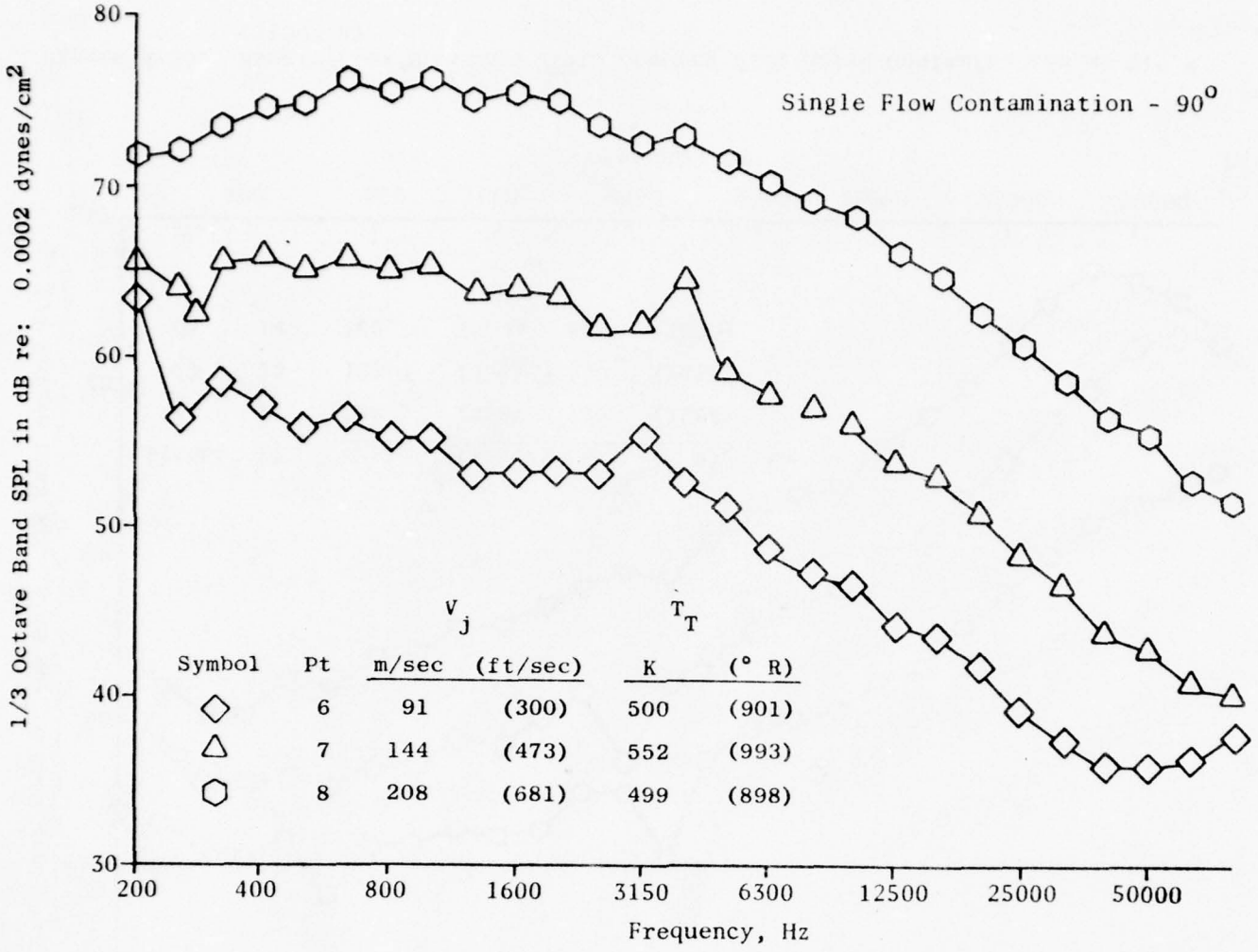

Figure 4-22. Single-Flow Spectrum Plots Showing Flow Noise Contamination at 500 K (1900° R).

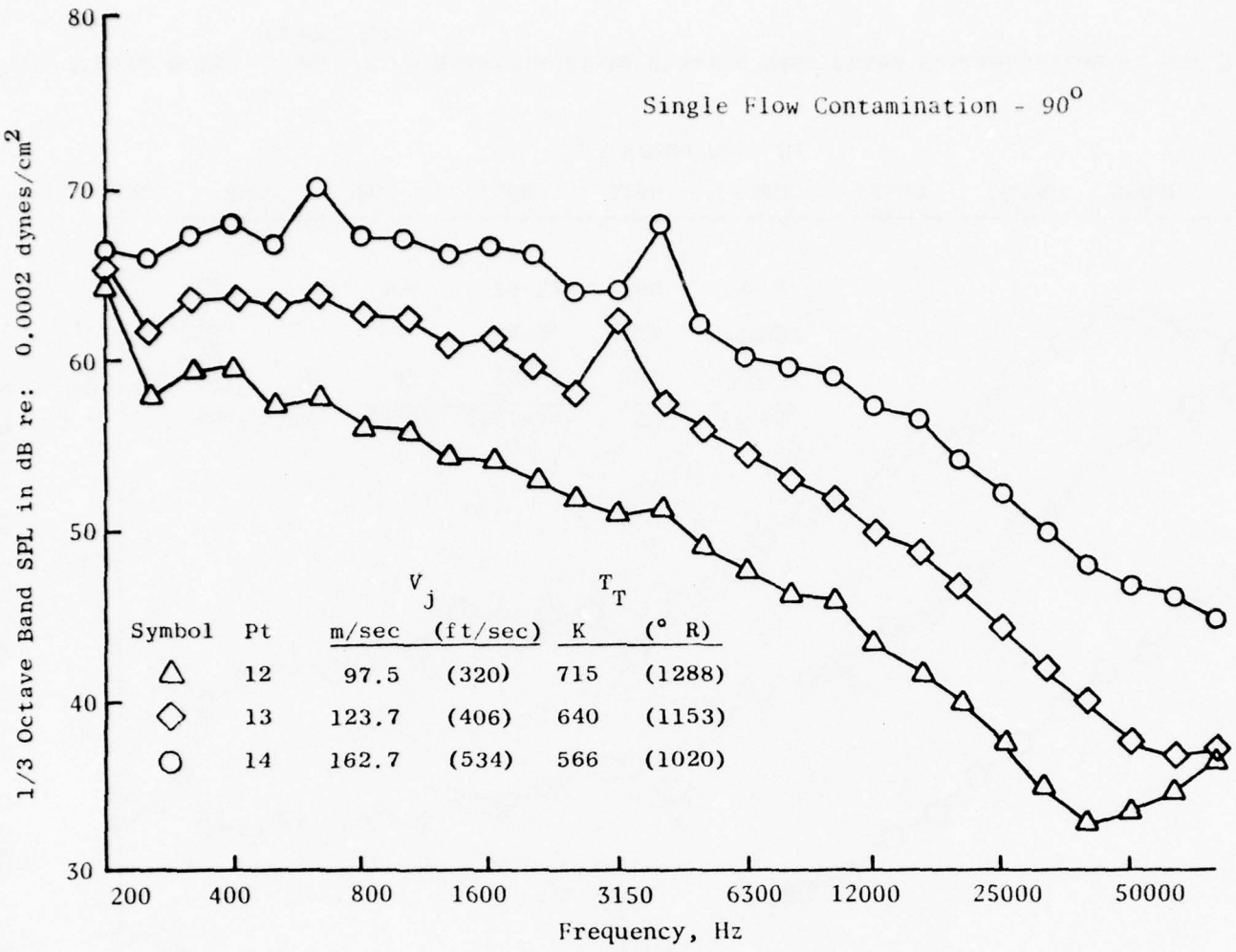

Figure 4-23. Single-Flow Spectrum Plots Showing Flow Noise Contamination at 610 K (1100° R).

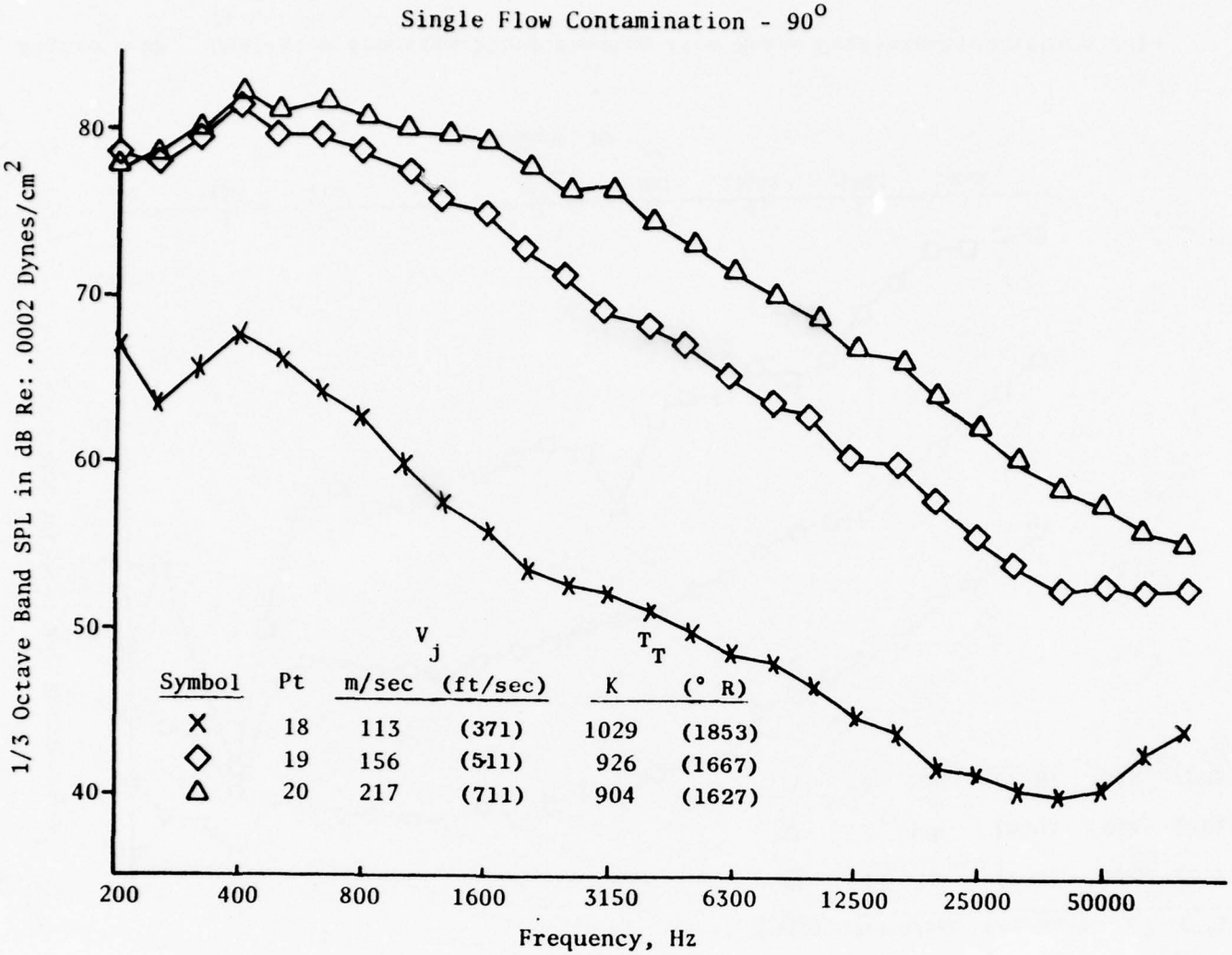

Figure 4-24. Single-Flow Spectrum Plots Showing Flow Noise Contamination at 945 K (1700° R).

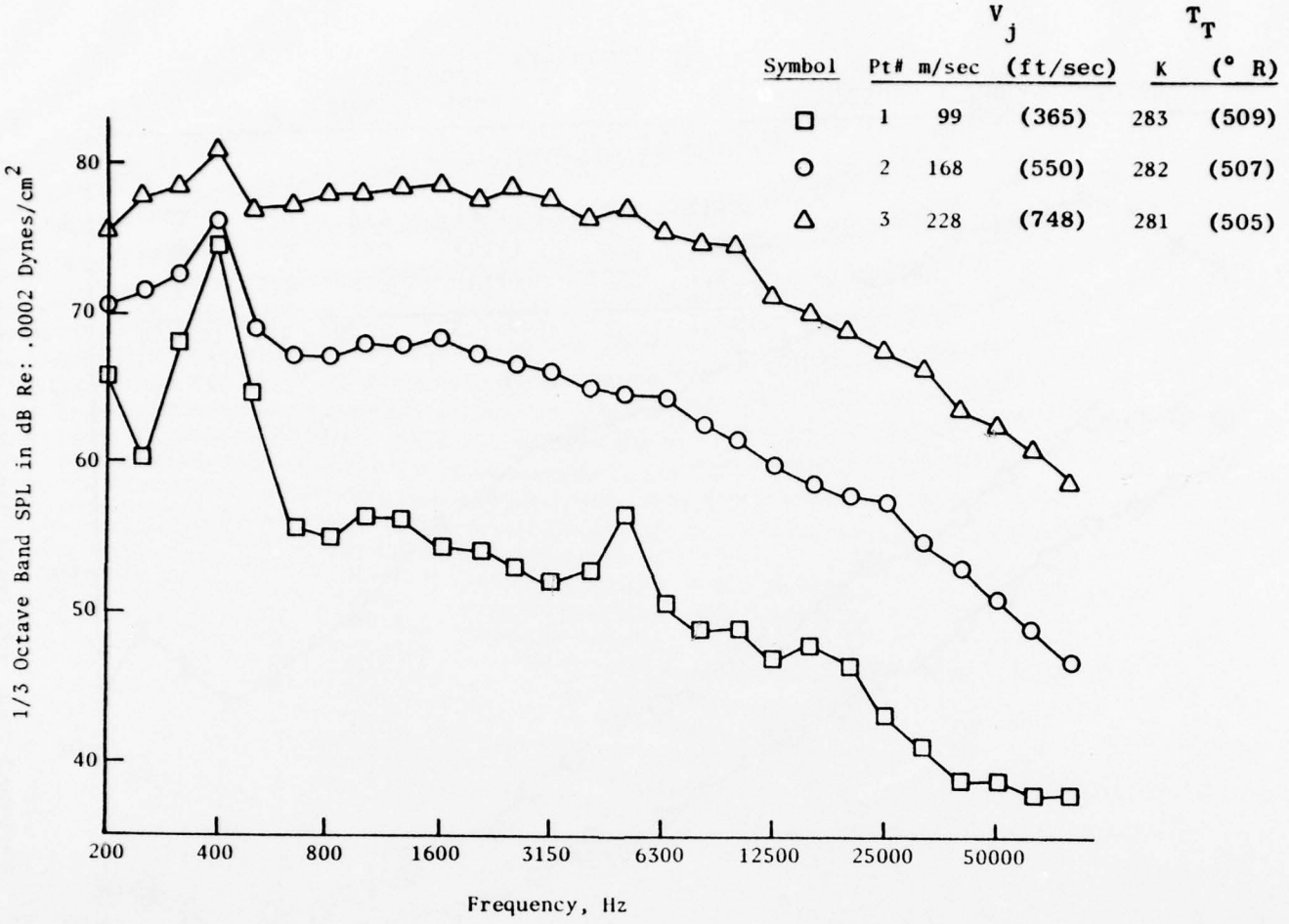

Figure 4-25. Dual-Flow Spectrum Plots Showing Flow Noise Contamination with a Cold Jet.

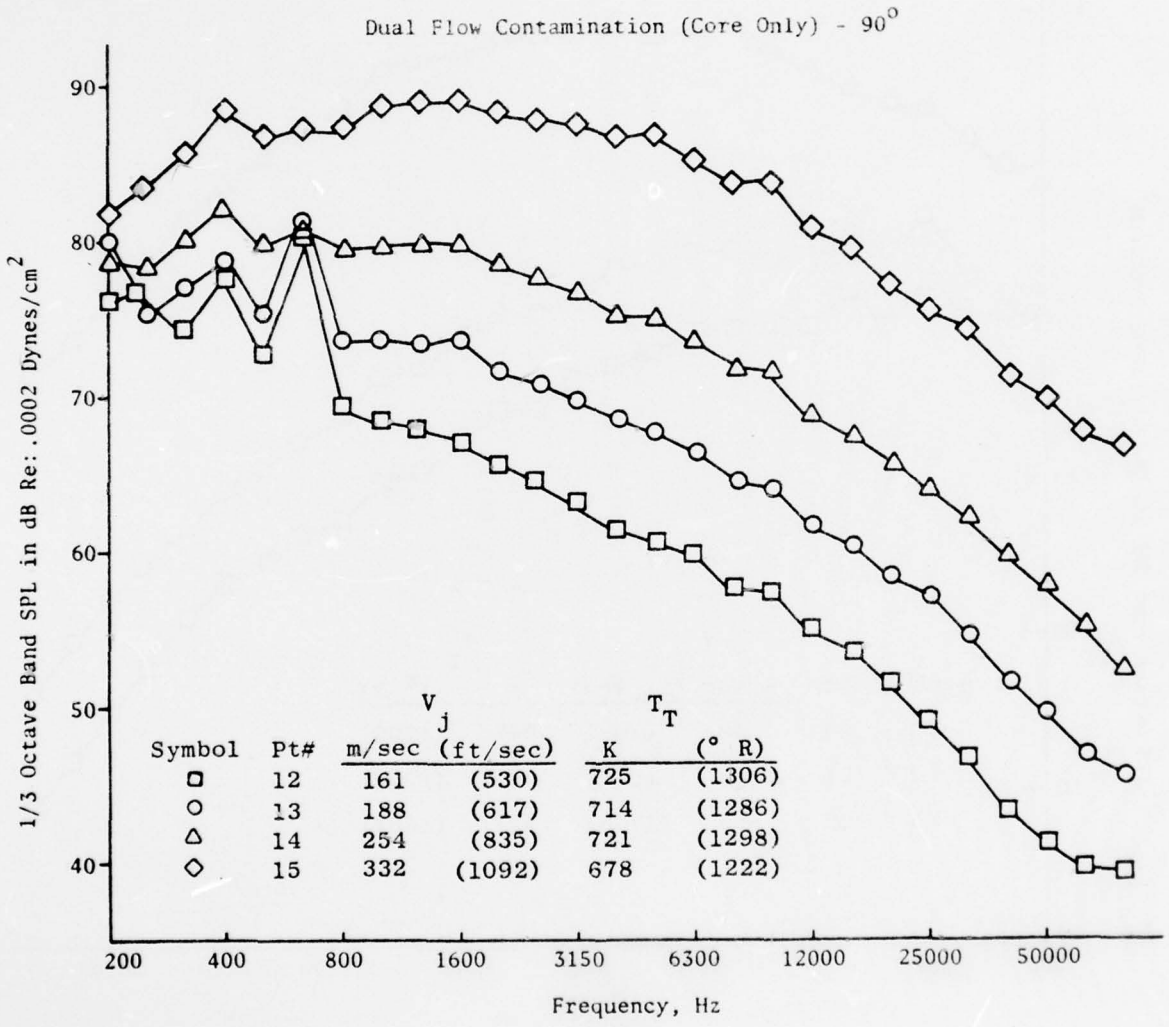

Figure 4-26. Dual-Flow Spectrum Plots Showing Flow Noise Contamination at 700 K (1260° R).

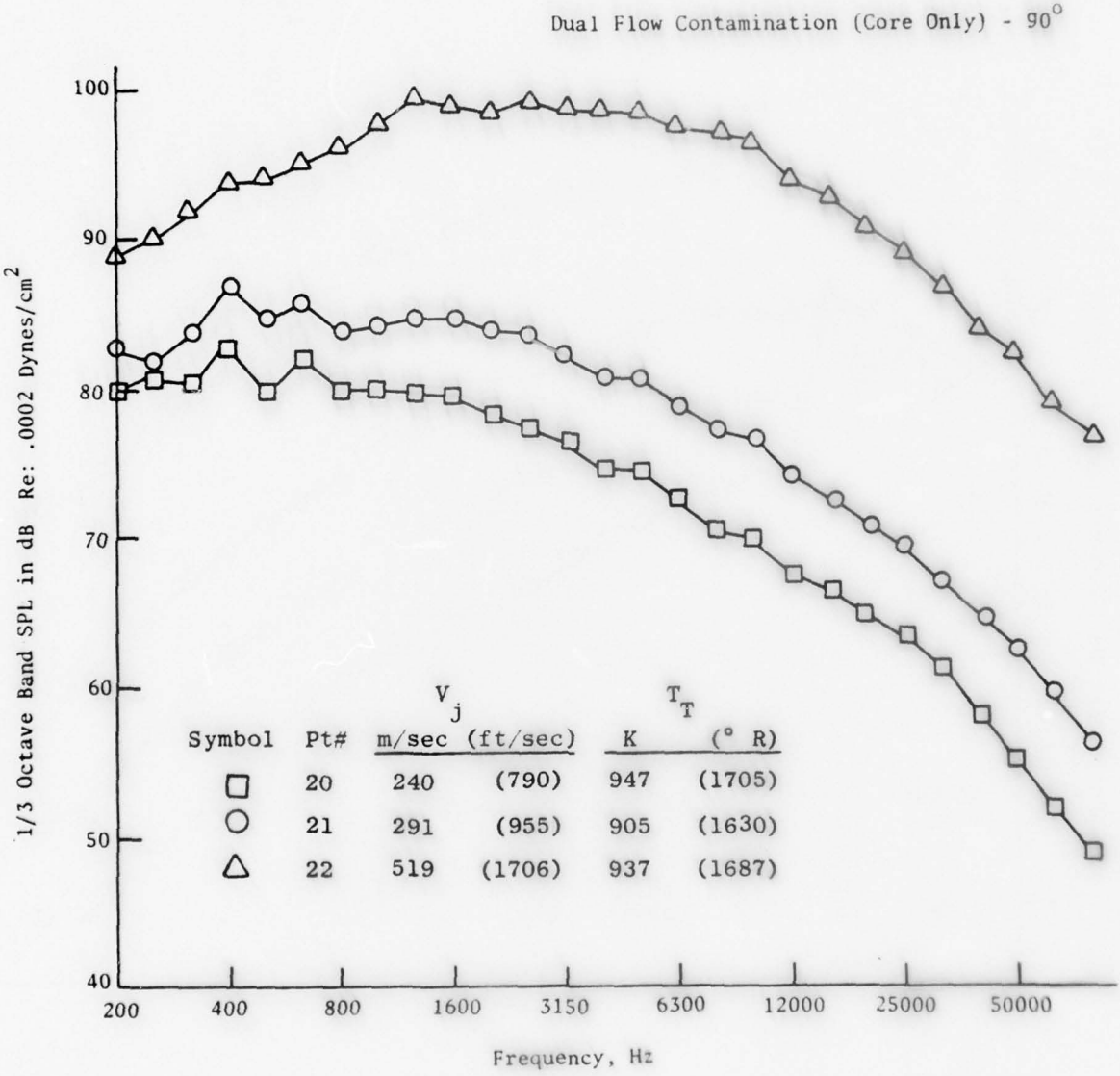

Figure 4-27. Dual-Flow Spectrum Plots Showing Flow Noise Contamination at 920 K (1656° R).

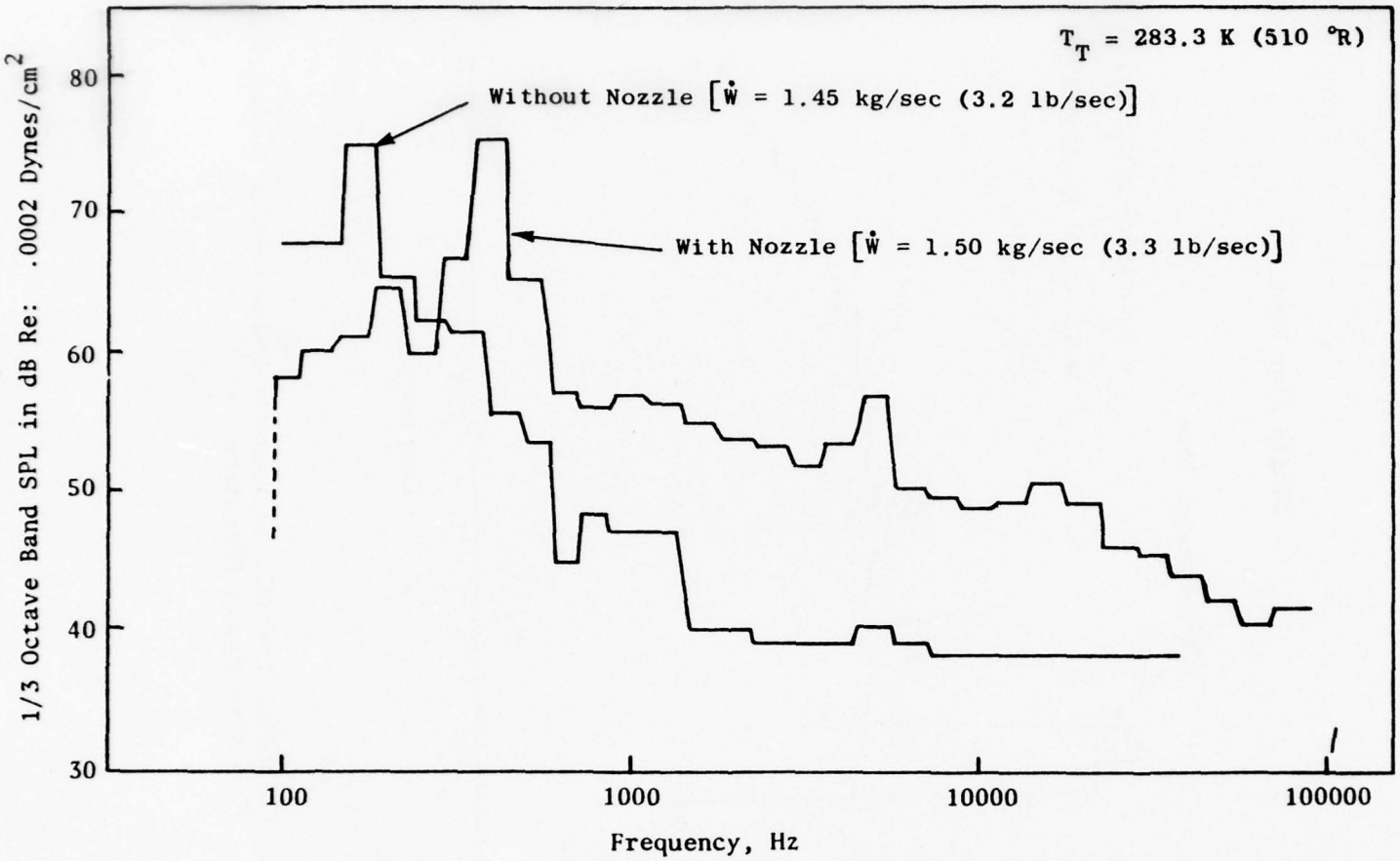

Figure 4-28. Flow Contamination Test with and without Nozzle.

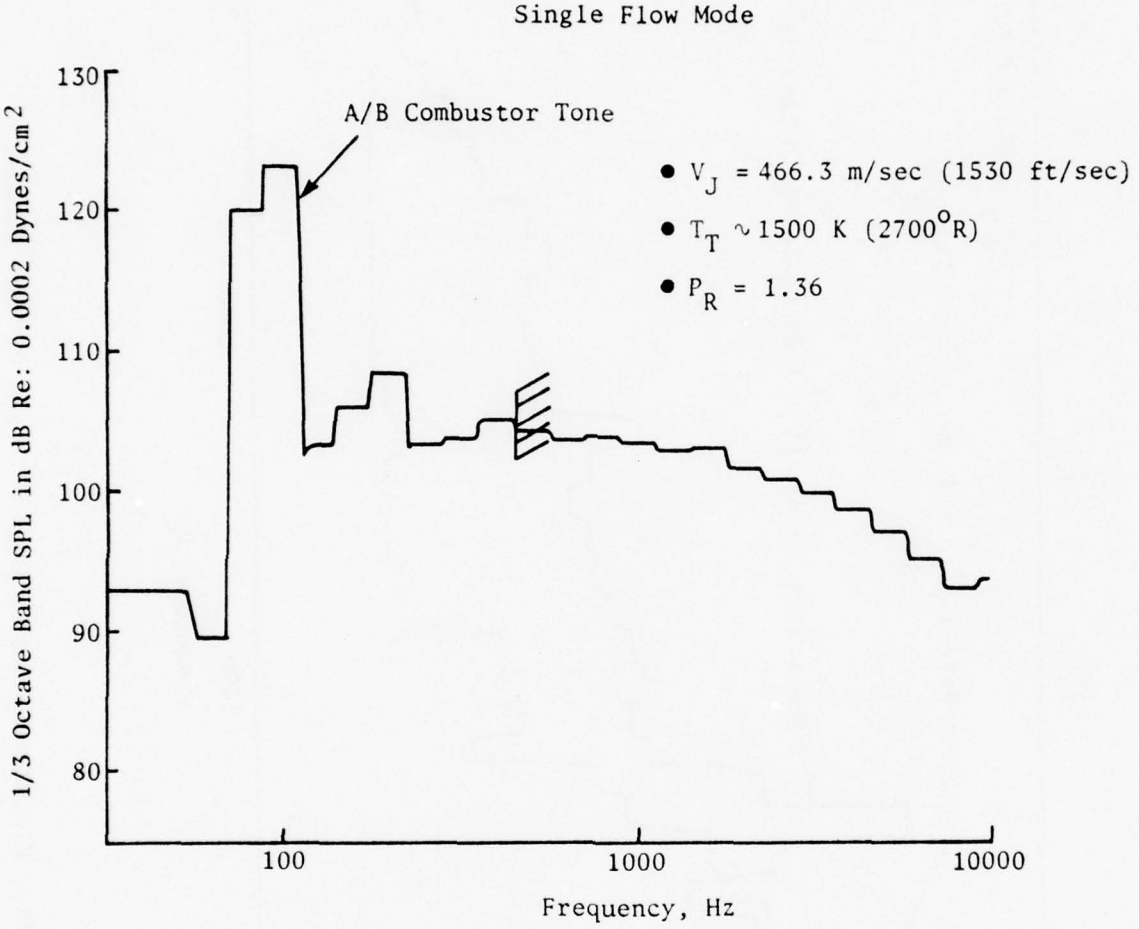

Figure 4-29. Combustor Instability Acoustic Contamination During Single-Flow Afterburner Operation.

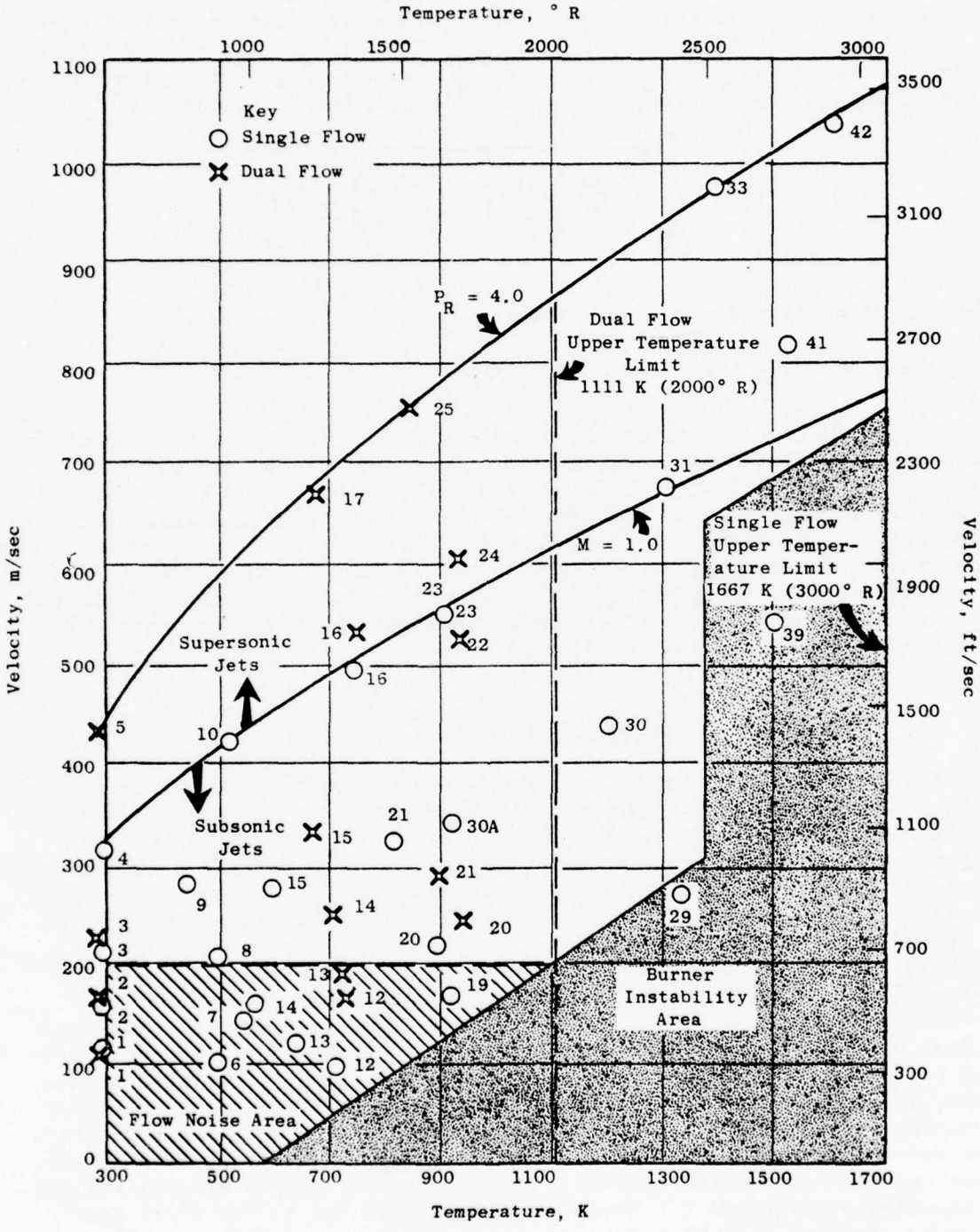

Figure 4-30. General Electric Anechoic Jet Noise Facility Operating Limits.

In Section 2.4.2, tolerances in the aerodynamic instrumentation were discussed in terms of percent error in T_T, P_T, and V_j. The rms deviation in overall sound power level (OAPWL) as a function of uncertainties in these aerodynamic parameters was calculated from the relationship:

$$\sigma_{PWL} = \sqrt{\left(\frac{\partial PWL}{\partial V_j}\right)^2 \sigma_{V_j}^2 + \left(\frac{\partial PWL}{\partial T_{T8}}\right)^2 \sigma_{T_{T8}}^2}$$

where an OAPWL dependence of the form:

$$PWL \propto 80 \log_{10} (V_j) - 10 \omega \log_{10} (\rho_8)$$

was assumed (ρ_8 is the jet static density and ω is the density exponent which has a complex dependence on velocity). The results are shown in Figures 4-31 and 4-32 as a function of variations in T_T and V_j for $V_j \geq 91$ m/sec (300 ft/sec) and $T_{T8} \geq 306$ K (550° R). From these figures, it is seen that (for both the single- and dual-flow aerodynamic measurement systems) a low velocity and a high temperature gave a large error in PWL. In the single-flow afterburner system, a minimum 1.5 dB standard deviation is seen as a result of the inaccuracies in platinum-rhodium thermocouples at ambient temperature flow conditions.

4.8 AIR ATTENUATION CORRECTIONS AND ACCURACY

The attenuation of sound over the distance from the jet source to the microphone will change with changes in the ambient air temperature and humidity from day to day. It is common practice in the General Electric Company and throughout industry to attempt to account for these differences by either correcting the data for air attenuation from the measured day values to a "standard day" of 15° C (59° F) and 70% relative humidity, or by removing all the air attenuation from the data. For low frequencies below 10 kHz, these corrections have been calculated using ARP 866 (References 2 and 3). This work extended the experimental data of Harris (Reference 8) taken at 20° C (68° F) to other temperatures using the theoretical work of Knesner (Reference 9). Harris' experiments, however, were only performed to 12.5 kHz narrowband, so he only gave corrections to the 8 kHz, 1/3-octave band (10 kHz in Reference 3). Extrapolations to higher frequency are somewhat difficult, since Knesner's single-relaxation theory does not fully account for all the energy transfer. Recently Bass, Bauer, Evans, and Sutherland (References 4 and 10) have developed a model for air attenuation predictions for frequencies up to 100 kHz at the fixed temperature of 20° C (68° F). They do not recommend that their model be extrapolated to other temperatures beyond a 5° C (9° F) spread. Research presently is underway (Reference 11) by Bass and Shields at the University of Mississippi to expand this model to the full range of temperature.

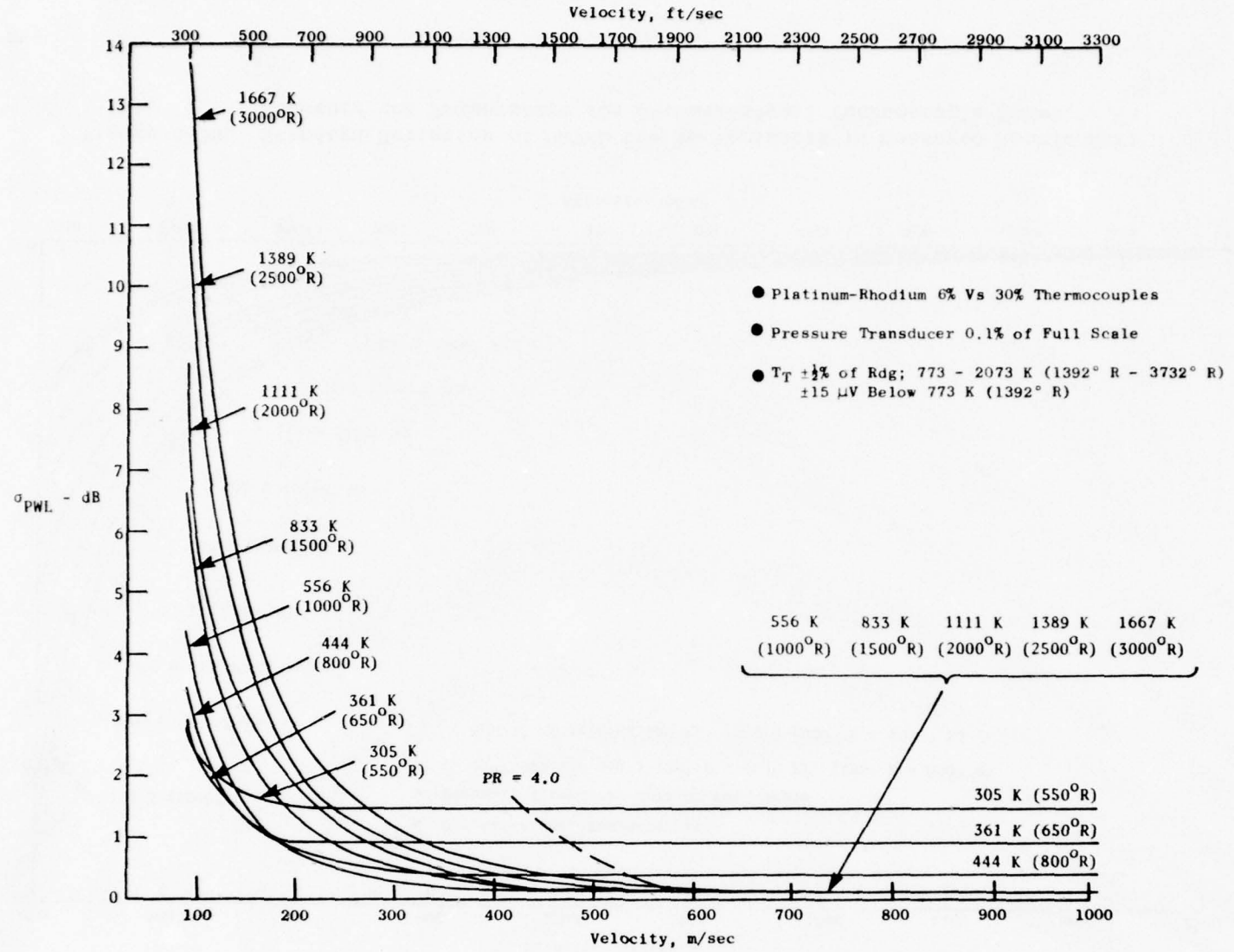

Figure 4-31. Standard Deviation of OAPWL Due to Variances in Measured Jet Nozzle Pressure and Temperature for Platinum Rhodium Thermocouple Rakes.

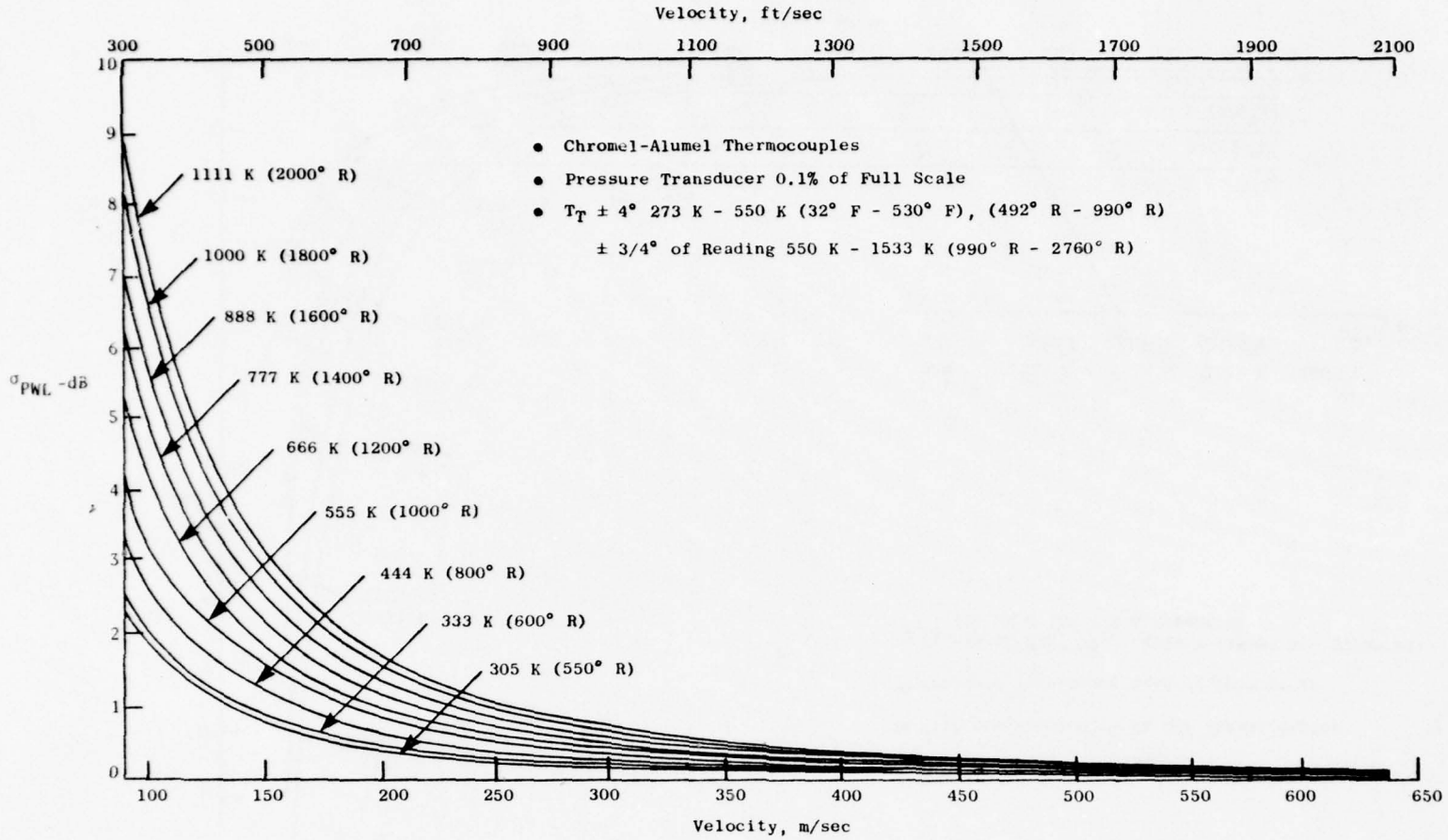

Figure 4-32. Standard Deviation of OAPWL Due to Variances in Measured Nozzle Exit Pressure and Temperature for Chromel Alumel Thermocouple Rakes.

A model was recently developed by Landon Evans of the Boeing Company which has been proposed as an American National Standard S-157 to the Standards Committee of the ASA. It is this model which has been used as a standard of comparison by the researchers at the University of Mississippi. A comparison of this model and the one proposed in Reference 13 revealed identical results.

The need for corrections at higher frequencies led to a General Electric Company extension to 80 kHz (Reference 12). These corrections were developed by extrapolations of the ARP 866 curves tempered by the application experience of scaling jet spectra from nozzle ranges from 1 inch to 4 feet in diameter. During the inverse square law testing of the chamber with air ball source (see Section 3.2), corrections to the high frequency were required to obtain the expected 6 dB per doubling decay. The GE model was tried, but was found to be inadequate to account for the full atmospheric absorption which was experienced. Fortunately, the ambient temperature during the test was within the 5° C (9° F) spread from 20° C (68° F) recommended for the Bass, Bauer, and Evans model. These predictions were found to give excellent results as discussed in Section 3.2. Subsequent testing has been performed over a wide range of temperatures where no verified model exists.

Errors in the corrections for air attenuation can be of two types: lack of accuracy and lack of precision. An accuracy error is encountered because of the lack of a good model, so a certain amount of bias or systematic error will be experienced which could be eliminated were a proper correction model known. Precision errors occur from random sources such as inaccuracies in the ambient temperature and humidity measuring equipment and instantaneous fluctuations in the temperature or humidity along the acoustic path. Fixed gradients in the chamber, as discussed in Section 3.3, will result in an accuracy error if they are not accounted for by a layer atmosphere or similar analysis. The lack of a good model for even the no-gradient case, however, does not justify the additional effort required to account for such gradients.

The Bass, Bauer, and Evans model was used for all the data in this report, even when the ambient temperature was beyond the recommended range.

The question of precision errors can be calculated from an analysis of variance study of the ARP 866A equations. The standard deviation of the air attenuation correction factor, σ_α, can be obtained from:

$$\sigma_\alpha = \sqrt{\left(\frac{\partial \alpha}{\partial T}\right)^2 \sigma_T^2 + \left(\frac{\partial \alpha}{\partial h}\right)^2 \sigma_h^2}$$

where α is the air attenuation correction, T is the temperature, and h is the absolute humidity. The choice of the standard deviation in temperature, T, and absolute humidity, h, are obtained by considering the variations which can occur in the measurement equipment and along the sound path. In Section 2.4.5, the accuracy of chromel alumel (CA) thermocouples used to measure the ambient temperature was designated at 51° F, while the relative humidity sensor had a guaranteed specification of ±2% relative humidity (RH). The steady-state gradients, which normally existed in the chamber, ranged from over 3° C (5.4° F) and 6 to 8% RH. Figure 4-33 shows these gradients displayed on a psychrometric chart. A variation of absolute humidity of 1.5 g/m^3 (8.8 grains of moisture per pound of dry air) appears to be representative. Figures 4-34 through 4-38 show the results of the analysis of the variance in the ARP 866A air attenuation model at frequencies of 1, 5, 10, 20, and 80 kHz. The contour plot of constant standard deviation of the air attenuation correction, σ_α, in dB is given by the islands for a 304.8-m (1000 ft) microphone distance. The appropriate standard deviation experienced over the distances given in Table 2-I are found by multiplying σ_α by the ratio of the radius in feet over 1000. The figures show a large possibility of precision errors depending on the ambient temperature and humidity; the largest errors occur at high frequency and low humidity. Figure 4-39 displays the error as a function of frequency for various % relative humidity at a 20° C (68° F) temperature for the 8.23 cm (27-foot) attenuation distance present in the chamber.

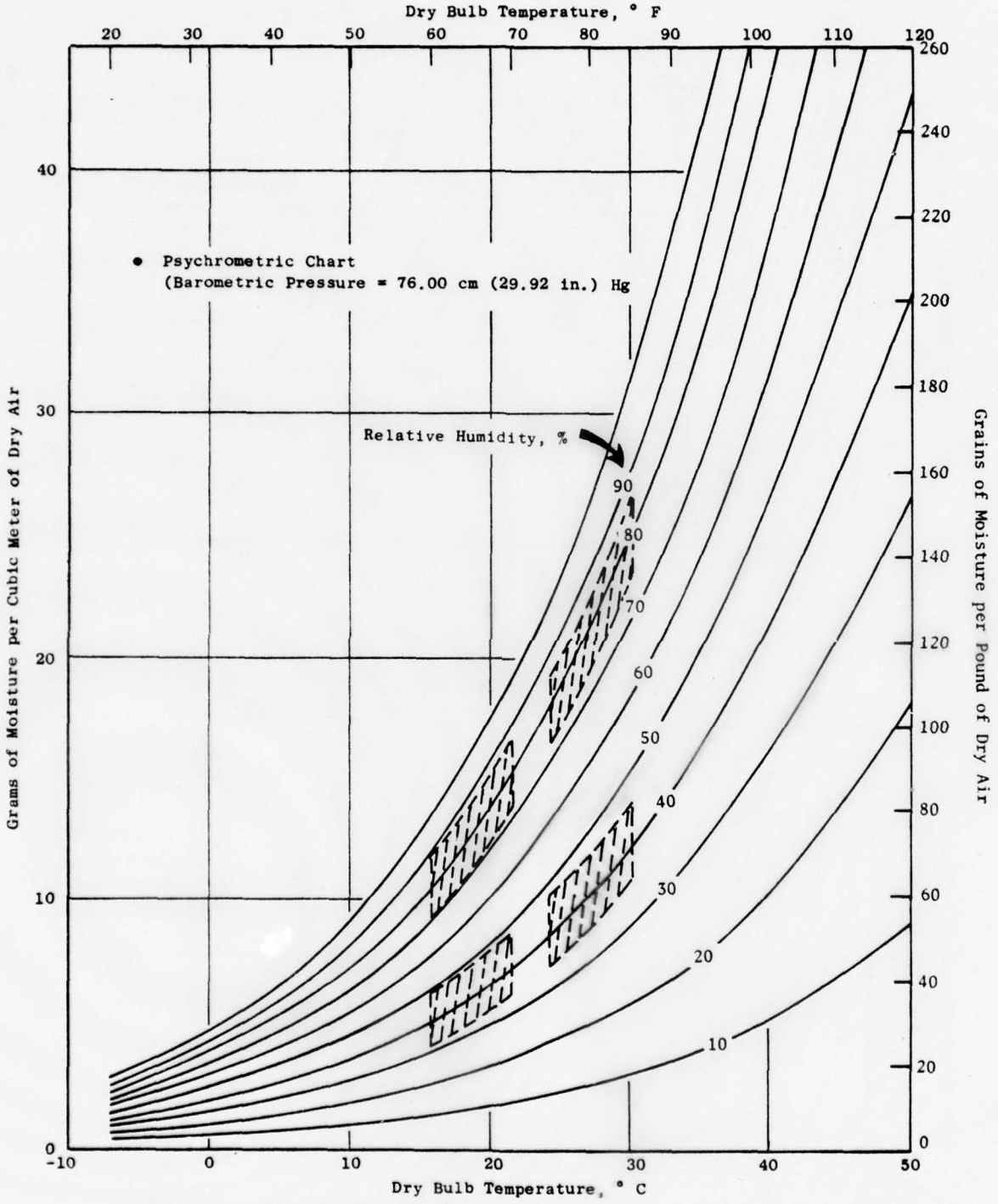

Figure 4-33. Psychrometric Chart Showing the Degree of Temperature and Humidity Excursions in the Chamber.

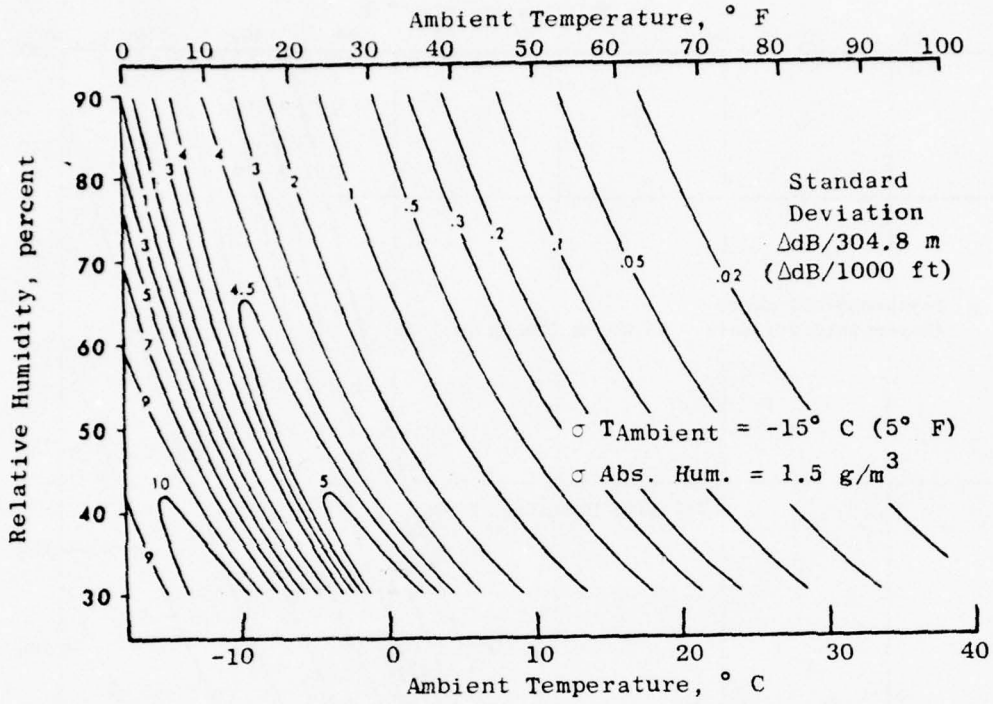

Figure 4-34. Atmospheric Attenuation Standard Deviation at 1000 Hz.

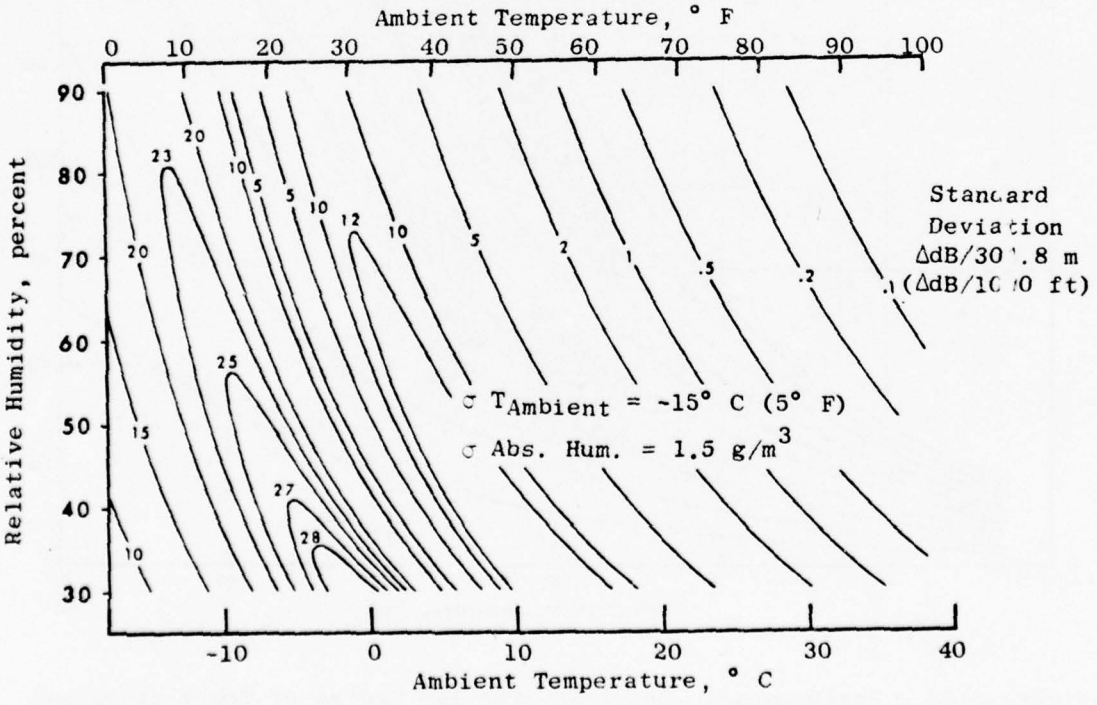

Figure 4-35. Atmospheric Attenuation Standard Deviation at 5000 Hz.

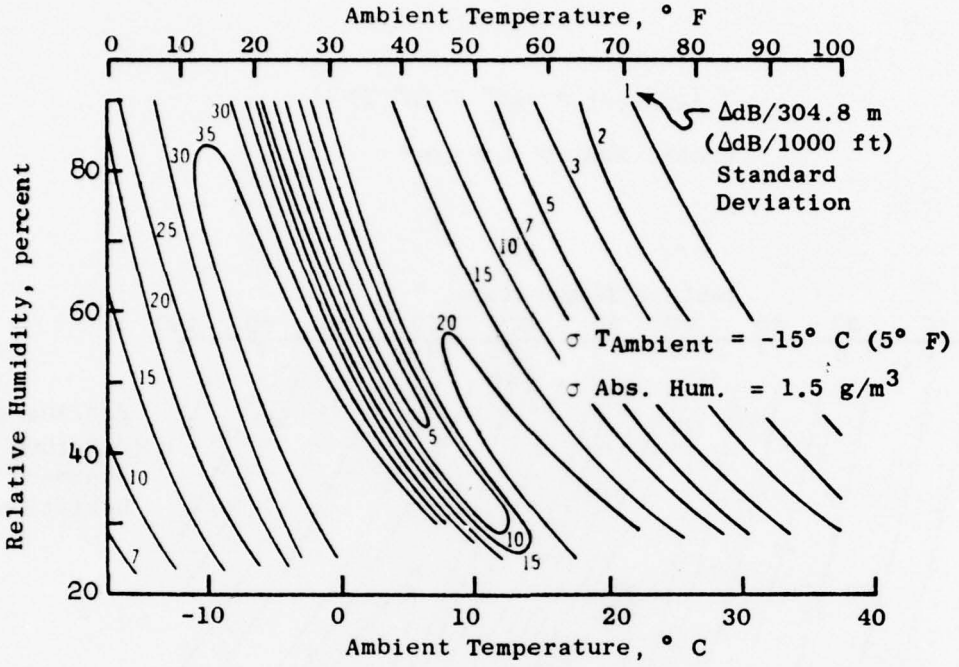

Figure 4-36. Atmospheric Attenuation Standard Deviation at 10,000 Hz.

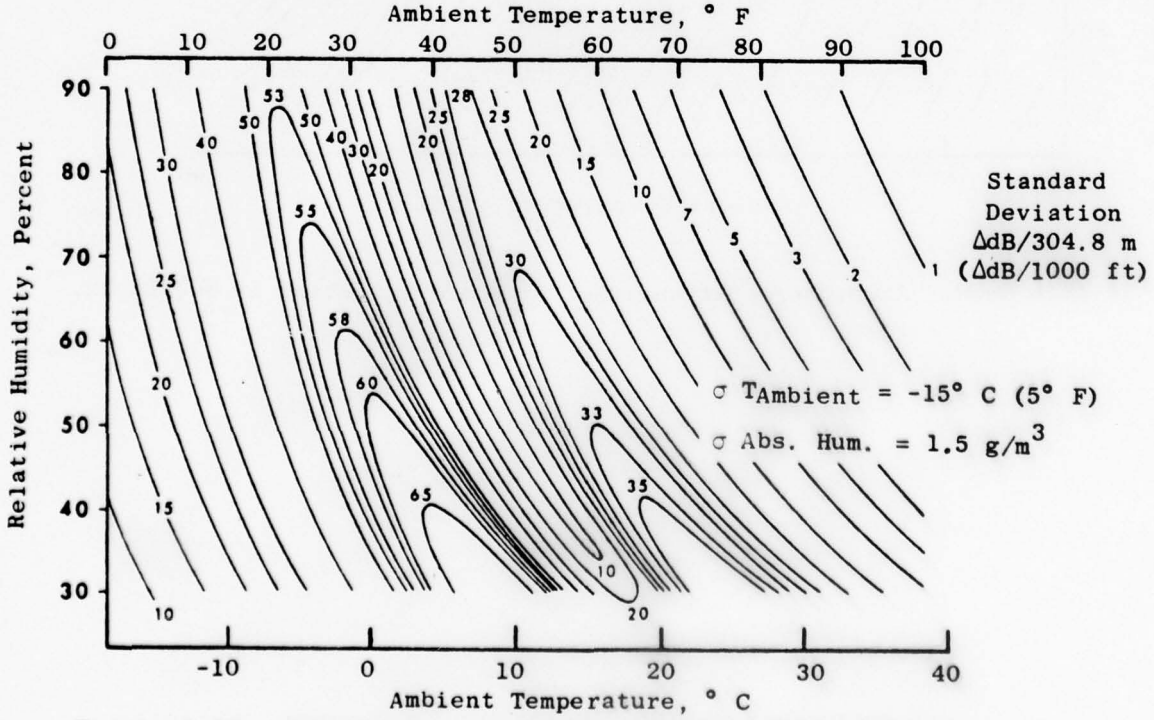

Figure 4-37. Atmospheric Attenuation Standard Deviation at 20,000 Hz.

σ $T_{Ambient}$ = -15° C (5° F)

σ Abs. Hum. = 1.5 g/m^3

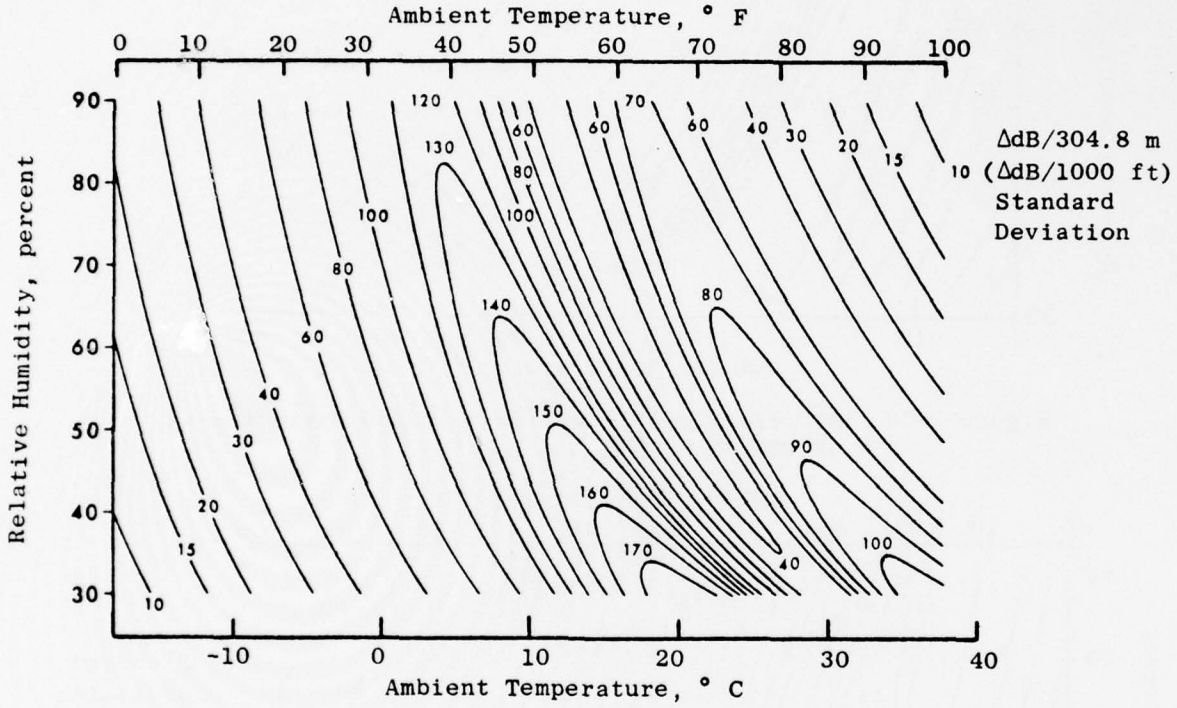

Figure 4-38. Atmospheric Attenuation Standard Deviation at 80,000 Hz.

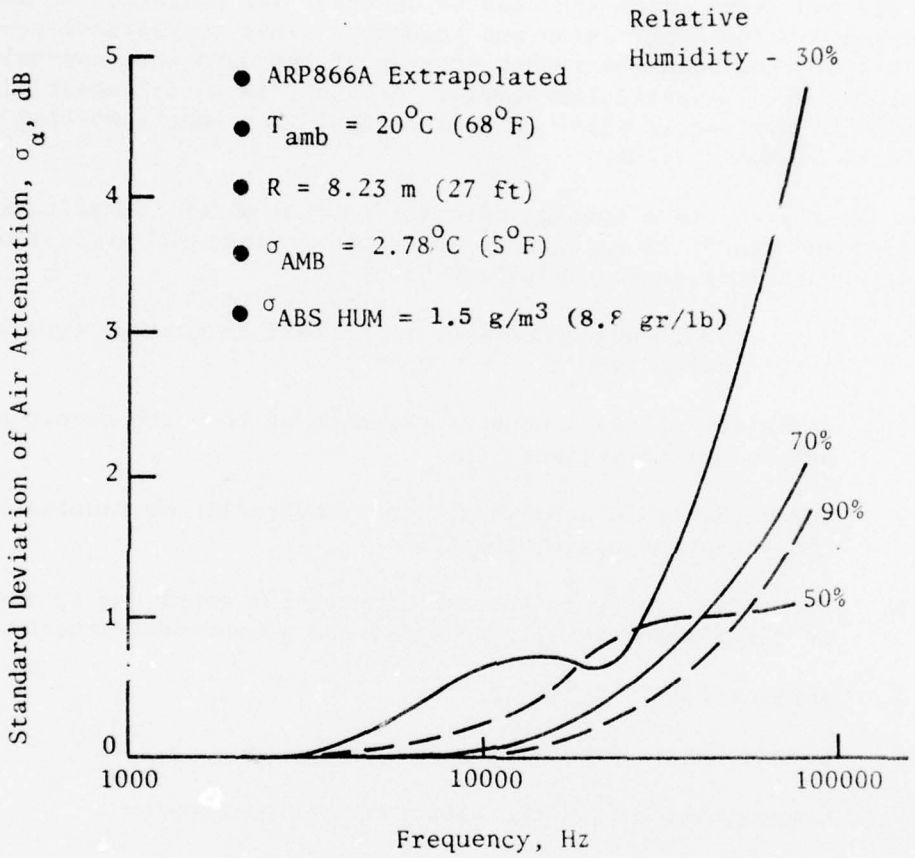

Figure 4-39. Standard Deviation of the Air Attenuation in the Anechoic Chamber at 20° C (68° F) due to Ambient Environmental Fluctuations.

5.0 ANALYSIS OF VARIANCE - OVERALL PRECISION OF THE ACOUSTIC MEASUREMENTS

5.1 INTRODUCTION

There are two terms which are used to describe the deviation of data from its expected value: precision and accuracy. In a statistical sense precision is concerned with the random scatter of the data when comparing the mean of the data with a particular sample. Accuracy is a term describing the amount of bias or systematic error in a data population when comparing the mean to a fixed or known value.

Figure 5-1 represents a montage of error sources which contaminate the pure jet noise and result in significant loss of accuracy and precision. Such biasing errors include contamination from:

Item 1. Nonanechoic environment and near-field deviations from inverse square law

Item 2. Variation of the frequency response of the data acquisition and reduction systems

Item 3. Inaccuracies in aerodynamic instrumentation or fluctuations in the jet aerodynamic conditions

Item 4. Precision errors in the air attenuation model due to environmental fluctuations, gradients, and measurement inaccuracies

Item 5. Ambient levels in the chamber

Item 6. Contamination from piping and combustors

Item 7. Contamination from the electronic noise floor.

The problem is then defined. Given an acoustic facility which generates a typical frequency spectrum such as shown by the symbols on Figure 5-1, make the necessary modification or establish appropriate correction factors to the data so the facility will produce the desired jet noise spectra indicated by the dashed line on Figure 5-1. Furthermore, the precision of the final corrected sound pressure level with frequency will exhibit specific standard deviations from the lowest frequency of interest to 80 kHz as indicated by the precision band on the figure.

For those effects which change the measured acoustic pressure by a multiplier (Items 1 to 4), the measured SPL is adjusted by a given adder:

$$SPL_m = SPL_{jet} + \sum_{i=1}^{K} \Delta_i$$

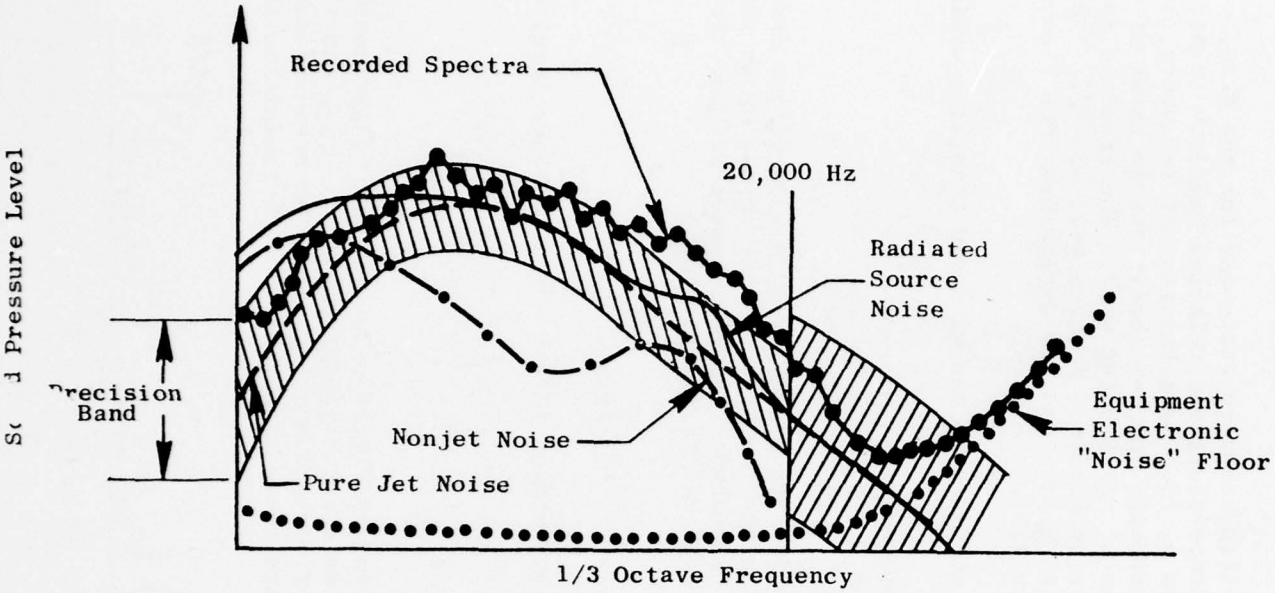

Figure 5-1. Montage of Possible Contaminants to Acoustic Measurements.

In this case, the standard deviation of measurement, σ_m, is simply the root mean square of each of the individual standard deviations.

$$\sigma_m = \sqrt{\sum_{i=1}^{K} \sigma_i^2}$$

To obtain a specific accuracy statement for the data, one must first specify the ambient temperature and relative humidity to determine the standard deviation of Item 4, (σ_4) as a function of frequency, from Figures 4-34 through 4-38. Then, specify the jet conditions in terms of velocity, temperature, and the type of rakes being used. The standard deviation of Item 3 (σ_3) can then be determined from Figures 4-31 or 4-32. The standard deviations from Items 1 and 2 (σ_1, σ_2) are determined from Figures 3-11, 3-39, and Table 4-I (Section 4.3).

An intermediate estimate of the measured precision variance can then be obtained as:

$$\sigma_{int} = \sqrt{\sigma_1^2 + \sigma_2^2 + \sigma_3^2 + \sigma_4^2}$$

Bias contaminations which are specified by a known floor level, SPL_i, such as Items 5, 6, and 7 influence the measured SPL depending on the numerical difference in level, δ_i, between the measurement without the contaminated floor and the noise level of the floor, viz.:

$$\delta_i = \left| SPL_{\text{no floor}} - SPL_{\text{floor } i} \right|$$

The magnitude of the adjustment to the no-noise floor level is given by:

$$SPL_m = SPL_{\text{no floor}} + 10 \log_{10} \left(1 + 10^{-\delta_i/10} \right)$$

This relation is plotted in Figure 5-2. The SPL measurement without the noise floor present has a variation given by $\sigma_{\text{no floor}}$ and the standard deviation of the floor variation is σ_{floor}. The standard deviation of the measured sound pressure level with the floor contamination included will be given by:

$$\sigma_m = \frac{\left[\left(10^{-\delta_i/5} \right) \left(\sigma_{\text{no floor}} \right)^2 + \left(\sigma_{\text{floor } i} \right)^2 \right]^{1/2}}{\left(1 + 10^{-\delta_i/10} \right)}$$

This relation is plotted in Figure 5-3.

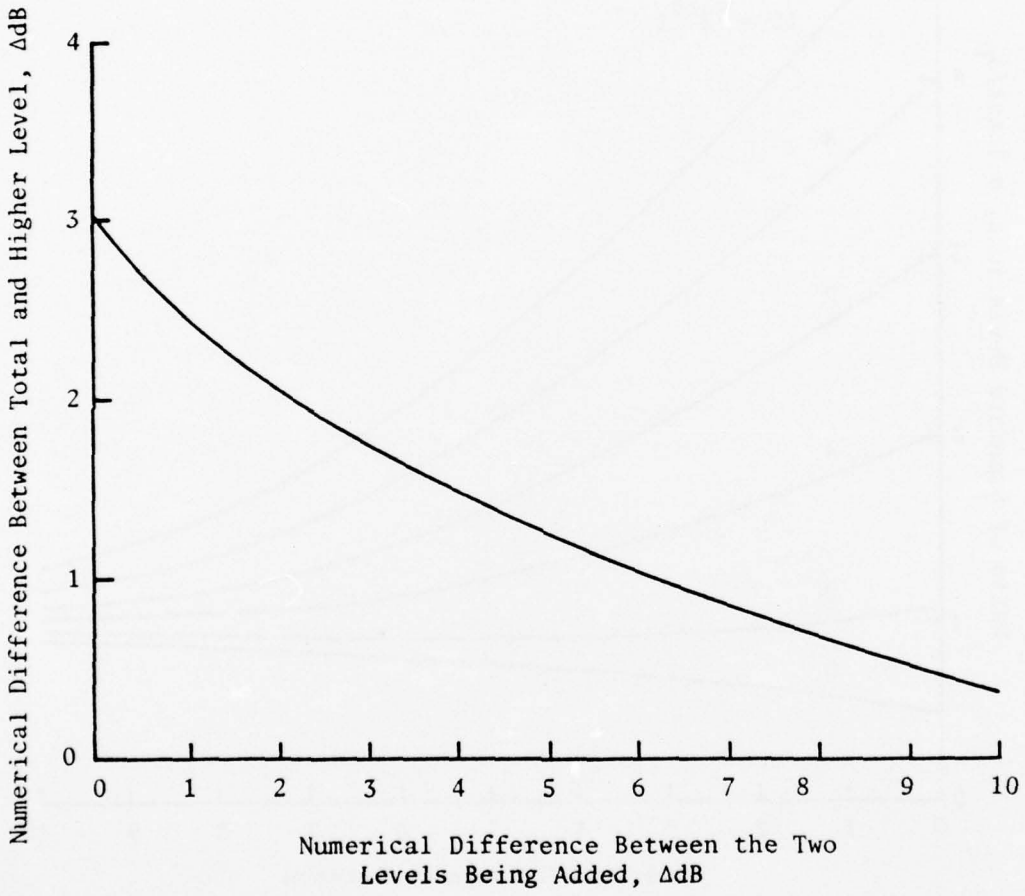

Figure 5-2. Effect of Adding Two Sound Levels on the Total Level.

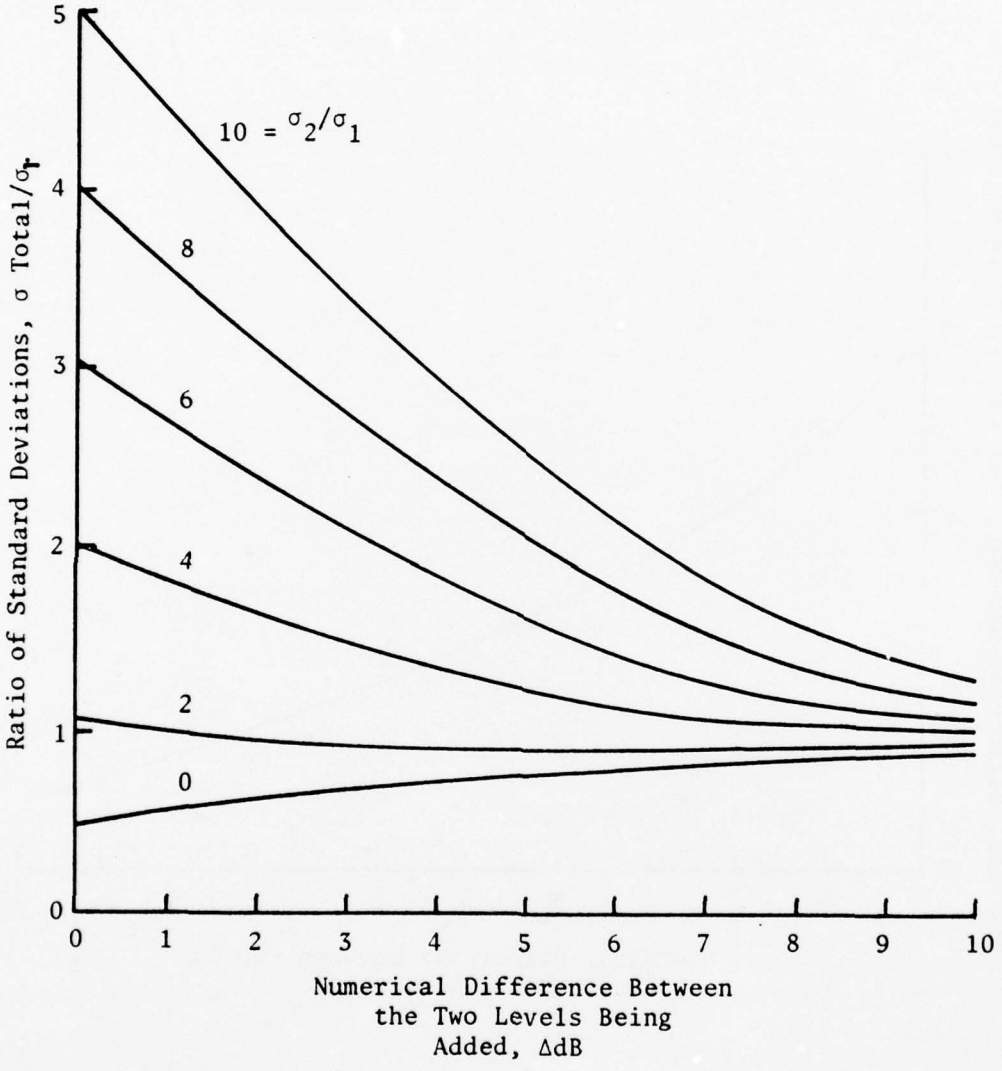

Figure 5-3. Effect of Adding Two Sound Levels with given Standard Deviations on the Standard Deviation of the Total Level.

With the jet velocity and temperature known a jet spectrum can be estimated. The dynamic range from this prediction to the contamination floors of Items 5, 6, and 7 can be determined by comparing Figures 4-10, 4-14, 4-15, and 4-16 against Figures 4-1, 4-6, and 4-19. The effect of the noise floor on the overall precision and ultimate standard deviation can then be determined by individually calculating the standard deviation ratio from Figure 5-3. The new estimated standard deviation is used to calculate the contribution from the next contamination level, etc. until the final total standard deviation is determined for each frequency.

5.2 CALCULATION OF THE PRECISION ERROR

This exercise was carried out for an ambient temperature of 15° C (68° F) and 70% relative humidity at three representative jet conditions:

Case	T_T K	T_T (° R)	V_J m/sec	V_J (ft/sec)
1	900	(1620)	427	(1400)
2	600	(1080)	305	(1000)
3	300	(540)	213	(700)

Table 5-I shows the intermediate standard deviation obtained from root sum square of the standard deviations from inverse square law testing which is σ_1 (Figure 3-11); acoustic instrumentation, σ_2 (Table 4-I); aerodynamic instrumentation, σ_3 (Figure 4-32); and fluctuations in the air attenuation correction at 70% RH, σ_4 (Figure 4-39).

The three jet spectra at 90° are shown on Figure 5-4 using SAE ARP 876 (Reference 14) prediction scheme. Superimposed are the contamination levels from ambient noise (Figure 4-10), microphone floor (Figure 4-1) and flow noise with the transmission loss subtracted (Section 4.6) to account for the attenuation by the nozzle (Figures 4-14, 4-15 and 4-16). The cell ambient noise is seen to have no effect on the jet levels. The microphone floor has minor influence on the 80 kHz and 100 kHz levels of Cases 2 and 3. Flow noise, corrected for nozzle attenuation, affects the jet noise below 630 Hz. Assuming a standard deviation of ±5 dB for both the flow noise and the microphone floor, the total standard deviation of the measurement was calculated from the values in Table 5-I using Figure 5-3. The results are given on Table 5-II.

Tape recorder noise floor would have the most severe effect on Case 3 since its spectrum peak is at the lowest frequency. This situation is studied in Figure 5-5 at the optimum gain and those conditions which may typically be experienced in practice (10 dB off and 20 dB off). The Wideband Group I recorder floor is seen to influence the jet spectra above 40 kHz to various degrees. Table 5-III presents the calculation of the total standard deviation from the values in Tables 5-I and 5-II using Figure 5-3.

Table 5-I. Standard Deviation Due to Deviation from Inverse Square Law, Acoustic and Aerodynamic Instrumentation Accuracy, and Air Attenuation Fluctuations.

f	Near Field σ_1* (Fig 3-11)	Frequency Response σ_2 (Table 4-I)	Aerodynamic Instrumentation σ_3 (Fig 4-32)	Air Attenuation Precision σ_4** (Fig 4-39)	σ_{int}
100	1.7	0.28	0.5	0	1.79
125	0.95	0.28	0.5	0	1.23
160	0.4	0.28	0.5	0	0.7
200	0.75	0.28	0.5	0	0.94
250	0.4	0.28	0.5	0	0.7
315	0.4	0.28	0.5	0	0.7
400	0.3	0.28	0.5	0	0.67
500	0.35	0.28	0.5	0	0.67
630	0.55	0.28	0.5	0	0.8
800	0.35	0.28	0.5	0	0.67
1000	0.4	0.28	0.5	0	0.7
1250	0.25	0.28	0.5	0	0.63
1600	0.45	0.28	0.5	0	0.73
2000	0.4	0.28	0.5	0	0.7
2500	0.4	0.28	0.5	0	0.7
3150	0.25	0.28	0.5	0	0.63
4000	0.35	0.28	0.5	0	0.67
5000	0.4	0.28	0.5	0	0.7
6300	0.45	0.28	0.5	0	0.73
8000	0.7	0.28	0.5	0	0.9
10000	0.6	0.33	0.5	0	0.84
12500	0.6	0.33	0.5	0.1	0.85
16000	0.75	0.33	0.5	0.2	0.98
20000	0.65	0.33	0.5	0.35	0.99
25000	0.6	0.33	0.5	0.5	0.99
31500	0.55	0.33	0.5	0.7	1.07
40000	0.7	0.33	0.5	0.95	1.33
50000	0.8	0.33	0.5	1.25	1.6
63000	0.8	0.33	0.5	1.6	1.89
80000	1.2	0.33	0.5	2.2	2.58
100000	0.75	0.33	0.5	3.0	3.15

* Most Severe Case

** At 70%

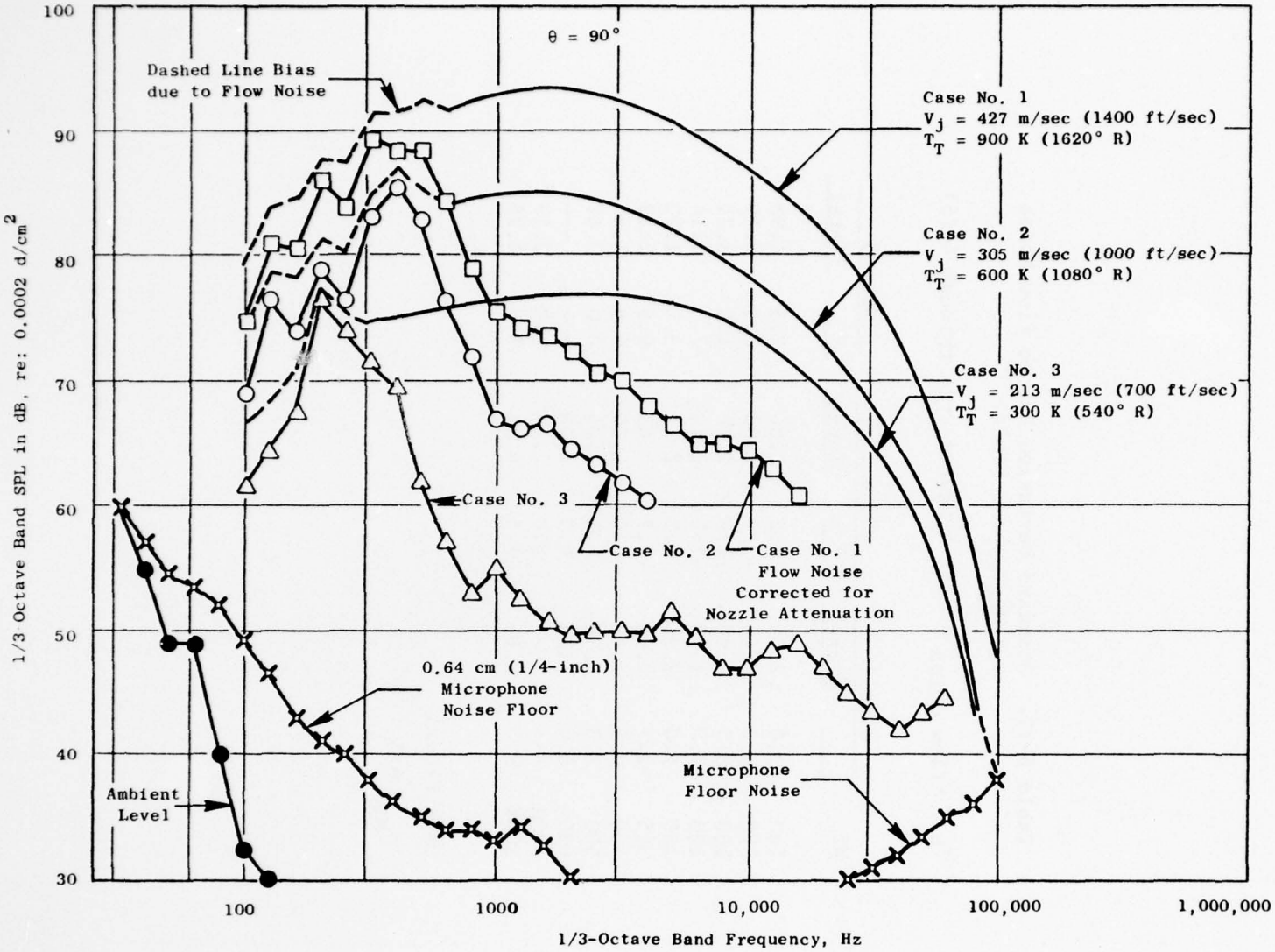

Figure 5-4. Overlay of Contamination Sources Added to Jet Noise.

Table 5-II. Standard Deviation Due to Flow Noise and Microphone Floor.

$\sigma_6 = \sigma_{\text{flow noise}} = 5$ dB (Figures 4-14 through 4-16)

Hz	Case 1		Case 2		Case 3	
	σ	σ_{Total}	σ	σ_{Total}	σ	σ_{Total}
100	3.0	2.05	4.5	1.86	3.5	1.98
125	-0.5	2.44	-2.0	2.08	1.5	2.19
160	2.0	1.98	2.0	1.98	1.0	2.25
200	-3.0	1.78	-1.5	2.14	-7.0	1.14
250	1.0	2.25	1.5	2.11	-3.0	1.73
315	-1.7	2.06	-2.7	1.81	0.5	2.39
400	0.5	2.38	-4.0	1.50	4.0	1.50
500	2.0	1.98	-1.0	2.24	13.0	0.68
630	6.4	1.14	6.9	1.08	---	---
80K	---	---	5.0	2.27	5.0	2.27
100K	9.5	2.85	-7.5	4.24	-7.5	4.25

(Mic Floor)

$\sigma_{\text{Mic}} = 5$

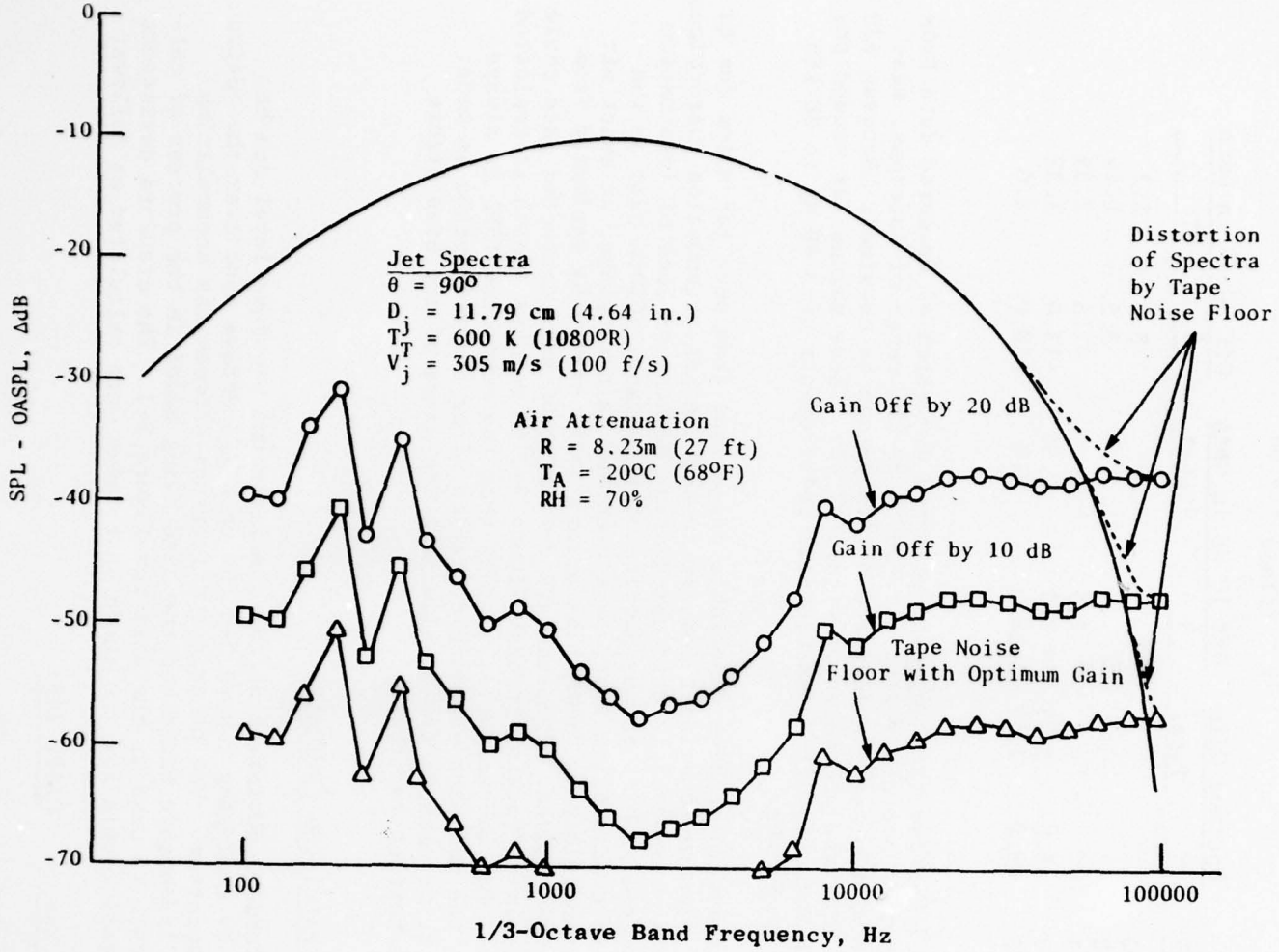

Figure 5-5. Example of Possible Electronic Noise Floor Contamination of Jet Noise Spectra.

Table 5-III. Contamination from Tape Recorder Floor.

(Case 2: T_T = 600 K (1080° R); V_j = 305 m/sec (1000 ft/sec)

$\sigma_7 = \sigma_{floor}$ = 3 dB

	Optimum Gain		Off 10 dB in Gain		Off 20 dB in Gain	
kHz	δ	σ_{Total}	δ	σ_{Total}	δ	σ_{Total}
40					8.5	1.2
50					3.5	1.44
63			7.5		-2.5	2.55
80	5.0	2.09	- 3.0	1.86	-13.0	2.32
100	-8.0	3.83	-18.0	3.0	-28.0	3.0

Figure 5-6 shows the composite standard deviation of measured data from all contamination sources. Over the 400 to 80 kHz range of interest, measurements to within ±2.5 dB standard deviation can be obtained. Between 630 Hz and 31.5 kHz, the precision is within ±1 dB. These values far exceed the FAA/DOT High Velocity Jet Noise Contract requirements of 3 dB up to 20 kHz and 5 dB up to 80 kHz.

Bias errors which give repeatable deviations from pure jet noise due to flow noise, electronic noise floor, or inaccurate air attenuation corrections have not been considered in this calculation because of lack of information about the degree of bias in any particular situation. Given data on the actual nozzle transmission loss, tape recorder gain settings, or exact air attenuation coefficients, such bias errors could easily be estimated from Figure 5-2 and removed. The standard deviation of such corrected data could then be calculated working through Figure 5-3 in reverse (which is replotted as Figure 5-7 for convenience). Notice that the corrected σSPL is always larger than the measured standard deviation after the correction is made; therefore, it is best to try to eliminate the cause of any bias errors rather than correct for them.

5.3 OASPL PRECISION ESTIMATE

The standard deviation of the overall sound pressure level can be determined by employing Figure 5-3 for each 1/3-octave band over the entire frequency spectrum. The numerical difference between the accumulating sum of the 1/3-octave bands and the band being added in the process of calculating OASPL is used as the axis for Figure 5-3. The standard deviations of the overall levels for the three test cases were calculated as follows:

Case	OASPL (dB)
1	0.26
2	0.29
3	0.21

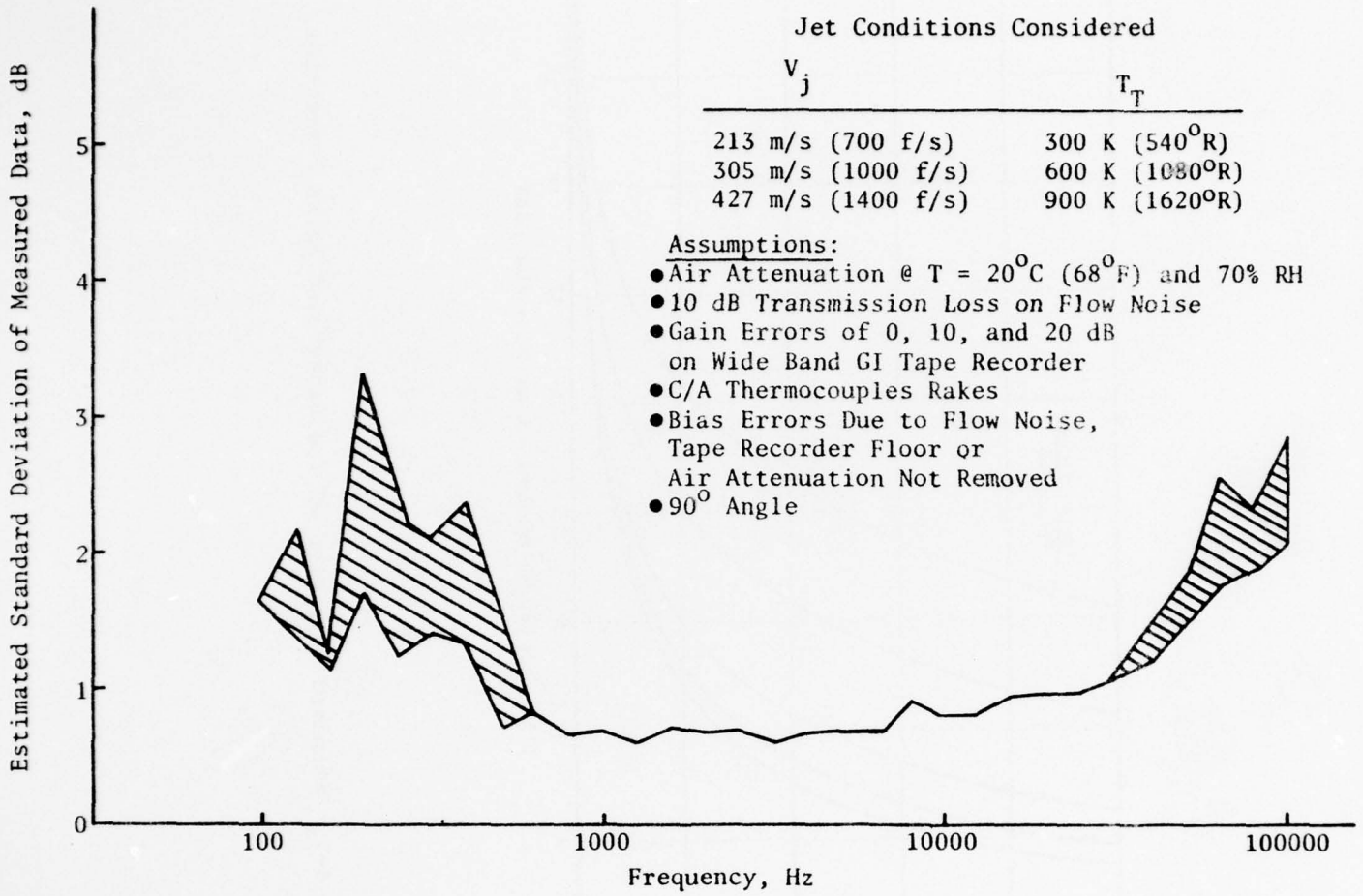

Figure 5-6. Estimated Standard Deviation of Measured Data due to all Contaminates in the General Electric Jet Noise Anechoic Chamber.

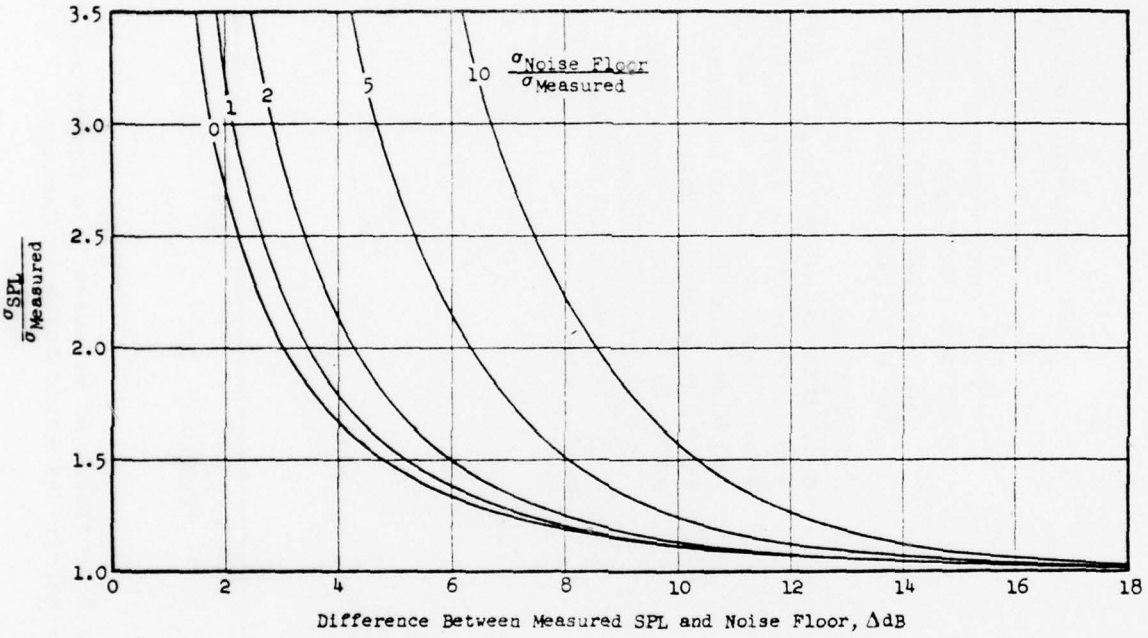

Figure 5-7. Standard Deviation of the Background Noise Correction.

AD-A042 327 GENERAL ELECTRIC CO CINCINNATI OHIO AIRCRAFT ENGINE GROUP F/G 14/2
HIGH VELOCITY JET NOISE SOURCE LOCATION AND REDUCTION. TASK 1. --ETC(U)
FEB 77 C T SAVELL, E J STRINGAS DOT-05-30034

UNCLASSIFIED R77AEG188 FAA-RD-76-79-1A NL

3 OF 3
AD A042327

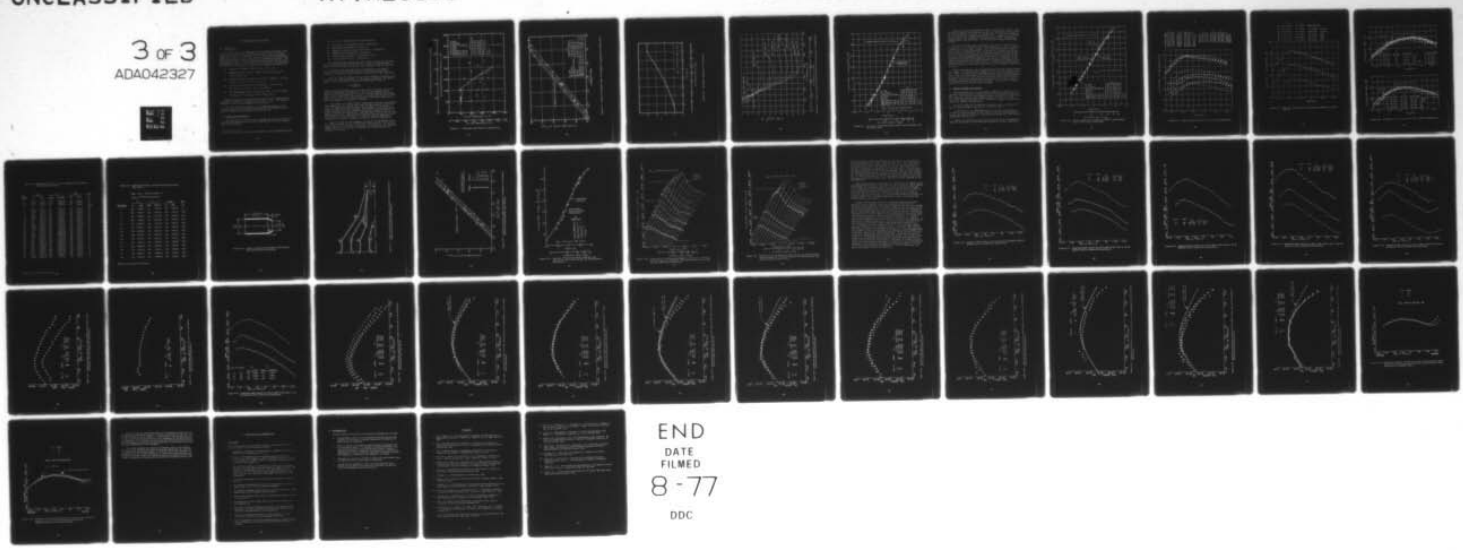

END
DATE FILMED
8-77
DDC

6.0 CERTIFICATION OF THE FACILITY

6.1 INTRODUCTION

As a final test of the cleanliness and free-field environment of the test facility, recorded and processed acoustic data from round conical nozzles were compared to "classical referee" data at similar aerodynamic conditions. These "classical" data consisted of previously published data which made the same claims to cleanliness and free-field properties. The comparisons are made in terms of the semiempirical scaling laws which have been proposed by Hoch, et al. (Reference 15) which include the jet temperature effects. In particular, all data will be compared with respect to:

- Lighthill's Parameter: OAPWL versus $\rho_o V_j^8 A_j/a_o^5$
- SNECMA/NGTE power relation: OAPWL-10 $\log_{10}$ $(A_j[\rho_j/\rho_{isa}]^{\omega})$ versus $\log_{10}$ (V_j/a_o)
- Overall 90° level variation with velocity: $OASPL_{90°}$ - 10 $\log_{10}$ $[A_j/R^2]$ $[\rho_j/\rho_{isa}]^{\omega}$ versus $\log_{10}$ (V_j/a_o)
- Acoustic power level* spectral variation: 1/3-octave PWL - 10 $\log_{10}$ $[A_j(\rho_j/\rho_{isa})^{\omega}]$ versus $\log_{10}$ (fD/V_j)
- 90° sound pressure level spectral variation: 1/3-octave $SPL_{90°}$ - 10 $\log_{10}$ $[A_j/R^2)$ $(\rho_j/\rho_{isa})^{\omega}]$ versus $\log_{10}$ (fD/V_j)

Whenever possible, the comparisons are made at points representing the aerodynamic boundaries or operating limits of the facility. The maximum variations of the data are expected at these points.

Only data inside the acoustically clean operating boundary of the facility are shown in these certification figures, contaminated data outside this domain having been shown in earlier sections.

6.2 REFEREE DATA PRESENTATION

A detailed search of the literature revealed that there are very little available data that satisfied both the cleanliness and free-field requirements of this program.

*Reference area used to calculate PWL is implied in the normalization factor.

Only six sets of external data were found suitable:

- University of South Hampton (Lush) - Reference 16
- NGTE (Ahuja and Bushell) - Reference 17
- NASA-Lewis (Olsen, Gutierrez, and Dorsch) - Reference 18
- SNECMA (Hoch and Duponchel) - Reference 15
- NGTE (Cocking and Bryce) - References 15 and 19
- Lockheed (Tanna, et al.) - Reference 20

The first three data sets were run with a cold jet while the last three were with heated jets up to 944 K (1700° R). Figure 6-1 shows the aerodynamic points (in terms of V_j and T_T) at which acoustic data were available.

In addition to the above data, the latest addition of the SAE A21 Committee proposed ARP 876 "GAs Turbine Jet Exhaust Noise Prediction" (Reference 14) which was used to represent a bench mark for data comparison.

Figure 6-2 shows the referee data in terms of Lighthill's parameter with various values of the K parameter. As postulated by Lighthill, the subsonic round jet in an atmosphere at rest has an acoustic power output of:

$$W = K\rho_o V_j^8 D_j^2 / a_o^5$$

Quoting Lighthill (Reference 21), "K is very closely constant in any given series of experiments, being about 0.3×10^{-4} for jets emerging from a nozzle with low turbulence level, 0.6×10^{-4} for jets emerging from straight pipes, and as large as 10^{-4} for jets with a very high level of initial turbulence." Most of the referee data in Figure 6-2 lies between these limits. A mean value appears to be about $K = 0.5 \times 10^{-4}$.

In jets whose core density differs substantially from that of the ambient (surrounding) air, the acoustic power output becomes dependent on the ratio ρ_j/ρ_o. An empirical correction in the form $10 \log(\rho_j/\rho_o)^\omega$, is found to account for this effect quite reliably. The exponent ω, generally ascribed to Hoch (Reference 15), has a complex dependence on velocity as shown by Figure 6-3 (taken from Reference 14). For high speed subsonic jets, it takes values between 0 and 1, indicating that heating of the jet leads to reduction of jet noise for cases where $\rho_j/\rho_o > 1$. Figure 6-4 shows the magnitude of the empirical correction in terms of jet velocity and total temperature.

Figure 6-5 shows the data presented in terms of the SNECMA/NGTE parameter. The line through the data is that found in Reference 15. This curve is high at high velocity, because the line was a fit to supercritical convergent nozzles with shocks in Reference 15; whereas, the Lockheed data are for shock-free C/D nozzles.

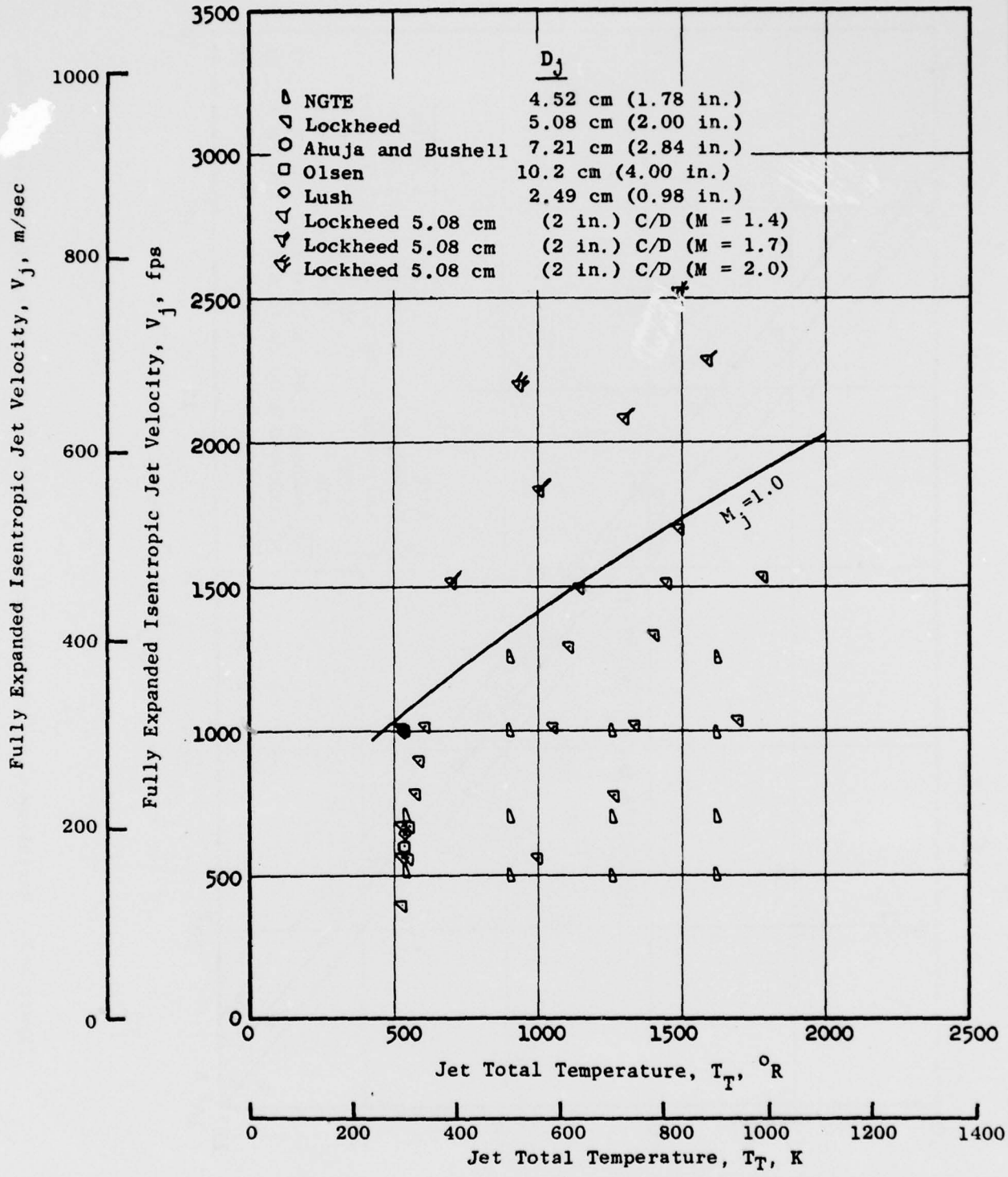

Figure 6-1. Aerodynamic Test Domain for Referee Data.

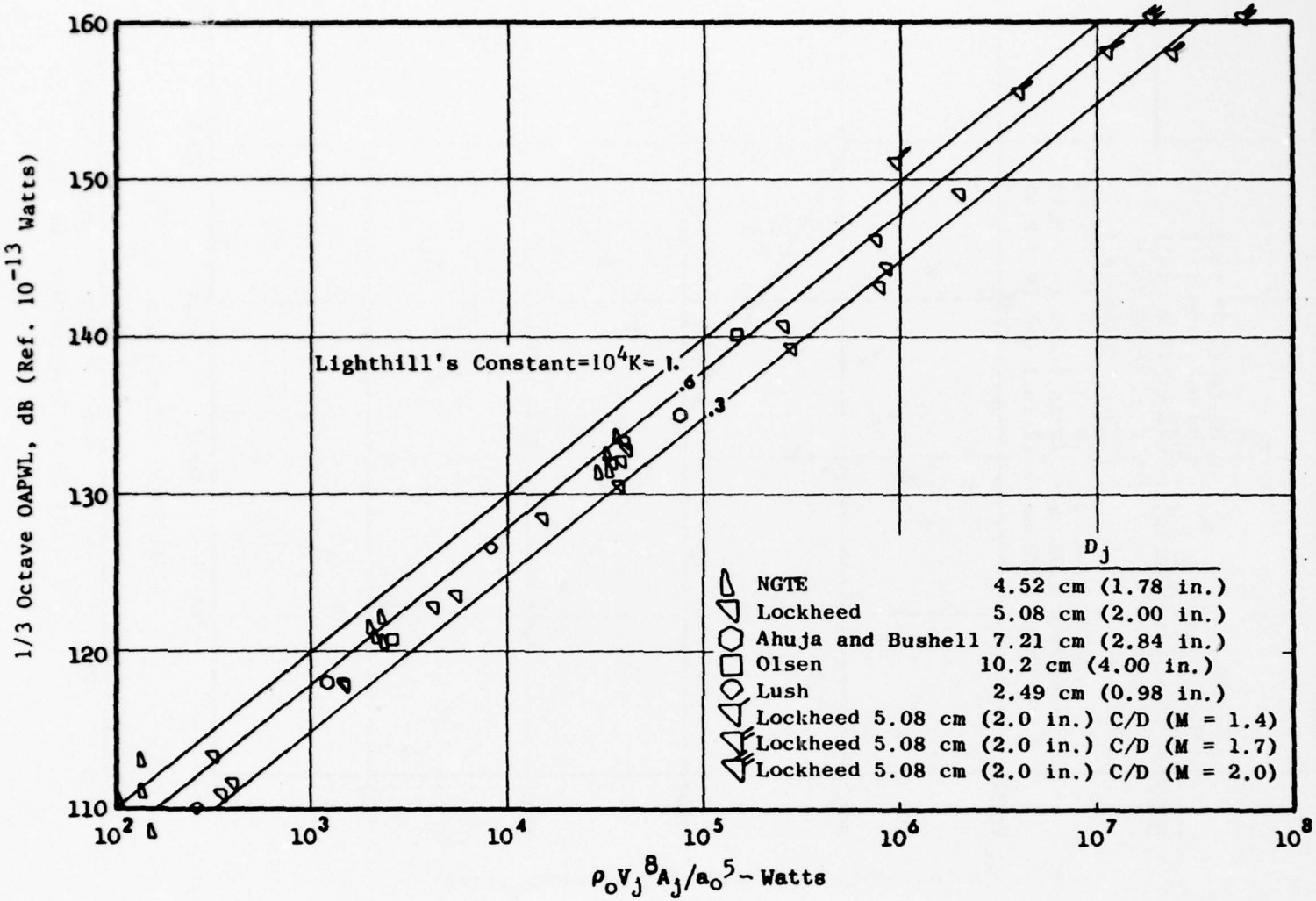

Figure 6-2. Variation of Overall Power with Lighthill's Parameter for Referee Data.

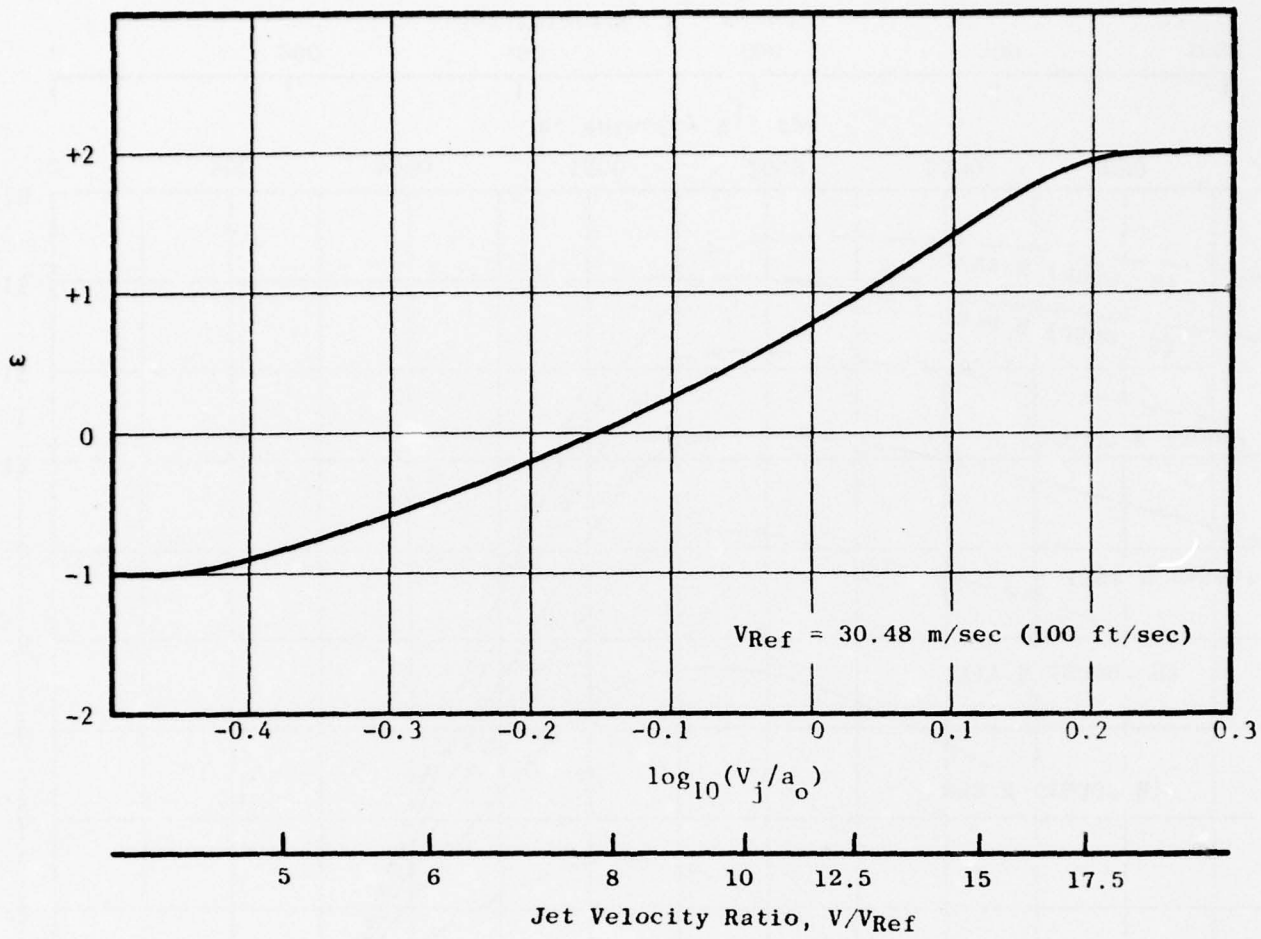

Figure 6-3. Jet Density Exponent Vs. Jet Velocity.

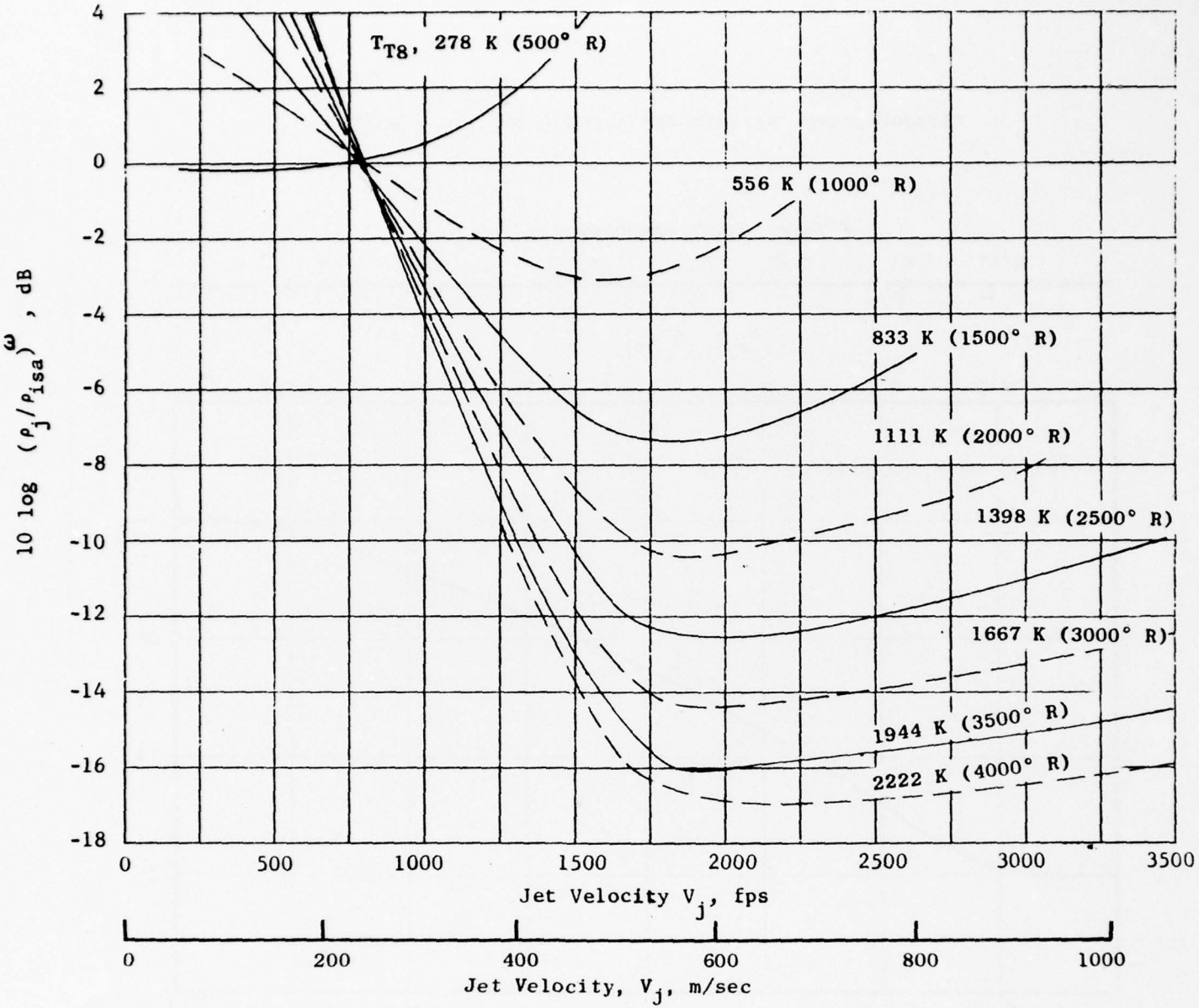

Figure 6-4. Variation of Density Correction Factor with Jet Velocity and Temperature.

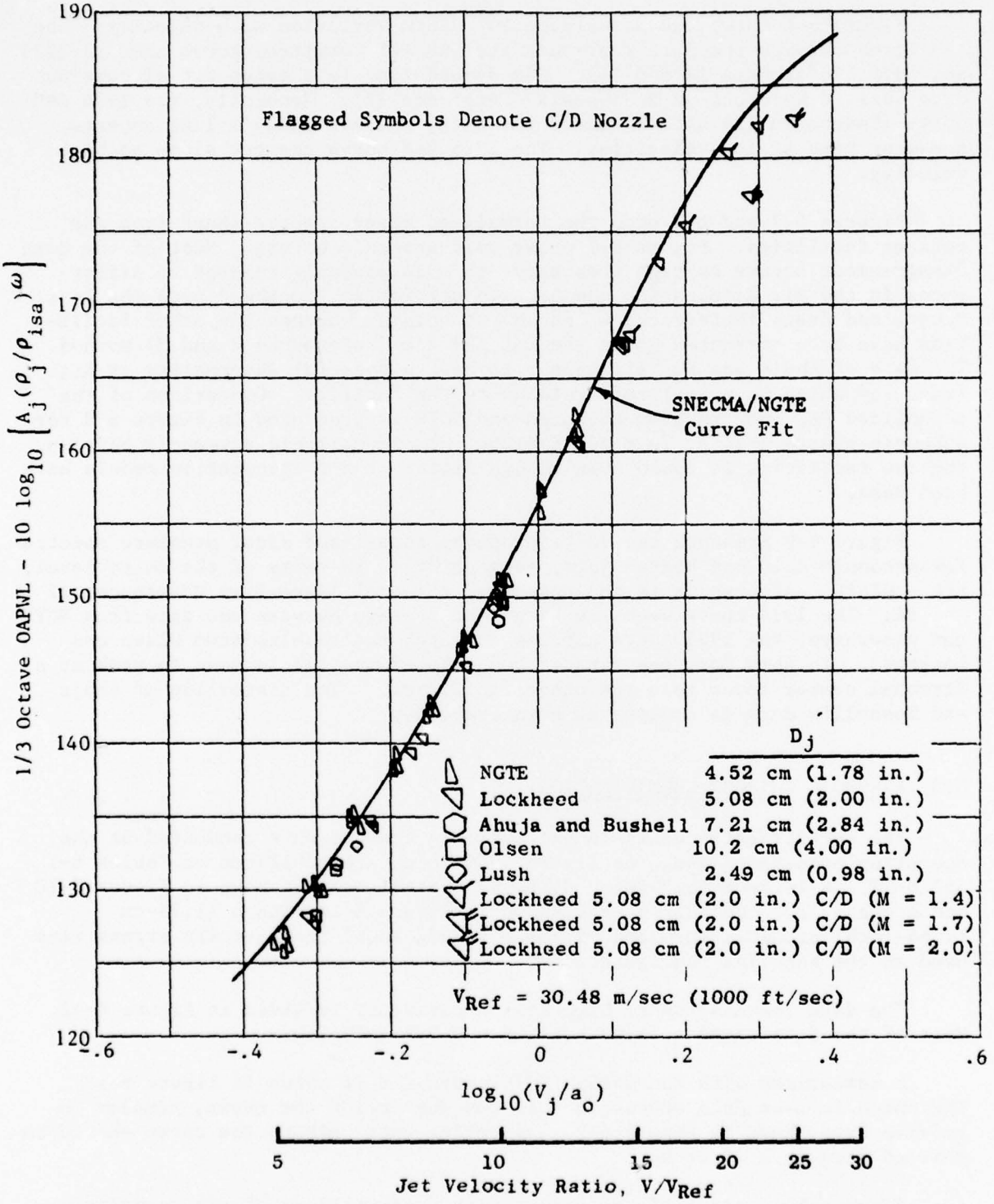

Figure 6-5. Variation of Normalized Overall Power with Jet Velocity for the Referee Data.

Figure 6-6 shows the normalized 90° OASPL variation with velocity. The two lines through the data represent the SAE A21 Committee curve used in 1974 and 1975 (References 12 and 14). The dashed line is a curve fit of numerous data derived by Stone of NASA-Lewis (Reference 22). Generally, the 1974 SAE curve (Reference 12) underpredicts the data, whereas Stone's line appears somewhat high at low velocities. The 1975 SAE curve changes slope at high velocity.

Figures 6-7 and 6-8 show the normalized power spectra shape from the referee facilities. Figure 6-7 shows cold subsonic points. Most of the data disagreement occurs at high frequency; this is probably related to differences in the air attenuation models. In particular, Lockheed uses the Bass, Bauer, and Evans (References 4 and 10) technique, whereas the other facilities have been corrected using the SAE ARP 866 (References 2 and 3) method. The data of Ahuja and Bushell appear to have a spectral abnormality at high frequency which is most likely related to the facility. Comparison of the normalized PWL spectra from Lockheed and NGTE is presented in Figure 6-8 for subsonic heated jets at T_T = 700 K (1260° R). Remarkable agreement between the two facilities is found even though different air attenuation models have been used.

Figure 6-9 presents the 90° microphone normalized sound pressure spectra for subsonic cold and heated jets, respectively, in terms of the delta level, SPL - OASPL. Also shown is the suggested spectral lines from References 12 and 14. The 1974 curve seems to be a good average between the data from NGTE and elsewhere; the 1975 curve appears to match the results from Olsen and Lockheed. In this form the data at Lush (Reference 16) is seen to peak at a Strouhal number lower than the other facilities. The distortion of Ahuja and Bushell's data is obvious at high frequency.

6.3 ANECHOIC CHAMBER CERTIFICATION

The certification tests in the anechoic chamber were conducted at the operating conditions shown on Figure 4-30 which are tabulated as Tables 6-I and 6-II. A 14.5-cm (5.7-inch) diameter conical nozzle shown in Figure 6-10 and a coannular, coplanar nozzle shown in Figure 6-11 with a 11.79-cm (4.64-inch) diameter core and 15.45-cm (6.082-inch) diameter fan stream were used as the baseline configurations.

The data correlation to Lighthill's parameter is given in Figure 6-12. Most of the data seems to best fit a $K = 0.5 \times 10^{-4}$ line.

A comparison with the SNECMA/NGTE curve fit is shown in Figure 6-13. The anechoic room data appear to fall somewhat below the curve, similar to referee data shown in Figure 6-5, indicating that perhaps the curve should be shifted down by 1 dB or so.

Figures 6-14 and 6-15 are carpet-plot presentations of the normalized OASPL for the single-flow and dual-flow installation testing, respectively.

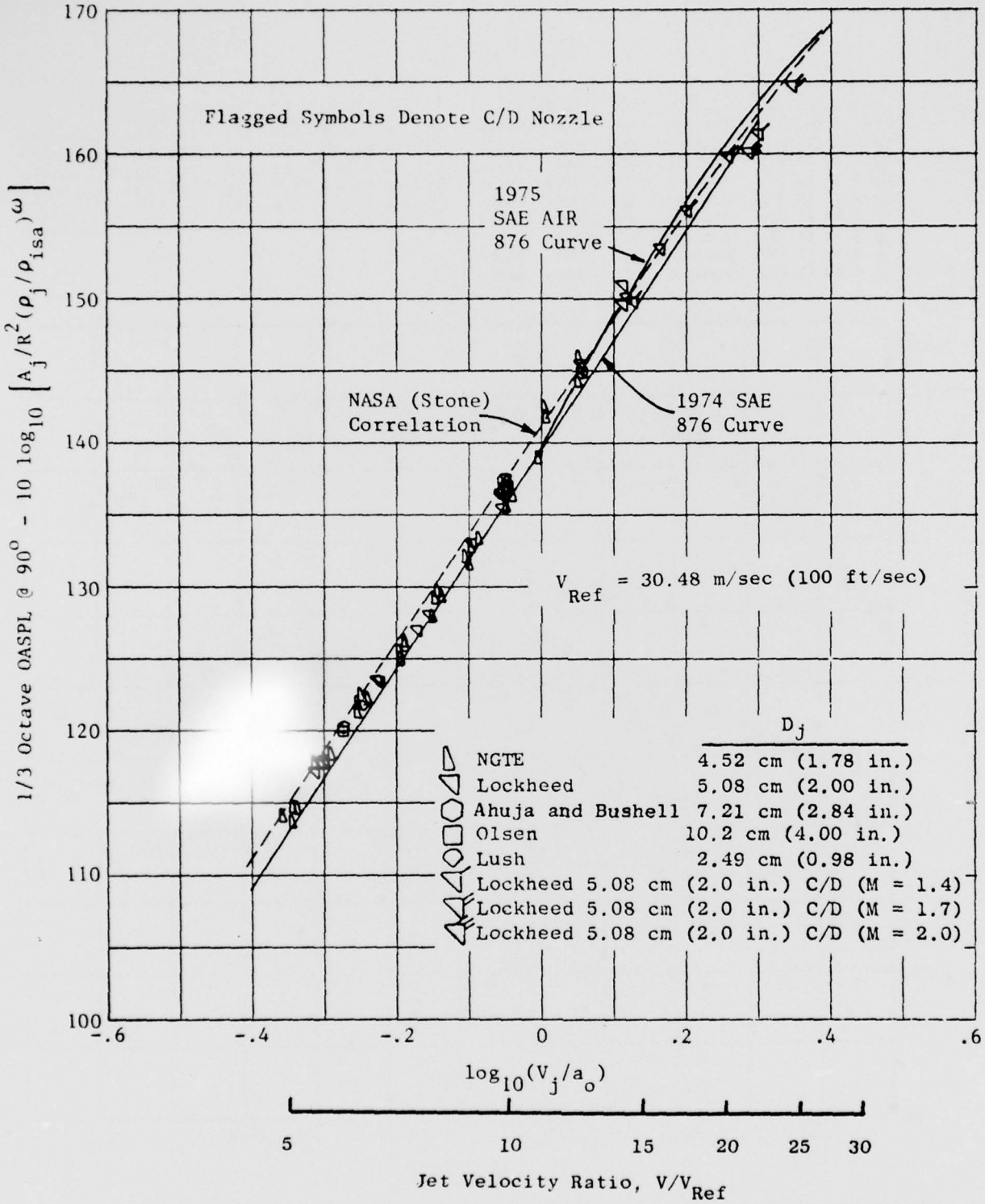

Figure 6-6. Velocity Dependence of Normalized Overall Sound Pressure Level at 90° for the Referee Data.

D_j cm (in.)	T_T	V_j m/sec (ft/sec)	
◇ 10.2 (4.00)	Ambient	183 (600)	Olsen
□ 10.2 (4.00)	Ambient	303 (994)	Olsen
⬡ 7.21 (2.84)	Ambient	183 (600)	Ahuja
⬡ 7.21 (2.84)	Ambient	305 (1000)	Ahuja
◇ 2.49 (0.98)	Ambient	195 (640)	Lush
◇ 2.49 (0.98)	Ambient	300 (984)	Lush
△ 4.52 (1.78)	Ambient	157 (514)	NGTE
△ 4.52 (1.78)	Ambient	220 (722)	NGTE
△ 4.52 (1.78)	Ambient	309 (1014)	NGTE

D_j cm (in.)	T_T K (° R)	V_j m/sec (ft/sec)	
◁ 5.08 (2.00)	293 (528)	171 (562)	Lockheed
◁ 5.08 (2.00)	293 (528)	205 (674)	Lockheed
◁ 5.08 (2.00)	293 (528)	309 (1013)	Lockheed
◁ 5.08 (2.00)	303 (545)	172 (565)	Lockheed
◁ 5.08 (2.00)	309 (557)	207 (678)	Lockheed
◁ 5.08 (2.00)	336 (605)	310 (1017)	Lockheed

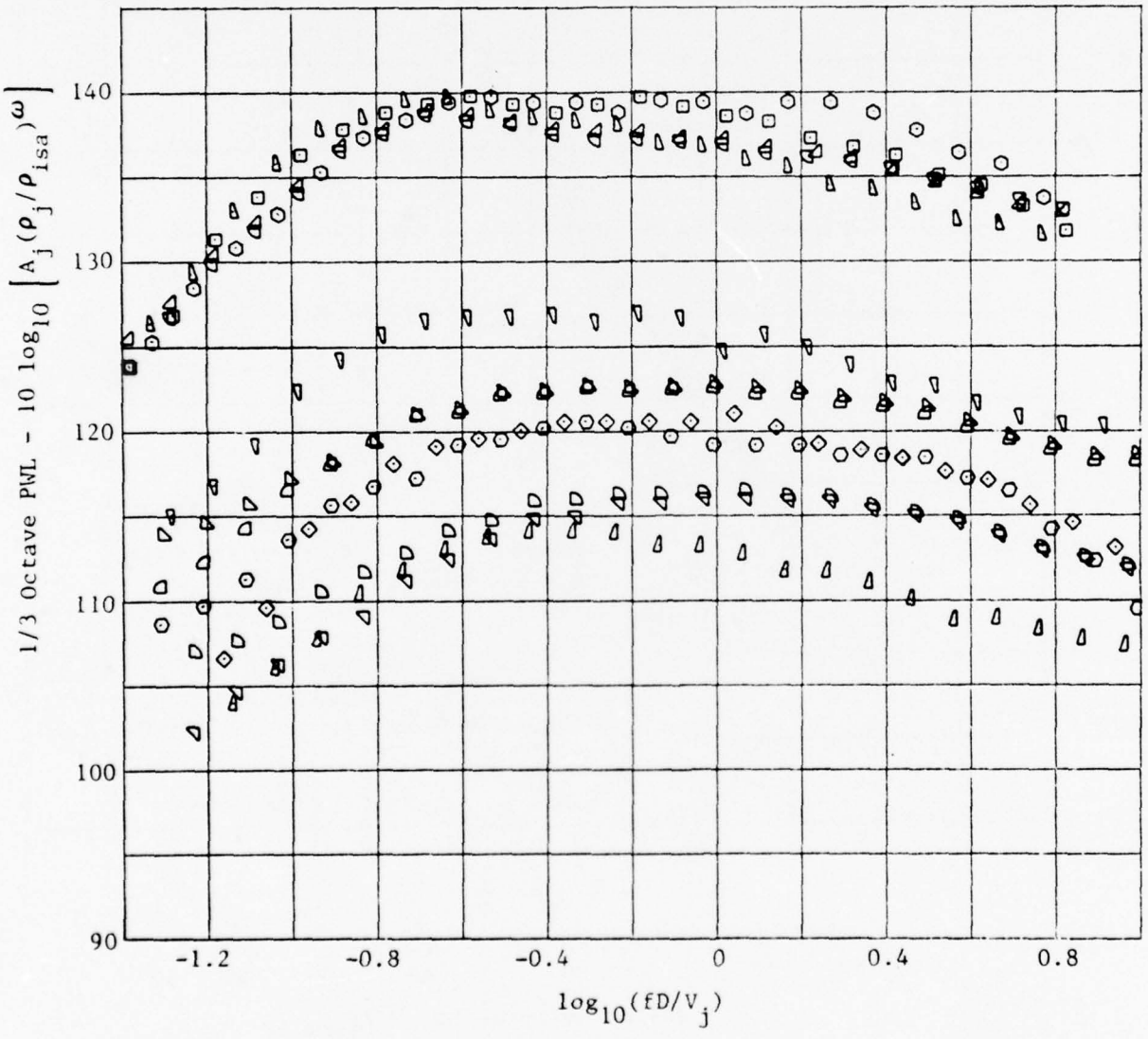

Figure 6-7. Normalized Power Spectra for the Cold Jet Referee Data.

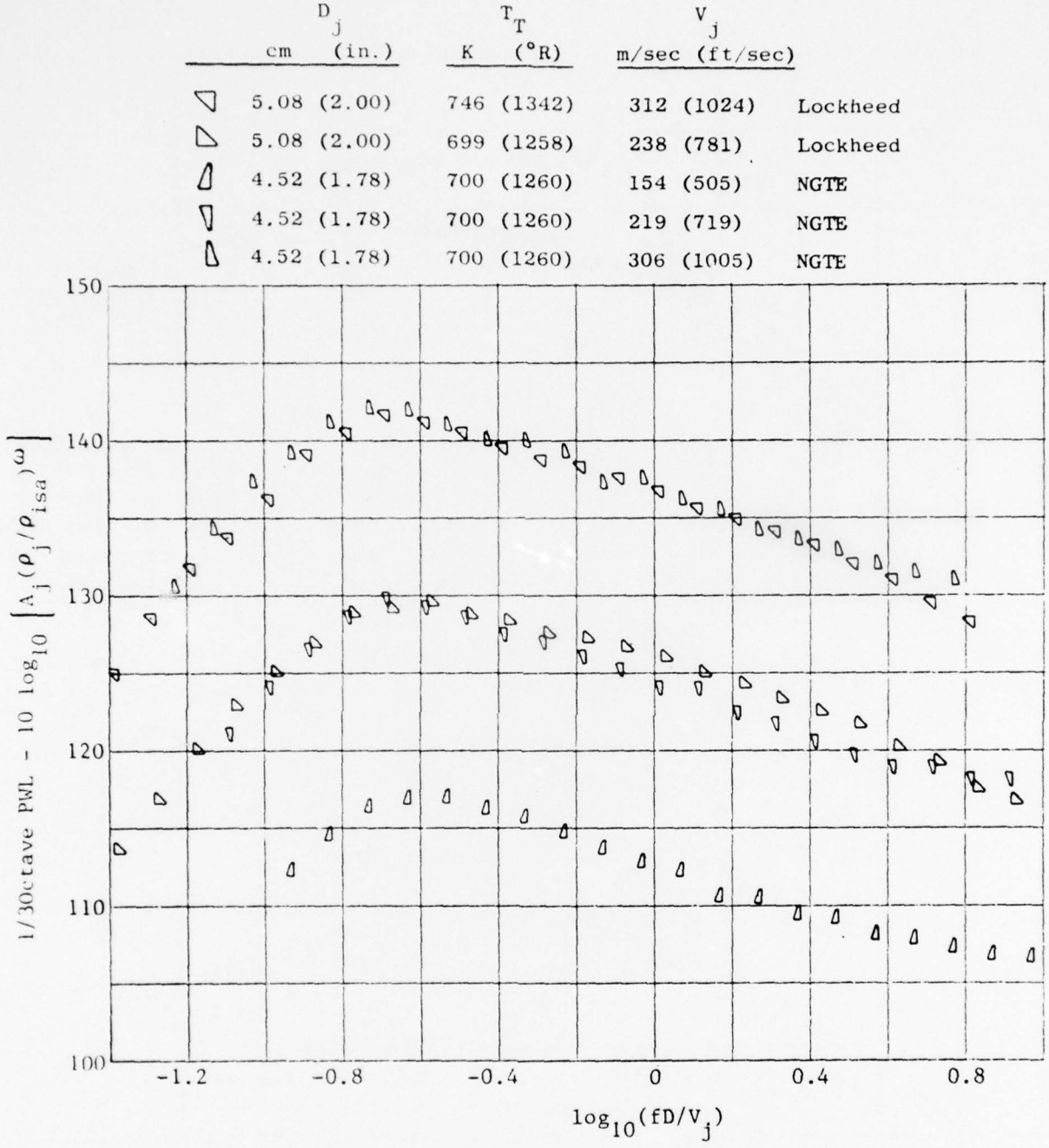

Figure 6-8. Normalized Power Spectra for Lockheed and NGTE Data at 700 K (1260° R).

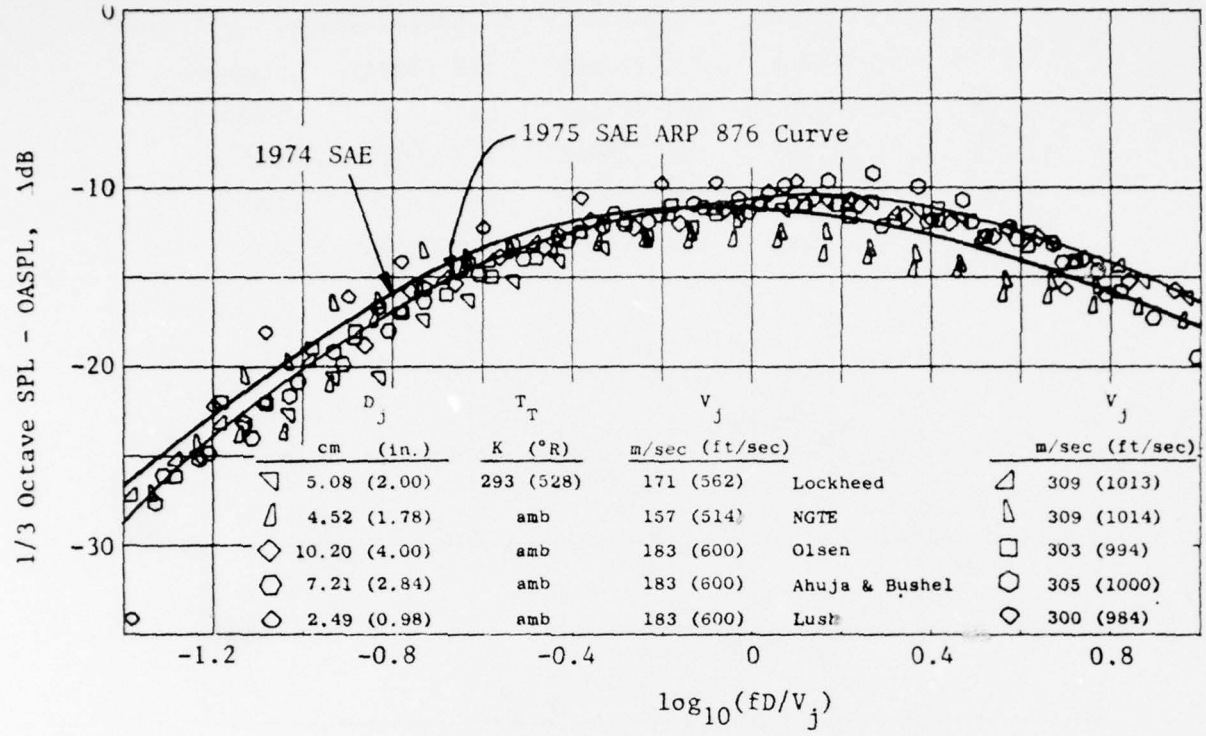

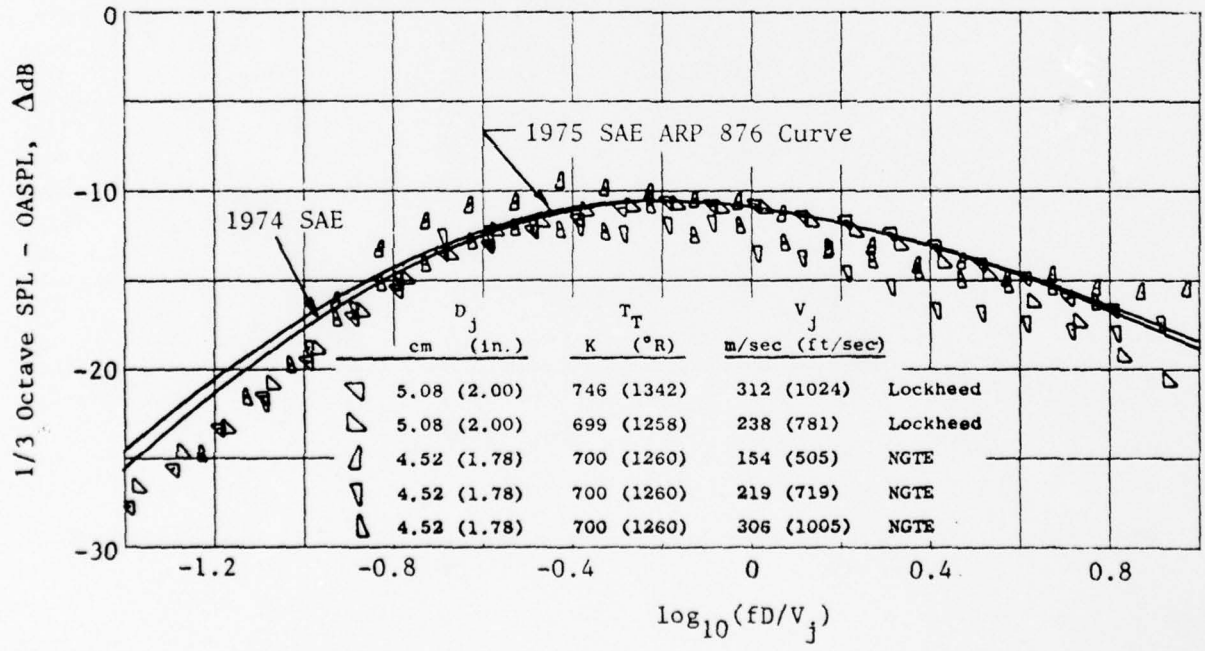

Figure 6-9. SPL Spectra at 90° for Cold and 700 K (1260° R) Referee Data.

Table 6-I. Single-Flow 14.478 cm (5.7 inch) Diameter Conical Nozzle Certification Test Points

Data Point	T_{T8} K	T_{T8} (°R)	V_j m/sec	V_j (ft/sec)	T_{amb} K	T_{amb} (°R)	R/H %
01	320.6	(576.7)	82.1	(269.57)	270	(518.0)	55
02	320.5	(576.5)	146	(480.10)	270	(519.0)	53
03*	321	(578.0)	210	(689.39)	271	(520.0)	51.4 72.6
1	293.7	(528.3)	75	(260.48)	270	(517.5)	80
2	292.1	(525.4)	139	(458.5)	270	(519.3)	80
3	290.8	(523.1)	210	(691.56)	260	(499.7)	81
4*	292	(525.6)	315	(1032.06)	260	(499.9)	80
6	496.5	(893.0)	101	(334.6)	261	(502.9)	67
7	52097	(937.0)	139	(459.5)	261	(503.3)	66
8*	499	(897.8)	207	(680.86)	262	(505.1)	65
9*	446	(803.2)	283	(928.6)	263	(506.0)	64
10*	524	(943.1)	420	(1378.39)	261	(502.98)	68
12	726.0	(1305.8)	161	(531.66)	255	(492.0)	63
13	715.2	(1286.4)	188	(617.17)	255	(492.0)	63
14	721.6	(1298.0)	254	(835.29)	255	(492.0)	63
15*	604	(1087.1)	275	(902.07)	263	(506.2)	65
16*	748	(1347.1)	492	(1613.33)	260	(501.0)	71
19	926.7	(1666.8)	167	(550.78)	260	(500.6)	80
20*	904	(1627.0)	216	(710.40)	260	(501.0)	80
21*	827	(1488.2)	321	(1054.19)	260	(501.2)	82
23*	914	(1645)	546	(1792.61)	260	(501.0)	84
29*	1344	(2420.20)	268	((880.40)	263	(506.6)	64
30A	929	(1670.9)	342	(1124.4)	264	(507.8)	62
30*	1214	(2185.4)	437	(1434.28)	264	(507.8)	62
31*	1321	(2378.2)	673	(2209.47)	264	(508.2)	61
33	1411.1	(2538.0)	968	(3179.84)	264	(508.5)	61
39*	1517	(2731.1)	536	(1758.39)	265	(510.9)	59
41*	1544	(2780.0)	812	(2663.37)	265	(510.9)	59
42	1625.3	(2923.2)	1062	(3486.2)	265	(509.1)	60
18	1030.1	(1852.8)	113	(371.21)	264	(508.9)	18

*Used for certification evaluation

Table 6-II. Dual-Flow Coannular, Coplanar Nozzle Certification Test Points.

$D_{Fan + Core}$ = 15.48 cm (6.082 in.)

D_{Core} = 11.786 cm (4.64 inch);

Data Point	T_T		V_j		T_{amb}		R/H
	K	(^oR)	m/sec	(ft/sec)	K	(^oR)	%
1	283	(509.2)	111	(364.75)	256	(494.0)	63
2	281	(507.1)	167	(549.52)	256	(493.0)	63.8
3*	282	(508.3)	228	(747.38)	256	(493.0)	64.3
4	281	(506.2)	317	(1041.96)	256	(493.0)	64.3
12	725	(1305.8)	161	(531.66)	255	(492.0)	66.4
13	715	(1286.4)	188	(617.16)	255	(492.0)	66.4
14*	700	(1260.0)	251	(822.93)	255	(492.0)	66.7
15*	678	(1221.5)	333	(1091.93)	255	(492.0)	65.3
16*	756	(1361.7)	532	(1747.23)	255	(492.0)	66.3
20	947	(1704.7)	240	(789.92)	254	(489.0)	60.0
21	905	(1629.8)	290	(954.47)	255	(492.0)	64.0
22*	937	(1687.4)	520	(1705.1)	255	(492.0)	65.9
23*	942	(1694.7)	563	(1846.22)	254	(490.0)	68.1
24*	939	(1691.2)	605	(1985.01)	254	(489.0)	68.8

*Used for certification evaluation.

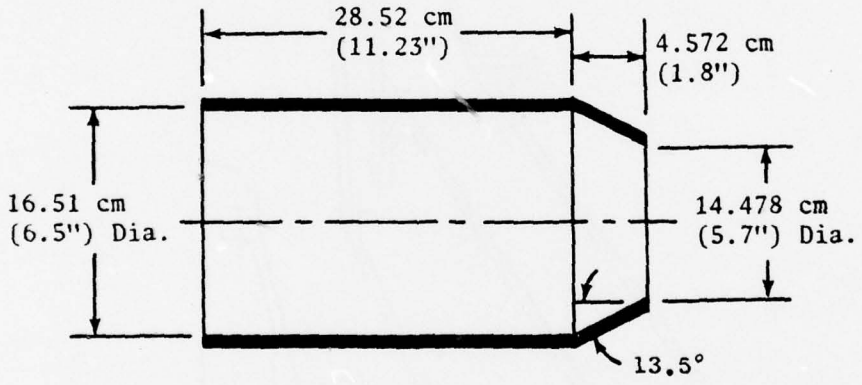

Figure 6-10. Shape of Single-Flow Convergent Conical Nozzle Used for Certification Testing.

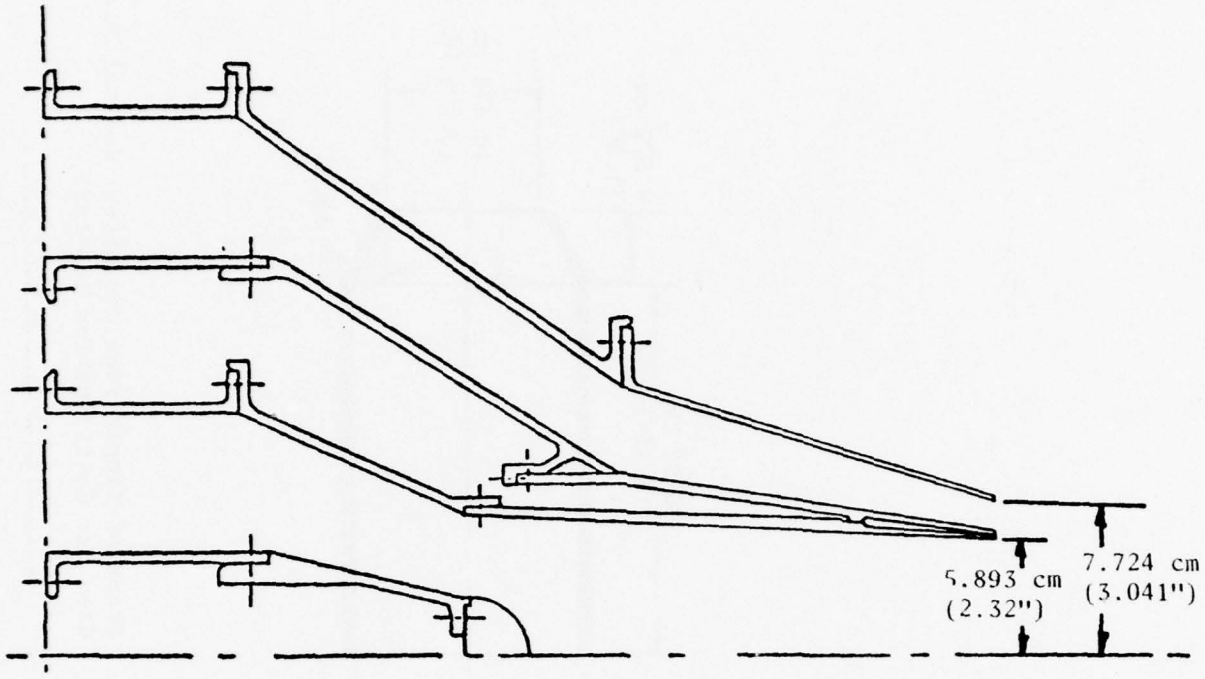

Figure 6-11. Shape of the Dual-Flow, Coannular, Coplanar Convergent Conical Nozzle Used for Certification Testing.

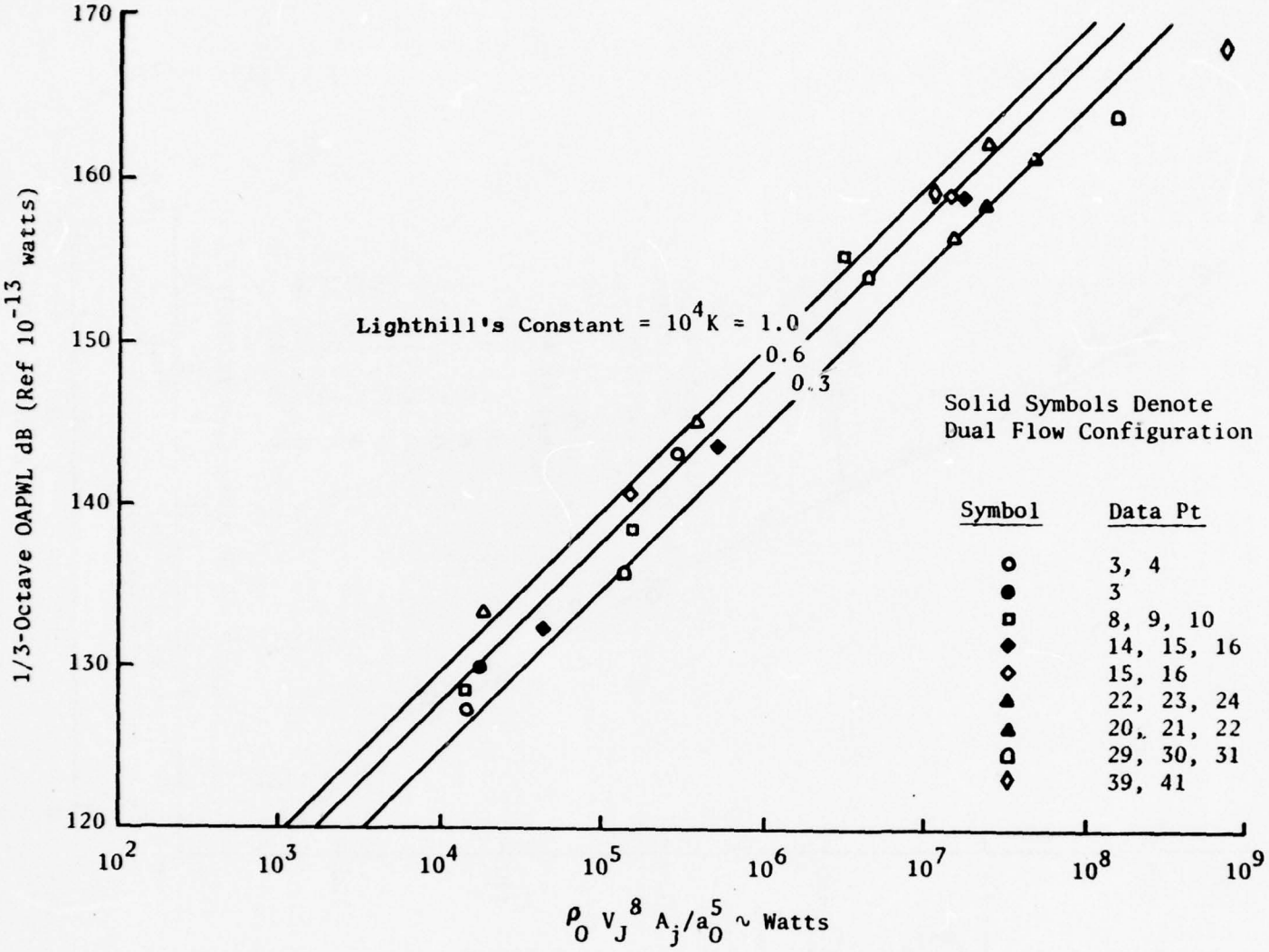

Figure 6-12. Variation of Overall Power with Lighthill's Parameter for the General Electric Jet Noise Anechoic Test Facility.

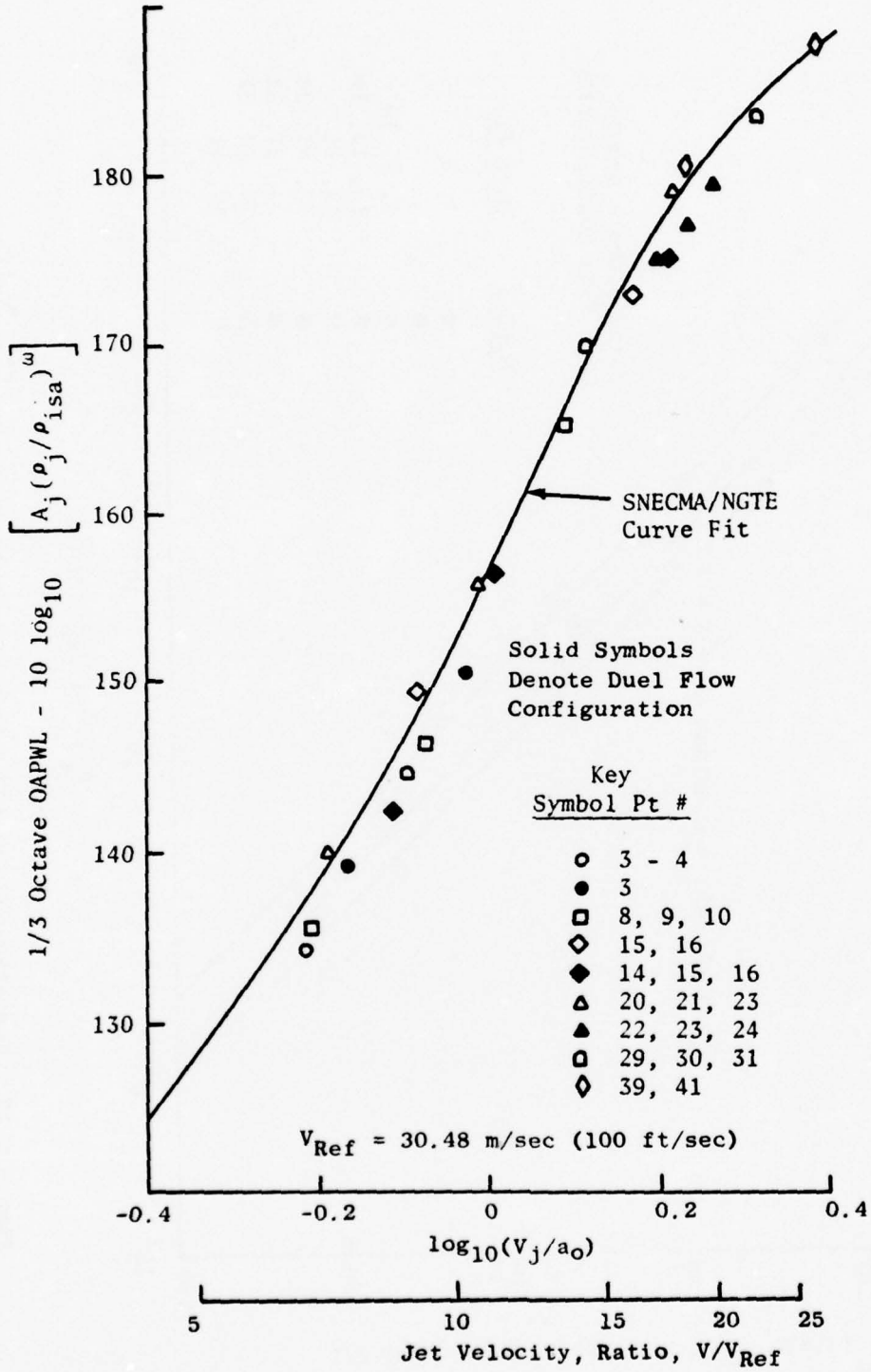

Figure 6-13. Variation of Normalized Overall Power with Jet Velocity for the General Electric Jet Noise Anechoic Test Facility.

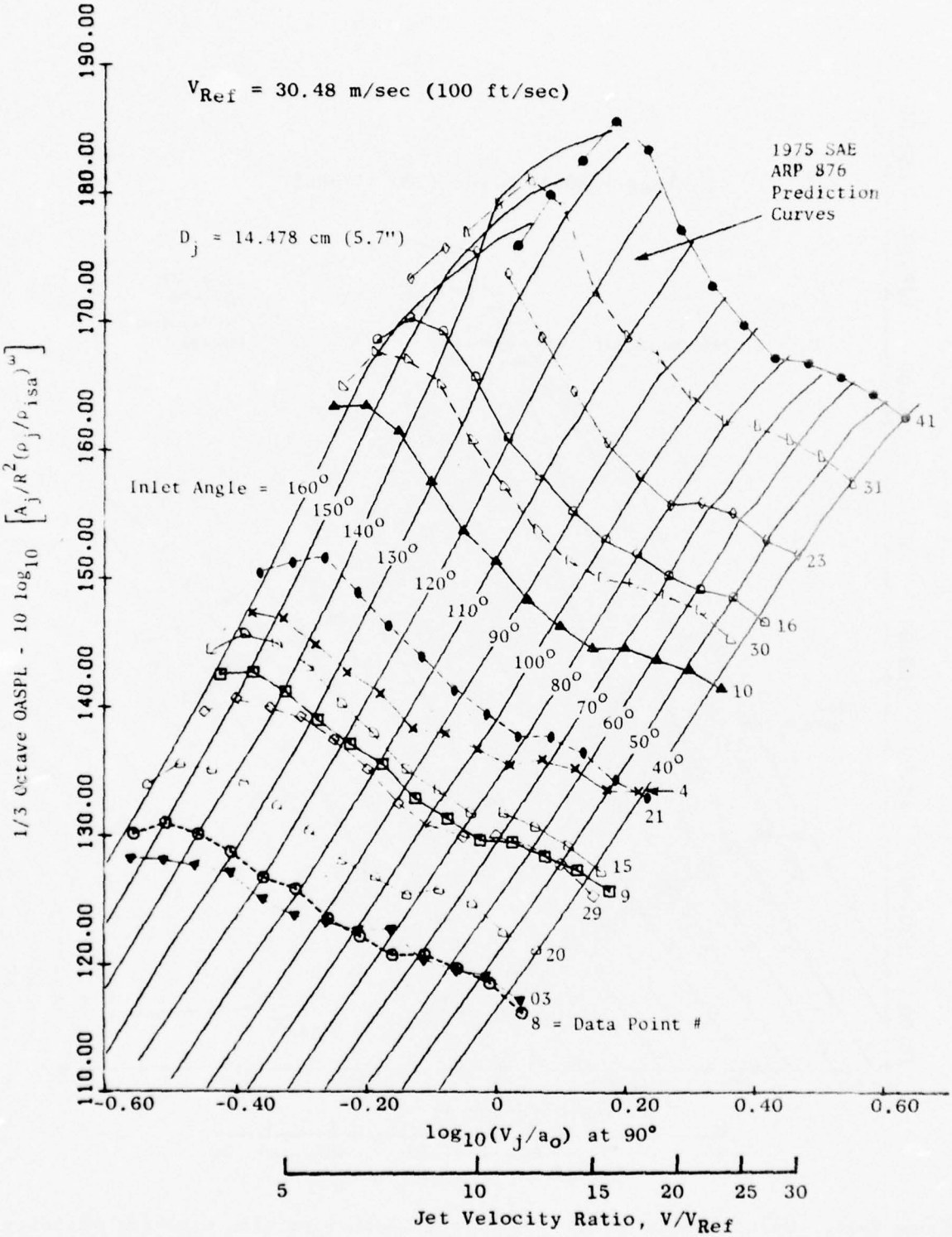

Figure 6-14. Carpet Plots of the Normalized OASPL Variation with Jet Velocity and Inlet Angle for the General Electric Jet Noise Anechoic Test Facility Single-Flow Installation.

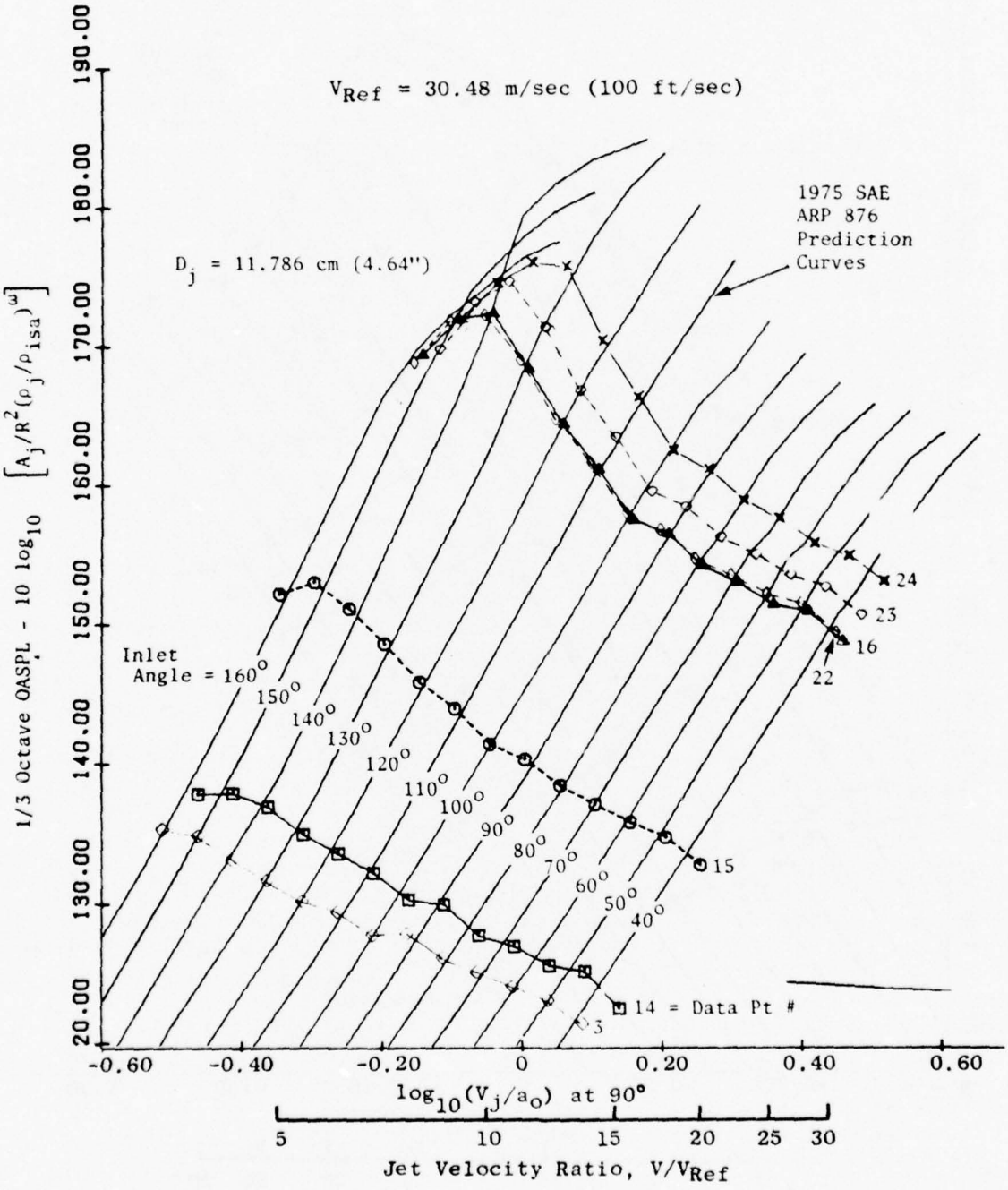

Figure 6-15. Carpet Plots of the Normalized OASPL Variation with Jet Velocity and Inlet Angle for the General Electric Jet Noise Anechoic Test Facility Dual-Flow Installation.

The plot gives jet noise variation with jet velocity as well as the directivity distribution with acoustic angle from the inlet. The scale shown on the abscissa is the $\log_{10}$ (V_j/a_o) value for each of the data points to be used in 90° angle curve. The scale for each of the other angles can be obtained by shifting the abscissa by 0.05 [Δ $\log_{10}$ (V_j/a_o)]. All the data are seen to fall within ±1 dB of the SAE prediction line at the 90° station. The largest deviations appear to occur at the 160° angle which may be due to lack of adequate data used to generate the SAE design curves (note in Reference 12, only data between 60° to 150° were shown); furthermore, the design curves are constantly evolving as more and better data are assembled by the SAE Committee.

Power spectra shape for the single-flow installations at temperatures of approximately 300 K (540° R), 500 K (900° R), 700 K (1260° R), 900 K (1620°R), 1278 K (2300° R), and 1530 K (2754° R) are given as Figures 6-16 through 6-21, respectively. The corresponding spectra from the dual-flow installation are given as Figures 6-22 through 6-24 for 300 K (540° R), 700 K (1260° R), and 940 K (1690° R). The spectra display a smooth shape and follow the expected inverse velocity variation when plotted as a function of Strouhal number. The jet diameter dependence is seen to be removed when normalized by Strouhal number.

Figures 6-25 through 6-33 give the normalized sound pressure level spectra for 90° at the same conditions as Figures 6-16 through 6-24; practical, referee spectra (e.g. proposed revised SAE 876) are also included in Figures 6-25 through 6-33. The spectral shape is excellent with both jet velocity and diameter dependence being removed by the Strouhal number parameter. The spectral plots were made with the data corrected to standard day conditions of 15° C (59° F) and 70% relative humidity from the actual conditions during the test day. Design curves such as Figures 6-25 through 6-33 can also be presented with all air attenuation removed (i.e., "lossless data") rather than with 8.23 m to 10.67 m (27 to 35 feet) of standard day air attenuation as shown in Figure 6-34. Tables 6-I and 6-II show that most of the testing was performed at ambient temperatures which exceed the ±5° C (±9° F) variation from the calibrated 20° C (59° F) for the Bass, Bauer, and Evans (Reference 4) air attenuation model. Using this model produced high frequency scatter and divergence from test day to test day; therefore, the new model (Section 4.8) proposed as the American National Standard S-157 (Sutherland, Bass, Piercy, and Evans; Reference 13) was applied to the data corrected to standard day shown on Figure 6-25. These data are shown on Figure 6-35; results indicate that scatter is reduced. The curl-up at high frequencies is suspected of being the interception of data with the electronic noise floor of the tape recorder. Corrections to standard day were chosen for the presentation in Figures 6-25 through 6-33 since the numerical magnitude of the corrections are smaller and have less impact on the data. The lossless data in Figure 6-35 appear to fit the 1974 SAE design curve better (see Figure 6-9) than the 1975 line.

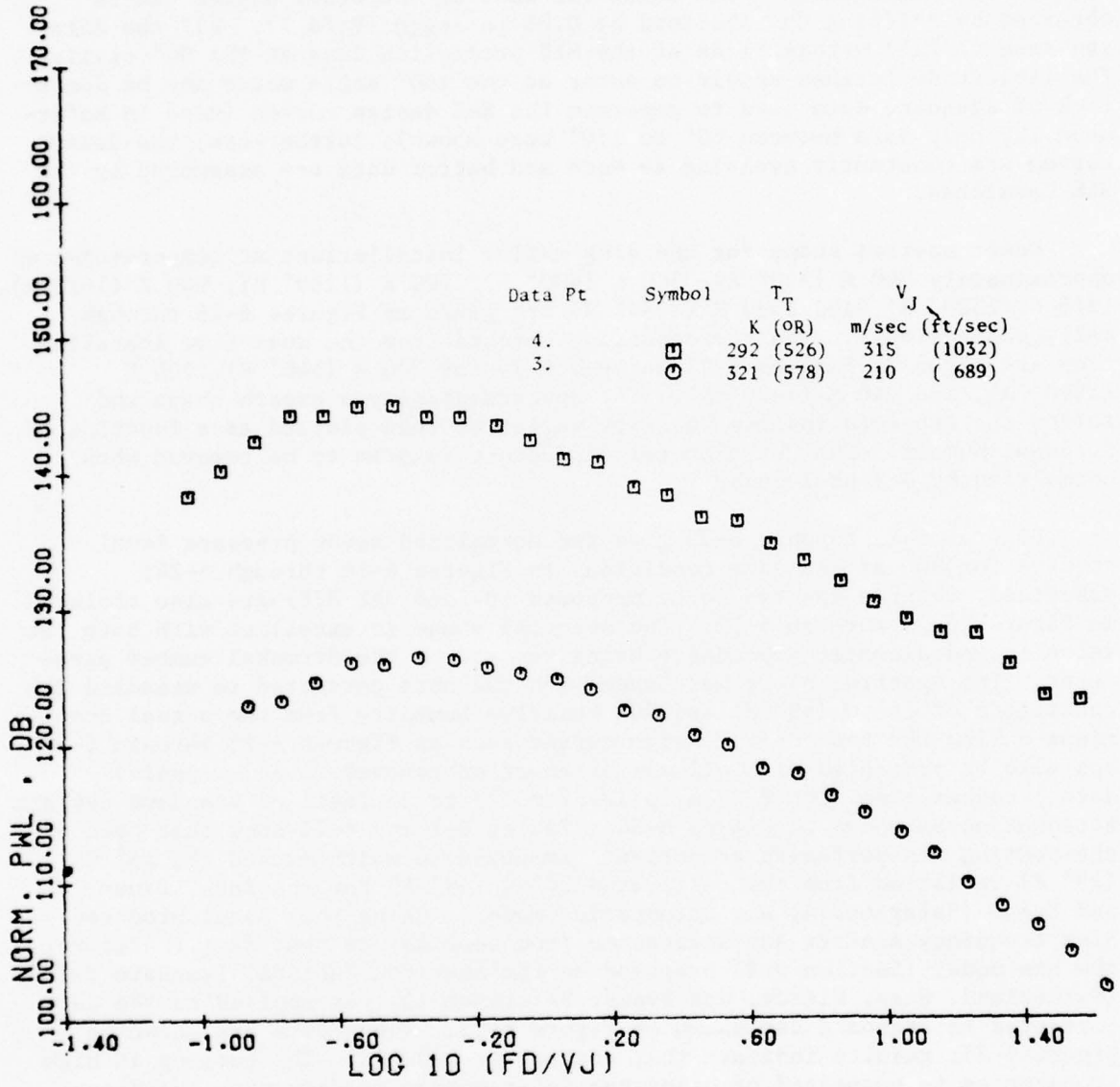

Figure 6-16. Normalized Power Spectra for Cold Jets in the General Electric Anechoic Facility Single-Flow Installation.

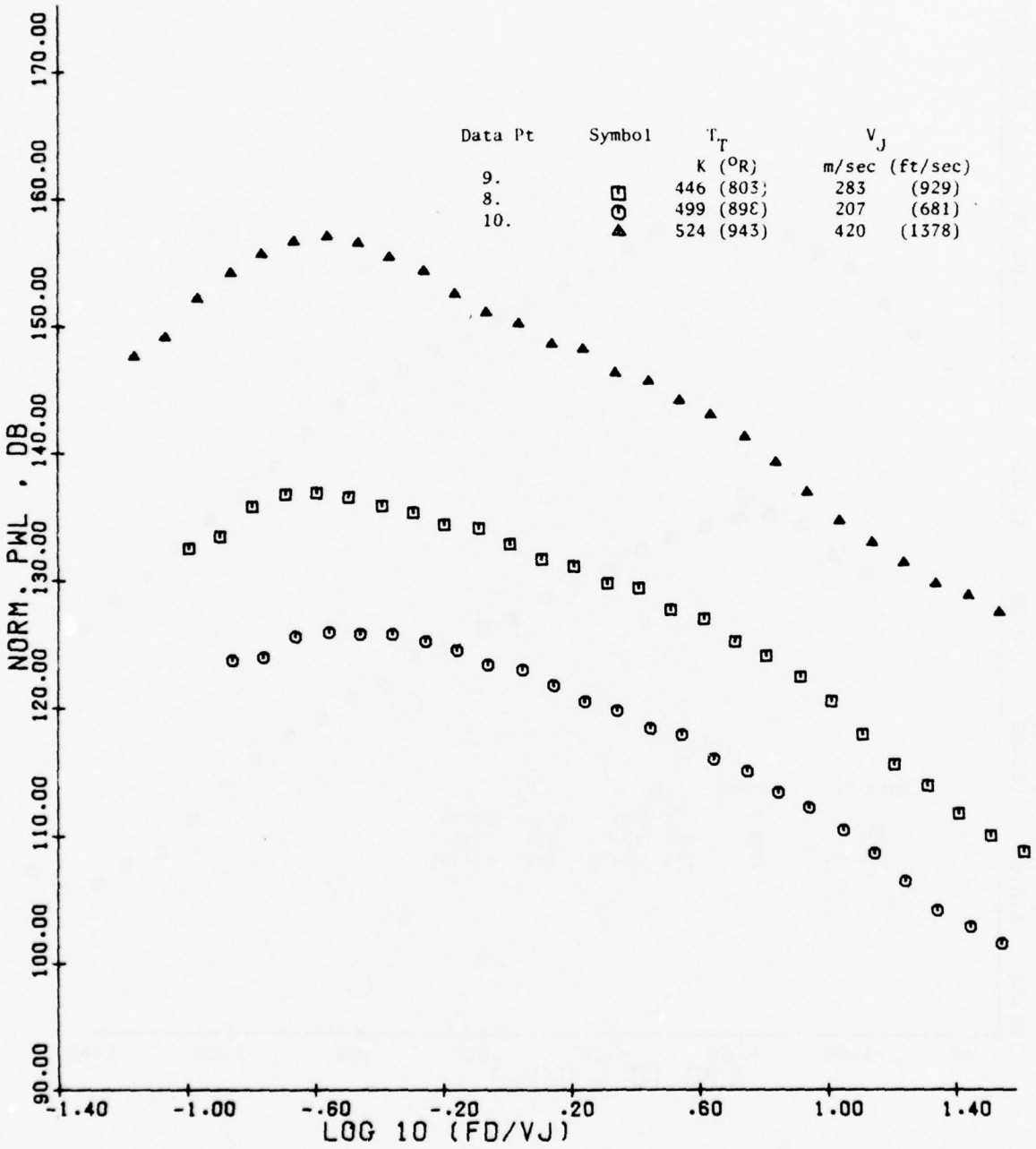

Figure 6-17. Normalized Power Spectra for 500 K (900° R) Hot Jets in the GE Anechoic Facility Single-Flow Installation.

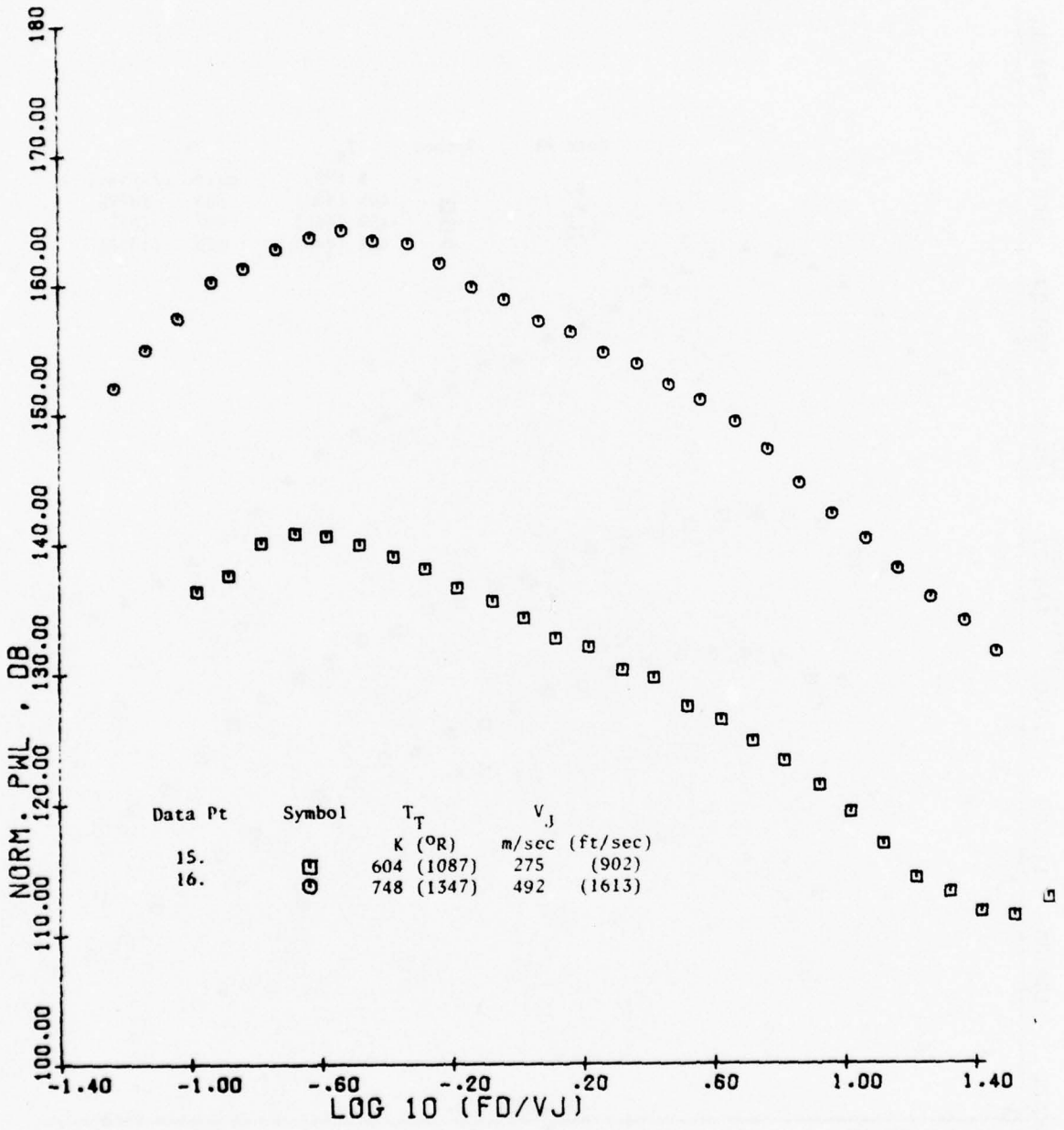

Figure 6-18. Normalized Power Spectra for 700 K (1260° R) Hot Jets in the GE Anechoic Facility Single-Flow Installation.

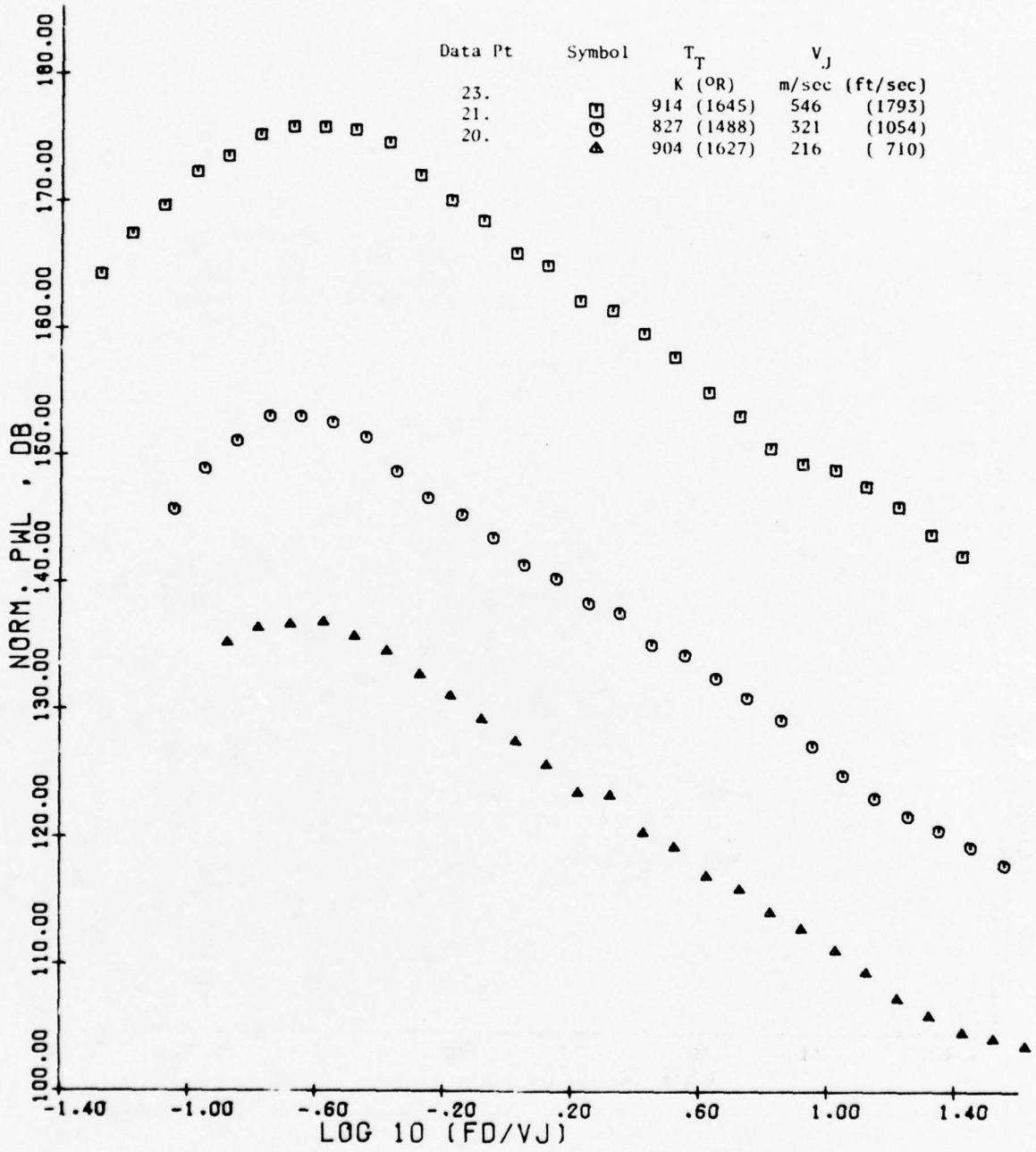

Figure 6-19. Normalized Power Spectra for 900 K (1620° R) Hot Jets in the GE Anechoic Facility Single-Flow Installation.

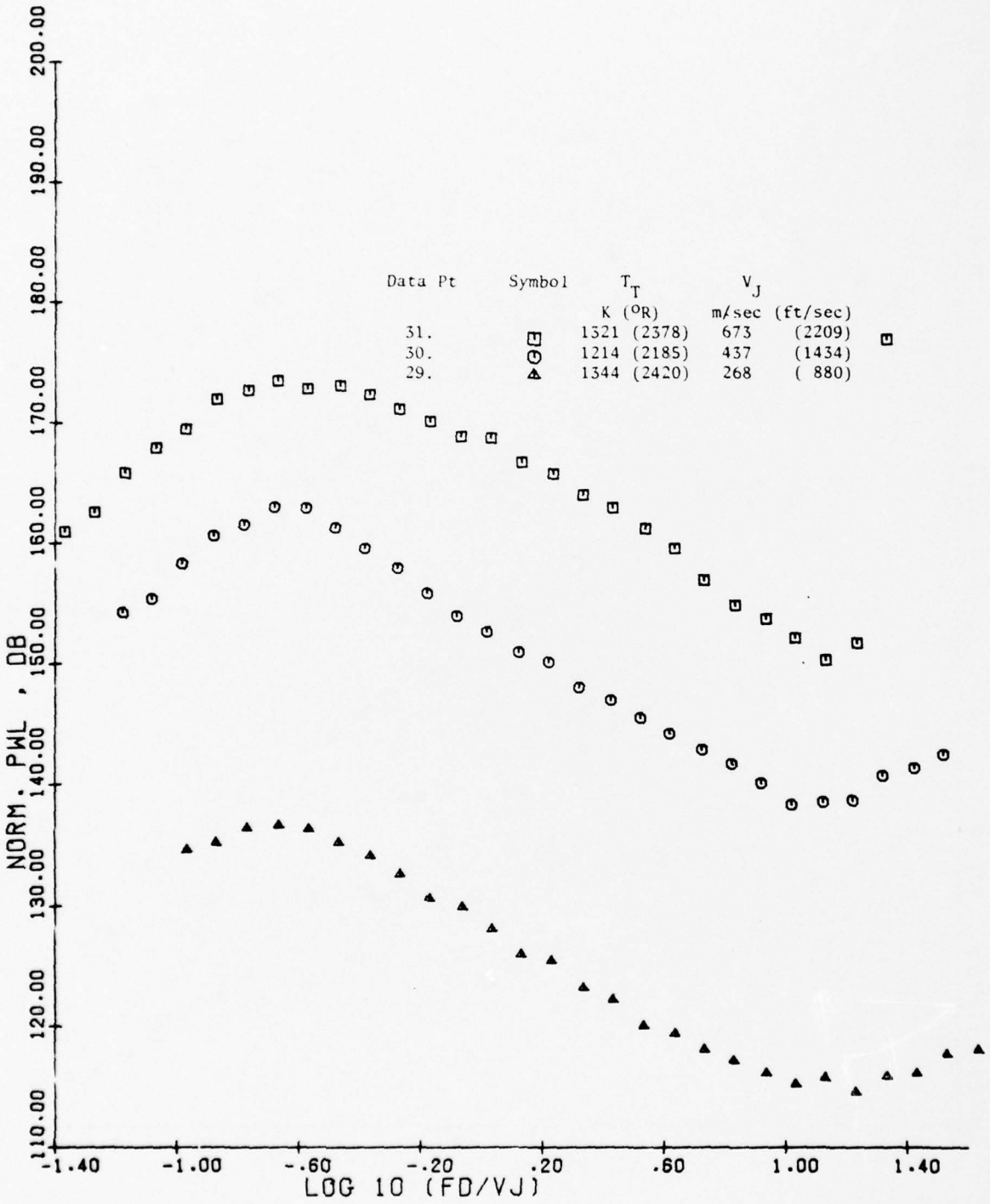

Figure 6-20. Normalized Power Spectra for 1278 K (2300° R) Hot Jets in the GE Anechoic Facility Single-Flow Installation.

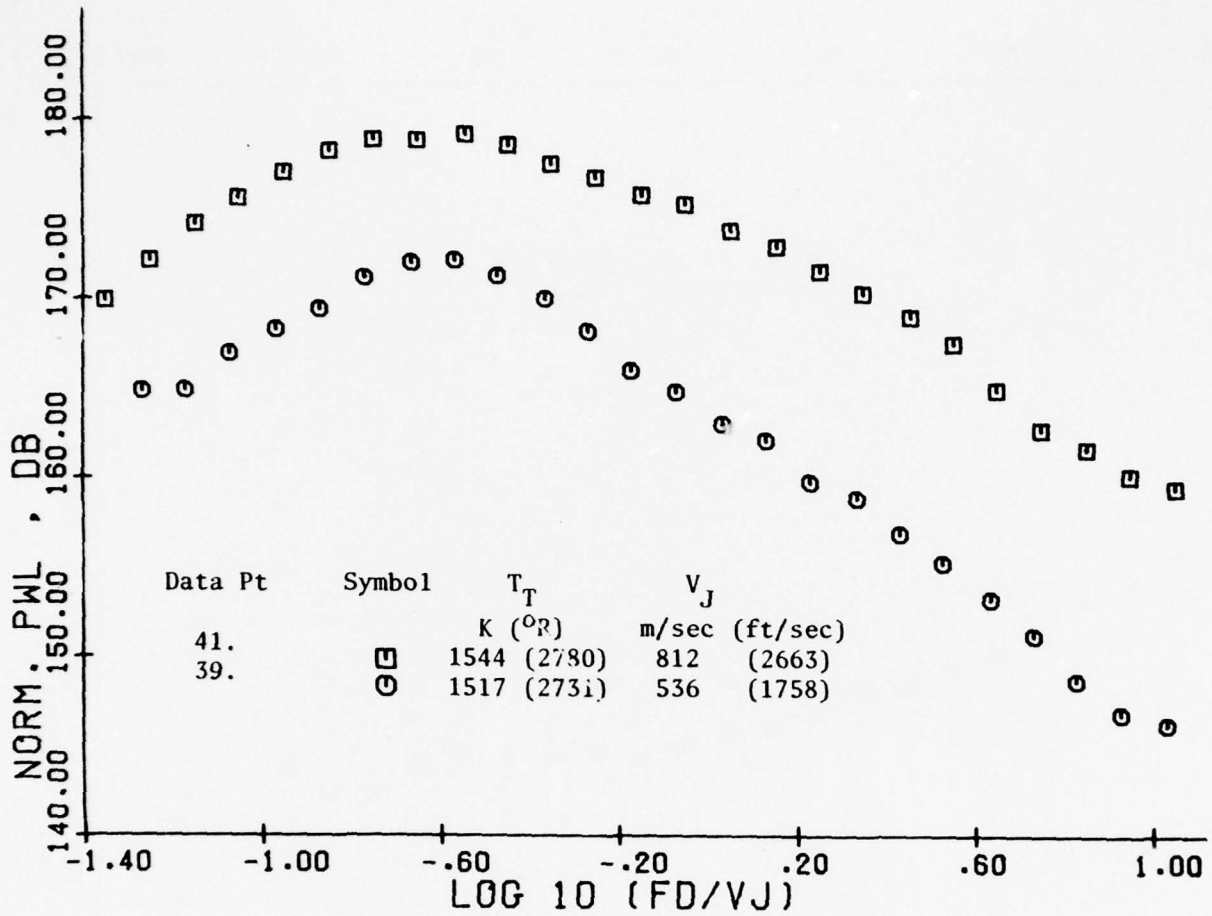

Figure 6-21. Normalized Power Spectra for 1530 K (2754° R) Hot Jets in the GE Anechoic Facility Single-Flow Installation.

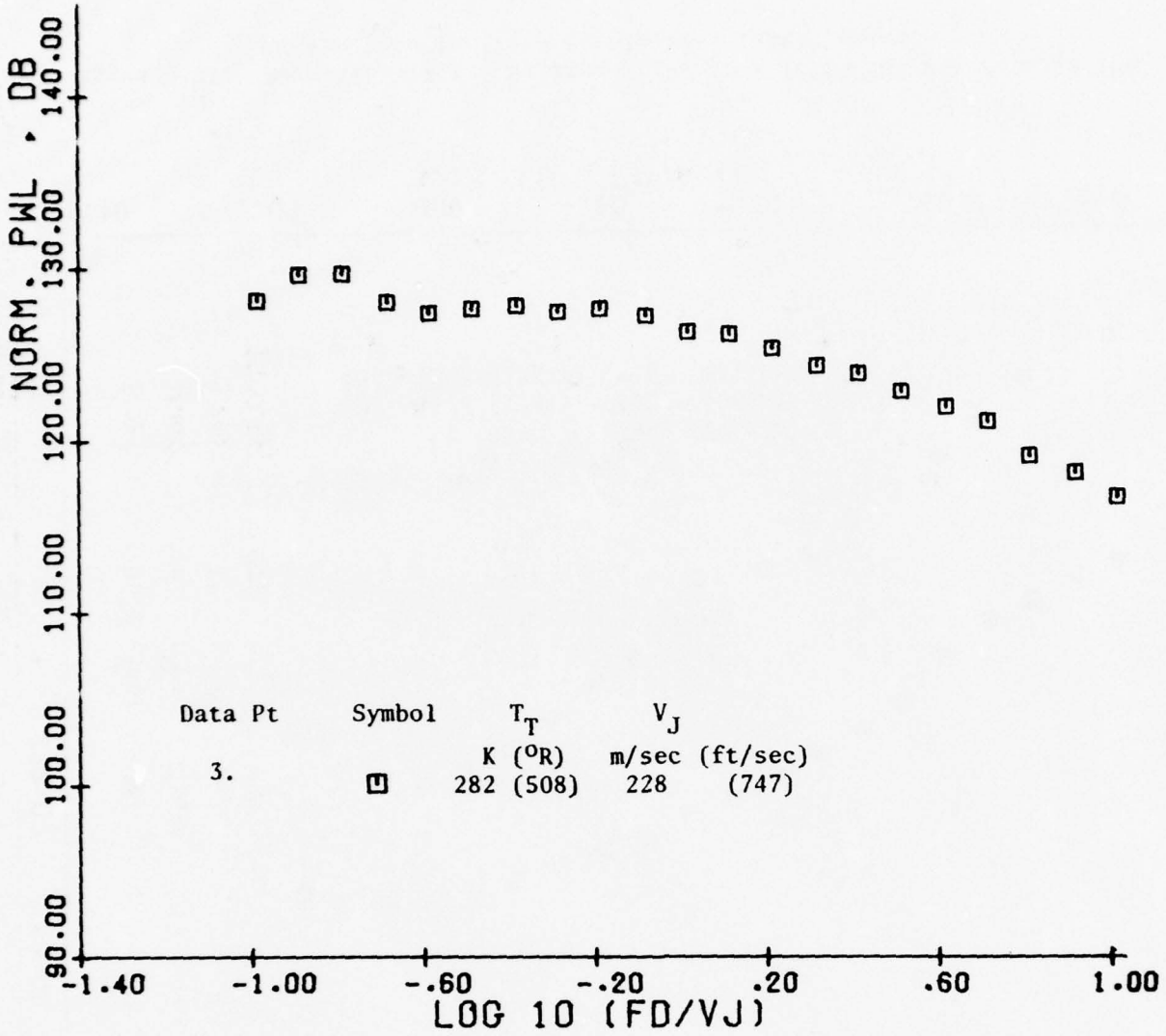

Figure 6-22. Normalized Power Spectra for Cold Jets in the GE Anechoic Facility Dual-Flow Installation.

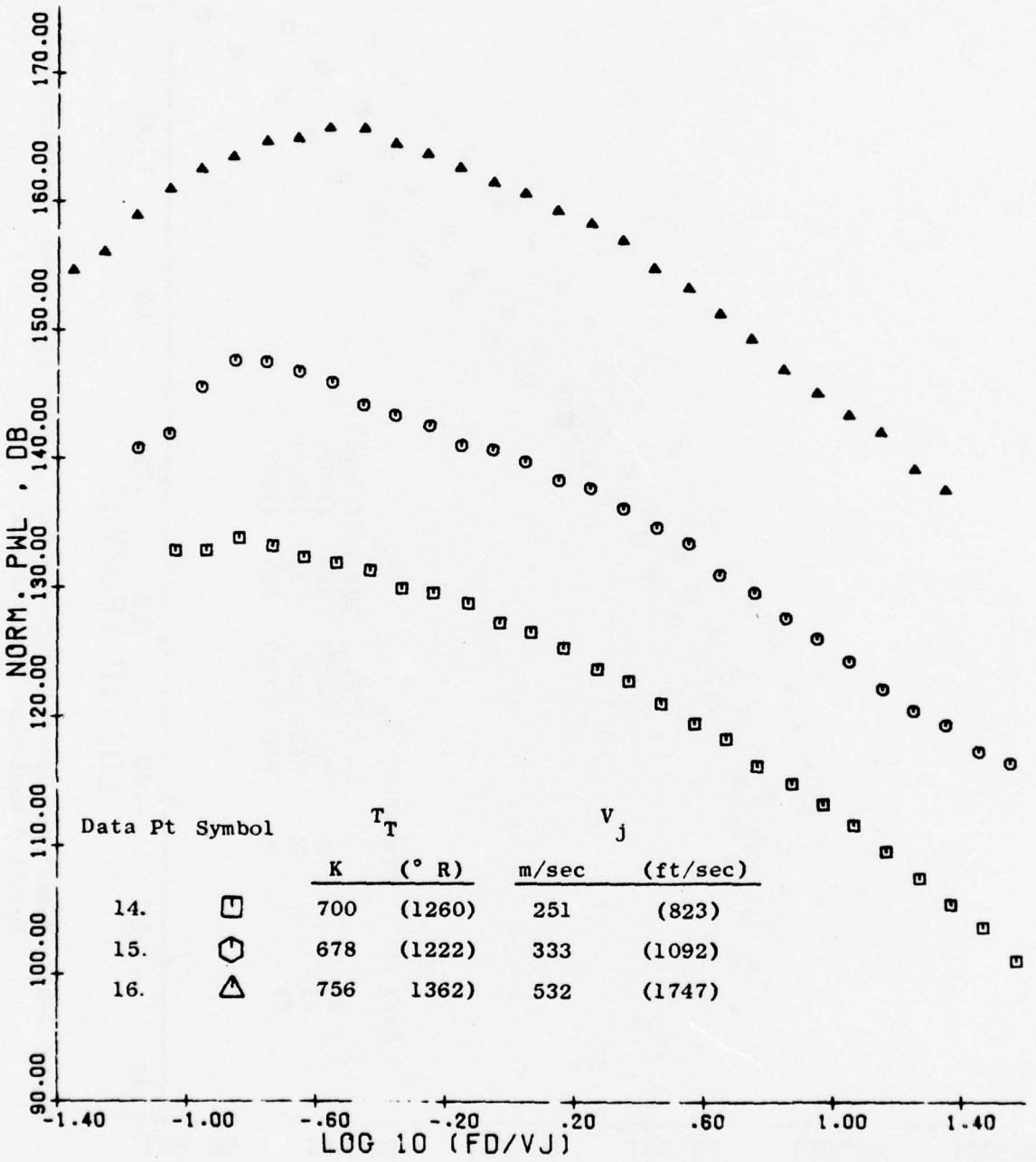

Figure 6-23. Normalized Power Spectra for 700 K (1260° R) Hot Jets in the GE Anechoic Facility Dual-Flow Installation.

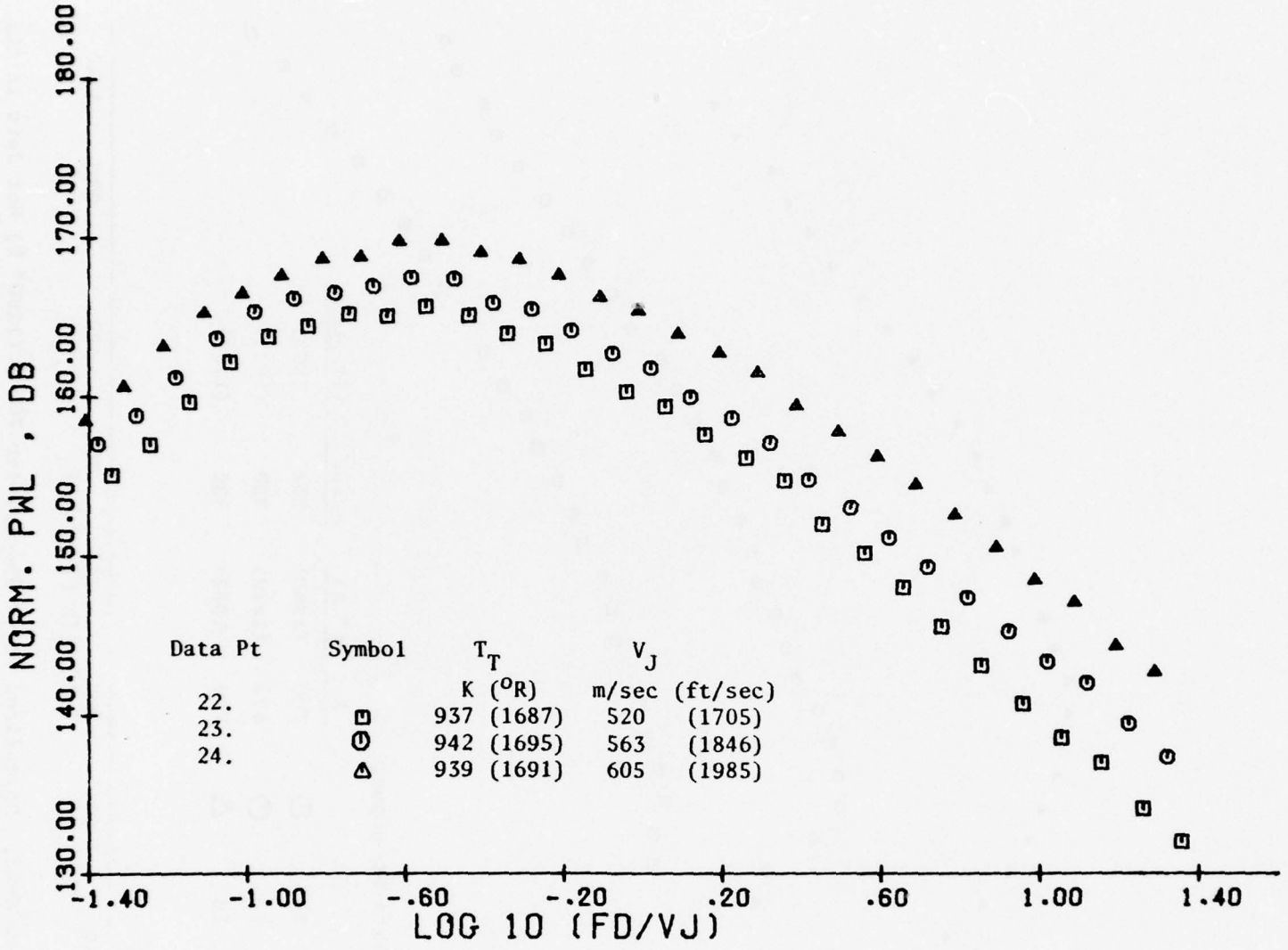

Figure 6-24. Normalized Power Spectra for 939 K (1690° R) Hot Jets in the GE Anechoic Facility Dual-Flow Installation.

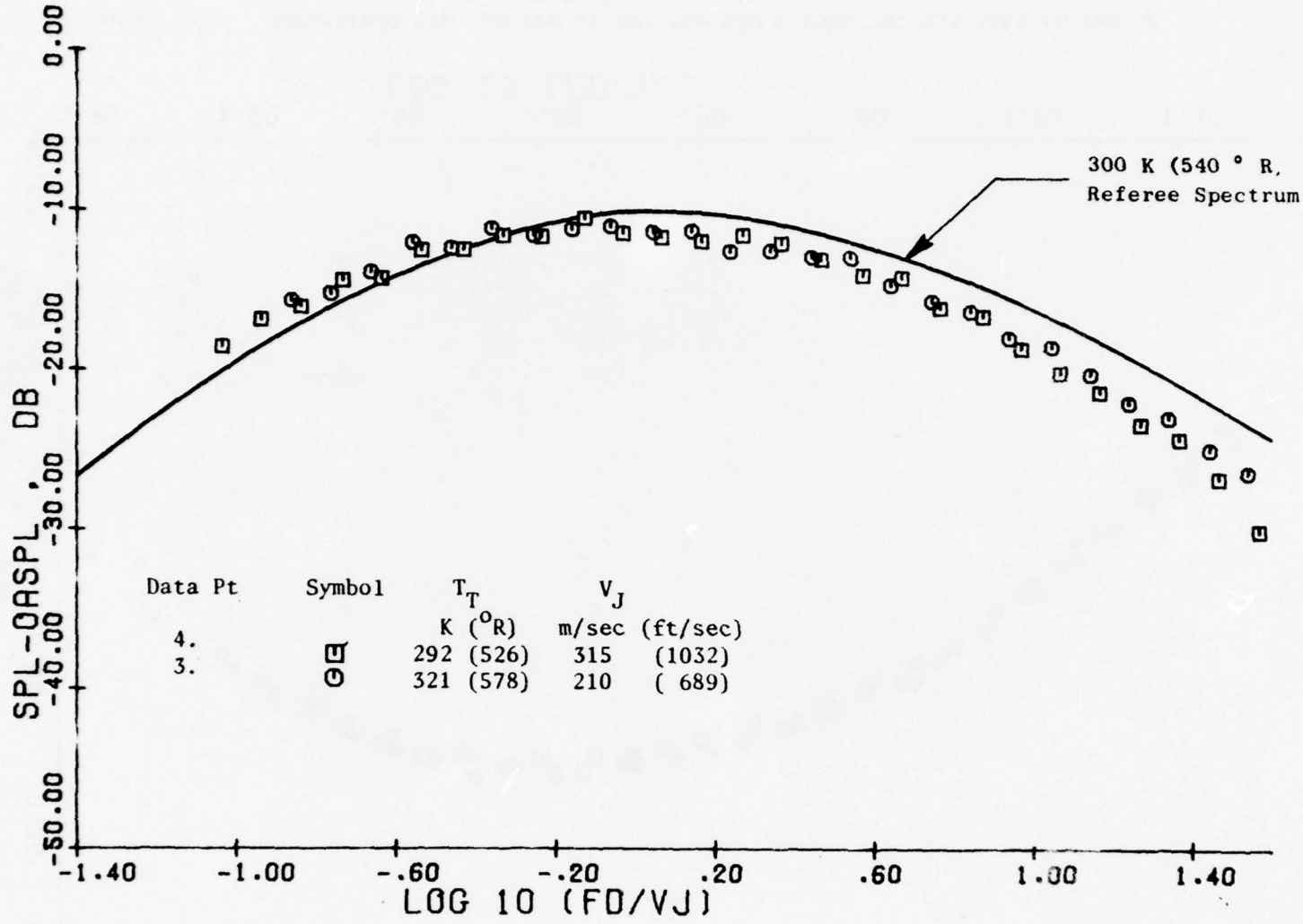

Figure 6-25. Normalized SPL Spectra at 90° for Cold Jets in the GE Anechoic Facility Single-Flow Installation.

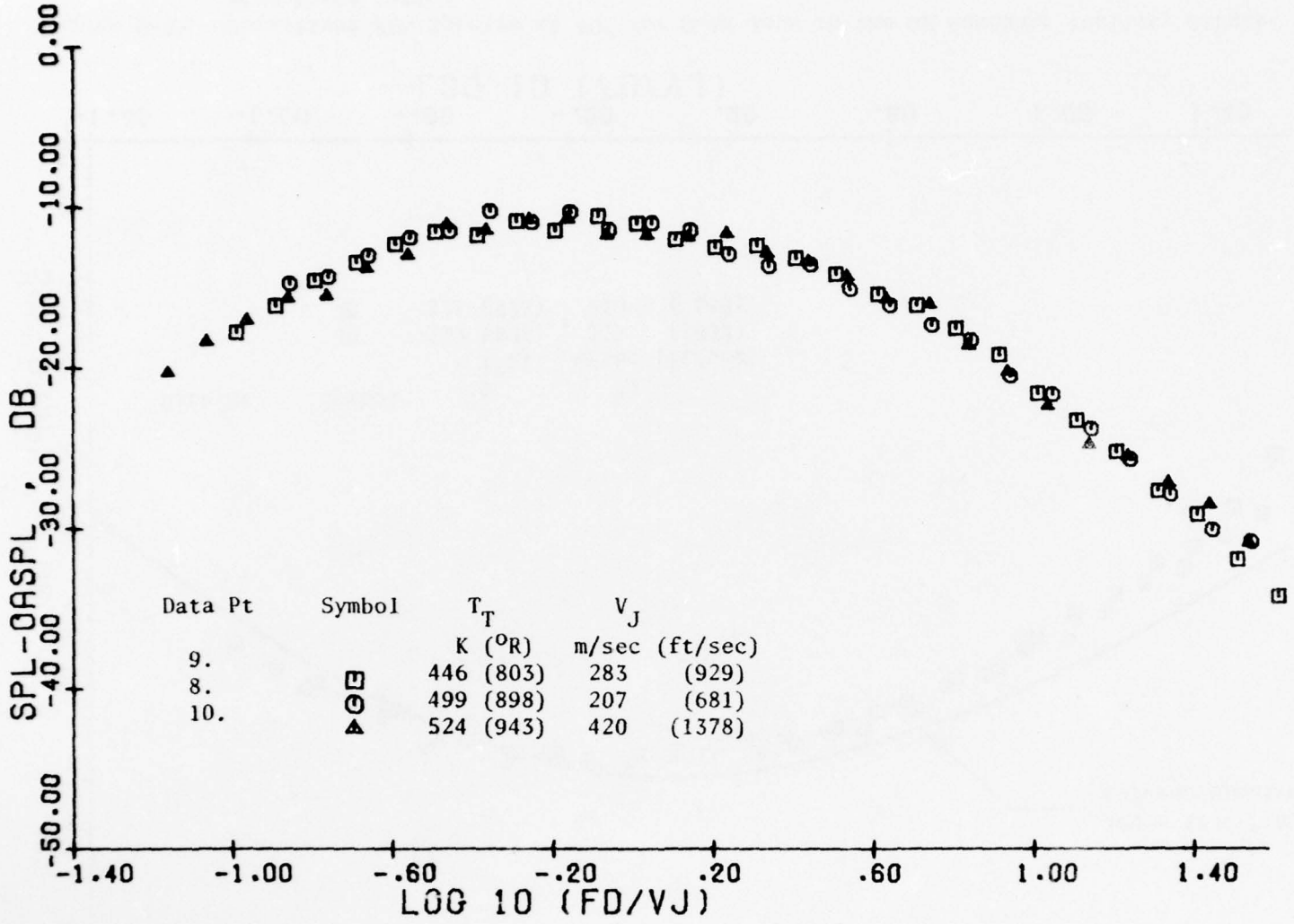

Figure 6-26. Normalized SPL Spectra at 90° for 500 K (900° R) Hot Jets in the GE Anechoic Facility Single-Flow Installation.

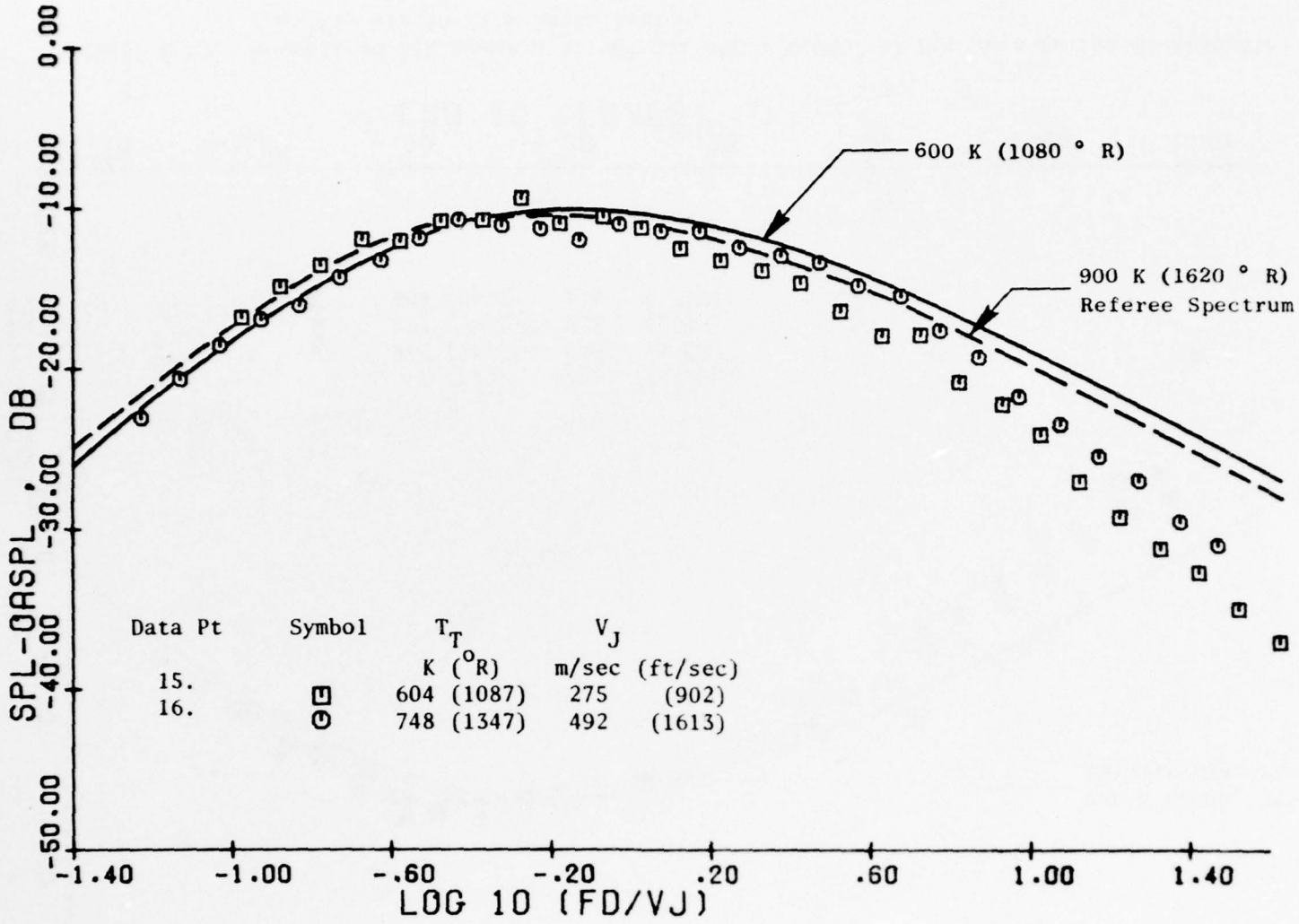

Figure 6-27. Normalized SPL Spectra at 90° for 700 K (1260° R) Hot Jets in the GE Anechoic Facility Single-Flow Installation.

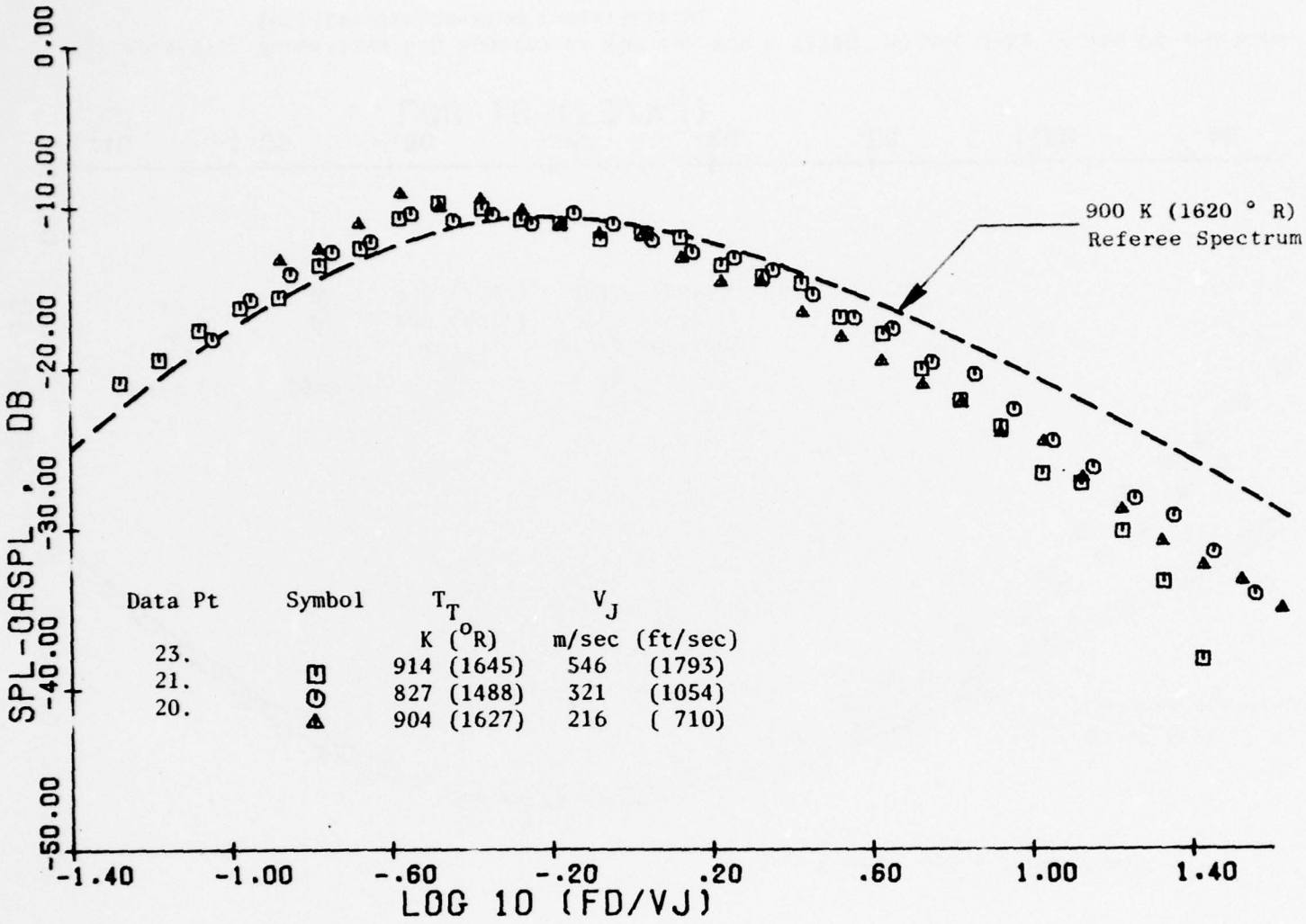

Figure 6-28. Normalized SPL Spectra at 90° for 900 K (1620° R) Hot Jets in the GE Anechoic Facility Single-Flow Installation.

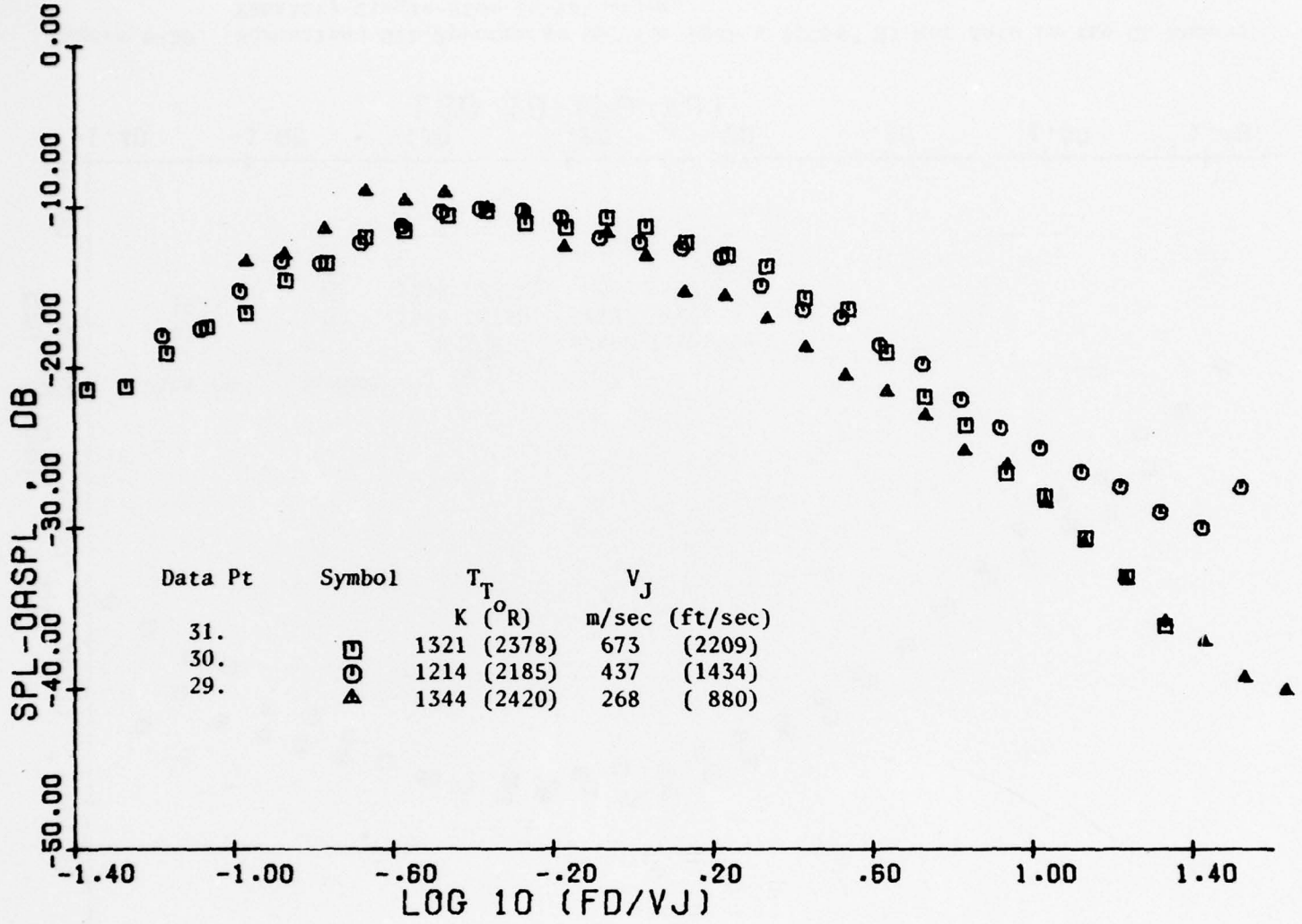

Figure 6-29. Normalized SPL Spectra at 90° for 1278 K (2300° R) Hot Jets in the GE Anechoic Facility Single-Flow Installation.

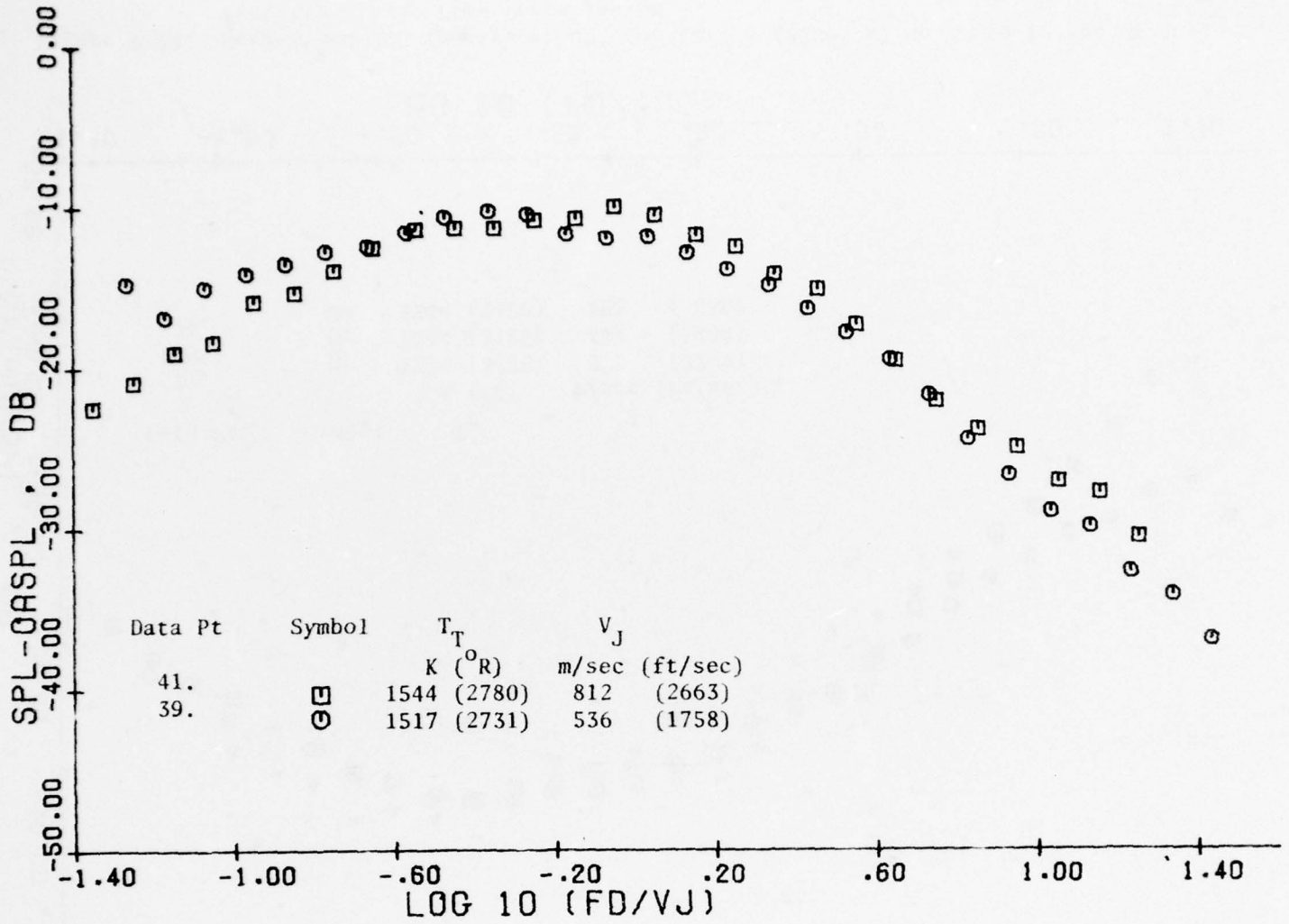

Figure 6-30. Normalized SPL Spectra at 90° for 1530 K (2754° R) Hot Jets in the GE Anechoic Facility Single-Flow Installation.

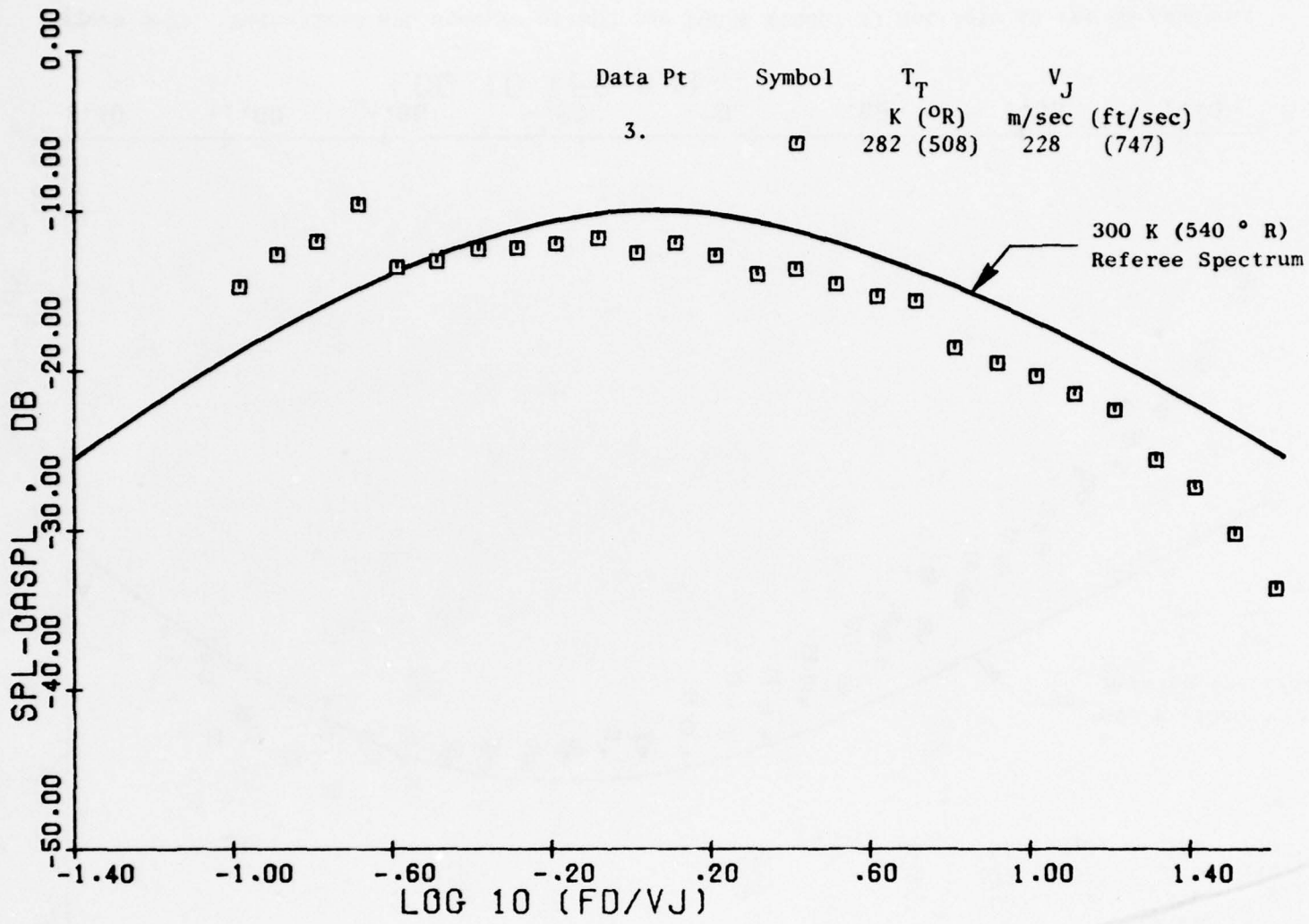

Figure 6-31. Normalized SPL Spectra at 90° for Cold Jets in the GE Anechoic Facility Dual-Flow Installation.

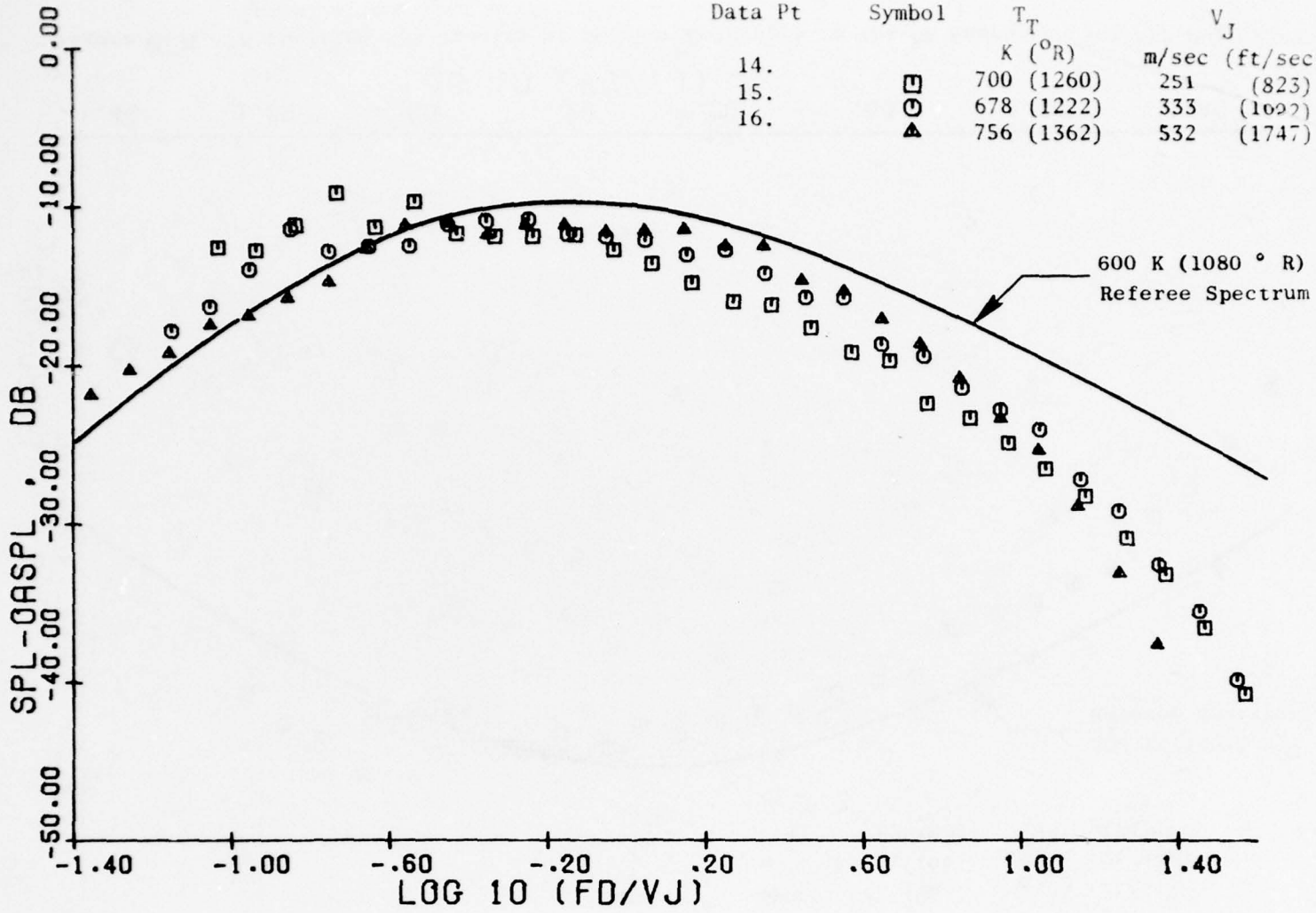

Figure 6-32. Normalized SPL Spectra at 90° for 700 K (1260° R) Hot Jets in the GE Anechoic Facility Dual-Flow Installation.

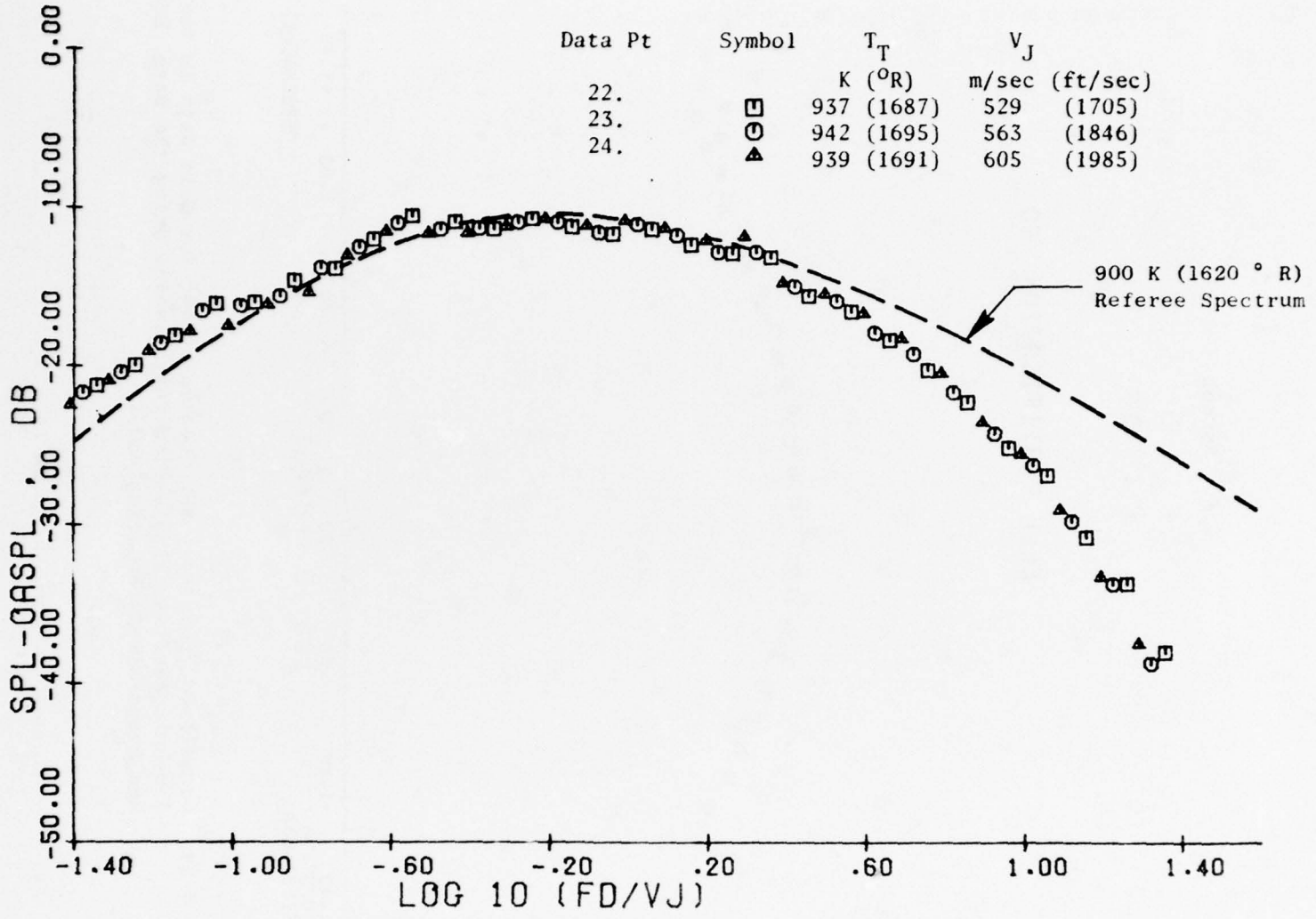

Figure 6-33. Normalized SPL Spectra at 90° for 939 K (1690° R) Hot Jets in the GE Anechoic Facility Dual-Flow Installation.

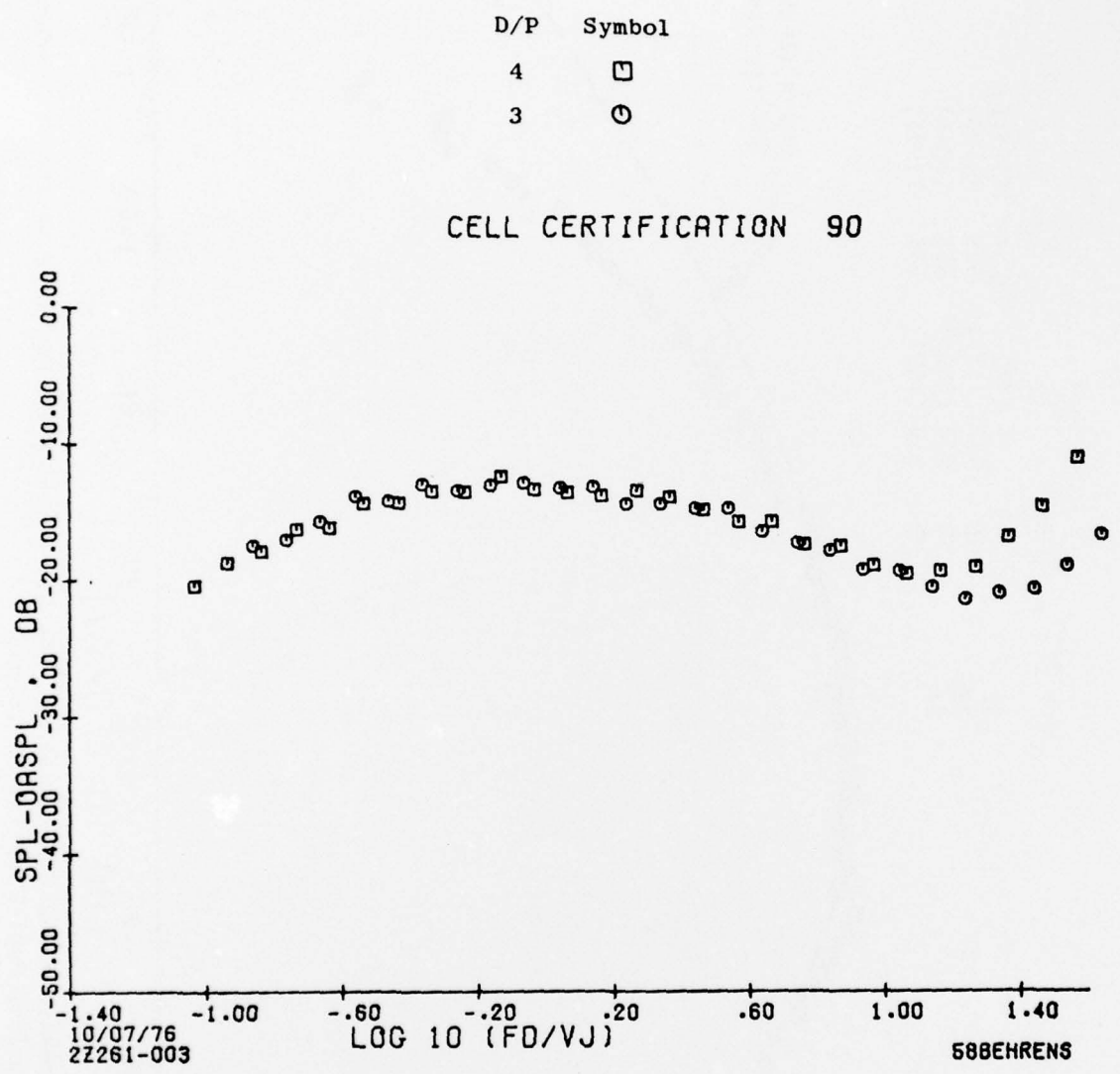

Figure 6-34. Normalized "Lossless" SPL Spectra at 90° for Cold Jets in the GE Anechoic Facility Single-Flow Installation Using the Bass, Bauer, and Evans Air Attenuation Model.

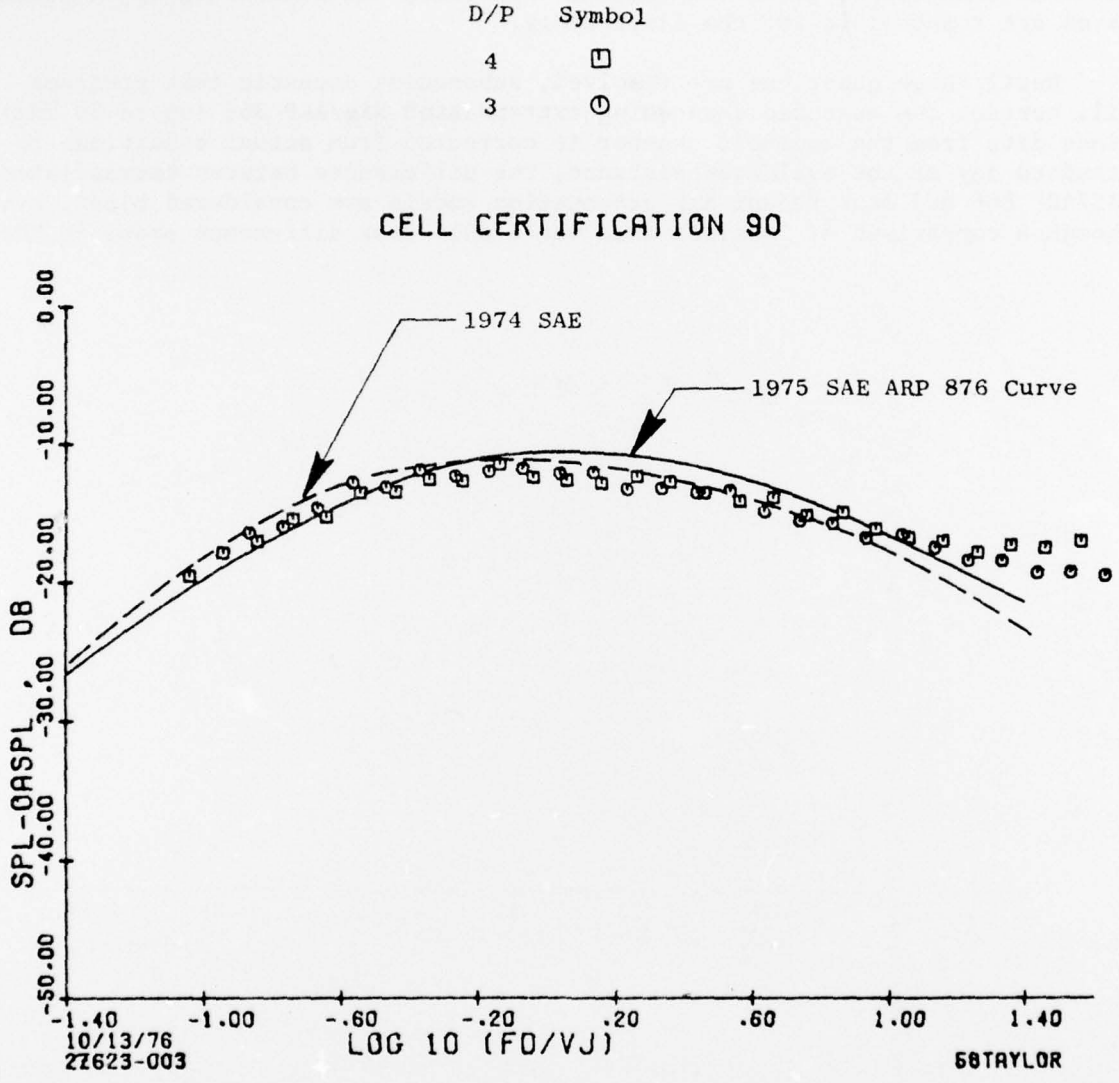

Figure 6-35. Normalized "Lossless" SPL Spectra at 90° for Cold Jets in the GE Anechoic Facility Single-Flow Installation Using the "Proposed Standard" Air Attenuation Model.

Even the latest air attenuation model did not adequately correct all the measured data to different distances or scale sizes without causing some curl up, particularly at the aft angles. A detailed study verified that this curl up was not caused by electronic noise, so an inadequate air attenuation model was suspected. It is believed that near-field and distributed source effects, and wind temperature gradients causing channeling and scattering of the sound waves are responsible for the discrepancy.

Until these questions are resolved, subsequent acoustic test programs will correct the measured data using extrapolated SAE/ARP 866 (up to 80 kHz). Since data from the anechoic chamber is corrected from actual conditions to standard day at the evaluated distance, the differences between extrapolated SAE/ARP 866 and most recent air attenuation models are considered minor, even though a comparison of lossless data would show some difference above 40 kHz.

7.0 CONCLUSIONS AND RECOMMENDATIONS

7.1 CONCLUSIONS

The previous analysis of the General Electric Jet Noise Anechoic Test Facility has resulted in the following conclusions:

1. Aerodynamic testing can be accomplished to a temperature of 1667 K (3000° R) and a pressure ratio of 4.5.

2. Acoustic testing should not be conducted below 213 m/sec (700 ft/sec) up to 1111 K (2000° R), below a pressure ratio of 1.1 from 1111 K (2000° R) to 1390 K (2500° R), and below a pressure ratio of 1.8 above 1390 K (2500° R).

3. The precision accuracy of the facility is within ±2.5 dB standard deviation over the 400 Hz to 80 kHz frequency range of interest and within 1 dB between 630 Hz and 31.5 kHz. The chief sources of precision error are flow noise at low frequency and tape recorder floor along with air attenuation measurement inaccuracies at high frequencies.

4. The anechoic environment is excellent over the range from 200 Hz to 80 kHz.

5. The standard microphone stations are in the farfield for nozzles smaller than 17.3 cm (6.8 in.) effective diameter.

6. Environmental gradients are extreme at low velocities and very high temperatures near the chamber roof and corner.

7. Tape recorder dynamic range becomes a problem at the angles closest to the jet axis.

8. Contamination from the chamber ambient noise or microphone floor are insignificant.

9. The accuracy of the aerodynamic and acoustic instrumentation was excellent. The largest variability occurred when using the high temperature platinum rakes at low temperatures.

10. Flow noise contamination appears to affect measured jet noise levels below jet velocities of 213 m/sec (700 ft/sec).

11. Exact relationships for the air attenuation model at high frequency are yet unknown, so a bias error in the correction factors is possible.

7.2 RECOMMENDATIONS

From the previous conclusions, the following recommendations are drawn:

1. An experimental study of air attenuation characteristics at high frequency as a function of ambient temperature and relative humidity should be conducted.

2. After a reliable air attenuation model has been established (the Bass and Shields models, for example) detailed experimental study into near-field effects, distributed source effects, wind and temperature gradients, channeling, and scattering of sound in the neighborhood of the jet should be conducted to determine the proper air attenduation corrections to be applied to jet noise.

3. Improved data acquisition systems to obtain increased dynamic range at angles near the jet axis should be developed.

4. A study of the transmission loss of flow and combustor noise through nozzles needs to be conducted to determine the absolute level of contamination from these sources.

REFERENCES

1. Anon, "Chapter 4: Flow Measurement Instruments and Apparatus Part 5 - Measurement of Quantity of Materials," ASME PTC 19.4;4, ASME, New York, 1959.

2. Anon, "Standard Values of Atmospheric Absorption as a Function of Temperature and Humidity for Use in Evaluating Aircraft Flyover Noise," SAE ARP 866, 1964.

3. Anon, "Standard Values of Atmospheric Absorption as a Function of Temperature and Humidity," SAE ARP 866A, March 15, 1975.

4. Bass, H.R., Bauer, H.J., and Evans, L.B.; "Atmospheric Absorption of Sound: Analytic Expressions," JASA, Volume 52, 5 (Part 2), 1972.

5. Burren, R.H., Dean, P.D., and Tanna, H.K.; "A New Anechoic Facility for Supersonic Hot Jet Noise Research at Lockheed Georgia," 86th Meeting of the Acoustic Society of America, Los Angeles, October, 1973.

6. Chu, W.T.; "Certification of the USC Jet Noise Facility," USCAE 131, University of Southern California, April 1975.

7. Beranek, L.L.; "Noise Reduction," McGraw-Hill, 1960.

8. Harris, C.M.; "Absorption of Sound in the Audio Frequency Range," JASA, Volume 35, 1963.

9. Knesner, H.O.; "Interpretation of the Anomalous Sound Absorption in Air and Oxygen in Terms of Molecular Collisions," JASA, Volume 5, 1933.

10. Evans, L.B., Bass, H.E., and Sutherland, L.C.; "Atmospheric Absorption of Sound, Theoretical Predictions," 5 (Part 2), JASA, Volume 51, 1972.

11. Shields, F.D., and Bass, H.D.; "A Study of Atmospheric Absorption of High Frequency Noise - University of Mississippi, NAS3, 19431.

12. Anon, "Jet Exhaust Noise Predictions," Proposed AIR 876, SAE A21 Committee, New York, New York, September 1974.

13. Sutherland, L.C., Piercy, J.E., Bass, H.E., and Evans, L.B.; "A Method for Calculating the Absorption of Sound by the Atmosphere," ASA paper, November 1974.

14. Anon, "Gas Turbine Jet Exhaust Noise Prediction," Proposed ARP 876, SAE A21 Committee, New York, New York, July 1975.

15. Hoch, R.G., Duponchel, J.P., Cocking, B.J., and Bryce, W.D.; "Studies of the Influence of Density on Jet Noise," Journal of Sound and Vibration, 28 (4), pp. 649-668, 1973.

16. Lush, P.A.; "Measurements of Subsonic Jet Noise and Comparison with Theory," J. Fluid Mech., Volume 46, pt. 3, pp. 477-500, 1971.

17. Ahuja, K.K., and Bushell, K.W.; "An Experimental Study of Subsonic Jet Noise and Comparison with Theory," Journal of Sound and Vibration, 30 (3), pp. 317-341, 1973.

18. Olsen, W.A., Gutierrez, O.A., and Dorsch, R.G.; "The Effect of Nozzle Inlet Shape, Lip Thickness and Exit Shape on Subsonic Jet Noise," NASA TMS 68182, Lewis Research Center, 1973.

19. Cocking, B.J.; "The Effect of Temperature on Subsonic Jet Noise," NGTE Report No. R331, May 1974.

20. Tanna, H.K., and Dean P.D.; "Results for the AFAPL/DOT Contract," Lockheed Georgia Company. To be published in Journal of Sound and Vibration.

21. Lighthill, M.J.; "Sound Generated Aerodynamically," the Bakerian Lecture 1961, Proc. Roy Soc., Volume 267A, Page 172, May 1962.

22. Stone, J.R.; "Interim Prediction Method for Jet Noise," NASA TMX 71618, NASA Lewis Research Center, 1974.